December 2018

# Tissue Engineering Platforms for Cardiac Pathology in Diabetes: In Vitro and In Vivo Studies

Laura Elizabeth McCallum
*Clemson University*, lauramccallum22@gmail.com

# TISSUE ENGINEERING PLATFORMS FOR CARDIAC PATHOLOGY IN DIABETES: IN VITRO AND IN VIVO STUDIES

---

A Dissertation
Presented to
the Graduate School of
Clemson University

---

In Partial Fulfillment
of the Requirements for the Degree
Doctor of Philosophy
Bioengineering

---

by
Laura Elizabeth McCallum
December 2018

---

Accepted by:
Dr. Agneta Simionescu, Committee Chair
Dr. Dan Simionescu
Dr. Martine LaBerge
Dr. Ying Mei
Dr. John Bruch

## ABSTRACT

425 million people have diabetes worldwide, and by 2045 this number is estimated to increase to 629 million. The risk for cardiovascular diseases such as cardiomyopathy, hypertension, and atherosclerosis increase 5 and 2-fold for diabetic women and men respectively. Diabetic cardiomyopathy (DCMP) is a ventricular dysfunction that occurs in patients with diabetes independent of coronary artery disease, hypertension or valvular abnormalities. Hyperglycemia and dyslipidemia cause metabolic disturbances that adversely affect myocardial cells and extracellular matrix. These modifications alter overall myocardial structure and cardiac function, which can lead to heart failure.

As of now there is no specific marker for this disease and diagnosis is the same as other cardiomyopathies. Elucidating early stages of this disease is vital for early diagnosis, treatment, and possible therapy targets. Currently, rodent models and 2D cell cultures have been employed to analyze DCMP, however there are notable differences between rodents and humans that provide challenges when studying DCMP and cell cultures lack an extracellular matrix and dynamic environment crucial to the progression of this disease.

Our overall goal was to use tissue engineering to bridge this gap by developing platforms to study pathological mechanisms at the cellular and extracellular level. We examined cardiac tissue engineered constructs in: (1) a perfusion 3D Kube minibioreactor and (2) an electromechanical bioreactor customized in our lab. Each platform contained decellularized myocardium seeded with human cardiomyocytes for

two weeks; “diabetic” conditions were simulated by increased glucose concentration. We were able to better mimic physiological conditions with our electromechanical bioreactor, compared to static and non-diabetic conditions, as well as to 2D cell culture. Methods for detecting cellular and matrix changes associated with DCMP were validated in a type 1 diabetic rodent model. Our tissue engineering platform shows promise for unveiling early cellular and matrix modifications in DCMP. This system could also be useful for studying human cells in other cardiac diseases, test treatments, and precondition myocardial-like tissue prior to implantation.

## DEDICATION

This dissertation is dedicated, first and foremost, to Jesus Christ, my Lord and savior. Psalms 84:12; Jeremiah 29:11; Romans 12:21.

It is also dedicated to my family- past, present, and future. For my mother, who spent countless hours teaching me at home outside of school and imparted the importance of grit. For my sister, who taught me to be myself by being open and honest. For my father, who inspired me to pursue bioengineering and instilled the love of problem solving. For my Mockie and Papa, who showed me that determination and hard work are essential for success.

## ACKNOWLEDGMENTS

A special thank you to Dr. Agneta Simionescu, my advisor, mentor, and lab mom. You have instilled your love of research, continual learning, teaching, and mentoring in me. You have gone above and beyond the call of mentoring by providing support through difficult times. Likewise, many thanks to Dr. Dan Simionescu- lab dad. Thank you both for believing in me, even when I did not, and for providing an unparalleled, inspirational environment for research and growth.

I would also like to thank my committee members Dr. Martine LaBerge, Dr. Ying Mei, and Dr. John Bruch. You have all provided wonderful support and alternative perspectives for this research. Your feedback and advice have been key in shaping this project, as well as my individual professional development.

I would like to thank all past and present graduate students of the Cardiovascular and Tissue Engineering and Regenerative Medicine Lab and Biocompatibility and Tissue Regeneration Lab for their friendship and support- Jeremy Mercuri, Lee Sierad, James Chow, Jason Schulte, Mike Jaeggli, Katy Jaeggli, George Fercana, Chris DeBorde, Allison Kennamer, Anna Lu Carter, Margarita Portilla, Megan Casco, Jhilmil Dhulekar, Spencer March, Tasha Topoluk, Richard Pascal, Grace Dion, Satyam Patel, Elizabeth Fontaine, Lisa Larrew, Eric Wright, Katelyn Rye, Jessica Canavan, Christopher Ferriera, Alex Bina, Brady Culbreth, Clayton Compton, Harrison Smallwood, Robert Marti, Josh Rodriguez, Joshua Biggs, James McManus, David Pollard, Bethany Lefeber, Nathan Adams, Collin Owens, and Chip Herbert. Also, a thank you to undergraduates I started with in the lab- Harleigh Warner, Devon Bowser, and Laine Shaw. A massive thank you

to our past undergraduate lab cheerleader- Maddy Raudat. A significant thanks to undergraduate researchers who worked directly on this project- Kaitlin McClure, Charles Pickens, and Anthony Alerre.

A great thank you to Clemson University Department of Bioengineering and its staff, past and present, including: Maria Torres, Leigh Humphries, Michelle Kirby, Cassie Gregory, Chad McMahan, Teri Townsend, Jessica Lang, Sherri Morrison, Maranda Arnold, Mellissa McCullough, Jennifer Hogan, and Tammy Rothell. You are the backbone of the department and have provided much support. An enormous thank you to Clara Ditty- a departmental inspiration and one of the strongest people I know. Many thanks to friends made within the department. You have all made this home.

## TABLE OF CONTENTS

Page

**Table of Contents (Continued)**

Page

**Table of Contents (Continued)**

Page

**Table of Contents (Continued)**

Page

## Table of Contents (Continued)

Page

## LIST OF TABLES

## LIST OF FIGURES

## List of Figures (Continued)

## List of Figures (Continued)

## List of Figures (Continued)

## List of Figures (Continued)

# CHAPTER 1: REVIEW OF LITERATURE

## 1.1 Introduction

The total global economic burden of diabetes mellitus in 2017 was estimated at $850 billion.[1] 425 million people have diabetes worldwide, and by 2045 this number is estimated to increase to 629 million.[1] The risk for cardiovascular disease increases 5 and 2 fold for diabetic women and men respectively.[2] Diabetics have higher instances of cardiovascular disease such as diabetic cardiomyopathy, hypertension, and atherosclerosis, with elevated occurrences of myocardial infarctions and strokes within these patients due to atherosclerotic plaque ruptures.[3] Diabetic cardiomyopathy (DCMP) can manifest in diabetic patients and it is estimated 19-26% of diabetic patients experience heart failure.[4] DCMP is a ventricular dysfunction that occurs in patients with diabetes independent of coronary artery disease, hypertension or valvular abnormalities. Excessive utilization of circulating free fatty acids (FFA) creates a highly oxidative environment that supersedes the endogenous antioxidant defense mechanism of cells, leading to oxidative stress, lipotoxicity, autophagy, and apoptosis of cardiomyocytes. The hyperglycemic environment causes the formation and accumulation of advanced glycation endproducts (AGEs) in the extracellular matrix, fibrosis, and, lastly, heart failure.[5] As of now, mainly rodent models and two dimensional (2D) cell cultures have been employed to analyze DCMP. However, there are notable differences between rodents and humans that provide challenges when studying DCMP and 2D cultures lack a dynamic, three dimensional (3D) environment crucial to the progression of this disease.[6] There is a need for a more accurate model to investigate DCMP for early diagnosis and

test potential therapies. This gap can be bridged with the development of a reproducible, native-like tissue engineered model of the myocardium utilizing the tissue engineering paradigm of combining a scaffold, cells, and biochemical and physical stimuli.

### 1.2 The Heart and Myocardium

The heart is responsible for pumping blood throughout the body to supply oxygen, nutrient, and waste exchange. It is a highly stressed organ as it beats between 60 and 100 beats per minute. It is comprised of four chambers, four heart valves, and utilizes a network of blood vessels in the circulatory system for transportation.[7] Within the body, the heart is located left to the midline posterior to the sternum and rotated slightly so that its right border is located more anteriorly, and the left border is located more posteriorly. A fibrous sac and serous lining called the pericardium, surrounds the heart to provide an almost frictionless environment for the continuous movement of this organ. The normal adult human heart is typically 12cm in length, 8cm wide, 6cm thick, and weighs between 250 and 350 grams.[8]

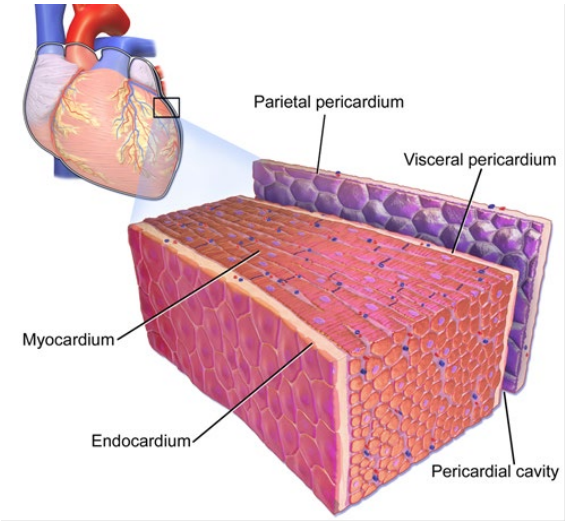


**Figure 1.1:** The layers of the heart wall.[7]

The heart wall consists of three layers; the epicardium, myocardium, and endocardium with blood vessels and capillaries incorporated (**Figure 1.1**). The outer epicardium is comprised of epithelium and connective tissue and fat; the middle myocardium is made of mainly cardiomyocytes (CMs) and fibroblasts (FBs); and the inner endocardium contains endothelium and areolar connective tissue.[7]

*1.2.1 The Extracellular Matrix of the Myocardium*

The extracellular matrix (ECM) of healthy myocardium is a dynamic environment, undergoing constant, balanced turnover in its normal state. It is made of collagens (type I, III, IV, V, and VI), elastin, glycoproteins (laminins, fibronectin, periostin, fibromodulin, and vitronecin), proteoglycans (versican, lumican, and biglycan), glycosaminoglycans (hyaluronic acid and dermatan sulfate), and matricellular proteins.[9]

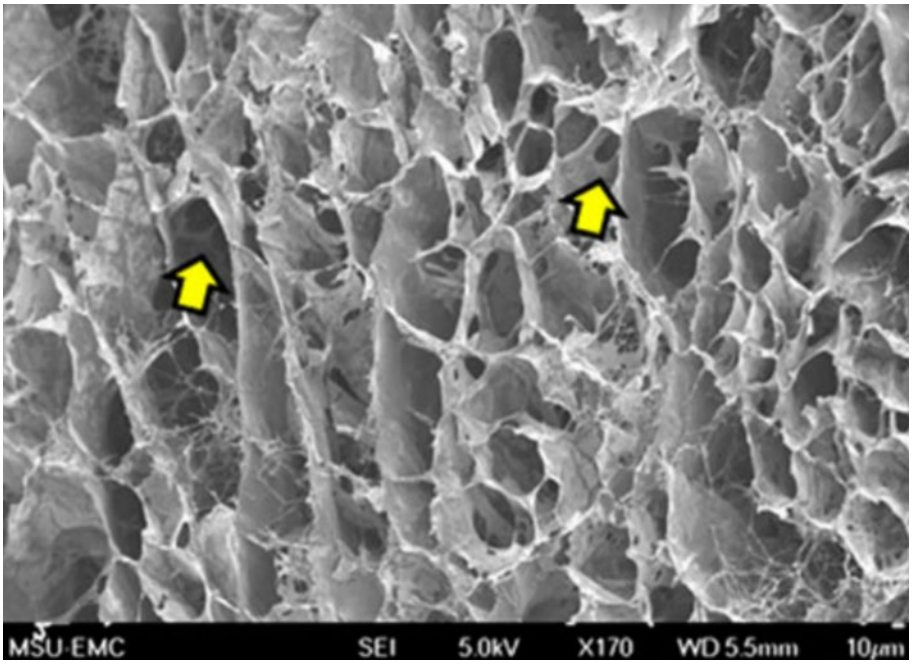


**Figure 1.2:** Scanning electron microscopy (SEM) image of acellular myocardium, illustrating the collagenous network of the ECM that supports native cells.[10] Arrows=cell voids.

These extracellular molecules are secreted by cells in the heart, mainly the FBs, and provide mechanical and biochemical support of the cells (**Figure 1.2**) by facilitating cell adhesion and differentiation. Collagens provide strength and resilience for the highly stressed environment and proteoglycans are receptors on cell surfaces. Proteoglycans provide cushioning for the cells and glycosaminoglycans are responsible for storage of growth factors and cell hydration.[11]

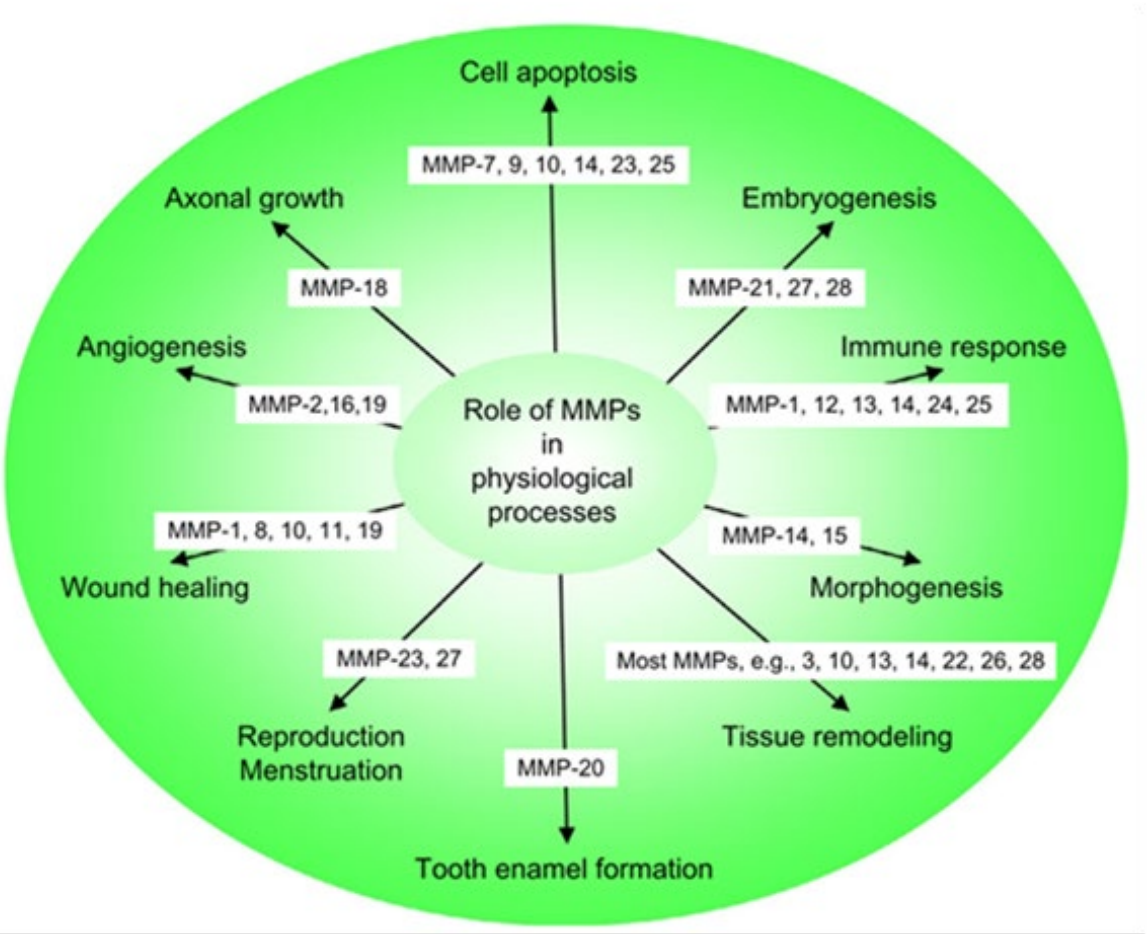


**Figure 1.3:** Roles of MMPs in physiological processes.[12]

Matrix metalloproteinases (MMPs) are a family of zinc-dependent endoproteases produced by cells. MMPs play an important role in ECM turnover by breaking down various ECM proteins, such as collagens and elastin.[9] They are also vital for tissue invasion, immune responses, vascularization, and cell proliferation, migration, and differentiation (**Figure 1.3**). Resident growth factors in the ECM are proteolytically cleaved and released by MMPs for cellular uptake.[12] Besides degradation of ECM, MMPs can degrade cell receptors to terminate migratory signaling and cell migration. Within the human body, 23 types of MMPs are known to exist, along with 4 endogenous, homologous tissue inhibitors of MMPs (TIMPs). TIMPs are endogenous and bind to MMPs at a 1:1 ratio. MMPs are controlled at multiple levels including messenger ribonucleic acid (RNA) expression, activation of proenzyme to the active form, and binding of TIMPs.[12]

*1.2.2 The Cells of the Myocardium*

The myocardium is composed of two main cell types, the cardiomyocytes (CMs) and fibroblasts (FBs) (**Figure 1.4**). Even though CMs occupy the largest volume in the heart, around 75%, their populations are only around 30-40%. FBs make up the majority of the heart's population. Smaller populations of vascular smooth muscle cells (SMCs) and endothelial cells (ECs) are also found, as they comprise the vascular network in the myocardium.[13]

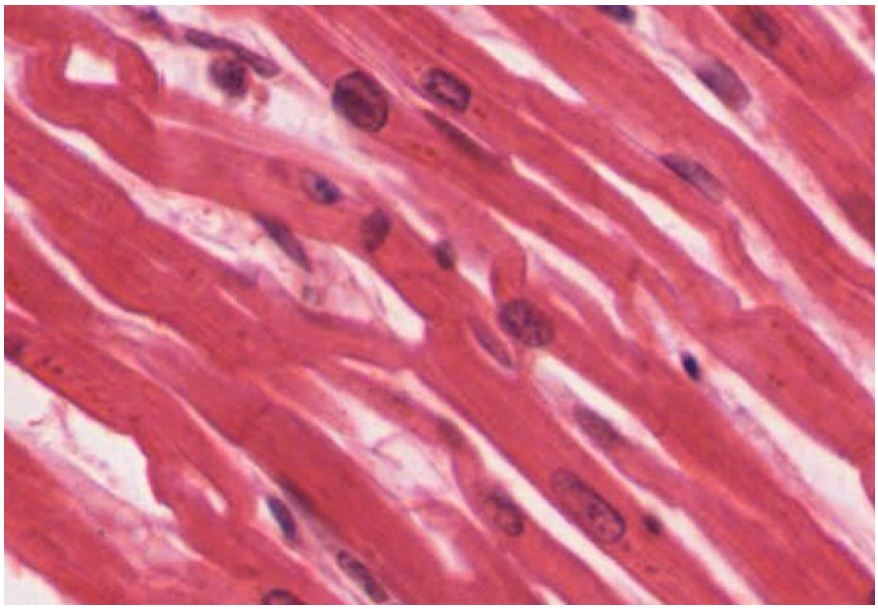

**Figure 1.4:** Hematoxylin and eosin staining of human myocardium.[14] 40x; purple=nuclei; pink=cytoplasm, tissue.

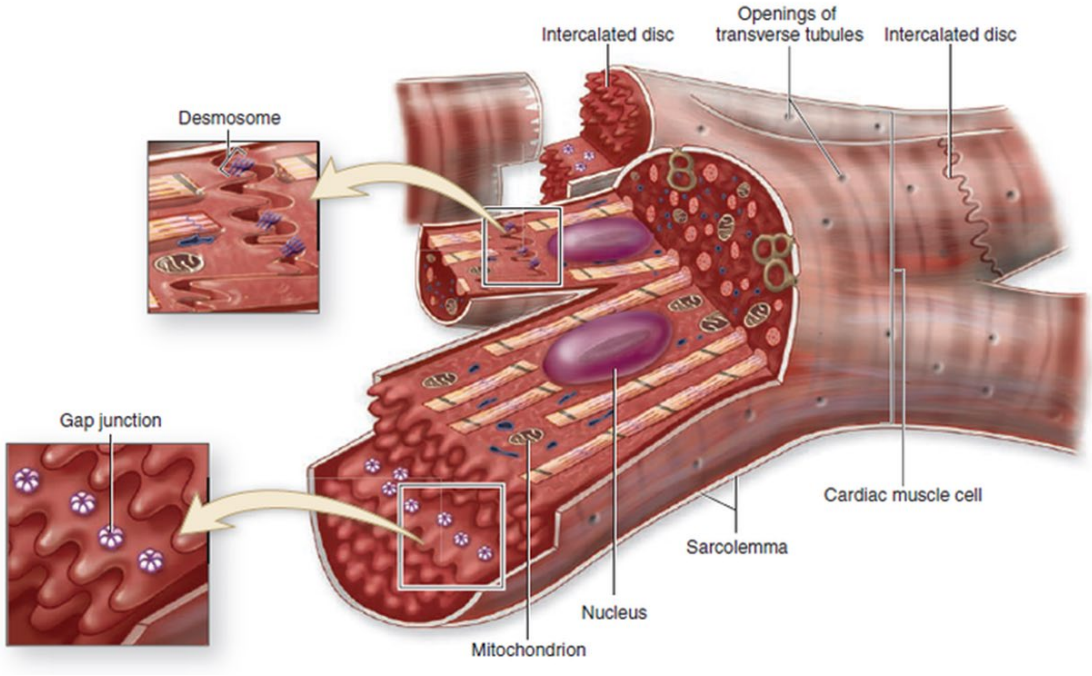


**Figure 1.5**: Cardiomyocyte cross section.[7]

CMs allow for contraction of the ventricles and atria. Myocytes in the ventricle are long and narrow, and can be 10 to 25 um in diameter and 50 to 100 um in length, while myocytes in the atrium are oval and are less than 10 um in diameter and around 20 um in length.[15] CMs have one or two nuclei and form Y-shaped branches that join to adjacent CMs via intercalated discs (**Figure 1.5**).[7] Intercalated discs allow for force to be transmitted from one CM to another, while gap junctions allow for electrical transmission between cells.[8] Mitochondria account for 60% of the cell volume, providing cellular energy through the production of adenosine 5'-triphosphate (ATP) and can also prevent intercellular calcium overload through calcium uptake.[15]

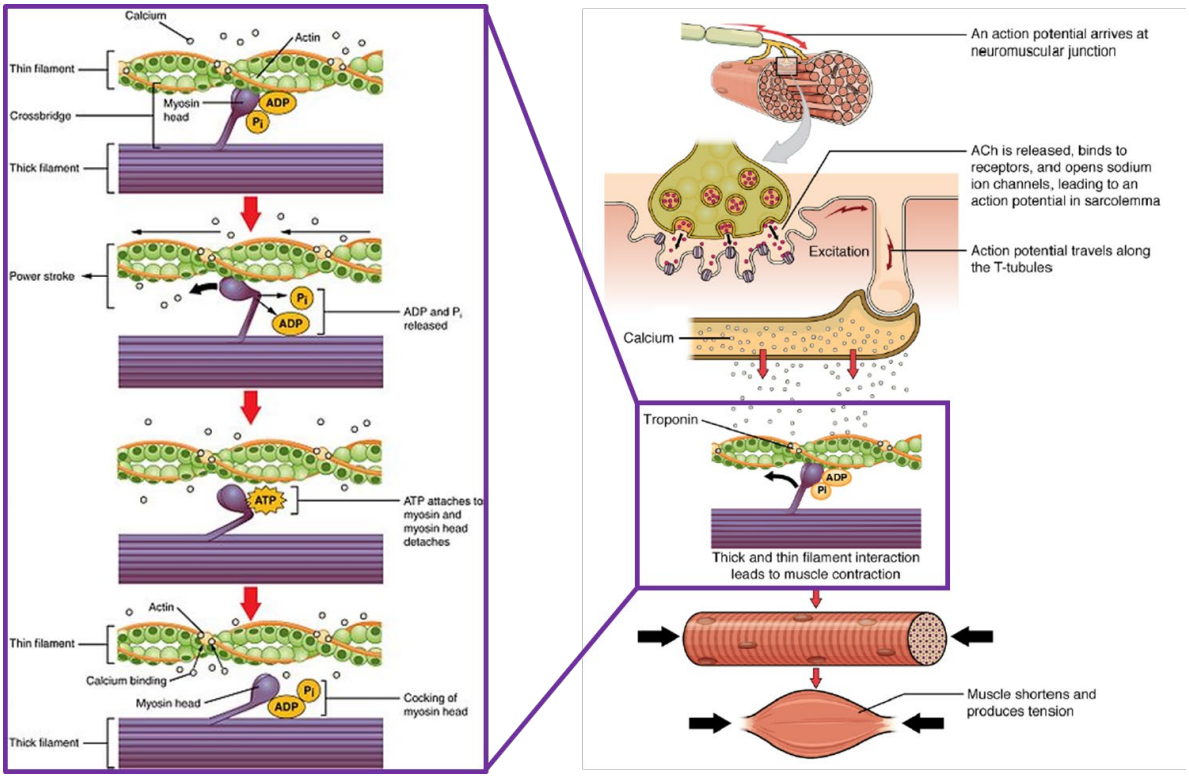


**Figure 1.6:** Excitation-contraction of a cardiomyocyte.[14]

Contraction of CMs is possible through an intricate network of proteins organized in sarcomeres, which are composed of thick and thin filaments (**Figure 1.6**). Myosin and actin comprise thick and thin filaments, respectively. CM contraction is set in motion by an action potential that travels along the sarcolemma into the transverse tubule (T-tubule) and depolarizes the cell membrane. This in turn opens calcium channels to allow calcium in the cell. Intracellular calcium rapidly increases as the sarcoplasmic reticulum releases even more calcium in response. Calcium binds to troponin-C on the thin filaments, inducing a conformational change and exposing myosin binding sites on the actin filament. This binding leads to ATP hydrolysis, which results in a conformational change of the actin-myosin complex and a sliding of the filaments, causing the sarcomere to shorten. Shortening in this unit is responsible for the overall contraction of the cell. The sarcomere length is restored with lowered cytosolic calcium concentration and a ATP binding to the myosin head at the end of this cycle.[8]

The structural integrity of the heart relies mainly on FBs, as they are very proliferative and produce interstitial collagen for the maintenance of the ECM. They also contribute to cardiac development, cell-signaling, and electro-mechanical function. FBs are interspersed throughout the myocardium.[13] Cardiac FBs are elongated, contain one nucleus, and have high cellular activity as they have an intricate endoplasmic reticulum and a large Golgi apparatus. FBs are very dynamic in nature and can change phenotypes during injury states to become myofibroblasts. Myofibroblasts enhance the inflammatory response by secreting cytokines during injury. Cardiac injuries such as ischemia can initiate FB phenotypic changes and recruitment to the site of injury, leading to fibrosis[16]

Blood vessels within the heart supply the myocardium and resident cells with oxygen and nutrients. Due to its great energy demands, the myocardium is highly vascularized, with an average distance of 12um between capillaries.[17] They are comprised of FBs, SMCs, and ECs. ECs line the lumen or tunica intima of the vessel, forming a non-thrombogenic surface (**Figure 1.7**) SMCs form the tunica media, the layer surrounding the tunica intima, and FBs sheath the outermost layer of the vessel, the adventitia or tunica externa. These cells communicate with each other via physical contact and soluble or secreted molecules to regulate vessel maintenance, as well as tone and blood pressure.[18]

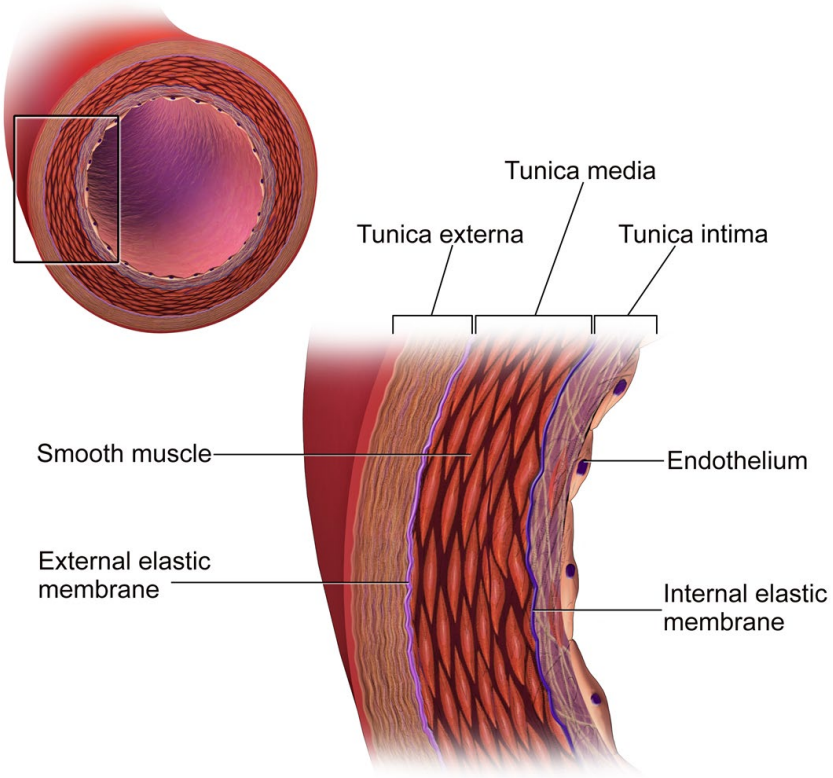


**Figure 1.7:** Structure of a blood vessel wall.

## 1.3 Cardiac Disease of the Myocardium

### *1.3.1 Coronary Artery Disease and Myocardial Infarction*

Coronary artery disease is characterized by atherosclerosis in one or both coronary arteries, which are the main vessels that supply the myocardium with oxygen and nutrients. This can lead to ischemia of the myocardium, myocardial infarction, and even sudden death.[3] As atherosclerotic plaque ruptures within the artery due to inflammatory mechanisms; a thrombus forms and occludes the vessel. Necrosis of the tissue supplied by this vessel quickly occurs, followed by inflammation. As mentioned before, FBs are very dynamic and during an injury state become myofibroblasts. After a MI, macrophages in the infarcted region secrete transforming growth factor-beta (TGF-β), which guides FBs to myofibroblasts. Myofibroblasts remodel the infarcted tissue by secreting collagen I and III, creating a fibrous patch.[19]

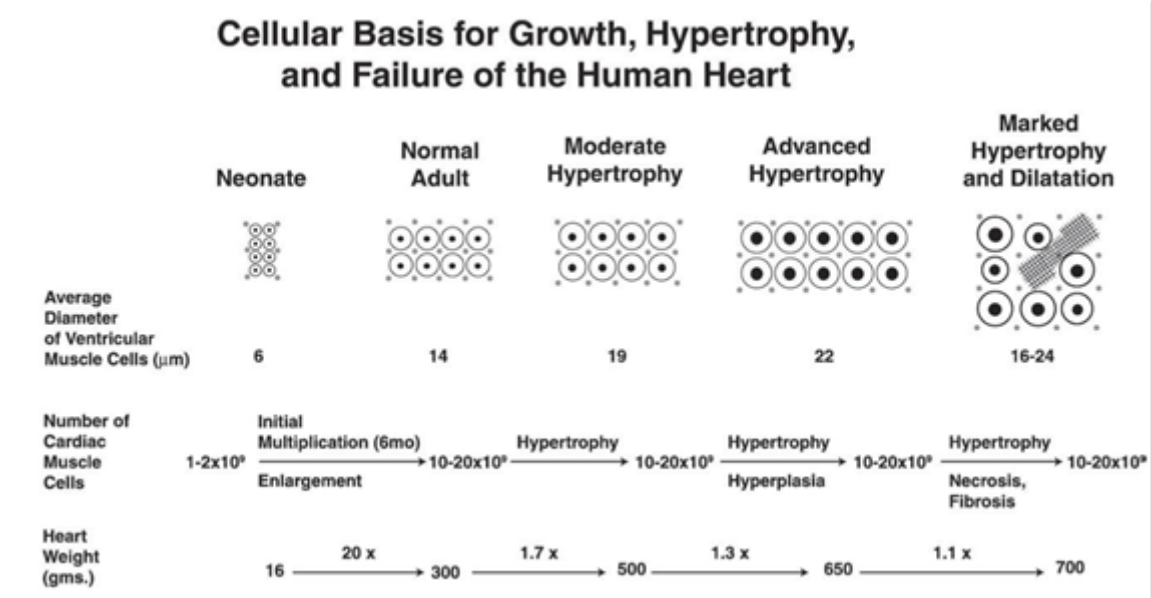


**FIGURE 1.8:** Illustration of ventricular CM hypertrophy compensation after MI and ischemia of the myocardium, leading to irreversible dilation followed by heart failure.[20]

After myofibroblasts remodel the infarct area, the overall mechanics of the heart are altered. CMs become hypertrophied to compensate for the lost CMs and maintain original cardiac output (**FIGURE 1.8**).[20] This compensation works short term, however over time CM hypertrophy and fibrosis of the ECM, lead to enlargement of the heart or dilation, and may end in heart failure.[21]

*1.3.2 Cardiomyopathies*

Cardiomyopathy is defined as a disease of the heart muscle, mainly of the left ventricle. It is marked by decreased systolic and/or diastolic function of the heart, which leads to heart failure. Main classifications of cardiomyopathy include; dilated, hypertrophic, and restrictive (**Figure 1.9**), and arrhythmogenic, without noticeable heart size or shape change.[22]

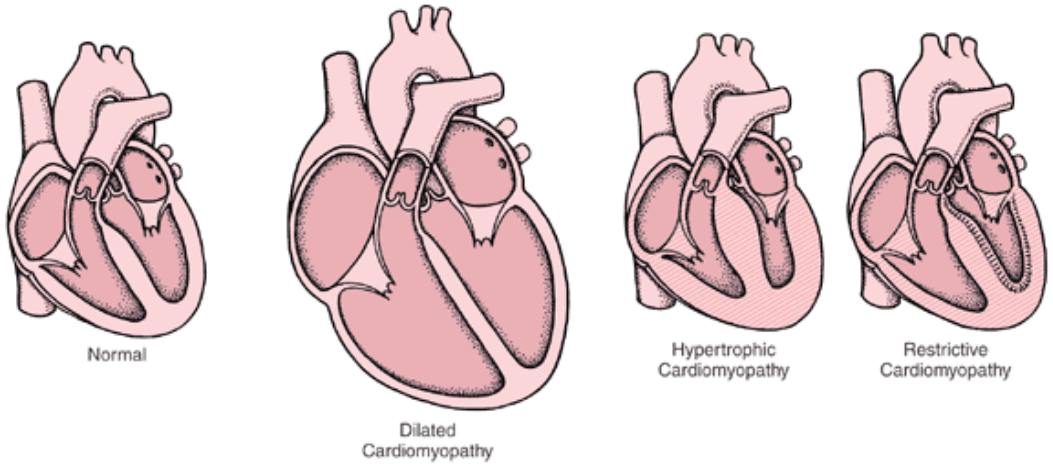


**Figure 1.9:** Gross morphological changes associated with dilated, hypertrophic, and restrictive cardiomyopathies. Dilated cardiomyopathy is marked by ballooning; hypertrophic by noticeably thickened walls; and restrictive by stiffened walls.[23]

**Dilated cardiomyopathy** is defined as ventricular chamber dilation and systolic dysfunction with normal ventricular thickness in the absence of abnormal loading conditions, such as hypertension.[24] It has an estimated prevalence of up to 1:250 and 30-50% of cases are genetic in nature.[25–28] Some cases are idiopathic and other causes include myocardial infections, systemic disorders, drugs and toxins, and endocrine and metabolic disorders.[29–31] Clinical presentations include cardiac arrhythmias, heart failure, and in some cases sudden death.[32] Hallmarks of this cardiomyopathy include an increase in ventricular mass, affecting mainly the left ventricle, a ballooning of the heart into a spherical shape, and floppy myocardium. There is loss of a proper apex leading to altered blood flow mechanics and a reduced ejection fraction, which can lead to mural thrombi.[30,33] At the microscopic level, interstitial and perivascular fibrosis is present in the myocardium and the endocardium.[32] CMs are the most affected, with myofibril loss and varying morphological changes. Many CMs undergo apoptosis which results in a mixture of hypertrophic CMs with enlarged nuclei and thin, lengthened CMs in the myocardium.[34]

**Hypertrophic cardiomyopathy** is defined as the presence of increased ventricular wall thickness or mass in the absence of any loading conditions sufficient to cause observed abnormality.[33] It has a prevalence of 1:500 worldwide.[35] The etiology is genetic, with sarcomeric hypertrophic cardiomyopathy being the most common, followed by mitochondrial disorders and metabolic or storage disease.[36,37] Genetic screening is important for diagnosis, as myocardial hypertrophy precedes symptoms and the disease can remain stable and under the radar.[38] Clinical presentations include left ventricular

dysfunction, heart failure, and sudden death.[39,40] In this form of cardiomyopathy, the myocardium is thick, ranging from mild, 13-15mm, to massive, 30mm.[33] Focal hypertrophy is found throughout the myocardium, mainly focused on the basal anterior septum and anterolateral free wall, which can lead in extreme cases to myocardial bridging. The mitral valve is often affected with enlarged leaflets, hypertrophied and abnormally positioned papillary muscles, and short chordae, which can lead to subaortic obstruction.[40] Microscopically in the myocardium there is an overall spatial disorganization of myofibers and single CMs, with replacement and interstitial fibrosis.[35,37] Morphologically, CMs have increased y-branching and side-to-side junctions, a whorled appearance, and herringbone pattern. CMs also have decreased distribution of desmin, intercalated disks, and z-bands.[33] Vascular cells are also affected, smooth muscle cells become hypertrophied and intimal thickening and perivascular fibrosis are present.[35]

**Restrictive cardiomyopathy** is defined as reduced diastolic relaxation of the left or both ventricles that can occur from many different pathologies. Diastolic filling is inhibited with an increase in ventricular filling pressure, while systolic function remains unchanged.[41,42] Causes are wide ranging and can be isolated or systemic in nature, as well as idiopathic. Amyloidosis, sarcoidosis, scleroderma, storage disease, toxicity, postirradiation therapy, and genetic mutations are some known causes.[42,43] Clinical presentations include diastolic dysfunction and heart failure. Biatrial enlargement occurs with unchanged atrial-ventricular valves and left ventricular wall thickness. Volume of the ventricles can remain unchanged or be decreased. Due to the ranging pathologies

leading to restrictive cardiomyopathy, macro and micro changes can vary, depending on the cause. For example, in sarcomeric restrictive cardiomyopathy, the atria are disproportionately dilated compared to normal ventricular size, while in amyloidosis, the atria are only mildly enlarged and the left ventricular wall can be affected in some cases.[41] Microscopically, interstitial fibrosis of myofibers and CMs are found in sarcomeric restrictive cardiomyopathy, while CMs in amyloidosis are atrophic. Amyloid deposits are the hallmark of amyloidosis and can be found histologically in the myocardium, endocardium, valves, arteries and veins.[33]

**Arrhythmogenic cardiomyopathy** is rare and defined as a genetic heart disease mainly affecting the right ventricle. It is a progressive myocardial injury where CMs are replaced by fibroadipose tissue.[44,45] Worldwide it is estimated to have prevalence up to 1:2000.[46] Mainly desmosomal proteins of intercalated disks are mutated, such as armadillo proteins plakiglobin (JUP) and desmocollin-2 (DSC2), however other proteins, such as TGF-β3 and desmin can be affected.[46,47] Clinical manifestations include ventricular arrhythmias, heart failure and an increase in sudden death, especially in juveniles and athletes.[44,48] With this cardiomyopathy there is no noticeable heart size or shape change. The external two-thirds of the right ventricle is normally effaced, and in some cases the left ventricle can be as well. The pulmonary infundibulum and outer right ventricle wall are the areas most affected.[33] In this disease, a mixture of atrophic and hypertrophic CMs with vacuolar degeneration are found in the myocardium, separated by interstitial fibrosis. CMs are lost and replaced by fibrous or fibroadipose tissue.[47] Lymphocytes and macrophages can also be found in the diseased myocardium.[33]

*1.3.3 Diagnosis and Treatments*

Coronary artery disease and cardiomyopathy are often diagnosed via symptoms or physical examination. They are verified through echocardiograms, electrocardiograms, cardiac angiograms, cardiac magnetic resonance imaging (MRI), cardiac positron emission tomography (PET), and occasionally an endomyocardial biopsy.[22] Symptoms include fatigue, weakness, shortness of breath, palpitations, light headedness, fainting, and chest pain. Treatments can include lifestyle changes such as diet and exercise and drugs, including but not limited to, blood thinners, angiotensin converting enzyme (ACE) inhibitors, diuretics, corticosteroids, aldosterone, angiotensin II, beta, or calcium channel blockers.[3] When a myocardial infarction occurs, speedy reperfusion is critical in limiting infarct size and percutaneous coronary intervention with balloon angioplasty with or without a stent is often utilized to reopen the occluded vessel. Coronary artery bypass is another treatment method to supply blood to the ischemic tissue.[21] Pacemakers, implanted cardioverter defibrillators, and left ventricular assist devices may be utilized depending on the severity.[3] Unfortunately, these treatments will only slow the progression of these diseases and they will ultimately lead to heart failure where the only treatment is whole heat transplantation.

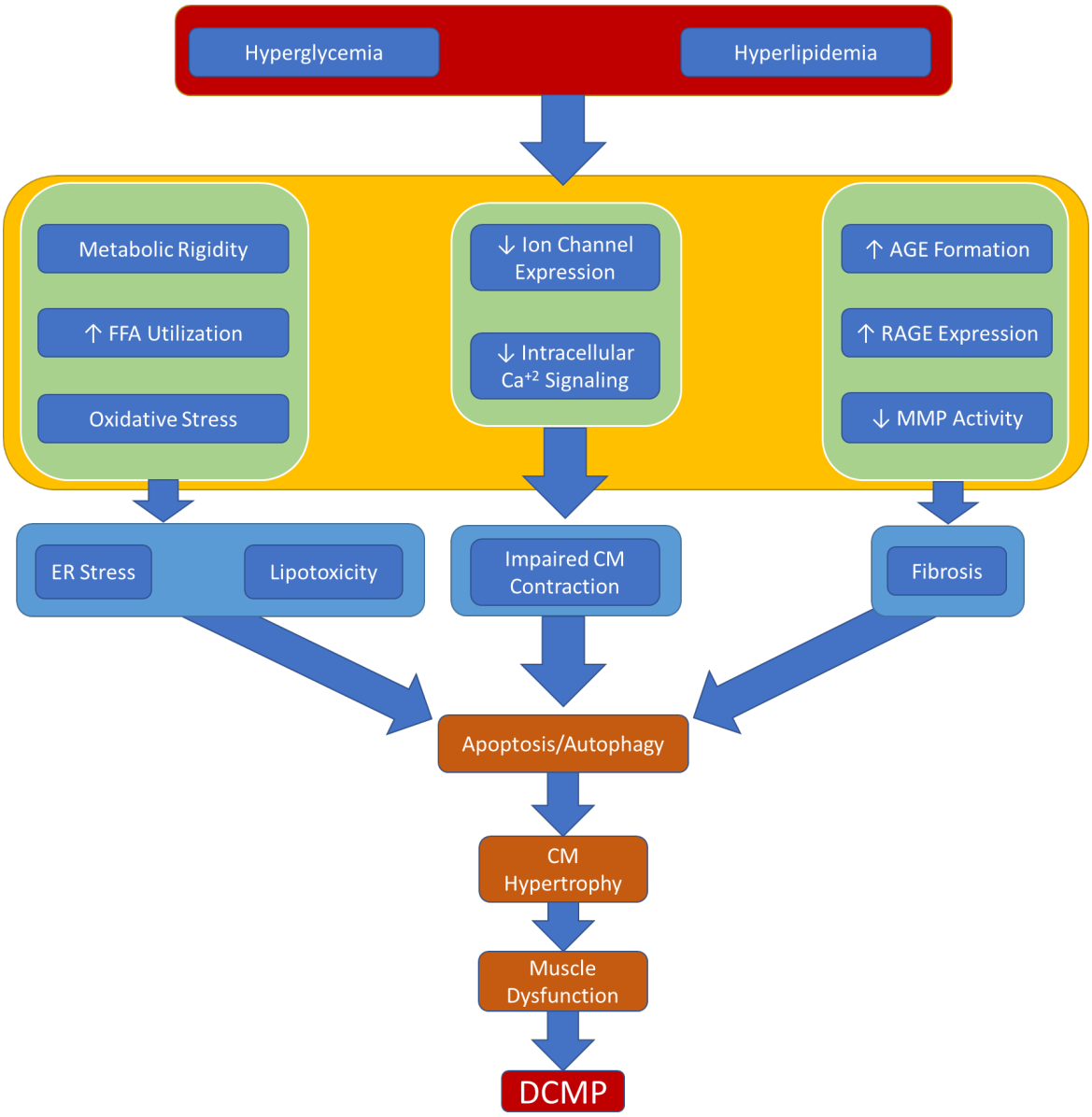


**Figure 1.10:** Diagram highlighting alterations in the myocardium caused by a diabetic environment that lead to DCMP.

## 1.4 Diabetic Cardiomyopathy

Diabetic cardiomyopathy (DCMP) is defined as a ventricular dysfunction that occurs in diabetic patients independent of coronary artery disease, hypertension, or valvular abnormalities.[49,50] Metabolic alterations caused by high glucose and dyslipidemia contribute to the onset and progression of DCMP (**Figure 1.10**). Within the ventricle, especially the left, fibrosis and microvascular disease changes the normal structure and function of myocardium. Normal cellular function is changed by a metabolism shift, leading to lipid peroxidation and the buildup of reactive oxygen species (ROS), which cause apoptosis and autophagy.[50] Diabetic patients have higher instances of coronary artery disease, as well as hypertension and atherosclerosis, due to this hyperglycemic and hyperlipidemic milieu.[3]

### *1.4.1 Diabetes Mellitus*

Normally, the body regulates blood glucose levels via a feedback loop to either release insulin or glucagon, to maintain homeostasis. During high glucose levels, islet of Langerhans beta cells in the pancreas (**Figure 1.11**) release insulin (**Figure 1.12**). Insulin binds to tyrosine kinase insulin receptors on target cells, inserting glucose transporters (GLUT4) on the cell surface for glucose transport (**Figure 1.13**). The liver then converts excess glucose to glycogen for storage and other cells begin to take up glucose via GLUT4. During low glucose levels, islet alpha cells release glucagon, which signals the liver to convert glycogen to glucose and release it into the blood (**Figure 1.14**). However, this homeostasis is disrupted with the metabolic disease diabetes, leading to not only prolonged hyperglycemia, but also a plethora of health issues.[51]

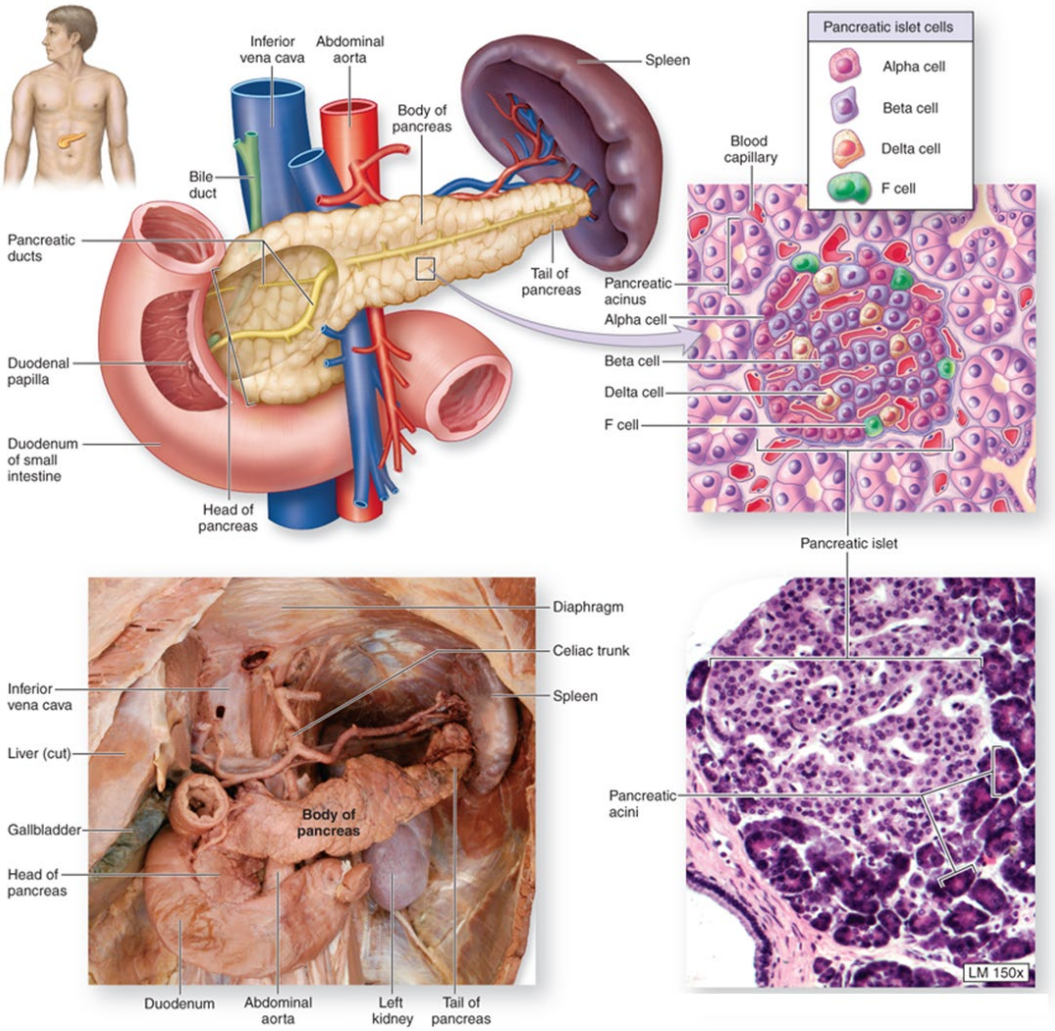


**Figure 1.11:** Anatomy of the pancreas and islet cells.[7]

There are two main types of diabetes. Type 1 diabetes is known as insulin dependent diabetes or juvenile onset diabetes. It is characterized by destruction of beta cells in the pancreas. This can occur due to an autoimmune disorder triggered by genetic or environmental factors. Some cases of type 1 diabetes are idiopathic. Type 2 diabetes is known as insulin resistant diabetes and is characterized by a decrease insulin secretion and synthesis. Type 2 diabetes is the most prevalent, accounting for 90% of diabetes.

This is due to the rise in the epidemic of obesity, especially in developing countries. Distribution of abdominal fat in obese type 2 diabetic patients, leads to alterations in cell receptors accompanied by resistance to endogenous insulin.[51,52]

Treatment of both types focus on control of blood glucose, as mismanagement of blood glucose levels by the patient lead to health problems, such as cardiovascular disease, and in extreme mismanagement cases, death.[3] Type 1 diabetes is treated with insulin therapy, accompanied by close monitoring of blood glucose levels with glucometers to determine insulin dosage, either through a pump or syringe. Blood glucose is also monitored in type 2 diabetes, however due to the nature of this type, lifestyle changes, such as healthy eating habits and exercise can be used to treat and even reverse this type.[53] Unlike type 1 diabetes, there is a wide spectrum associated with this type. When lifestyle changes are not enough, oral drugs such as metformin, sulfonylureas, thiazolindinediones (TZD), glucagon-like peptide 1 (GLP-1), and dipeptidyl peptidase inhibitors (DPP-4) may be used, and in extreme cases, insulin. Metformin increases insulin sensitivity and glucose uptake, while decreasing glucose gut absorption and hepatic gluconeogenesis. Sulfonylureas raise insulin release in beta cells. TZDs are peroxisome proliferator-activated receptor gamma agonists that improve insulin sensitivity, lipid profile, and blood glucose control. GLP-1 activates GLP-1 receptors, which boosts glucose-dependent insulin secretion and decreases glucagon secretion. DPP-4 or gliptins raise incretin levels (GLP-1), which has the same outcome as GLP-1 treatments.[54]

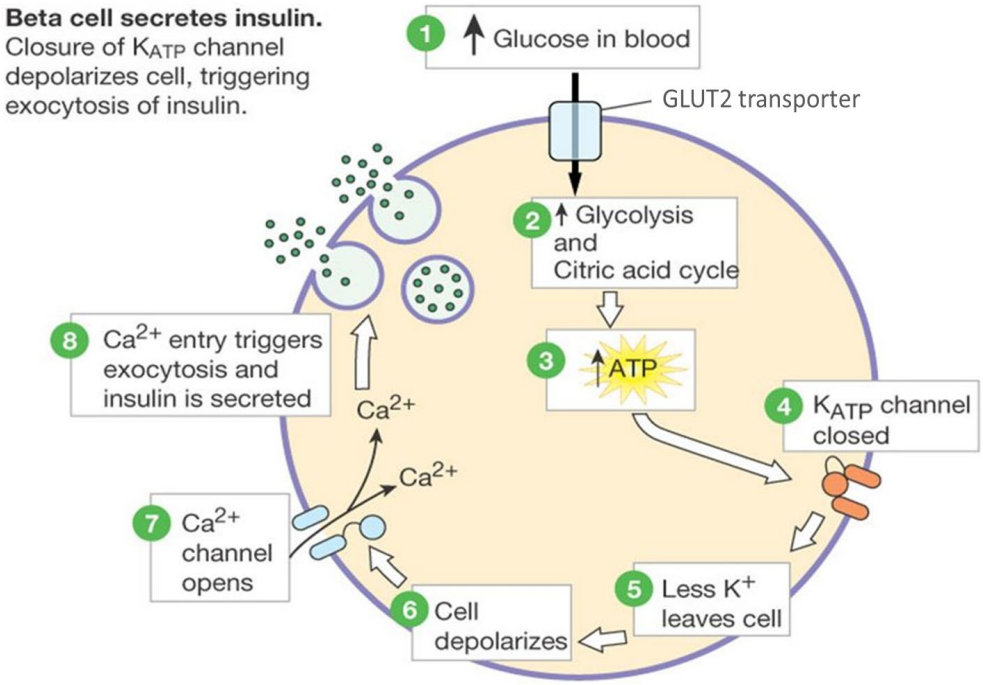


**Figure 1.12:** Glucose regulation of insulin secretion in pancreatic beta cells.[55]

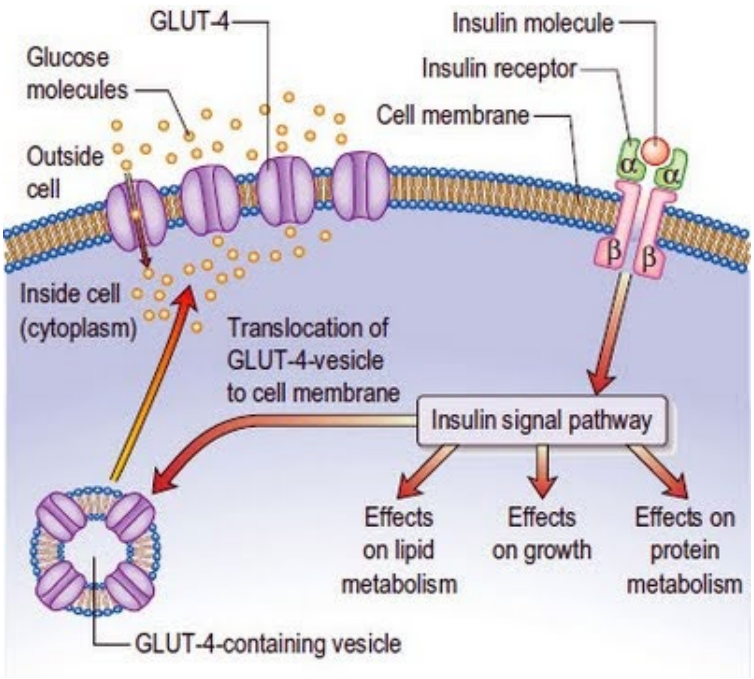


**Figure 1.13:** Translocation of GLUT4 to the target cell's membrane via tyrosine kinase insulin receptor binding to insulin for cellular glucose uptake.[55]

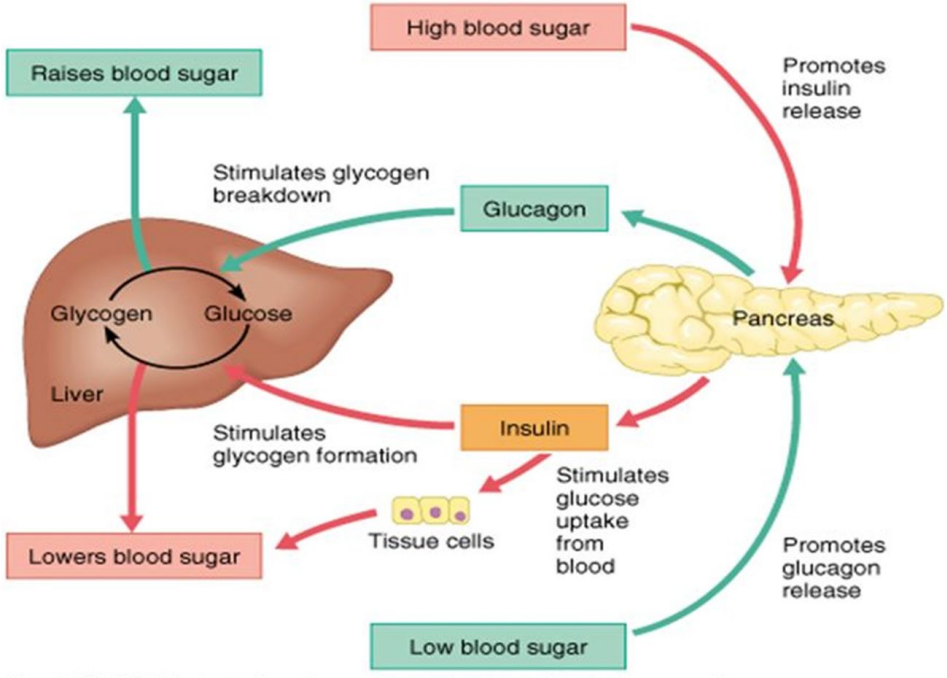


**Figure 1.14:** Blood glucose homeostasis.[56]

*1.4.2 Clinical Diagnosis and Treatment of Diabetic Cardiomyopathy*

Diagnosis of DCMP is the same as any cardiomyopathy described earlier, and as of now is unable to be diagnosed in asymptomatic patients.[57] Currently the only serological biomarker that can be used is brain natriuretic peptide, however it is a marker associated with several cardiac diseases.[58] Studies are ongoing to determine biomarkers, specifically microRNAs, that could be useful for DCMP diagnosis.[59,60]

Once patients are diagnosed with DCMP, emphasis is placed on glucose control and cardiomyopathy treatments are prescribed based on the individual.[61] For glucose control, type 1 diabetic patients continue with insulin therapy, while extra precautions are taken with management prescriptions for type 2 diabetics.[62] Sulfonylureas are often not prescribed as they may not function, due to heart failure being an insulin resistant state.[3]

TZDs increase fluid retention, so they are cautioned for use with class I and II heart failure and not recommended for use with class III and IV heart failure by the New York Heart Association (**Table 1.1**).[58] DCMP can be treated with, but not limited to, lifestyle changes, ACE inhibitors, angiotensin receptor blockers, direct renin inhibitors, beta blockers, calcium channel blockers and diuretics.[63,64] Depending on the severity and the symptoms, combinations of these can be used.[65] Calcium channel blockers are not recommended for heart failure patients with type 1 diabetes.[3] As the DCMP worsens, depending on the progression and individual, devices such as implantable cardioverter defibrillators, cardiac resynchronization devices, left ventricular assist devices, and even whole heart transplants may be employed. However, surgeries are risky, and one of the many criteria is that the patient have established glycemic control.[3] Unfortunately, there is no cure for DCMP, like other cardiomyopathies.

| New York Heart Association Classifications of Heart Failure | |
|---|---|
| Class I | Cardiac disease, but no symptoms and no limitations in normal physical activity |
| Class II | Mild symptoms and slight limitation during ordinary activity |
| Class III | Significant limitation in activity due to symptoms- comfortable only at rest |
| Class IV | Severe limitations- symptoms even while at rest |

**Table 1.1:** Classifications of heart failure from the New York Heart Association.[66]

Understanding of the progression of DCMP can be broken down into three stages. Molecular and cellular events from hyperglycemia and dyslipidemia cause structural alterations that lead to myocardial dysfunction and heart failure (**Table 1.2**).[3,65] However, this is a general understanding of the occurrence of this disease and as new knowledge of DCMP is brought to light, the progression and alterations may not be this rigid. Clinical findings hint at the possibility of two phenotypes associated with either type 1 diabetes or

type 2 diabetes, which are dilated cardiomyopathy with reduced left ventricular ejection fraction and restrictive cardiomyopathy with preserved left ventricular ejection fraction, respectively.[67]

| Stages | Molecular and Cellular Events | Alterations in Structure and Morphology | Myocardial Performance |
|---|---|---|---|
| Early | Metabolic disturbances: hyperglycemia, increased circulating free fatty acids, insulin resistance | Normal left ventricular dimensions, wall thickness, and mass | Impaired diastolic compliance with normal systolic function, or no obvious functional changes |
| | Altered calcium homeostasis | | |
| | Endothelial dysfunction | | |
| Middle | Cardiomyocyte injury, apoptosis, necrosis | Minor changes in structure: slightly increased heart mass, wall thickness, and/or ventricular dimensions | Significant changes in diastolic and systolic function |
| | Activation of cardiac fibroblasts leading to myocardial fibrosis | Cardiomyocyte hypertrophy | |
| | | Insignificant myocardial vascular changes | |
| Late | Hypertension | Significant changes in structure: increased heart size, wall thickness, and mass | Abnormal diastolic and systolic function |
| | Coronary artery disease | | |
| | Microangiopathy | | |
| | Cardiac autonomic neuropathy | Myocardial microvascular disease | |

**Table 1.2:** General progression of DCMP highlighted by three stages.[3]

*1.4.3 Metabolic Shift in Diabetes*

As mentioned before, left ventricular CMs have very high-energy demands. Within the human body, the heart utilizes the largest amount of energy per gram of tissue, roughly 20 times its own weight per day.[68] Approximately 70 percent ATP produced in the resting heart is due to FFA oxidation.[68] Uptake of FFAs into the CM is mediated via three transporters; cluster of differentiation 36 (CD36), fatty acid transport protein 1, and plasma membrane form of fatty acid binding protein. CD36 is stored in intracellular vacuoles (~50%) where it can be recruited to the sarcolemma membrane for the uptake of FFA under conditions such as muscle contraction, and stimulation by insulin and caffeine.[68] Physiologically, there is flexibility in the heart, allowing for shifts in the utilization of glucose and free fatty acids (FFA). Nutrients increase myocardial insulin

signaling and plasma insulin levels within the body. This leads to translocation of GLUT4 and CD36 to the CM sarcolemma, for glucose and FFA uptake, respectively, in order to supply myocardial energy substrates.[57]

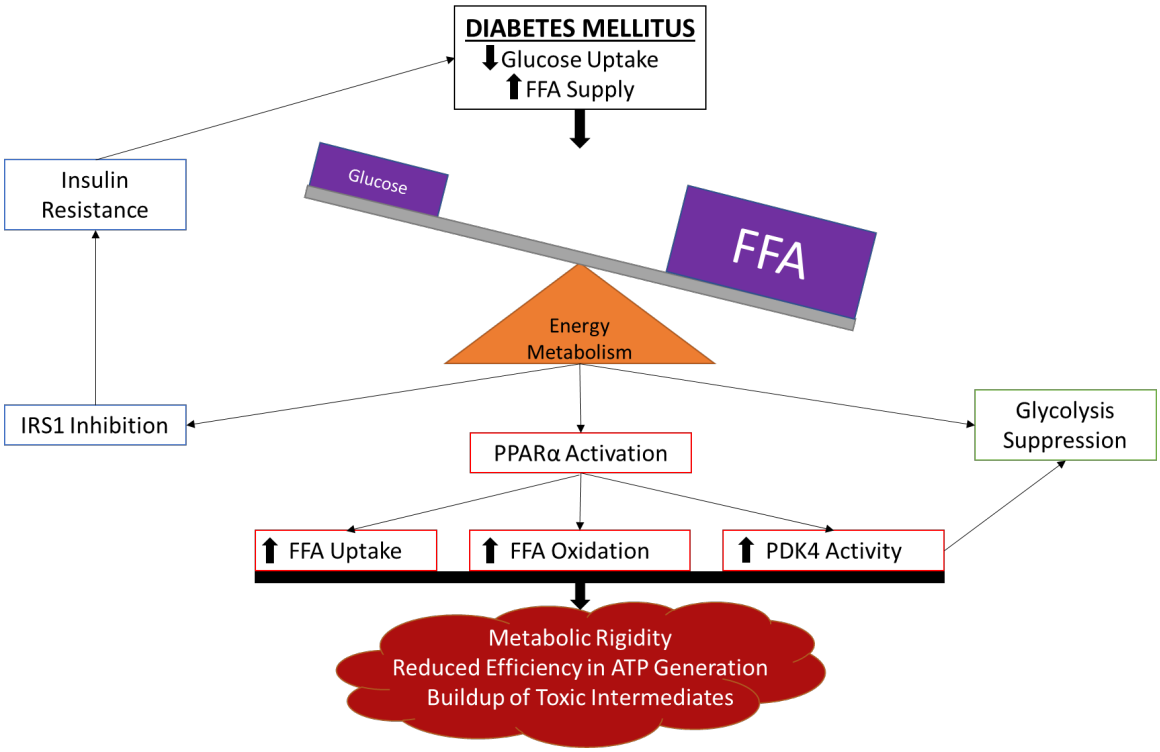


**Figure 1.15:** Pathophysiology of diabetes mellitus on energy metabolism in the heart.[68]

In the diabetic heart, this plasticity is lost, due to increased FFA in the circulation and depletion of GLUT4 (**Figure 1.15**).[69] High FFA levels activate transcription factor peroxisome proliferator-activated receptor alpha (PPARα) in the CM nucleus, leading to increased myocardial FFA oxidation and utilization via upregulation of CD36 expression, thus upregulating mitochondrial fatty acid beta-oxidation.[70] Insulin signaling is suppressed as insulin receptor substrate 1 (IRS1) is inhibited from accumulation of FFA and their derivatives.[68] CD36 is highly expressed on the sarcolemma, while GLUT4 returns to its intracellular location.[71] In this unbalanced environment, mitochondrial

oxidation capacity is exceeded and mitochondrial fission is increased, resulting in mitochondrial fragmentation with an accumulation of ROS, which can lead to apoptosis.[72,73] Increased circulating FFA also lead to inhibition of pyruvate dehydrogenase through pyruvate dehydrogenase kinase 4 (PDK4), impairing glycolysis and causing the buildup of glycolytic intermediates and intracellular lipids, such as ceramides.[74] This lipid accumulation decreases contractile function, hinders physiological autophagy, and impairs insulin signaling, leading to increased apoptosis within the myocardium.[58] These metabolic alterations ultimately lead to ROS production, lipotoxicity, CM death and hypertrophy, altered calcium handling and myocardial fibrosis.[57]

*1.4.4 Oxidative Stress*

Within the healthy cardiovascular system, a balance exists between ROS production and their removal by antioxidants.[75] Production of ROS is a naturally occurring process within the body and sources of ROS arise from non-enzymatic, enzymatic, and mitochondrial reactions.[76] Non-enzymatic formation of ROS occurs via autoxidation of glucose as well as a reaction between protein and glucose (**Figure 1.19**).[64,77] Sources of enzymatic formation of ROS are nitric oxide synthase (NOS), nicotinamide adenine dinucleotide phosphate (NADPH) oxidase, and xanthine oxidase.[64] The mitochondrial respiratory chain also provides a source of ROS, during oxidation phosphorylation.[78] In the physiological state, ROS play an important role in cell signaling, biosynthesis, and is an anti-infectious defense and a balance exists between ROS formation and antioxidant defense mechanisms.[79] Enzymatic and non-enzymatic

defense mechanisms in the body eliminate ROS. Enzymatic mechanisms such as superoxide dismutase (SOD) and glutathione reductase are important in removal of ROS.[80] Non-enzymatic antioxidants include glutathione, coenzyme $Q_{10}$, and vitamins A, E, and C.[76] This balance is important, as elevated ROS leads to oxidative stress, a harmful state which can alter cellular function and lead to cell death.[49]

As mentioned before, the loss of metabolic plasticity in the diabetic heart leads to increased FFA oxidation in CM mitochondria followed by ROS accumulation. Due to high energy demands of CM, it is theorized that the mitochondria are responsible for the majority of ROS production in this diseased state.[81] This influx of ROS supersedes endogenous antioxidant defense mechanisms, leading to oxidative stress.[82] Constant oxidative stress degenerates proteins, deoxyribonucleic acid (DNA), and lipids within the cells (**Figure 1.16**) causing cellular dysfunction that leads to apoptosis and autophagy.[83]

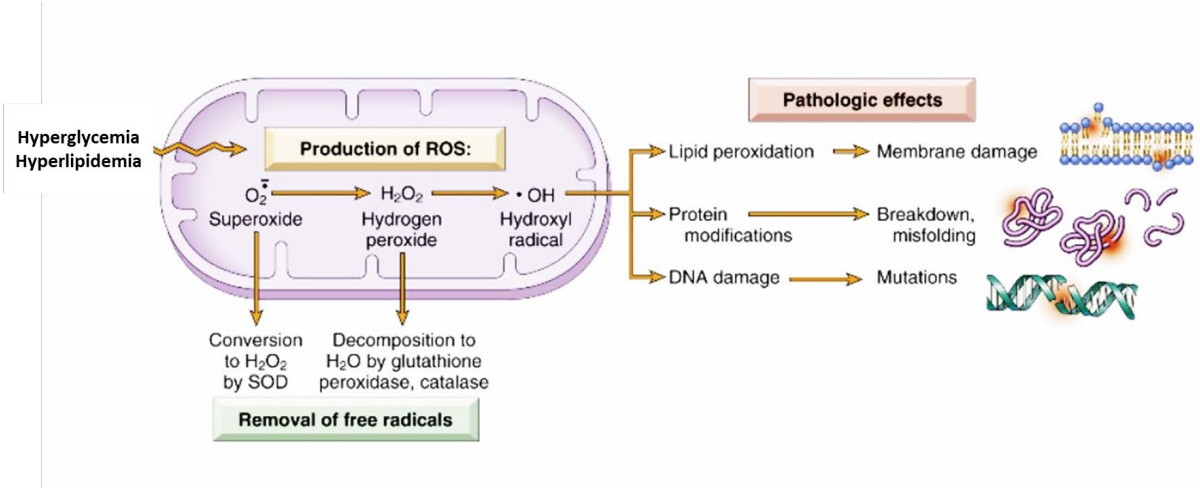


**Figure 1.16:** Schematic of pathologic outcomes of mitochondrial ROS production and prolonged oxidative stress due to hyperglycemia and hyperlipidemia.[84]

*1.4.5 Impaired Cardiomyocyte Contraction*

Intracellular calcium in the CM is responsible for excitation-contraction coupling during cellular contraction at the micro-scale and myocardial compression at the macro-level.[85] Calcium enters the cell through L-type calcium ion channels ($I_{Ca\text{-}L}$), which activates calcium release from endoplasmic reticulum and sarcoplasmic reticulum via ryanodine receptors (RyRs), leading to increases of calcium that binds to troponin C, activating contraction. Relaxation of CMs occurs through the release of calcium from troponin C, followed by calcium uptake via sarcoplasmic/endoplasmic reticulum $Ca^{+2}$-ATPase (SERCA), $Na^{+2}/Ca^{+2}$ exchanger (NCX), sarcolemmal $Ca^{+2}$-ATPase, and mitochondrial $Ca^{+2}$ ATP uniport.[86]

In the diabetic environment, dysfunctional intracellular calcium signaling and lower expressions of ion channels, SERCA, NCX, RyRs, and decreased myofilament calcium sensitivity in CMs lead to an imbalance in calcium homeostasis (**Figure 1.17**).[87] Hyperglycemia upregulates protein kinase C (PKC) and downregulates protein kinase A (PKA), which causes depression of outward potassium currents ($I_{to}$) and $I_{Ca\text{-}L}$ and L-type calcium channel expression.[88] High glucose also increases phosphorylated phospholamban (PLB) which reduces activity of SERCA and decreases overall SERCA and NCX expression.[89] Calcium homeostasis is furthermore upset with the dysfunction of RyR due to hyperphosphorylation, causing leakage of calcium during diastole and depletion of sarcoplasmic reticulum calcium stores.[74] Sensitivity of myofibrils to calcium are compromised with phosphorylation of troponin I and T from increased PKC activation, which leads to slower cross-bridge cycling.[90] AGEs produced in high glucose

conditions irreversibly bind between calcium handling proteins, such as SERCA and RyR, leading to their inactivation.[91] Myosin switches from the alpha to beta isoform in diabetes slows actin-myosin kinetics and depresses myosin and myofibrillar ATPase activity.[92] N2B to N2BA titin ratios shift towards N2BA, a more elastic isoform, and titin becomes hyperphosphorylated, causing contraction dysfunction.[92] Overall, these alterations in calcium handling are detrimental to cardiac efficiency and are obvious in slowed CM contraction and relaxation, prolonged action potential duration, and reduced shuttling of intracellular calcium.[87]

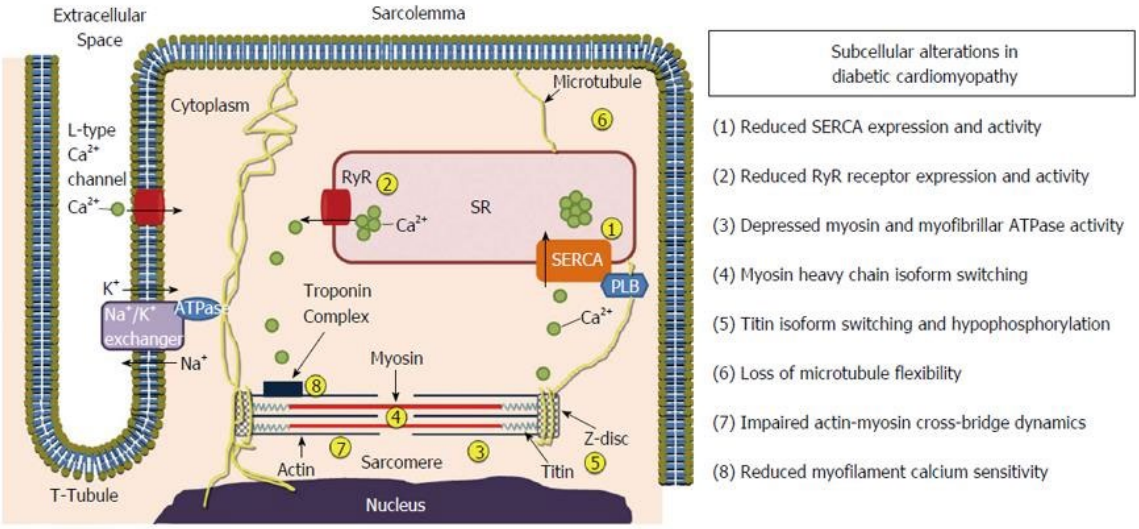


**FIGURE 1.17:** Alterations within the cardiomyocyte in diabetic cardiomyopathy that cause contraction dysfunction and reduced cardiac efficiency.[92]

*1.4.6 Endoplasmic Reticulum Stress*

The endoplasmic reticulum (ER), comprised of rough and smooth regions, is the main site for synthesis and processing of proteins and lipids in the secretory pathway. Within the closed ER lumen, newly polypeptide chains synthesize, fold and mature.[7]

These posttranslational modifications and folding interactions optimize protein function before correctly folded proteins are exported to the Golgi apparatus and transported to intracellular organelles or extracellular membrane. The ER also is a storage site for calcium.[93] Accumulation of unfolded or misfolded protein within the lumen of the ER induces ER stress. This mechanism of action is triggered to restore homeostasis and can lead to the unfolded protein response (UPR).[94] Conditions such as radiation, hypoxia, ischemia, oxidation, dysregulation of calcium, altered metabolism, or DNA mutations lead to ER stress.[95]

Increased circulated FFAs and hyperglycemia cause a metabolic shift, accumulation of ROS, and issues of calcium handling within the CM.[96] These in turn lead to ER stress and the UPR to control protein quality. There are three main pathways that are utilized during the UPR; inositol-requiring enzyme 1 (IRE1), protein kinase RNA-like ER kinsase (PERK), and activating transcription factor 6 (ATF6) pathways (**Figure 1.18**).[97] In the unstressed state, these sensors are bound to binding protein (BiP) and remain inactive.[98] When misfolded proteins are present in the ER lumen, BiP unbinds from IRE1, PERK, and ATF6, allowing it to attach to misfolded proteins to serve as a chaperone.[99] Misfolded proteins have exposed hydrophobic regions, which BiP readily binds to.[97] Once IRE1 is activated, it becomes phosphorylated by PKA and splices X-box binding protein 1 (XPB1) messenger RNA, yielding transcription factor XBP1s for expression of UPR target genes, upregulation of ER chaperones, and exportation and degradation of misfolded proteins.[100] IRE1 also activates Jun N terminal kinase (JNK) which can lead to apoptosis and autophagy.[101] After unbinding of BiP, PERK

phosphorylation of eukaryotic translation initiation factor 2 alpha (eIF2α) reduces protein translation, while increasing activating transcription factor 4 (ATF4), which induces transcription of CCAAT/-enhancer-binding protein homologous protein (CHOP). ATF4 and CHOP upregulate genes involved in protein synthesis and ER associated degradation (ERAD).[93] PERK also phosphorylates nuclear factor (erythroid-derived 2)-related factor2 (Nrf2), which turns on genes that combat oxidative stress.[102] In the ATF6 signaling pathway, unbinding of BiP frees ATF6 from the ER and is translocated to the Golgi apparatus, where it is cleaved by resident proteases.[97] This cleaved cytoplasmic domain activates genes involved in lipid biosynthesis, protein folding, ER expansion, and ERAD.[103] Under prolonged ER stress, these pathways lead to autophagy and apoptosis.[96]

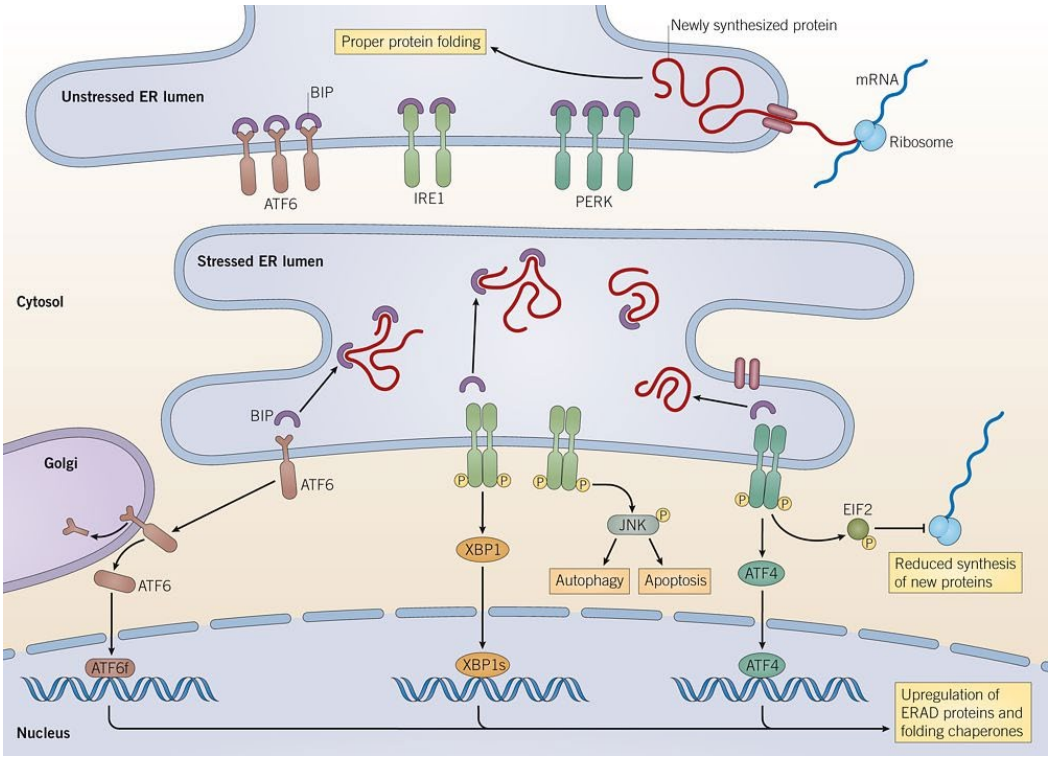


**Figure 1.18:** Illustration of ER stress and the UPR, leading to the activation of the ATF6, IRE1, and PERK pathways in response.[101,104]

*1.4.7 Extracellular Matrix Changes*

During hyperglycemia, an influx of glucose leads to the formation of advanced glycation end-products (AGEs), form irreversible cross-links within lipids and proteins, such as collagen, laminin, and elastin, and cause fibrosis.[105] This cross-link is formed by the Maillard reaction via a Schiff base and Amadori product (**Figure 1.19**). Matrix metalloproteinases are unable to degrade these irreversible ECM modifications, causing an imbalance in physiological ECM turnover.[106] AGE formation can induce cardiac FB proliferation and elevated collagen production.[107] Accumulation of AGEs lead to vascular disease, as when it binds to a receptor for AGEs (RAGE), it increases endothelial permeability to macromolecules.[108] Oxidative stress upregulates RAGE expression, which in turn causes increased NADPH oxidase expression, mitochondrial oxidase activation, and suppresses endogenous antioxidant activity.[109] This establishes a positive feedback loop between ROS formation and RAGE expresssion.[106]

Inhibition of matrix metalloproteinase (MMP) activity, macro and microvascular disease, and altered AGE and RAGE expression lead to myocardial thickening and fibrosis (**Figure 1.20**).[111,112] Fibrosis causes the myocardium to stiffen and vascular disease decreases nutrient transport within the myocardium, inducing cell death in this vicious cycle.[50] As CMs undergo apoptosis and autophagy, the ventricle must continue to pump at the same rate, so the surviving CMs must compensate for ones that have died off. To do so CMs enlarge and become hypertrophied.[113] As they are continually overstressed mechanically and as more CMs continue to die in the toxic diabetic environment, the myocardium function gradually declines, ending in heart failure.

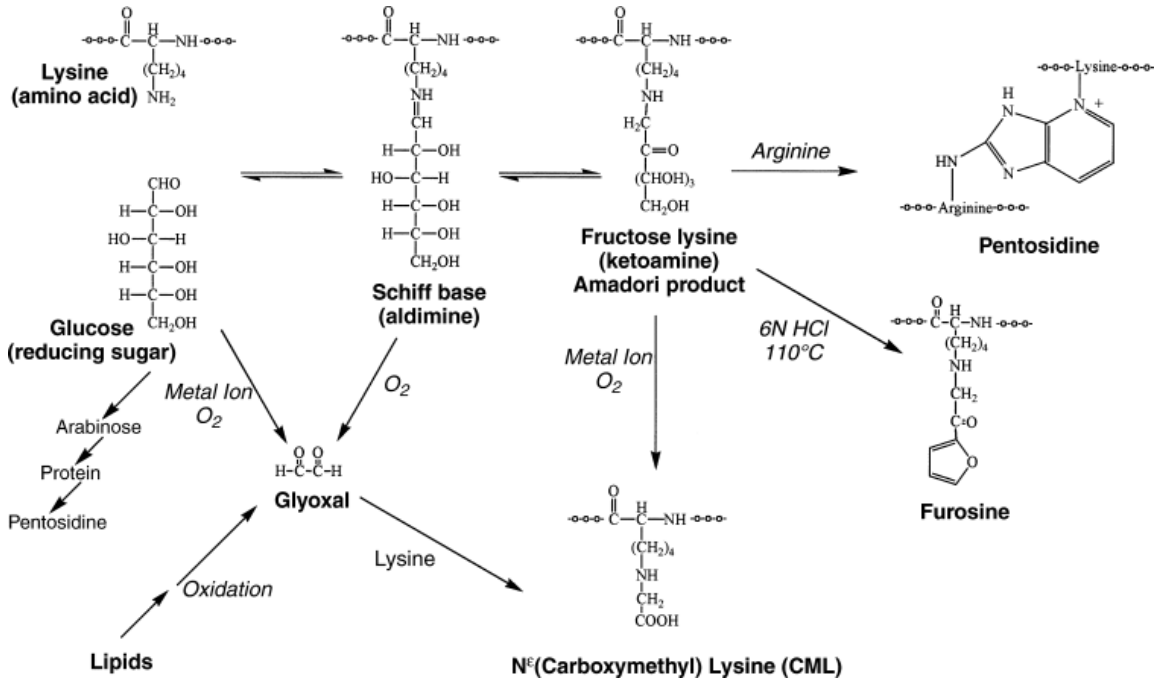


**Figure 1.19:** Mechanism for AGE formation via glycoxidation.[110]

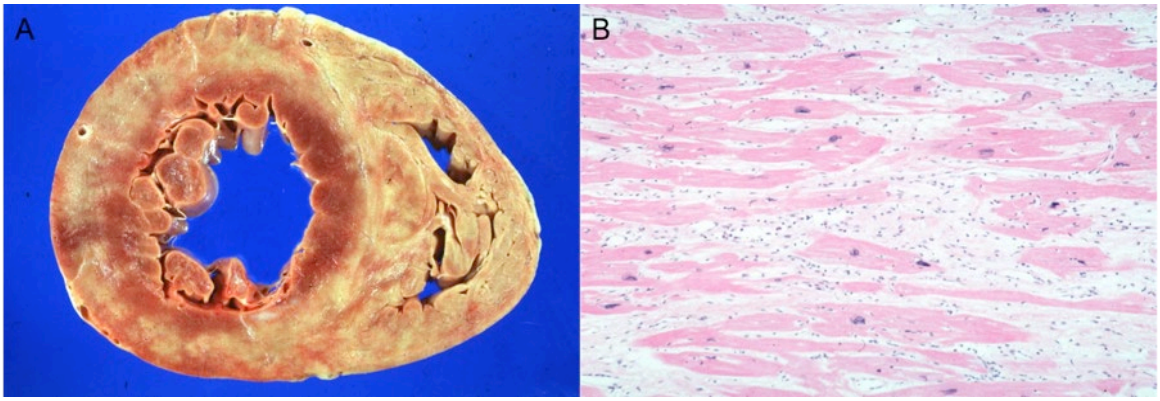


**Figure 1.20:** Autopsy of a heart with DCMP. (A) Gross anatomy showing hypertrophy of the left ventricle. (B) Hematoxylin and eosin staining showing fibrosis and cardiomyocyte hypertrophy within the left ventricle.[113]

*1.4.8 Potential Antioxidant Therapies*

Researchers have started focusing on antioxidant therapies to combat elevated ROS in within the diabetic environment.[114,115] One method of interest is increasing intracellular SOD content. This is a favorable countermeasure; however, SOD isoforms are very large, making them difficult to permeate the cells, and they have a very short half-life. **Mito-TEMPO** ((2-(2,2,6,6-tetramethylpiperidin-1-oxyl-4-ylamino)-2-oxoethyl) triphenylphosphonium chloride) is a mimetic form of SOD, that is more stable and smaller, allowing it to overcome these barriers (**Figure 1.21**).[116] Ni et al. tested mito-TEMPO in type 1 diabetes streptozotocin (STZ) and type 2 diabetes db/db mouse models. They found in both animal models that daily injections of mito-TEMPO for 30 days inhibited mitochondrial ROS generation, prevented intracellular oxidative stress levels, decreased apoptosis, and reduced myocardial hypertrophy in diabetic hearts.[78]

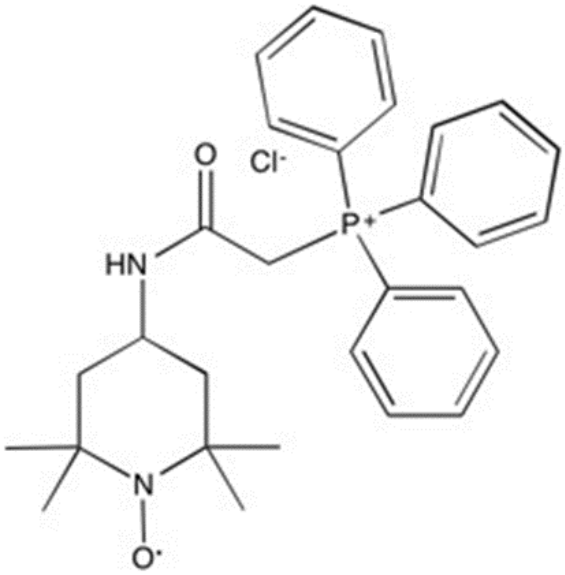


**Figure 1.21:** Structure of mito-TEMPO.[117]

**Rutin** is another appealing antioxidant. It is a citrus flavonoid found in a variety of plants (**Figure 1.22**).[118] Bhandary et al. investigated a series of flavonoids in a study to determine if all or any would have a protective effect on ischemic/reperfused rat hearts. To test different concentrations of flavonoids, harvested rat hearts, subjected them to ischemia, reperfused them, and then perfused treatments through them. They found that rutin enhanced SOD activity and had consistent protective effects in ischemic/reperfusion injury.[80] In other studies performed by Saklani et al. and Wang et al. on STZ induced type 1 diabetic rats, rutin treatments significantly protected hearts against diabetic oxidative stress, improved electrocardiography parameters, apoptosis, and inflammation in the diabetic hearts.[118,119]

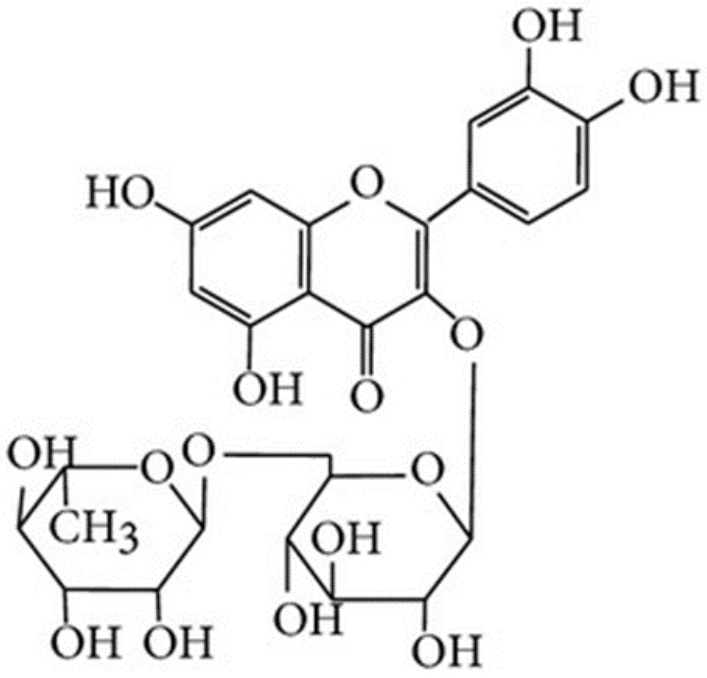


**Figure 1.22:** Structure of Rutin.[120]

**Coenzyme-Q10** is an antioxidant that is endogenously synthesized and is a lipophilic cofactor of the mitochondrial electron transport chain (**Figure 1.23**). It is available as a non-prescription oral dietary supplement and has been shown to be beneficial when used with other therapies for chronic heart failure.[121] Blasio et al. studied the effect of coenzyme-Q10 on an exacerbated diabetic cardiomyopathy mouse model with reduced phosphoinositide 3-kinase (PI3K) signaling, which upregulates NADPH oxidase. 6-week-old dominant negative PI3K p110α mice were treated with STZ and after 4 weeks were treated with coenzyme-Q10. Within this aggravated model, coenzyme Q10 reduced left ventricular diastolic dysfunction, CM fibrosis and hypertrophy, expression of atrial natriuretic peptide, connective tissue growth factor, and β-myosin heavy chain.[77]

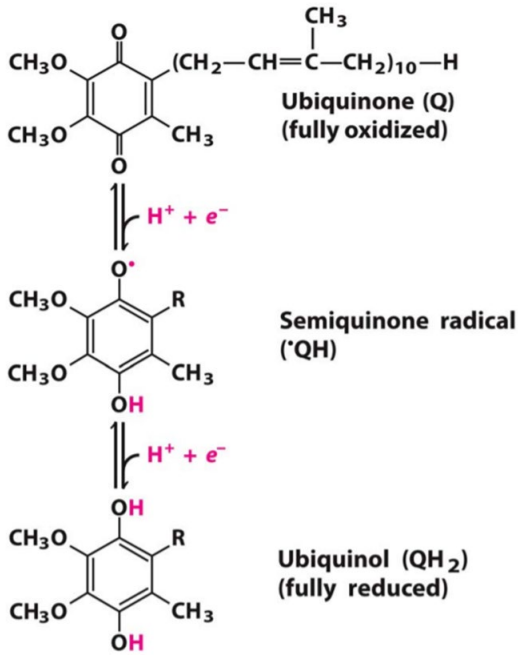


**Figure 1.23:** Reduction of ubiquinone (coenzyme-Q10) to ubiquinol through semiquinone intermediate.[122]

There has also been a shift towards naturally occurring plant-based antioxidants, such as curcumin, garlic, and broccoli.[123] Turmeric powder, with the active polyphenol **curcumin** (**Figure 1.24**), has been used as a spice for cooking and medicinal purposes in Asia for thousands of years.[124] Yu et al. treated type 1 diabetic induced STZ rats with oral administrations of curcumin and found that it attenuated myocardial dysfunction, cardiac fibrosis, AGE accumulation, oxidative stress, apoptosis, and inflammation in the diabetic rat hearts.[125] Sahebkar et al. performed a meta-analysis of eight randomized controlled clinical trials and found curcumin treatments significantly reduced pro-inflammatory cytokine tumor necrosis factor alpha (TNFα).[126]

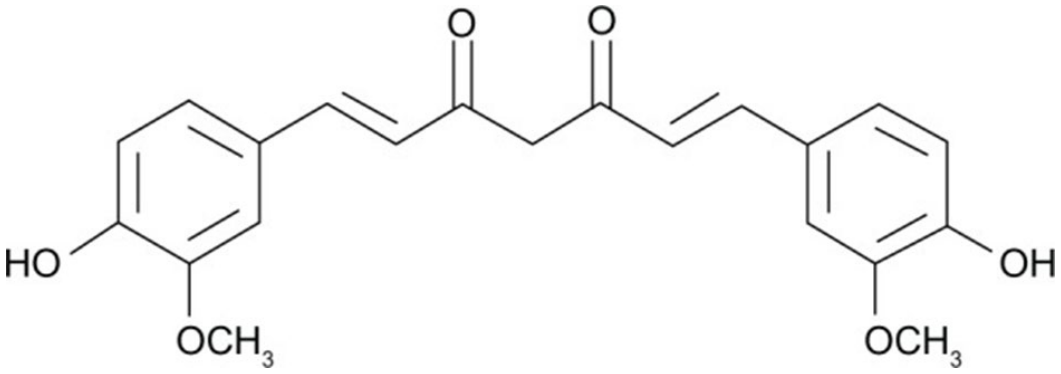


**Figure 1.24:** Structure of curcumin.[127]

There are many ongoing investigations of other potential antioxidants not only for treatment of cardiac disease in diabetes, but also cardiovascular diseases in general, cancer, arthritis, autoimmune disorders, phycological diseases, neurological issues, etc.[114] Many of these antioxidants are on the market in non-prescription supplemental forms, however additional research into dosage and effect, as well as monitoring of production need to be performed. Antioxidants target sources of many diseases, making it a promising therapeutic avenue.

## 1.5 Cardiac Tissue Engineering

Tissue-engineered models have been used to address discrepancies between animals and humans to investigate diseased states. These organotypic models aim to replicate specific architecture and relevant physiological function of the tissue for analysis.[128] This is useful for studying disease progression, as well as drug screening and treatment testing. Myocardial tissue engineering combines cells, scaffolds, and cues to create a structure and network similar to the native tissue. Many groups are looking to the promise of tissue-engineered myocardium, not only for the study of normal and diseased myocardium, but also for the hope of creating functional myocardium as a treatment for heart disease.[129] This overlap has led to the rise of different approaches to develop tissue-engineered myocardium that have the crossover potential to be used for modeling and diseased tissue replacement.

### *1.5.1 Cardiac Scaffolds*

Scaffolds for cardiac tissue engineering are utilized to provide an environment comparable to native myocardial ECM for cells to attach and align, interact with each other, transmit load, and conduct electric signals. The scaffold must also be able to be remodeled by the cells (i.e.- biodegradable) and have similar mechanical properties to withstand physiological cyclic strains and stresses.[130] It should be biocompatible and have porosity that promotes vascularization and diffusion of oxygen and nutrients to support the seeded cells.[131]

Biomaterials utilized for cardiac scaffolds include, synthetic, natural, and combination. Several natural materials employed include collagen, fibrin, hyaluronic

acid, Matrigel, and preparations of native heart matrix. Some synthetic materials applied include polyesters such as poly(lactic acid) and poly(glycolic acid), poly(lactones), polyurethanes, and polysebasic acid.[130] Combinations of synthetic and natural materials such as poly(e-caprolactone) and gelatin or collagen have also been used.[132] Scaffolds can further be categorized by method of fabrication such as hydrogel, prefabricated matrices, decellularized tissue, and cell sheets. Advantages and disadvantages that should be taken into consideration when deciding on a method to use (**Table 1.3**).[131]

| Scaffold | Source | Advantages | Disadvantages |
|---|---|---|---|
| Hydrogels | Natural, Synthetic and Mixed | In-situ injection of cells | Fragile, prone to breakage |
| | | Lessened immune response | |
| Prefabricated | Natural, Synthetic and Mixed | Easy to engineer and manipulate 3D forms | Optimal porosity needs to be maintained |
| | | | Exact ECM structure difficult to create |
| Decellularized | Natural | Vascularization | Difficulties reseeding |
| | | Immune response eliminated | |
| | | Native ECM protiens retained | |
| Cell Sheets | Natural | Easy to scale up in 3D form | Fragile and difficult to handle |
| | | Easy to manipulate | Limited thickness |

**Table 1.3:** Types of scaffold fabrication methods with materials that can be used and some advantages and disadvantages of each.[131]

**Hydrogels** are produced by crosslinking water-soluble polymers. They can be made from natural or synthetic materials or combinations. Cells can integrate and grow in the scaffold.[131] To increase cell anchoring and integration, growth factors and peptides, such as arginylglycylaspartic acid (RGD) for cell adhesion. Hydrogels are favorable vehicles for cardiac cell and/or growth factor in-situ injection, as it can increase delivery efficiency via protective encapsulation and catheters can be used for transport, eliminating the need for invasive surgery and use of drugs or anesthesia.[131] Encapsulation by hydrogels can also alleviate immunogenic responses post implantation. For cardiac applications, this scaffold type is limited by its ability to withstand physiological forces

seen in the heart.[133] Wang et al. injected crosslinker tetraaniline-polyethylene glycol diacrylate and thiolated hyaluronic acid, along with adipose derived stem cells and plasmid DNA encoding endothelial nitric oxide synthases (eNOs) nanocomplexes into the myocardium of rat infarct models. In rats there was an increase in ejection fraction, shortened QRS interval, smaller infarction size, less fibrosis, and higher vessel density within the hearts.[134] Tang et al. injected human cardiac stem cells in thermosensitive poly(N-isopropylacrylamineco-acrylic acid) nanogel into mouse and pig myocardial infarction models. In mice and pigs treated with cells and hydrogels, cardiac function was preserved and scar size was decreased.[135]

**Prefabricated matrices** are useful for cardiac tissue engineering, as mechanical properties, behavior, porosity, size, and degradability are tailorable.[131] These scaffolds can be made from natural, synthetic, or combination materials. Pores of these scaffolds can be tailored by methods such as, porogen leaching, freeze drying, phase separation, and electro-spinning. Difficulties can arise in using preformed matrices, as it is difficult to exactly recapitulate ECM and overall organ structure with this method.[131] Gu et al. fabricated cardiac patches with electro spun elastomeric polyester urethane urea and polyester ether urethane urea with incorporated recombinant adeno-associated virus-green fluorescent protein (GFP) labelled- to test addition and release of viral vectors in infarcted rat models. GFP was expressed even after 12 weeks and mechanical support provided by the scaffold improved remodeling and provided support to the compromised infarct tissue.[136] Tsui et al. constructed cardiac scaffolds from electroconductive-acid modified silk fibroin-poly(pyrrole) substrates patterned with nanoscale ridges and

topography similar to native ECM. Human induced pluripotent stem cell (iPSC) cardiomyocytes were cultured on this material for 21 days and showed increased cellular organization and sarcomere development, with increased connexin-43 expression.[137]

**Tissue decellularization** (decell) is a method that uses the organ itself to provide the 3D structure of interest through detergent washes to remove cells and cellular material, leaving the ECM and vasculature intact. Decelling is a favorable method, as immunogenic material is removed and native ECM, such as collagen, elastin, and laminin, is retained, allowing for patient specific cells to be integrated into the native scaffold to create an individually tailored tissue.[138] One obstacle to overcome with this scaffold is homogenous cell seeding. Perea-Gil et al. tested decellularized porcine myocardium and human pericardium that were reseeded with or without porcine adipose mesenchymal stem cells in porcine myocardial infarct models. Both scaffolds with or without cells restored function of myocardium post infarction and integrated with the underlying tissue via neovascularization.[139] Decell is based on the idea that nature is the best engineer. Recently, other vascularized things in nature, such as plants, have been researched. Gershlak et al. decellularized spinach and parsley leaves and roots were performed and seeded with human cells. Human iPSC cardiomyocytes seeded showed contractile function and calcium handling capabilities over the course of 21 days.[140]

**Cell sheets** are considered a scaffold free approach and are employed to overcome the obstacle of low cell concentrations and inflammatory reactions of scaffolds. They are fabricated by culturing cells on poly-N-isopropylacrylamide, a temperature sensitive polymer, until they are confluent.[141] At 37 degrees Celsius, the cell culture

dishes are hydrophobic and cell adhesive. The monolayer of cells can be detached from the polymer at 32 degrees Celsius, leaving the ECM and proteins intact. These fragile sheets can then be layered to a maximum thickness of 80um to form tissue.[131] Shudo et al. implanted a bilayered cell sheet of rat endothelial progenitor cells (EPCs) and rat mesenchymal stem cells differentiated into smooth muscle cells (SMCs) into a rat model of ischemic cardiomyopathy. Rats treated with the EPC-SMC cell sheet had increased mature vessel density, decreased cardiac fibrosis, increased left ventricular ejection fraction, and decreased left ventricular dimensions.[142] Sakaguchi et al. fabricated 10um thick cell sheets with neonatal rat CMs at 30 degrees Celsius in order to slow metabolism and allow for myocardial tissue formation and prevascularization. Lower temperature cultured cell sheets were implanted under the skin of nude rats and developed denser prevascular networks compared to cell sheets cultured in normal conditions, showing promise for cardiac applications.[143]

*1.5.2 Cardiac Cell Sources*

To develop functional myocardium for cardiac tissue engineering applications, there are several cell sources for consideration. Some sources are acceptable for implantation, while others are only suitable for disease modeling and screening for individual patient therapies. Allogenic sources include CMs, embryonic stem cells (ESCs), cardiac progenitor cells (CPCs), and cardiac stem cells (CSCs). Autologous sources include adipose derived stem cells (ADSCs), skeletal myoblasts, bone marrow derived stem cells (BMDSCs), and iPSCs (**FIGURE 1.25**).[131] Allogenic sources have been investigated, however complications arise with activation of the immune response.

CPCs and CSCs are difficult to source, as they are estimated to make up 1% of total cells in the heart. It is also problematic acquiring CMs from healthy hearts, as they will be used for whole organ transplantation.[132] There are ethical concerns with ESCs and when transplanted in vivo, tumors can form and they may induce arrhythmias.[144]

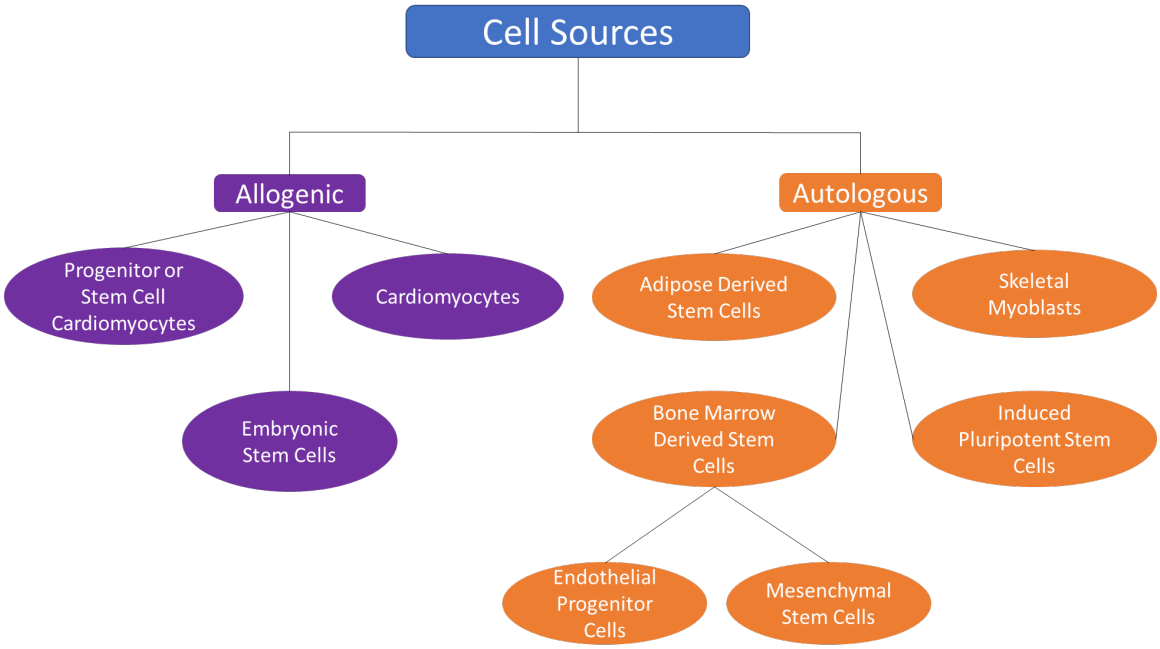


**FIGURE 1.25:** Diagram of potential allogenic and autologous cell sources for cardiac tissue engineering.[131]

Autologous skeletal myoblasts have been investigated for transplantation treatments of diseased myocardium, as they are easy to isolate, resistant to ischemia and fatigue. However, with skeletal myoblast transplantation there is an increased risk of arrhythmias as they fail to structurally integrate into the myocardium and beat independently of neighboring CMs.[144] BMDSCs are another potential source from which mesenchymal stem cells (MSCs) and EPCs can be isolated from. MSCs are easy to isolate, can differentiate into CM-like cells in vivo and in vitro, however they have a low

differentiation efficiency.[145] They have been shown to improve left ventricular ejection fractions in animal myocardial infarction models when directly injected into infarct or when administered intravenously.[146] EPCs have been shown to increase neovascularization and cardiac function in infarct models, though low numbers limit their use.[147] iPSCs can be derived from adult cells, however this is a long, costly process, with low efficiency of 0.01-0.1 percent.[132] Problems arise with the use of iPSCs in vivo, as there are concerns with tumor formation and iPSCs differentiated into CMs from patients with cardiomyopathy have been shown to retain diseased phenotypes.[148] ADSCs are easy to isolate and are widely available within the body. In preclinical studies, they have been shown to decrease infarct size and survival. In the PRECISE trial in Europe ADSC treated patients with ischemic cardiomyopathy had a reduction in inducible ischemia and improvement in peak oxygen consumption at 18 months.[149]

*1.5.3 Cardiac Bioreactors*

Merging scaffolds and cells with a bioreactor, certain conditions can be met to produce a more physiologically relevant environment to precondition myocardial-like tissue prior to implantation or create models for the study of disease states. Preconditioning increases cell functionality, as well as guides cells towards myocardial cell lineages such as CMs.[150] Physiological myocardial environment recapitulation in a bioreactor requires addition of elements such as, perfusion, electrical stimuli, and mechanical loading, which can be added to necessary controlled conditions such as pH, temperature, and nutrients.[129,151] If the thickness of the myocardial-like tissue is greater than ~150um, perfusion is necessary for oxygen diffusion.[17]

It has been established that electrical stimulation affects cell alignment, differentiation, metabolic activity, protein synthesis, connexin 43 expression, conduction velocity, calcium handling, and force generation.[150] Physiological electrical properties such as rectangular shape and 2ms duration at 5V/cm and 1Hz are successful in inducing these changes.[152] Radisic et al. cultured neonatal rat CMs on collagen sponges and subjected them to an electrical stimulus (2 ms, 5 V/cm, 1 Hz), comparable to native myocardium for 5 days utilizing carbon rods. Cells were aligned and coupled; intercalated discs, gap junctions, myofibrils, and T-tubules formed; and important proteins such as troponin I, α-actinin, connexin 43, α- and β-myosin heavy chain increased.[153]

Mechanical strain is also important for CM alignment and maturation. Zimmerman et al. mechanically loaded (cyclic stretch at 10%, 2 Hz) neonatal rat CMs seeded on collagen I scaffolds for 7 days and found that CMs more closely resembled adult myocardial tissue when compared to 6-day old native neonatal rat myocardium. They observed morphological changes such as a basement membrane, well developed T-tubules, cell alignment along the construct and increases in myofilaments, sarcomeric organization, gap junctions, desmosomes, adherens junctions.[154]

Electrical and mechanical stimuli combined improve CM functional properties over electrical or mechanical stimulation alone. Morgan and Black subjected neonatal rat CMs in fibrin gel on latex tubing to electrical (rectangular pulse, 1ms, 3V/cm, 1Hz) and mechanical (5% stretch, 50% duty cycle, 1Hz) stimulation in an electromechanical bioreactor they constructed (**Figure 1.26**) for 14 days. They found that combined

electromechanical stimuli enhanced myocardial-like tissue function by increasing expression of SERCA2a, troponin T, protein kinase B (Akt), proteins responsible for cell-cell communication and contractility.[155]

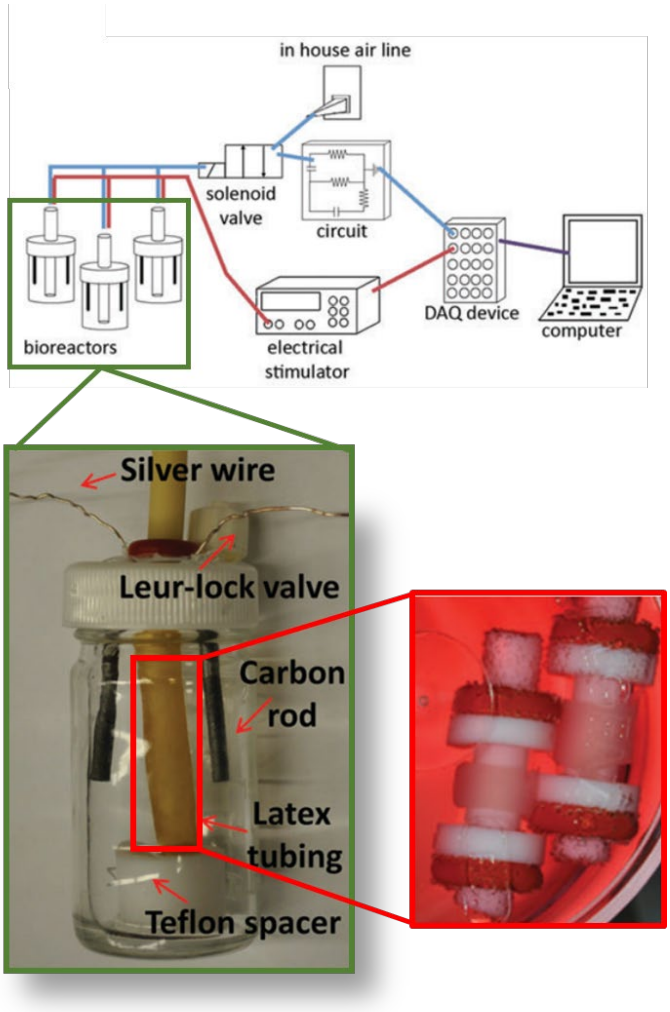


**Figure 1.26:** Electromechanical bioreactor produced in the Black Laboratory.[155]

*1.5.4 Current Diabetic In Vivo and In Vitro Cardiac Models*

Animal models are currently used to understand early cardiac alterations in diabetes and heart failure, while cadaveric hearts have been used to study end stages heart failure in diabetic patients. Animal models are useful, however there are many

physiological discrepancies between humans and animal models.[156] Rodent models, particularly rat and mouse, are the typical choice for diabetic cardiac research, as they are relatively inexpensive, easy to house and care for.[156] Mouse models are employed as they are easy to manipulate genetically.[74] Type 1 diabetic rodent models such as the streptozotocin (STZ) induced diabetes in rat or mouse model, OVE26 mouse, and Akita diabetic mouse are common for cardiac diabetes studies.[156] Standard type 2 diabetes models include the Zucker diabetic fatty rat (ZDF), db/db mouse, and ob/ob mouse.[6] While these models have been helpful in determining alterations that could be occurring in diabetic myocardium, and have been widely accepted, there are major discrepancies between humans and the rodent models. Rodents have a higher heart rate, differing electrophysiological properties of CMs, and varying circulating lipid concentrations when compared to humans.[6] One of the major discrepancies often overlooked for rodent models are differences in the immune response when compared to humans. Diabetes is a prolonged inflammatory disease.[65] Taking into consideration marked differences seen among host immune responses in human patients and rodent subcutaneous implants, there most assuredly are differences between rodent models and patients in this extended inflammatory disease.[157] Inconsistencies also exist in the progression of cardiac alterations in these diabetic rodent models and within the models themselves. Depending on the lineage of the rodent, genetic manipulation, and severity of obesity and diabetes, some models are more susceptible to changes and show a rapid progression of diabetes and heart failure.[6] For example, when comparing type 2 diabetic models, cardiac efficiency is markedly lower for db/db and ob/ob mice, but does not change for ZDF

rats.[158–160] In the Akita type 1 diabetic model it has been shown depending on the study that cardiac size can remain the same or increase.[161,162] Disparities may arise depending on the sex of the animal. Akita male mice are usually more favorable for diabetes research as female Akita mice have less pronounced hyperglycemia when compared to their male counterparts.[163]

In vitro models have been employed to study cardiac alterations in diabetes and changes that occur in specific cell types, however their models have either lacked a dynamic 3D environment with an ECM or utilized animal cells instead of human cells.[148,164] Song et al. statically cultured rat neonatal cardiomyocytes on collagen scaffolds in either low (1g/L) or high (4.5g/L) glucose with or without insulin (20μM) for 8 days. They saw poor electric properties and an increased ratio of myosin heavy chain isoform β to α in high glucose cultures.[164] Drawnel et al. cultured human iPSC derived cardiomyocytes, from two type 2 diabetic patients and a non-diabetic patient and subjected them for two days to either a manufacturer's maintenance medium without glucose or a "diabetic" medium with glucose (10mM), as well as endothelin-1 (10nM) and cortisol (1μM) to dull insulin sensitivity. iPSC-CMs from type 2 diabetic patients showed baseline cardiomyopathy (CM hypertrophy, loss of sarcomeric integrity) without being cultured in "diabetic" medium and normal iPSC-CMs cultured in "diabetic" medium showed baseline cardiomyopathy as well.[148]

**1.6 Conclusions**

The risk for cardiac disease is dramatically increased in diabetic patients. This is due to the diabetic environment, as hyperglycemia and dyslipidemia cause metabolic

disturbances that adversely affect myocardial cells and ECM. These modifications aggregate to alter overall myocardial structure and cardiac function, leading to DCMP. As of now there is no specific marker for this disease and diagnosis is the same as other cardiomyopathies. Elucidating early stages of this disease is vital for determining markers for early diagnosis, treatment, and possible therapy targets. As of now, animal models and 2D studies have been utilized to understand early changes associated with DCMP, however there are discrepancies with animal models and 2D studies fail to recapitulate the ECM and dynamic environment. Tissue engineering is vital in bridging this gap. By combining scaffolds, cells, and biochemical and physical stimuli, we can elucidate early alterations in DCMP, as well as test potential therapies for treatment.

### 1.7 Chapter 1 References


1. International Diabetes Federation. *Eighth edition 2017*. (2017).
2. Boudina, S. & Abel, E. D. Diabetic cardiomyopathy revisited. *Circulation* **115,** 3213–3223 (2007).
3. McGuire, D. K. & Marx, N. *Diabetes in Cardiovascular Disease: A Companion to Braunwald's Heart Disease*. (Saunders, 2015).
4. Jia, G., Hill, M. A. & Sowers, J. R. Diabetic cardiomyopathy: An update of mechanisms contributing to this clinical entity. *Circ. Res.* **122,** 624–638 (2018).
5. Wang, J., Song, Y., Wang, Q., Kralik, P. M. & Epstein, P. N. Causes and characteristics of diabetic cardiomyopathy. *Rev Diabet Stud* **3,** 108–117 (2006).
6. Bugger, H. & Abel, E. D. Rodent models of diabetic cardiomyopathy. *Dis Model Mech* **2,** 454–466 (2009).
7. McKinley, M. & O'Loughlin, V. D. *Human Anatomy*. *Human Anatomy* (The McGraw-Hill Companies, 2012).
8. Iaizzo, P. A. Handbook of cardiac anatomy, physiology, and devices, third edition. *Handb. Card. Anatomy, Physiol. Devices, Third Ed.* 1–817 (2015). doi:10.1007/978-3-319-19464-6
9. Zamilpa, R. & Lindsey, M. L. Extracellular matrix turnover and signaling during cardiac remodeling following MI: Causes and consequences. *J. Mol. Cell. Cardiol.* **48,** 558–563 (2010).
10. Wang, B. *et al.* Structural and biomechanical characterizations of porcine myocardial extracellular matrix. *J. Mater. Sci. Mater. Med.* **23,** 1835–1847 (2012).
11. Mouw, J. K., Ou, G. & Weaver, V. M. Extracellular matrix assembly: A multiscale

deconstruction. *Nat. Rev. Mol. Cell Biol.* **15,** 771–785 (2014).
12. Cui, N., Hu, M. & Khalil, R. A. *Biochemical and Biological Attributes of Matrix Metalloproteinases*. *Progress in Molecular Biology and Translational Science* **147,** (Elsevier Inc., 2017).
13. Camelliti, P., Borg, T. K. & Kohl, P. Structural and functional characterisation of cardiac fibroblasts. *Cardiovasc Res* **65,** 40–51 (2005).
14. Betts, J. G. *et al. Anatomy and Physiology*. (OpenStax, 2013).
15. Opie, L. H. *Heart Physiology: From Cell to Circulation*. (Lippincott Williams & Williams, 2004).
16. Baum, J. & Duffy, H. S. Fibroblasts and myofibroblasts: what are we talking about? *J. Cardiovasc. Pharmacol.* **57,** 376–9 (2011).
17. Mannhardt, I., Marsano, A. & Teuschl, A. Vascularization for Tissue Engineering and Regenerative Medicine. 1–14 (2017). doi:10.1007/978-3-319-21056-8
18. Lilly, B. We Have Contact: Endothelial Cell-Smooth Muscle Cell Interactions. *Physiology* **29,** 234–241 (2014).
19. Baum, J. & Duffy, H. S. Fibroblasts and myofibroblasts: what are we talking about? *J Cardiovasc Pharmacol* **57,** 376–379 (2011).
20. Buja, L. M. & Vela, D. Cardiomyocyte death and renewal in the normal and diseased heart. *Cardiovasc Pathol* **17,** 349–374 (2008).
21. Bonow, R. O., Mann, D. L., Zipes, D. P. & Libby, P. *Braunwald's Heart Disease*. *Braunwald's Heart Disease* (Saunders, 2011).
22. Sims, J. Cardiomyopathy. *The Gale Encyclopedia of Medicine* **2,** 856–859 (2011).
23. Darling, D. Cardiomyopathy. *Encyclopedia of Science* (2016).
24. Jefferies, J. L. & Towbin, J. A. Dilated cardiomyopathy. *Lancet* **375,** 752–762 (2010).
25. Herman, D. S. *et al.* Truncations of Titin Causing DilatedCardiomyopathy. *N. Engl. J. Med.* **366,** 9 (2012).
26. Hershberger, R. E., Hedges, D. J. & Morales, A. Dilated cardiomyopathy: the complexity of a diverse genetic architecture. (2013).
27. Lakdawala, N. K. *et al.* Familial dilated cardiomyopathy caused by an alpha-tropomyosin mutation: the distinctive natural history of sarcomeric dilated cardiomyopathy. *J Am Coll Cardiol* **55,** 320–329 (2010).
28. Burke, M. A. *et al.* Molecular profiling of dilated cardiomyopathy that progresses to heart failure. *JCI Insight* **6,** 18 (2016).
29. Norton, N. *et al.* Exome sequencing and genome-wide linkage analysis in 17 families illustrate the complex contribution of TTN truncating variants to dilated cardiomyopathy. *Circ. Cardiovasc. Genet.* **6,** 144–153 (2013).
30. Mcnally, E. M., Golbus, J. R. & Puckelwartz, M. J. Review series Genetic mutations and mechanisms in dilated cardiomyopathy. *J. Clin. Invest.* **123,** 19–26 (2013).
31. Haas, J. *et al.* Alterations in cardiac DNA methylation in human dilated cardiomyopathy. *EMBO Mol Med* **5,** 413–429 (2013).
32. Assomull, R. G. *et al.* Cardiovascular Magnetic Resonance, Fibrosis, and Prognosis in Dilated Cardiomyopathy. *J. Am. Coll. Cardiol.* **48,** 1977–1985

(2006).
33. d'Amati, G. & Giordano, C. in *Cardiovasc Pathol* 435–483 (Elsevier Inc, 2016). doi:10.1016/b978-0-12-420219-1.00011-2
34. Hong, B. K. *et al.* Apoptosis in Dilated Cardiomyopathy. **15,** (2000).
35. Coppini, R. *et al.* Late sodium current inhibition reverses electromechanical dysfunction in human hypertrophic cardiomyopathy. *Circulation* **127,** 575–584 (2013).
36. Lan, F. *et al.* Abnormal calcium handling properties underlie familial hypertrophic cardiomyopathy pathology in patient-specific induced pluripotent stem cells. *Cell Stem Cell* **12,** 101–113 (2013).
37. Ho, C. Y. *et al.* T1 measurements identify extracellular volume expansion in hypertrophic cardiomyopathy sarcomere mutation carriers with and without left ventricular hypertrophy. *Circ. Cardiovasc. Imaging* **6,** 415–422 (2013).
38. Bos, J. M. *et al.* Characterization of a Phenotype-Based Genetic Test Prediction Score for Unrelated Patients With Hypertrophic Cardiomyopathy. *Mayo Clin Proc* **89,** 10 (2014).
39. Maron, B. J. *et al.* Prevention of sudden cardiac death with implantable cardioverter-defibrillators in children and adolescents with hypertrophic cardiomyopathy. *J Am Coll Cardiol* **61,** 1527–1535 (2013).
40. Maron, B. J. & Maron, M. S. Hypertrophic cardiomyopathy. *Lancet* **381,** 242–255 (2013).
41. Gupta, A., Singh Gulati, G., Seth, S. & Sharma, S. Cardiac MRI in restrictive cardiomyopathy. *Clin Radiol* **67,** 95–105 (2012).
42. Brodehl, A. *et al.* Mutations in FLNC are Associated with Familial Restrictive Cardiomyopathy. *Hum. Mutat.* **37,** 269–279 (2016).
43. Huby, A. C. *et al.* Disturbance in Z-disk mechanosensitive proteins induced by a persistent mutant myopalladin causes familial restrictive cardiomyopathy. *J Am Coll Cardiol* **64,** 2765–2776 (2014).
44. Asimaki, A., Kl??ber, A. G., MacRae, C. A. & Saffitz, J. E. Arrhythmogenic cardiomyopathy - New insights into disease mechanisms and drug discovery. *Prog. Pediatr. Cardiol.* **37,** 3–7 (2014).
45. Kant, S., Holthöfer, B., Magin, T. M., Krusche, C. A. & Leube, R. E. Desmoglein 2–Dependent Arrhythmogenic Cardiomyopathy Is Caused by a Loss of Adhesive FunctionCLINICAL PERSPECTIVE. *Circ. Cardiovasc. Genet.* **8,** 553–563 (2015).
46. Basso, C., Bauce, B., Corrado, D. & Thiene, G. Pathophysiology of arrhythmogenic cardiomyopathy. *Nat Rev Cardiol* **9,** 223–233 (2012).
47. Lorenzon, A. *et al.* Homozygous Desmocollin-2 Mutations and Arrhythmogenic Cardiomyopathy. *Am J Cardiol* **116,** 1245–1251 (2015).
48. Naidoo, A., Naidoo, K., Yende-zuma, N. & Gengiah, T. N. The Hippo Pathway is ACtivated and is a Causal Mechanism for Adipogenesis in Arrhymogenic Cardiomyopathy. *Circ Res* **114,** 161–169 (2014).
49. Murarka, S. & Movahed, M. R. Diabetic cardiomyopathy. *J Card Fail* **16,** 971–979 (2010).

50. Maisch, B., Alter, P. & Pankuweit, S. Diabetic cardiomyopathy - Fact or fiction? *Herz* **36,** 102–115 (2011).
51. Kaul, K., Tarr, J. M., Ahmad, S., Kohner, E. M. & Chibber, R. Chapter 1 Introduction To Diabetes Mellitus. *Diabetes An Old Dis. a New Insight* 1–11 (2012). doi:10.1007/978-1-4614-5441-0
52. American Diabetes, A. Diagnosis and classification of diabetes mellitus. *Diabetes Care* **33 Suppl 1,** S62-9 (2010).
53. Long-term effects of lifestyle intervention or metformin on diabetes development and microvascular complications over 15-year follow-up: the Diabetes Prevention Program Outcomes Study. *Lancet Diabetes Endocrinol.* **3,** 866–875 (2015).
54. Kahn, S. E., Cooper, M. E. & Del Prato, S. Pathophysiology and treatment of type 2 diabetes: perspectives on the past, present, and future. *Lancet* **383,** 1068–1083 (2014).
55. Silverthorn, D. U. *Human Physiology: An Integrated Approach*. (Pearson/Benjamin Cummings, 2004).
56. Marieb, E. N. *Human Anatomy & Physiology*. (Benjamin Cummings, 2001).
57. Lee, W. S. & Kim, J. Diabetic cardiomyopathy: Where we are and where we are going. *Korean J. Intern. Med.* **32,** 404–421 (2017).
58. Asghar, O. *et al.* Diabetic cardiomyopathy. *Clin Sci* **116,** 741–760 (2009).
59. León, L. E. *et al.* Subclinical detection of diabetic cardiomyopathy with microRNAs : science fiction or science fact ? *J. Diabetes Res.* **2016,** (2016).
60. Guo, R. & Nair, S. Role of microRNA in diabetic cardiomyopathy: From mechanism to intervention. *Biochim. Biophys. Acta - Mol. Basis Dis.* **1863,** 2070–2077 (2017).
61. Falcão-Pires, I. *et al.* Distinct mechanisms for diastolic dysfunction in diabetes mellitus and chronic pressure-overload. *Basic Res. Cardiol.* **106,** 801–814 (2011).
62. Falcão-Pires, I. & Leite-Moreira, A. F. Diabetic cardiomyopathy: Understanding the molecular and cellular basis to progress in diagnosis and treatment. *Heart Fail. Rev.* **17,** 325–344 (2012).
63. Gilbert, R. E. & Krum, H. Heart failure in diabetes: effects of anti-hyperglycaemic drug therapy. *Lancet* **385,** 2107–2117 (2015).
64. Voulgari, C., Papadogiannis, D. & Tentolouris, N. Diabetic cardiomyopathy: from the pathophysiology of the cardiac myocytes to current diagnosis and management strategies. *Vasc Heal. Risk Manag* **6,** 883–903 (2010).
65. Fang, Z. Y., Prins, J. B. & Marwick, T. H. Diabetic cardiomyopathy: evidence, mechanisms, and therapeutic implications. *Endocr. Rev.* **25,** 543–567 (2004).
66. Braunschweig, F. *et al.* New York Heart Association functional class, QRS duration, and survival in heart failure with reduced ejection fraction: implications for cardiac resychronization therapy. *Eur. J. Heart Fail.* **19,** 366–376 (2017).
67. Seferović, P. M. & Paulus, W. J. Clinical diabetic cardiomyopathy: A two-faced disease with restrictive and dilated phenotypes. *Eur. Heart J.* **36,** 1718–1727 (2015).
68. Bayeva, M., Sawicki, K. T. & Ardehali, H. Taking diabetes to heart--deregulation of myocardial lipid metabolism in diabetic cardiomyopathy. *J Am Hear. Assoc* **2,**

e000433 (2013).
69. Feuvray, D. & Darmellah, A. Diabetes-related metabolic perturbations in cardiac myocyte. *Diabetes Metab.* **34,** 3–9 (2008).
70. Bayeva, M., Sawicki, K. T. & Ardehali, H. Taking diabetes to heart--deregulation of myocardial lipid metabolism in diabetic cardiomyopathy. *J. Am. Heart Assoc.* **2,** e000433 (2013).
71. Battiprolu, P. K. *et al.* Diabetic cardiomyopathy and metabolic remodeling of the heart. *Life Sci.* **92,** 609–615 (2013).
72. Galloway, C. A. & Yoon, Y. Mitochondrial dynamics in diabetic cardiomyopathy. *Antioxid Redox Signal* **22,** 1545–1562 (2015).
73. Kobayashi, S. & Liang, Q. Autophagy and mitophagy in diabetic cardiomyopathy. *Biochim. Biophys. Acta - Mol. Basis Dis.* **1852,** 252–261 (2015).
74. Bugger, H. & Abel, E. D. Molecular mechanisms of diabetic cardiomyopathy. *Diabetologia* **57,** 660–671 (2014).
75. Stratmann, B. & Tschoepe, D. The diabetic heart: sweet, fatty and stressed. *Expert Rev. Cardiovasc. Ther.* **9,** 1093–6 (2011).
76. Lombardi, R. *et al.* Resolution of established cardiac hypertrophy and fibrosis and prevention of systolic dysfunction in a transgenic rabbit model of human cardiomyopathy through thiol-sensitive mechanisms. *Circulation* **119,** 1398–1407 (2009).
77. Blasio, M. J. De *et al.* Free Radical Biology and Medicine Therapeutic targeting of oxidative stress with coenzyme Q 10 counteracts exaggerated diabetic cardiomyopathy in a mouse model of diabetes with diminished PI3K ( p110 α ) signaling. *Free Radic. Biol. Med.* **87,** 137–147 (2015).
78. Ni, R. *et al.* Free Radical Biology and Medicine Therapeutic inhibition of mitochondrial reactive oxygen species with mito-TEMPO reduces diabetic cardiomyopathy. **90,** 12–23 (2016).
79. Varvarovska, J. *et al. Impact of Oxidative Stress on Diabetes Mellitus and Inflammatory Bowel Diseases*. (Nova Science Publishers, Inc., 2008).
80. Bhandary, B. *et al.* The Protective Effect of Rutin against Ischemia / reperfusion-associated Hemodynamic Alteration through Antioxidant Activity. *Arch Pharm Res* **35,** 1091–1097 (2012).
81. Kayama, Y. *et al.* Diabetic cardiovascular disease induced by oxidative stress. *International Journal of Molecular Sciences* **16,** (2015).
82. Anderson, E. J. *et al.* Substrate-specific derangements in mitochondrial metabolism and redox balance in the atrium of the type 2 diabetic human heart. *J Am Coll Cardiol* **54,** 1891–1898 (2009).
83. Goldin, A., Beckman, J. A., Schmidt, A. M. & Creager, M. A. Advanced glycation end products: Sparking the development of diabetic vascular injury. *Circulation* **114,** 597–605 (2006).
84. Kumar, V., Abbas, A., Fausto, N. & Aster, J. *Robbins and Cotran Pathologic Basis of Disease*. (Elsevier, 2009).
85. Suarez, J. *et al.* Restoring mitochondrial calcium uniporter expression in diabetic mouse heart improves mitochondrial calcium handling and cardiac function. *J.*

*Biol. Chem.* **293,** 8182–8195 (2018).
86. Thapa, K. *et al.* Dysregulation of the calcium handling protein, CCDC47, is associated with diabetic cardiomyopathy. *Cell Biosci.* **8,** 45 (2018).
87. Lebeche, D., Davidoff, A. J. & Hajjar, R. J. Interplay between impaired calcium regulation and insulin signaling abnormalities in diabetic cardiomyopathy. *Nat. Clin. Pract. Cardiovasc. Med.* **5,** 715–724 (2008).
88. Tse, G., Lai, E. T. H., Tse, V. & Yeo, J. M. Molecular and Electrophysiological Mechanisms Underlying Cardiac Arrhythmogenesis in Diabetes Mellitus. *J. Diabetes Res.* **2016,** (2016).
89. Yokoe, S. *et al.* Inhibition of phospholamban phosphorylation by O-GlcNAcylation: Implications for diabetic cardiomyopathy. *Glycobiology* **20,** 1217–1226 (2010).
90. Jweied, E. E. *et al.* Depressed cardiac myofilament function in human diabetes mellitus. *Am. J. Physiol. Circ. Physiol.* **289,** H2478–H2483 (2005).
91. Cheng, Y. S., Dai, D. Z., Dai, Y., Zhu, D. D. & Liu, B. C. Exogenous hydrogen sulphide ameliorates diabetic cardiomyopathy in rats by reversing disordered calcium-handling system in sarcoplasmic reticulum. *J. Pharm. Pharmacol.* **68,** 379–388 (2016).
92. Waddingham, M. T. Contractile apparatus dysfunction early in the pathophysiology of diabetic cardiomyopathy. *World J. Diabetes* **6,** 943 (2015).
93. Hussain, H., Maldonado-Agurto, R. & Dickson, A. J. The endoplasmic reticulum and unfolded protein response in the control of mammalian recombinant protein production. *Biotechnol. Lett.* **36,** 1581–1593 (2014).
94. Chen, Y. & Brandizzi, F. IRE1: ER stress sensor and cell fate executor. *Trends Cell Biol.* **23,** 547–555 (2013).
95. Battiprolu, P. K., Wang, Z. V. & Hill, J. A. in *Diabetes in Cardiovascular Disease: A Companion in to Braunwald's Heart Disease* 290–301 (2015).
96. Yang, L., Zhao, D., Ren, J. & Yang, J. Endoplasmic reticulum stress and protein quality control in diabetic cardiomyopathy ☆. *BBA - Mol. Basis Dis.* **1852,** 209–218 (2015).
97. Oakes, S. A. & Papa, F. R. The Role of Endoplasmic Reticulum Stress in Human Pathology. *Annu. Rev. Pathol. Mech. Dis.* **10,** 173–194 (2015).
98. Sano, R. & Reed, J. C. ER stress-induced cell death mechanisms. *Biochim. Biophys. Acta - Mol. Cell Res.* **1833,** 3460–3470 (2013).
99. Yang, L., Zhao, D., Ren, J. & Yang, J. Endoplasmic reticulum stress and protein quality control in diabetic cardiomyopathy. *Biochim Biophys Acta* **1852,** 209–218 (2015).
100. Salvadó, L., Palomer, X., Barroso, E. & Vázquez-Carrera, M. Targeting endoplasmic reticulum stress in insulin resistance. *Trends Endocrinol. Metab.* **26,** 438–448 (2015).
101. Todd, D. J., Lee, A. H. & Glimcher, L. H. The endoplasmic reticulum stress response in immunity and autoimmunity. *Nat. Rev. Immunol.* **8,** 663–674 (2008).
102. Iurlaro, R. & Muñoz-Pinedo, C. Cell death induced by endoplasmic reticulum stress. *FEBS J.* **283,** 2640–2652 (2016).

103. Hotamisligil, G. S. Endoplasmic Reticulum Stress and the Inflammatory Basis of Metabolic Disease. *Cell* **140,** 900–917 (2010).
104. ER Stress/Unfolded Protein Response. (2018). Available at: https://www.tocris.com/cell-biology/er-stress-upr.
105. Chow, J. P. *et al.* Mitigation of diabetes-related complications in implanted collagen and elastin scaffolds using matrix-binding polyphenol. *Biomaterials* **34,** 685–695 (2013).
106. Koulis, C., Watson, A. M. D., Gray, S. P. & Jandeleit-Dahm, K. A. Linking RAGE and Nox in diabetic micro- and macrovascular complications. *Diabetes Metab.* **41,** 272–281 (2015).
107. Turner, N. A. Inflammatory and fibrotic responses of cardiac fibroblasts to myocardial damage associated molecular patterns (DAMPs). *J. Mol. Cell. Cardiol.* **94,** 189–200 (2016).
108. Basta, G. Receptor for advanced glycation endproducts and atherosclerosis: From basic mechanisms to clinical implications. *Atherosclerosis* **196,** 9–21 (2008).
109. Soro-paavonen, A. *et al.* Receptor for Advanced Glycation End Products ( RAGE ) Atherosclerosis in Diabetes. *Vascular* **57,** 13–15 (2008).
110. Weiss, M. F. *et al.* Mechanisms for the formation of glycoxidation products in end-stage renal disease. *Kidney Int.* **57,** 2571–2585 (2000).
111. Bhalla, V. *et al.* Matrix metalloproteinases, tissue inhibitors of metalloproteinases, and heart failure outcomes. *Int J Cardiol* **151,** 237–239 (2011).
112. Bodiga, V. L., Eda, S. R. & Bodiga, S. Advanced glycation end products: Role in pathology of diabetic cardiomyopathy. *Heart Failure Reviews* **19,** (2014).
113. Anderson, P. GROSS: CARDIOVASCULAR: HEART: Diabetic Cardiomyopathy. *Pathology Education Informational Resource (PEIR) Digital Library* Diabetic Cardiomyopathy: Heart (2013).
114. Faria, A. & Persaud, S. J. Cardiac oxidative stress in diabetes: Mechanisms and therapeutic potential. *Pharmacol. Ther.* **172,** 50–62 (2017).
115. Huynh, K., Bernardo, B. C., Mcmullen, J. R. & Ritchie, R. H. Pharmacology & Therapeutics Diabetic cardiomyopathy : Mechanisms and new treatment strategies targeting antioxidant signaling pathways. *Pharmacol. Ther.* **142,** 375–415 (2014).
116. He, Q., Harris, N., Ren, J. & Han, X. Mitochondria-Targeted Antioxidant Prevents Cardiac Dysfunction Induced by Tafazzin Gene Knockdown in Cardiac Myocytes. **2014,** (2014).
117. Focus Biomolecules. *Mito-TEMPO | Mitochondria targeted antioxidant* (2016). Available at: https://focusbiomolecules.com/mito-tempo-mitochondria-targeted-antioxidant/.
118. Saklani, R., Kumar, S., Ipseeta, G., Mohanty, R. & Kumar, B. Cardioprotective effects of rutin via alteration in TNF- a , CRP , and BNP levels coupled with antioxidant effect in STZ-induced diabetic rats. *Mol. Cell. Biochem.* **420,** 65–72 (2016).
119. Wang, Y. B. I. N. *et al.* Rutin alleviates diabetic cardiomyopathy in a rat model of type 2 diabetes. *Exp. Ther. Med.* **9,** 451–455 (2015).
120. Zhao, C. *et al.* Optimization of ionic liquid based simultaneous ultrasonic-and

microwave-assisted extraction of rutin and quercetin from leaves of velvetleaf (Abutilon theophrasti) by response surface methodology. *Sci. World J.* **2014,** (2014).
121. Mortensen, S. A. *et al.* The effect of coenzyme Q10on morbidity and mortality in chronic heart failure: Results from Q-SYMBIO: A randomized double-blind trial. *JACC Hear. Fail.* **2,** 641–649 (2014).
122. Nelson, D. L. & Cox, M. M. *Principles of Biochemistry*. (W H Freeman & Co, 2008).
123. Sathibabu Uddandrao, V. V., Brahmanaidu, P., Nivedha, P. R., Vadivukkarasi, S. & Saravanan, G. Beneficial Role of Some Natural Products to Attenuate the Diabetic Cardiomyopathy Through Nrf2 Pathway in Cell Culture and Animal Models. *Cardiovasc. Toxicol.* **18,** 199–205 (2018).
124. Prasad, S., Gupta, S. C., Tyagi, A. K. & Aggarwal, B. B. Curcumin, a component of golden spice: From bedside to bench and back. *Biotechnol. Adv.* **32,** 1053–1064 (2014).
125. Yu, W. *et al.* Curcumin Alleviates Diabetic Cardiomyopathy in Experimental Diabetic Rats. *PLoS One* **7,** 1–11 (2012).
126. Sahebkar, A., Cicero, A. F. G., Simental-Mendía, L. E., Aggarwal, B. B. & Gupta, S. C. Curcumin downregulates human tumor necrosis factor-α levels: A systematic review and meta-analysis ofrandomized controlled trials. *Pharmacol. Res.* **107,** 234–242 (2016).
127. Farazuddin, M. *et al.* Chemotherapeutic potential of curcumin-bearing microcells against hepatocellular carcinoma in model animals. *Int. J. Nanomedicine* **9,** 1139–1152 (2014).
128. Vunjak Novakovic, G., Eschenhagen, T. & Mummery, C. Myocardial tissue engineering: In vitro models. *Cold Spring Harb. Perspect. Med.* **4,** (2014).
129. Gaetani, R., Doevendans, P. A. F., Messina, E. & Sluijter, J. P. G. Tissue Engineering for Cardiac Regeneration. **6,** 1–27 (2011).
130. Vunjak Novakovic, G., Eschenhagen, T. & Mummery, C. Myocardial tissue engineering: in vitro models. *Cold Spring Harb Perspect Med* **4,** (2014).
131. Chaudhuri, R., Ramachandran, M., Moharil, P., Harumalani, M. & Jaiswal, A. K. Biomaterials and cells for cardiac tissue engineering: Current choices. *Mater. Sci. Eng. C* **79,** 950–957 (2017).
132. Gorabi, A. M., Tafti, S. H. A., Soleimani, M., Panahi, Y. & Sahebkar, A. Cells, Scaffolds and Their Interactions in Myocardial Tissue Regeneration. *J. Cell. Biochem.* **118,** 2454–2462 (2017).
133. Hirt, M. N., Hansen, A. & Eschenhagen, T. Cardiac tissue engineering : State of the art. *Circ. Res.* **114,** 354–367 (2014).
134. Wang, W. *et al.* An injectable conductive hydrogel encapsulating plasmid DNA-eNOs and ADSCs for treating myocardial infarction. *Biomaterials* **160,** 69–81 (2018).
135. Tang, J. *et al.* Heart Repair Using Nanogel-Encapsulated Human Cardiac Stem Cells in Mice and Pigs with Myocardial Infarction. *ACS Nano* **11,** 9738–9749 (2017).

136. Gu, X. *et al.* Sustained viral gene delivery from a micro-fibrous, elastomeric cardiac patch to the ischemic rat heart. *Biomaterials* **133,** 132–143 (2017).
137. Tsui, J. H. *et al.* Conductive silk–polypyrrole composite scaffolds with bioinspired nanotopographic cues for cardiac tissue engineering. *J. Mater. Chem. B* (2018). doi:10.1039/C8TB01116H
138. Schulte, J. B., Simionescu, A. & Simionescu, D. T. The acellular myocardial flap: a novel extracellular matrix scaffold enriched with patent microvascular networks and biocompatible cell niches. *Tissue Eng Part C Methods* **19,** 518–530 (2013).
139. Perea-Gil, I. *et al.* Head-to-head comparison of two engineered cardiac grafts for myocardial repair: From scaffold characterization to pre-clinical testing. *Sci. Rep.* **8,** 1–13 (2018).
140. Gershlak, J. R. *et al.* Crossing kingdoms: Using decellularized plants as perfusable tissue engineering scaffolds. *Biomaterials* **125,** 13–22 (2017).
141. Fujita, B. & Zimmermann, W.-H. Myocardial Tissue Engineering for Regenerative Applications. *Curr. Cardiol. Rep.* **19,** 78 (2017).
142. Shudo, Y. *et al.* Layered smooth muscle cell–endothelial progenitor cell sheets derived from the bone marrow augment postinfarction ventricular function. *J. Thorac. Cardiovasc. Surg.* **154,** 955–963 (2017).
143. Sakaguchi, K. *et al.* Low-temperature culturing improves survival rate of tissue-engineered cardiac cell sheets. *Biochem. Biophys. Reports* **14,** 89–97 (2018).
144. Wang, F. & Guan Jianjun, J. Cellular cardiomyoplasty and cardiac tissue engineering for myocardial therapy. *Adv. Drug Deliv. Rev.* **62,** 784–797 (2010).
145. Wanjare, M. & Huang, N. F. Regulation of the microenvironment for cardiac tissue engineering. *Regen. Med.* **12,** 187–201 (2017).
146. Luger, D. *et al.* Intravenously delivered mesenchymal stem cells. *Circ. Res.* **120,** 1598–1613 (2017).
147. Demetz, G. *et al.* Overexpression of Insulin-Like Growth Factor-2 in Expanded Endothelial Progenitor Cells Improves Left Ventricular Function in Experimental Myocardial Infarction. *J. Vasc. Res.* **54,** 321–328 (2017).
148. Drawnel, F. M. *et al.* Disease modeling and phenotypic drug screening for diabetic cardiomyopathy using human induced pluripotent stem cells. *Cell Rep.* **9,** 810–820 (2014).
149. Henry, T. D. *et al.* The Athena trials: Autologous adipose-derived regenerative cells for refractory chronic myocardial ischemia with left ventricular dysfunction. *Catheter. Cardiovasc. Interv.* **89,** 169–177 (2017).
150. Kofron, C. M. & Mende, U. In vitro models of the cardiac microenvironment to study myocyte and non-myocyte crosstalk: bioinspired approaches beyond the polystyrene dish. *J. Physiol.* **595,** 3891–3905 (2017).
151. Carrier, R. L. *et al.* Perfusion Improves Tissue Architecture of Engineered Cardiac Muscle. *Tissue Eng.* **8,** 14 (2002).
152. Nunes, S. S. *et al.* Biowire: A platform for maturation of human pluripotent stem cell-derived cardiomyocytes. *Nat. Methods* **10,** 781–787 (2013).
153. Zimmermann, W. H. *et al.* Tissue engineering of a differentiated cardiac muscle construct. *Circ. Res.* **90,** 223–230 (2002).

154. Radisic, M. *et al.* Functional assembly of engineered myocardium by electrical stimulation of cardiac myocytes cultured on scaffolds. *Proc. Natl. Acad. Sci. U. S. A.* **101,** 18129–18134 (2004).
155. Morgan, K. Y. & Black, L. D. Mimicking Isovolumic Contraction with Combined Electromechanical Stimulation Improves the Development of Engineered Cardiac Constructs. *Tissue Eng. Part A* **20,** 1654–1667 (2014).
156. Fuentes-Antras, J. *et al.* Updating experimental models of diabetic cardiomyopathy. *J Diabetes Res* **2015,** 656795 (2015).
157. Aamodt, J. M. & Grainger, D. W. Extracellular matrix-based biomaterial scaffolds and the host response. *Biomaterials* **86,** 68–82 (2016).
158. Aasum, E., Hafstad, A. D., Severson, D. L. & Larsen, T. S. Age-dependent changes in metabolism, contractile function, and ischemic sensitivity in hearts from db/db mice. *Diabetes* **52,** 434–441 (2003).
159. Mazumder, P. *et al.* Impaired cardiac efficiency and increased fatty acid oxidation in insulin-resistant ob/ob mouse hearts. *Diabetes* **53,** 2366–2374 (2004).
160. Young, M. *et al.* Impaired long-chain faty acid oxidation and contractile dysfunction in obese zucker rat heart. *Diabetes* **51,** 2587–2595 (2002).
161. Bugger, H. *et al.* Type 1 diabetic akita mouse hearts are insulin sensitive but manifest structurally abnormal mitochondria that remain coupled despite increased uncoupling protein 3. *Diabetes* **57,** 2924–2932 (2008).
162. Lu, Z. *et al.* Decreased L-Type Ca 2+ Current in Cardiac Myocytes of Type 1 Diabetic Akita Mice Due to Reduced Phosphatidylinositol 3-Kinase Signaling. *Diabetes* **56,** (2007).
163. Basu, R. *et al.* Type 1 diabetic cardiomyopathy in the Akita (Ins2WT/C96Y) mouse model is characterized by lipotoxicity and diastolic dysfunction with preserved systolic function. *Am. J. Physiol. Heart Circ. Physiol.* **297,** H2096-108 (2009).
164. Song, H., Zandstra, P. W. & Radisic, M. Engineered heart tissue model of diabetic myocardium. *Tissue Eng Part A* **17,** 1869–1878 (2011).

# CHAPTER 2: RESEARCH MOTIVATION, SPECIFIC AIMS AND PROJECT SIGNIFICANCE

## 2.1 Introduction

As **diabetes mellitus** rises to epidemic proportions across the world, so follows an upsurge in the number of patients who have heightened risk of cardiovascular disease. The risk of cardiovascular disease, such as hypertension, diabetic cardiomyopathy, and atherosclerosis are increased in diabetic patients.[1,2] **Diabetic cardiomyopathy (DCMP)** is a ventricular dysfunction that specifically occurs in diabetic patients independent of coronary artery disease, hypertension or valvular abnormalities.[3]

Heart transplantation is the only cure for DCMP, which has a very long wait list.[4] Treatment is lumped in with other cardiomyopathies and heart failure, however these therapies only treat the symptoms and downstream complications that accompany heart failure without addressing the roots of the problem.[5] Understanding the fundamental **mechanisms in the early stages of DCMP** are vital for **early diagnosis and targeted therapies**. As of now, comprehension of this disease has depended on rodent models, cell culture models, and cadaveric human patient hearts.[6,7] Human DCMP cadaveric hearts have been useful for elucidating end stage cellular and extracellular changes and rodent and cell culture models have been utilized to fill in the gaps. However there are many discrepancies that exist between humans and rodents.[8–10] Human cells have been employed to examine specific cell type alterations associated with the diabetic environment, but this is in an oversimplified 2D static environment, lacking an extracellular matrix (ECM).[11]

**Our long-term goal** is to develop a tissue engineering platform to investigate mechanisms of early cellular and extracellular alterations of DCMP. To achieve this goal, we will examine known hallmarks of DCMP in two tissue-engineered models developed in our lab. This will be accomplished by containing tissue-engineered myocardium made by combining human cardiomyocytes and decellularized porcine myocardium in (1) a 3D Kube minibioreactor or (2) an in-house electromechanical bioreactor cultured in a high glucose environment.

**Preliminary studies** in our lab have shown cellular and extracellular alterations associated with DCMP in rat cardiomyocytes cultured in 3D Kube minibioreactors for 14 days in high glucose. Within our lab we have also developed a physiologically relevant myocardial electromechanical bioreactor. With these encouraging results we chose to move forward and examine early human cardiomyocytes (hCM) modifications in the 3D Kube minibioreactor, as well as our electromechanical bioreactor in a simulated "diabetic" environment with additional glucose. **We hypothesize** that by creating and utilizing tissue engineering platforms for modelling DCMP we can elucidate early alterations in hCM and the ECM to determine points for diagnosis and treatment.

## 2.2 Specific Aims

**Aim 1: Ascertain if tools and methods we employ are suitable for analysis and highlight DCMP alterations (Presented in Chapter 3)**

**Hypothesis:** Methods utilized will detect alterations in the ECM and cells of the heart caused by hyperglycemia and dyslipidemia in the diabetic environment

**Approach:** Hearts from normal and diabetic (streptozotocin type I induced) rats will be harvested and analyzed for this study 8 weeks after induction. Diabetic and DCMP cellular and ECM changes will be assessed via histological staining, western blotting, and specific assays. Alterations such as lipid accumulation, endogenous antioxidant mechanisms, advanced glycation endproduct (AGE) buildup, matrix metalloproteinase (MMP) activity, apoptosis, autophagy, endoplasmic reticulum (ER) stress, and perivascular and interstitial fibrosis.

**Aim 2: Assess suitability of human cardiomyocytes for the creation of a three-dimensional (3D), dynamic in vitro model of DCMP (Presented in Chapter 4)**

**Hypothesis:** hCMs will be modified and respond in a hyperglycemic milieu

**Approach:** Progenitor hCM will be cultured for two weeks in a high glucose environment (4.5g/L glucose) and compared to hCM cultured in normal glucose (1g/L glucose). Immunofluorescence, western blotting, and specialized kits and assays will be used to analyze the two groups. Cells will be analyzed for alterations such as lipid accumulation, lipid peroxidation, reactive oxygen species (ROS) generation, endogenous

antioxidant mechanisms, AGE buildup, receptor for AGE (RAGE) expression, MMP activity, apoptosis, autophagy, and ER stress.

**Aim 3: Develop a myocardial-like tissue platform using proper biochemical, mechanical, and electrical cues (Presented in Chapter 5)**

**Hypothesis:** Applying specific mechanical, electrical, and biochemical stimuli, cardiomyocytes seeded on scaffolds will mimic the organization and function of myocardial tissues

**Approach:** hCM from Aim 2 will be seeded into decellularized porcine myocardium and exposed to mechanical and electrical stimuli for 14 days via a modified Flexcell bioreactor to induce cell organization. Static controls will be cultured in tandem. Cell viability, as well as the presence of specific cardiac cell markers, such as connexin 43, sarcomeric α-actinin, desmin, and GATA-4 will be assessed. The extracellular matrix will also be analyzed for changes in collagen IV and laminin expression.

**Aim 4: Investigate cardiac cell and matrix modifications induced by oxidative stress in diabetic environment (Presented in Chapter 6)**

**Hypothesis:** High glucoxidative environments induce pathological modifications in cells and extracellular matrix

**Approach:** Lipid accumulation, endogenous antioxidant mechanisms, AGE accrual, MMP activity, apoptosis, autophagy, and ER stress will be assessed after the myocardial-like tissue is exposed to physiological-like conditions in vitro in either normal (1 g/L) or

high (4.5 g/L) glucose. Two bioreactor platforms will be tested for 14 days: (1) a 3D Kube perfusion minibioreactor and (2) an electromechanical bioreactor developed in our lab (from Aim 3).

### 2.3 Significance of Proposed Project

This project is expected to have a significant impact by bridging an existing gap in the understanding of early alterations of human cardiac cells and the extracellular matrix in DCMP and the diabetic environment with tissue engineering. Development of an organotypic, highly reproducible, systematic model will allow for strides to be made not only in the clarification of DCMP, diagnosis, and patient-tailored options for treatment and prevention, but in validating therapies and understanding the progression of DCMP.

### 2.4 Chapter 2 References


1 McGuire DK, Marx N. *Diabetes in Cardiovascular Disease: A Companion to Braunwald's Heart Disease*. 1st ed. Philadelphia, PA: Saunders; 2015.

2 Forbes JM, Cooper ME, 1997 ADA clinical practice recommendations, up O the, Tight blood pressure control and risk of macrovascular and microvascular complications in type 2 diabetes: UK 38 UPDSG, Abbott C, *et al.* Mechanisms of diabetic complications. *Physiol Rev* 2013;**93**:137–88. https://doi.org/10.1152/physrev.00045.2011.

3 Jia G, Hill MA, Sowers JR. Diabetic cardiomyopathy: An update of mechanisms contributing to this clinical entity. *Circ Res* 2018;**122**:624–38. https://doi.org/10.1161/CIRCRESAHA.117.311586.

4 Bonow RO, Mann DL, Zipes DP, Libby P. *Braunwald's Heart Disease*. 9th ed. Saunders; 2011.

5 Murarka S, Movahed MR. Diabetic cardiomyopathy. *J Card Fail* 2010;**16**:971–9. https://doi.org/10.1016/j.cardfail.2010.07.249.

6 Bugger H, Abel ED. Rodent models of diabetic cardiomyopathy. *Dis Model Mech* 2009;**2**:454–66. https://doi.org/10.1242/dmm.001941.

7 Michaelson J, Hariharan V, Huang H. Hyperglycemic and hyperlipidemic conditions alter cardiac cell biomechanical properties. *Biophys J* 2014;**106**:. https://doi.org/10.1016/j.bpj.2014.04.040.
8 Fuentes-Antras J, Picatoste B, Gomez-Hernandez A, Egido J, Tunon J, Lorenzo O. Updating experimental models of diabetic cardiomyopathy. *J Diabetes Res* 2015;**2015**:. https://doi.org/10.1155/2015/656795.
9 Bayeva M, Sawicki KT, Ardehali H. Taking diabetes to heart--deregulation of myocardial lipid metabolism in diabetic cardiomyopathy. *J Am Hear Assoc* 2013;**2**:e000433. https://doi.org/10.1161/JAHA.113.000433.
10 Aamodt JM, Grainger DW. Extracellular matrix-based biomaterial scaffolds and the host response. *Biomaterials* 2016;**86**:68–82. https://doi.org/10.1016/j.biomaterials.2016.02.003.
11 Maalouf RM, Eid AA, Gorin YC, Block K, Escobar GP, Bailey S, *et al.* Nox4-derived reactive oxygen species mediate cardiomyocyte injury in early type 1 diabetes. *AJP Cell Physiol* 2012;**302**:C597–604. https://doi.org/10.1152/ajpcell.00331.2011.

# CHAPTER 3: CHARACTERIZATION OF AN IN VIVO DIABETIC CARDIAC DISEASE MODEL

## 3.1 Introduction

The only cure for DCMP is a whole heart transplant.[4] There is no specific marker for this cardiomyopathy and it is diagnosed after symptom manifestation, including but not limited to, shortness of breath, fatigue, chest pain, and fluid retention.[5] As of now, treatment of DCMP is the same as other cardiomyopathies, with a focus on blood glucose control.[2] DCMP is a complex disease and understanding its progression is the key to determining distinct markers for early diagnosis, as well as targeted treatments.

Animal models have been widely utilized to understand the underlying mechanisms of DCMP and cardiac alterations associated with diabetes.[6] One of these popular models is the streptozotocin (STZ) type I diabetic rat model. This type I diabetic rat model is produced through tail vein injection of STZ, a glucosamine-nitrosourea antibiotic that causes beta cell necrosis, leading to insulin deficiency.[7] STZ is favorably up taken by beta cell GLUT2 glucose transporters in the pancreas as it has a similar structure to glucose.[7] This diabetic rat model has been shown to exhibit decreased glucose utilization, increased FFA oxidation, decreased mitochondrial function, impaired calcium handling, and increased oxidative stress.[6]

We hypothesized that by utilizing this diabetic STZ rat model, we could detect alterations in the ECM and cells of the heart caused by hyperglycemia and dyslipidemia in the diabetic environment.

## 3.2 Materials and Methods

### *3.2.1 Materials*

Streptozotocin was obtained from Sigma (S0130). Insulin used was Humulin N U-100 NPH from Lilly (Indianapolis, IN). AlphaTRAK® (GenII) test strip and the AlphaTRAK® Blood Glucose Monitoring System were from Abbot Laboratories, Animal Health (Abbott Park, IL). Bicinchoninic acid protein assay was from Pierce Biotech (Rockford, IL). Electrophoresis apparatus, gel imager and imaging software, chemicals, and molecular weight standards were from Bio-rad (Hercules, CA). BM Chemiluminescence Western Blotting kit (Mouse/ Rabbit) was obtained from Roche (Indianapolis, IN). The Vectastain Elite kit, ABC diaminobenzidine tetrahydrochlorine peroxidase substrate kit, and Vectashield mounting medium were from Vector Laboratories (Burlingame, CA). The following antibodies were used: rabbit anti-superoxide dismutase-2 (Abcam, ab13534), rabbit anti-advanced glycation endproducts (Abcam, ab23722), rabbit anti-protein kinase RNA-like endoplasmic reticulum kinase (Abcam, ab192591), rabbit anti-alpha-smooth muscle actin (Abcam, ab5694), rabbit anti-caspase-3 (Millipore, 06-735). Biotinylated anti-rabbit IgG was purchased from Vector Laboratories (Burlingame, CA). Movat's Pentachrome Kit was from Poly Scientific (Bay Shore, NY). All other chemicals were of the highest purity and purchased from Sigma-Aldrich Corporation (Lakewood, NJ).

*3.2.2 Rat Streptozotocin-Induced Diabetes Model*

Diabetic rat models were produced utilizing adult male Sprague-Dawley rats (n=20, weight 300-350g) after tail vein injection of a single dose of sterile filtered 55mg/kg streptozotocin (STZ) solution in 0.1M citrate buffer (pH 5). Control rats were given an equal volume of sterile citrate buffer (n=20). 3 days after diabetic induction, AlphaTRAK® (GenII) strips with the AlphaTRAK® Blood Glucose Monitoring System were used to measure levels of blood glucose 3-4 times a day. Diabetic rats were given subcutaneous injections of long-lasting insulin (2-4U Isophane) every other day after the establishment of diabetes (>400mg glucose/dL blood). This ensured blood glucose levels were maintained at reasonable ranges (400-600mg glucose/dL blood) and would prevent weight loss and ketonuria development. Adequate health parameters were maintained by closely monitoring glucose levels, individual weights, hydration status, and food and water consumption. Godley-Snell Research Center Animal Facility associated staff and attending university veterinarian provided food and water for the animals *ad libitum,* as well as animal care. 8 weeks after STZ or control injection, rats were humanely euthanized by carbon dioxide and hearts were harvested. Hearts for protein extraction were flash frozen in liquid nitrogen, transported on dry ice for storage at -20°C. For histological analysis, hearts were either fixed in 10% formalin before processing or embedded and frozen in optimal cutting temperature (OCT) compound. National Institute of Health (NIH) guidelines for the care and use of laboratory animals (NIH publication #86-23 Rev. 1996) were observed. The Animal Research Committee at Clemson University approved the animal protocol for this experiment.

*3.2.3 Histological Analysis*

Rat hearts were dissected into 4 coronal sections before paraffin processing and embedding, for more in-depth histological analysis. Movat's pentachrome staining was utilized to compare morphology between the normal and diabetic hearts (n=3 for each group). Rehydrated paraffin sections (5um) were stained using a Movat's pentachrome kit. Manufacturer's guidelines were followed.

Immunohistochemistry (IHC) was performed for detection of superoxide dismutase-2 (SOD-2), advanced glycation endproducts (AGE), and alpha-smooth muscle actin (α-SMactin) to compare diabetic and normal rat hearts (n=3 for each group). Briefly, antigen retrieval was performed on rehydrated paraffin sections (5um) with heated (90-100 degrees C, 10 min) 10mM citric acid (pH=7.4). Slides were permeabilized with 0.025% Triton X-100 for 5 minutes and then incubated in normal blocking serum for 45 minutes. Primary antibodies (rabbit anti-SOD-2 10ug/mL dilution, rabbit anti-AGE 4ug/mL dilution, or rabbit anti-a-SMactin 1ug/mL dilution) were incubated overnight at 4 degrees Celsius. Negative controls were obtained by omitting the primary antibody. Endogenous peroxidases were blocked with 0.3% hydrogen peroxide in 0.3% normal horse serum for 30 minutes. The secondary biotinylated anti-rabbit antibody was applied for 30 minutes. Antibody staining was visualized using the Vector ABC peroxidase substrate kit and then lightly counterstained with diluted hematoxylin, before mounting. A Zeiss Axiovert 40CFL microscope with AxioVision Release 4.6.3 digital imaging software (Carl Zeiss MicroImaging, Inc. Thornwood, NY) was utilized to obtain images.

*3.2.4 Lipid Staining*

Lipid accumulation was visualized via oil red O or sudan black staining on cryosectioned rat hearts (n=3 per group) and mounted with aqueous Vectashield mounting medium. Light images were taken on a Zeiss Axiovert 40CFL microscope, as described before. For oil red o, slides were fixed in 4% paraformaldehyde, rinsed in distilled, deionized water ($ddH_2O$), rinsed in 60% isopropanol, and stained in 0.3% Oil Red O in isopropanol solution. Slides were then rinsed twice in 60% isopropanol, stained in a 1 to 1 hematoxylin in $ddH_2O$ solution, and rinsed in $ddH_2O$.

For sudan black staining, were fixed in 4% paraformaldehyde, rinsed in $ddH_2O$, rinsed in 35% ethanol, followed by 70% ethanol, and stained in sudan black in 70% ethanol. Slides were rinsed twice in 70% ethanol, followed by a rinse in tap water, stained in a 1 to 1 hematoxylin in $ddH_2O$, and rinsed in $ddH_2O$.

*3.2.5 Detection of Caspase-3, SOD-2, AGE, and PERK*

Western blotting was employed to compare amounts of caspase-3, SOD-2, AGE, and protein kinase RNA-like endoplasmic reticulum kinase (PERK) between the diabetic (n=5) and normal (n=4) rat hearts. Proteins were extracted by pulverizing liquid nitrogen-frozen tissue samples from the left ventricular wall and homogenizing them in radioimmunoprecipitation assay (RIPA) extraction buffer (50mM Tris-HCl pH 7.4, 150mM sodium chloride (NaCl), 1mM ethylenediaminetetraacetic acid (EDTA), 1% Triton X-100, 1% Sodium Deoxycholate, 0.1% sodium dodecyl sulfate (SDS), with protease inhibitor cocktail). Protein concentrations in the samples were found using a bicinchoninic acid protein (BCA) assay. For each sample, 20ug of protein per lane was

loaded and a pre-stained molecular weight standard was loaded in one of the lanes. Protein from the gels were transferred to polyvinylidine fluoride membranes. Primary antibodies (rabbit anti-AGE 0.5ug/mL dilution, rabbit anti-SOD-2 1ug/mL dilution, rabbit anti-caspase-3 1ug/mL dilution, or rabbit anti-PERK 1ug/mL dilution) were applied overnight at 4 degrees C. The secondary antibody from the anti-mouse/rabbit kit was then applied for 45 minutes at room temperature. The polyvinylidine fluoride membranes were fluorescently tagged with detection solution from the anti-mouse/rabbit kit and then imaged using the Chemi-Doc™ XRS+ system from Bio-rad (Hercules, CA). Relative band intensities were determined using Bio-rad Image Lab Software Version 5.1, beta build 1.

Relative amounts of caspase-3 within the rat hearts (n=3 per group) were determined with the Caspase-3 Fluorogenic Spectroscopic Assay from BD Pharmingen (San Jose, CA). Manufacturer's protocol was followed. Intensities were measured using the Synergy H1 Hybrid Reader System from BioTek (Winooski, VT).

*3.2.6 Matrix Metalloproteinase Activity Analysis*

Protein extracts from hearts were extracted using the RIPA buffer method (above). Protein concentrations in the samples were found using a BCA assay. For each sample, 20ug of protein per lane were loaded into a gelatin zymography gel (n=2 per group), as was a pre-stained molecular weight standard into a separate lane. After electrophoresis separation, the zymography gel was washed in a triton-X solution and matrix metalloproteinases (MMPs) were activated with a brij-35 development buffer for 24 hours at 37 degrees C. After staining with Coomassie, MMP clear bands were imaged

using the Chemi-Doc™ XRS+ system and evaluated by densitometry using the using Bio-rad Image Lab Software.

*3.2.7 Glutathione Detection*

Protein extracts were taken from rat hearts using the RIPA buffer extraction method (above). Protein concentrations in the samples were found using a BCA assay. Glutathione was detected in rat hearts (n=3 per group) using Cell Technology's fluorescent thiol detection kit assay (Mountain View, CA). Manufacturer protocol was utilized. Intensities were measured the Synergy H1 Hybrid Reader System.

*3.2.8 Statistical Analysis*

Results are expressed at mean ± standard deviation (SD). Statistical analysis was performed between groups utilizing Welch's two-tailed t-test in excel. Significance was determined with an alpha (α) value of 0.05.

**3.3 Results**

*3.3.1 Extracellular Matrix Analysis*

Analysis of normal and diabetic rat hearts was performed to determine if ECM changes associated with DCMP were noticeable. On the macro scale, diabetic hearts markedly enlarged and dilated when compared to normal rat hearts (**Figure 3.1**). As seen in **Figure 3.2**, diabetic rat hearts had higher instances of fibrosis within the myocardium of the left ventricle and blood vessels, as revealed by Movat's pentachrome staining and IHC staining of α-SMactin. Analysis of MMPs revealed reduced activity in diabetic rat hearts (**Figure 3.3**).

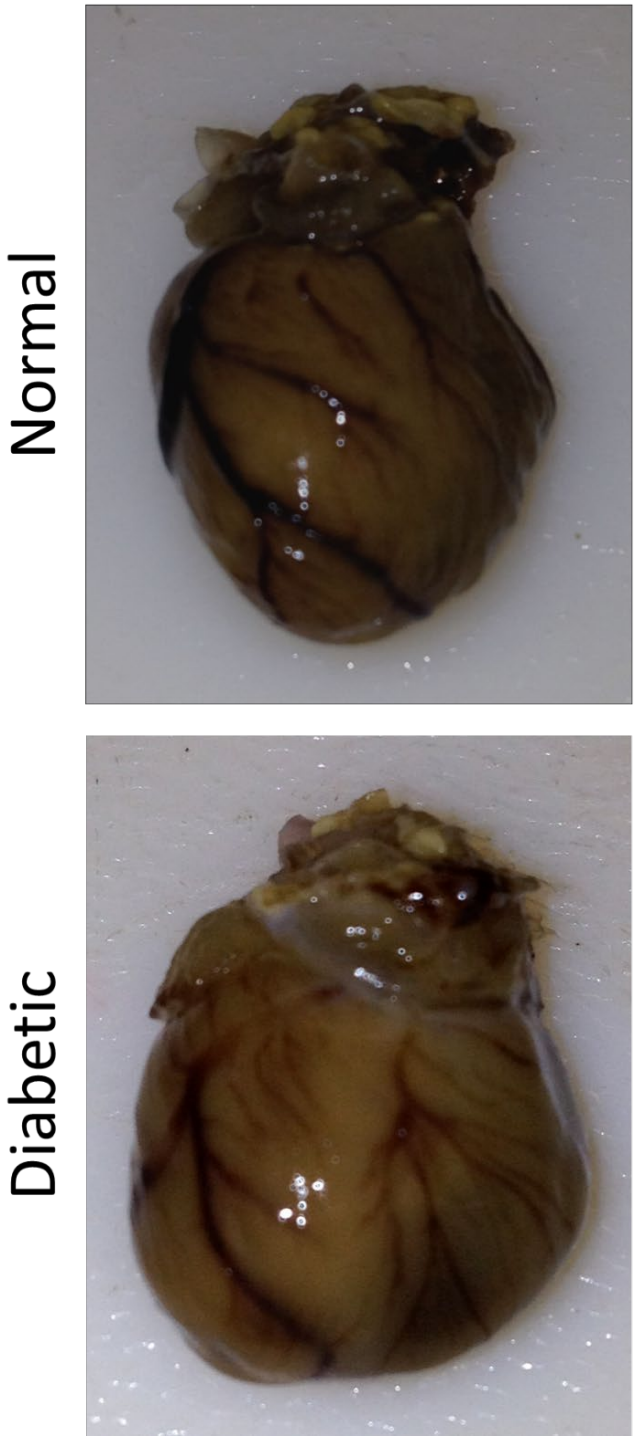


**Figure 3.1:** Harvested diabetic (bottom) and normal (top) rat hearts.

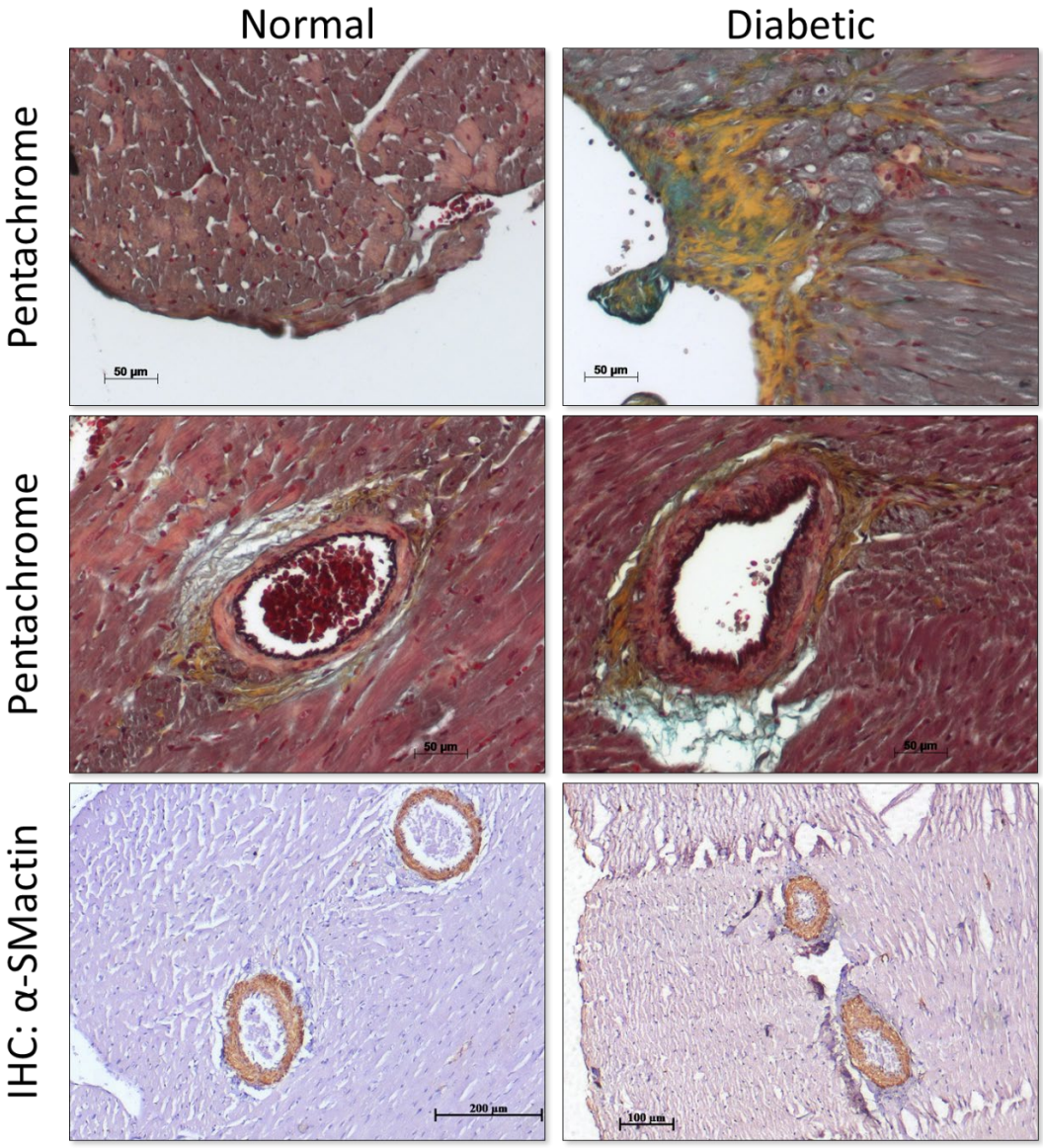


**Figure 3.2:** Extracellular matrix (ECM) analysis of normal and diabetic rat hearts. Movat's pentachrome staining (top and middle) of the left ventricle and blood vessels (black=nuclei or elastic fibers, yellow=collagen or reticular fibers, blue=ground substance or mucin, bright red=fibrin, red=muscle) in hearts. Immunohistochemistry (IHC) staining (bottom) was used for α-smooth muscle actin (α-SMactin, brown=positive, dark purple=nuclei) visualization. Negative controls not shown for IHC.

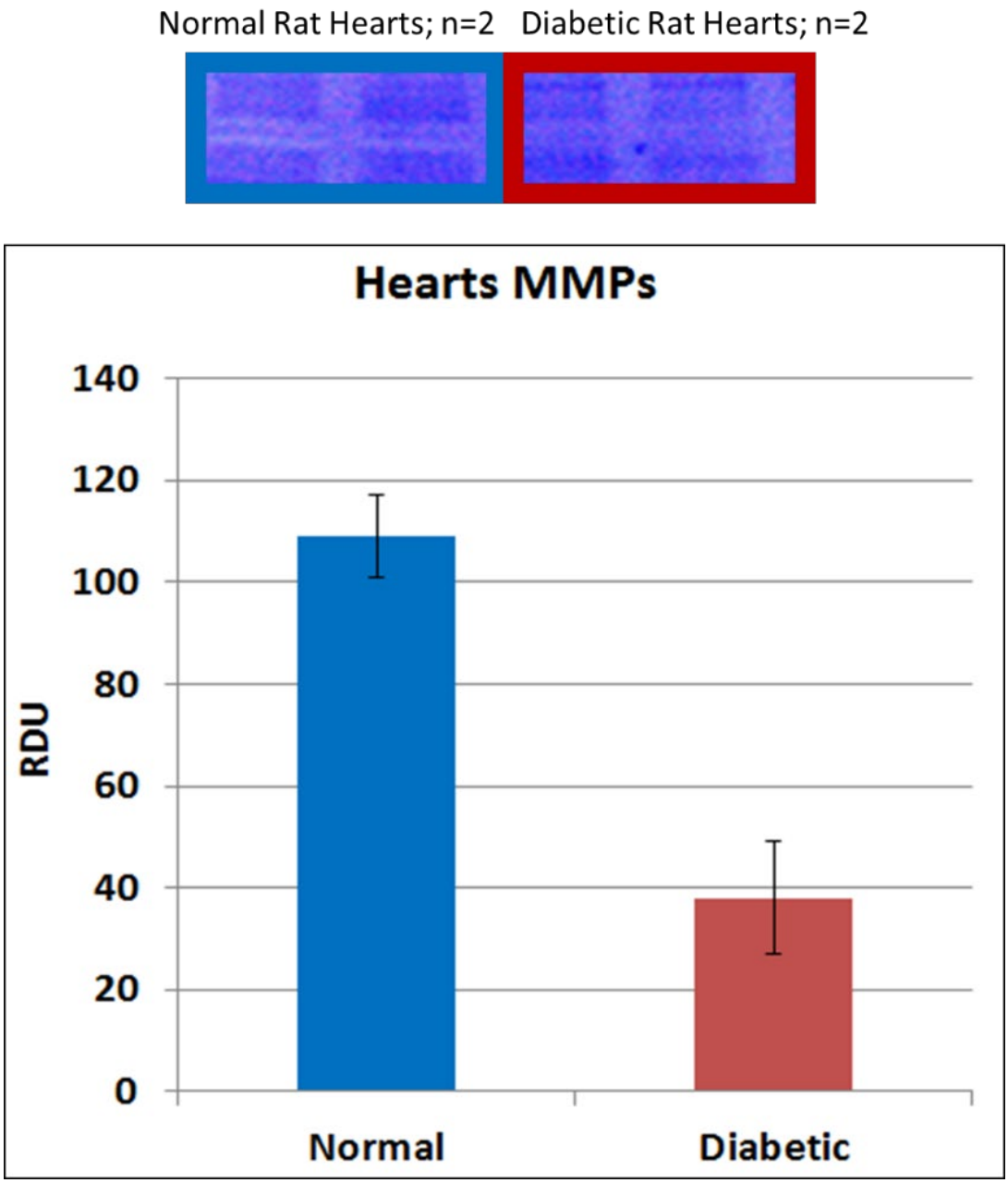


**Figure 3.3:** Matrix metalloproteinase (MMP) activity assessment in rat hearts. Gelatin zymography was used to determine MMP activity in diabetic and normal rat hearts. RDU= relative densitometry units.

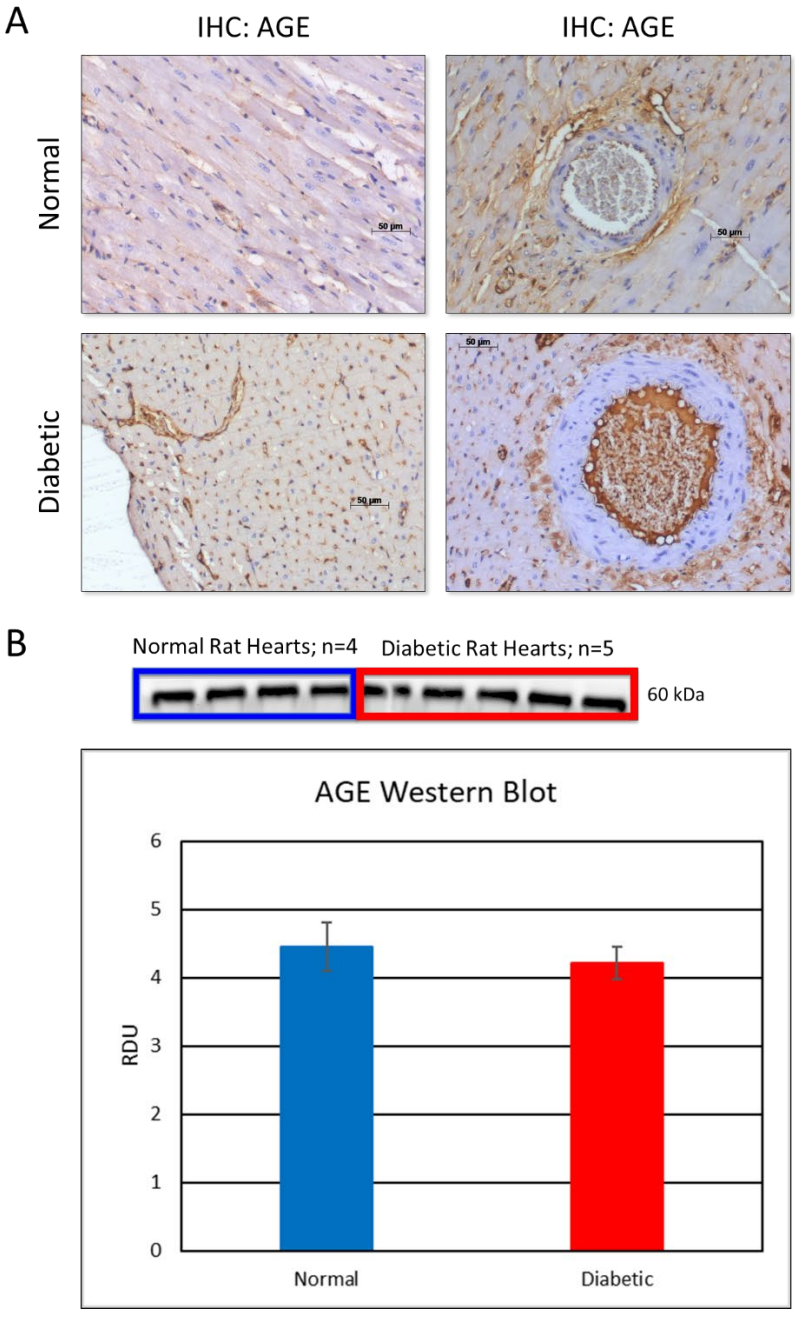


**Figure 3.4:** Advanced glycation endproducts (AGE) formation within normal and diabetic rat hearts. (A) Hearts were stained for AGEs via immunohistochemistry (IHC) (brown=positive, dark purple=nuclei). (B) AGEs in hearts were analyzed with western blotting. RDU= relative densitometry units.

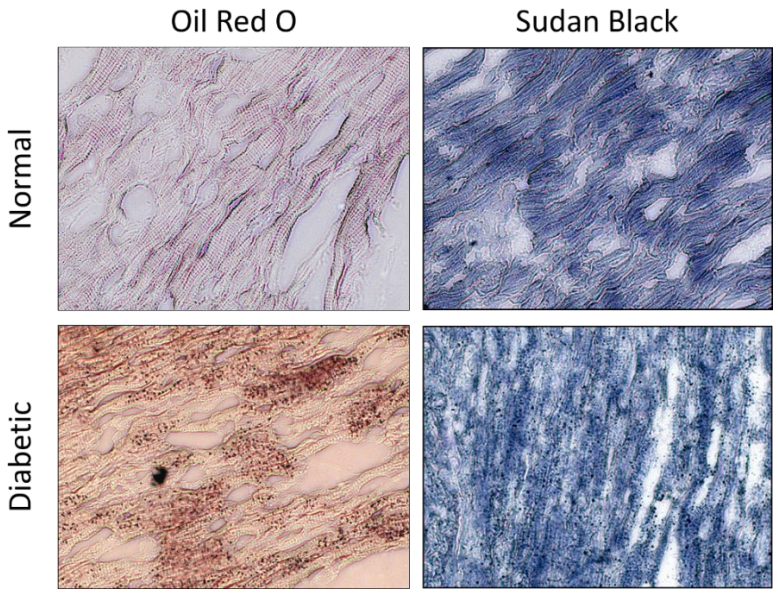


**Figure 3.5:** Lipid accumulation staining in diabetic and normal rat hearts. Lipids in hearts were visualized with oil red O (red=lipids) and sudan black (black=lipids) staining.

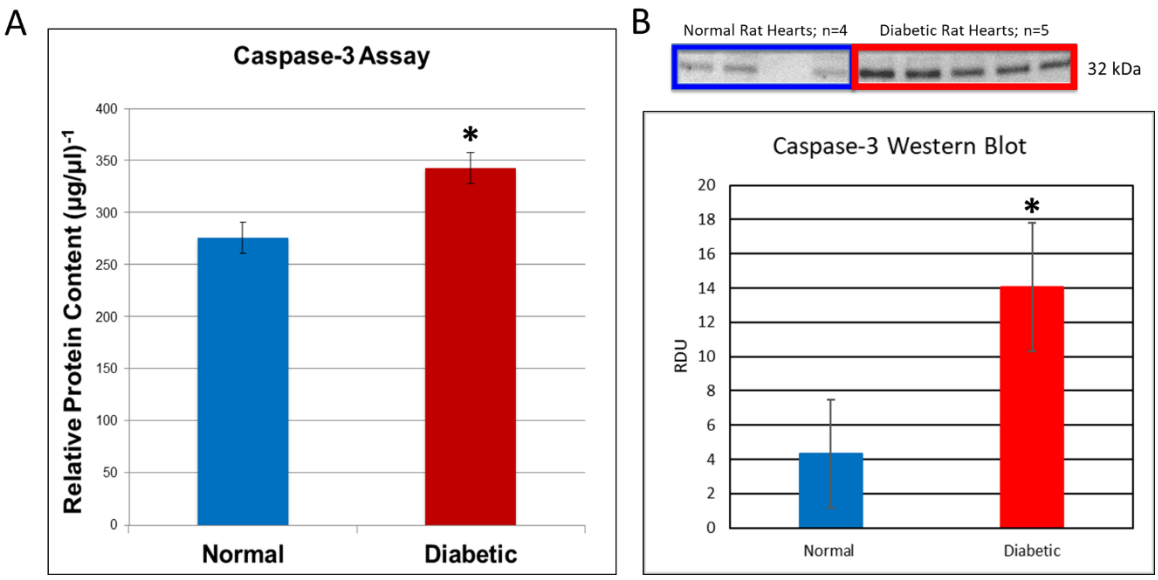


**Figure 3.6:** Investigation of apoptosis in rat hearts. Relative expression of caspase-3, an apoptosis marker, was measured with (A) a caspase-3 assay and (B) western blotting. * indicates statistical significance. RDU=relative densitometry units.

*3.3.2 AGE Formation, Lipid Accumulation, and Apoptosis*

As hyperglycemia and hyperlipidemia are hallmarks of DM and DCMP, we sought to compare diabetic rat hearts to normal rat hearts for glycoxidation and lipid accumulation. As shown in **Figure 3.4**, AGEs were present in both normal and diabetic rat heart tissue, as seen in IHC AGE staining. Western blot protein analysis of AGEs showed no significant difference between normal and diabetic rat hearts. AGE staining of blood vessels of the hearts demonstrated increased circulating AGEs in diabetic rat hearts. Staining of lipids via oil red O and sudan black, displayed higher lipid accumulation within the diabetic rat heart tissue (**Figure 3.5**). Hyperglycemia and hyperlipidemia can both lead to programmed cell death, known as apoptosis. Caspase-3, a marker of apoptosis, was used to investigate this. It was found via western blotting and a specific caspase-3 assay that caspase-3 expression was significantly increased, and therefore apoptosis, in diabetic rat hearts compared to normal rat hearts (**Figure 3.6**).

*3.3.3 Antioxidant Defense Mechanisms and Endoplasmic Reticulum Stress*

One element of DCMP is oxidative stress caused by an imbalance between reactive oxygen species (ROS) and antioxidant defense mechanisms, such as SOD-2 and glutathione. As observed in **Figure 3.7**, there was a significant reduction in SOD-2 and glutathione expression in diabetic rat hearts. IHC revealed normal rat hearts to have SOD-2 expressed throughout the tissue, while SOD-2 expression in diabetic rat hearts were concentrated in the myocardium. Western blot protein detection showed SOD-2 was significantly decreased in diabetic rat hearts. Glutathione content in diabetic rat hearts was also significantly decreased as measured by a glutathione assay.

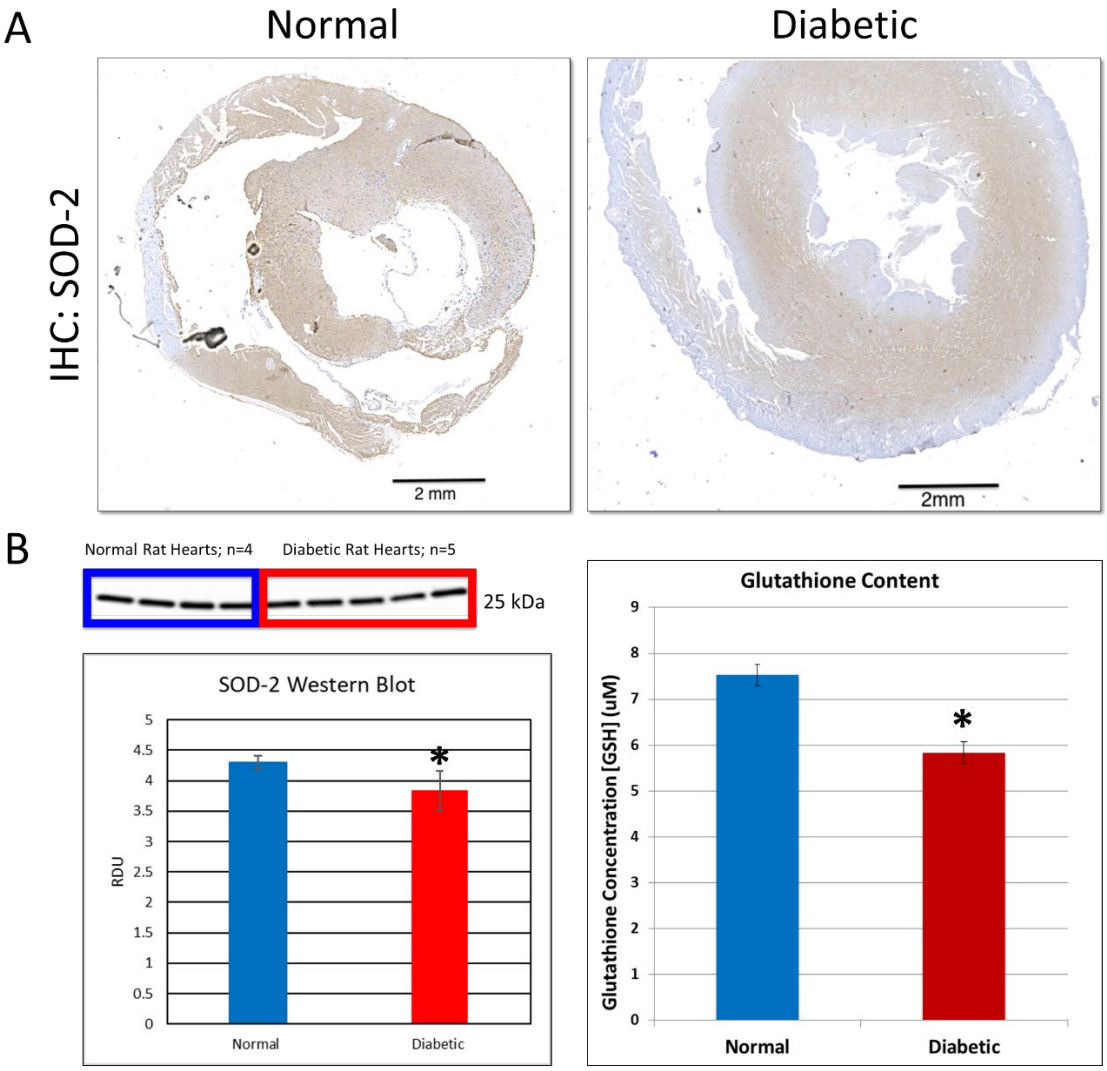


**Figure 3.7:** Antioxidant defense mechanisms utilized by normal and diabetic rat hearts. Superoxide dismutase-2 (SOD-2) was visualized with immunohistochemistry (IHC) (top) (brown=positive, dark purple=nuclei) and detected with western blotting (bottom left); results are in relative densitometry units (RDU). Glutathione was measured via an assay (bottom right).

Another trait of diabetes and DCMP is ER stress within cells due to buildup of misfolded proteins. Protein kinase RNA-like endoplasmic reticulum kinase (PERK) is upregulated in ER stress and its pathway triggers the unfolded protein response. Western blotting of this protein showed an upward trend in diabetic rat hearts.

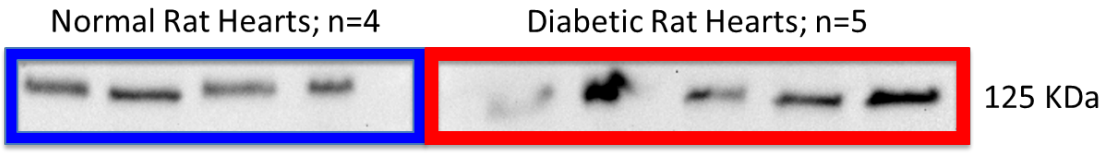


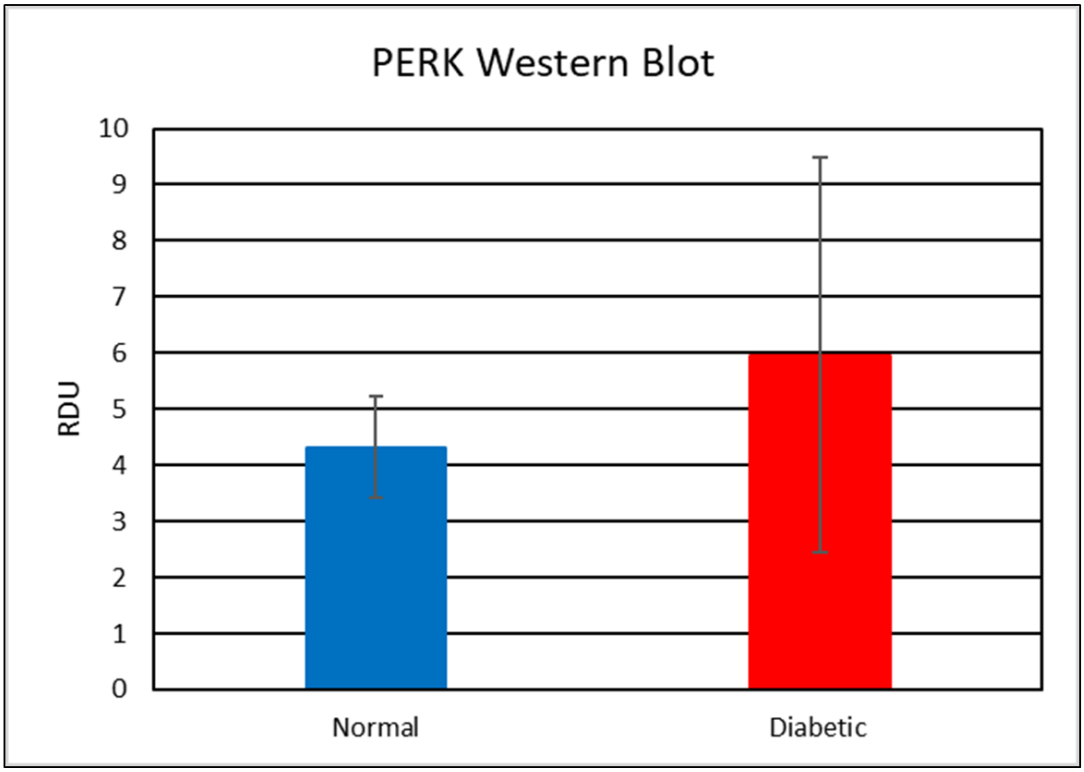


**Figure 3.8:** Endoplasmic reticulum (ER) stress in normal and diabetic rat hearts. Protein kinase RNA-like endoplasmic reticulum kinase (PERK), a marker for ER stress, was detected by western blotting. RDU= relative densitometry units.

### 3.4 Discussion

Experimental animal models have been employed for understanding cardiovascular alterations associated with diabetes, specifically DCMP. Known hallmarks of this disease at the cellular and extracellular levels, include fibrosis, buildup of AGEs, lipid accumulation, oxidative stress, ER stress, apoptosis, and autophagy.[8] In this study we sought to use a diabetic rat model to see if there were noticeable ECM and cellular alterations in the hearts associated with DCMP. We also wanted to optimize the tools and methods we were using in investigating and perceiving these changes.

The STZ diabetic type 1 model used for this study provided a baseline, as it has been thoroughly studied in literature and diabetic rat hearts from this experimental model have been shown to display alterations and characteristics of DCMP.[6] STZ is a popular diabetic rodent model as it is easily administered to the animal and takes less time to produce than genetic diabetic rodent models.[7] This model can also be combined with genetically altered rodents, making it favorable for specific research into genetic disorders combined with diabetes, exacerbated diabetic models, and knock out models.[9,10] While this is a popular experimental model, there are disadvantages that have been noted with intravenous STZ administration to create this diabetic state. One of the most significant is systemic genotoxic effects from the injected STZ.[11] Kume et. al. reported that there are changes in hepatic gene expression, such as downregulation of genes associated with lipid metabolism and glucose as soon as 48 hours after STZ administration. These modifications occurred before a rise in blood glucose levels, implying that genes unrelated to hyperglycemia might be altered.[12] It has also been

suggested that through a p38 mitogen-activated protein kinase-dependent oxidative stress mechanism STZ reduces cardiac function.[13] Problems can also arise within this model, as the intensity of diabetes developed within STZ treated rats can differ, explicitly seen in lack of mitochondrial dysfunction in STZ diabetic rats without ketosis.[14]

Within rat hearts that were treated with STZ and diabetic for 8 weeks, there were noticeable changes to the ECM as reported before, such as fibrosis.[15,16] Upon observation, diabetic rat hearts were increased in size and dilated when compared to normal hearts. Interstitial fibrosis was noticeably spread through the endocardium and myocardium of left ventricle of diabetic rat hearts, whereas it was not in normal rat hearts. Perivascular fibrosis within the diabetic myocardium was also noticed with an increased amount of collagen and thickened walls. This could be due to an imbalance between collagen production and degradation, as MMP activity was also lowered in diabetic hearts. The diabetic condition is a prolonged, highly inflammatory state and inflammation activates increased collagen production through myofibroblast activation.[17,18]

As the hyperglycemia and dyslipidemia are traits of a diabetic environment, we investigated glycoxidation, specifically the presence of AGEs, and lipid accumulation within the rat heart tissue.[19,20] We found there was no significant difference in AGE expression within the tissue of normal and diabetic hearts, however AGEs circulating within diabetic blood vessels was visibly higher as seen in staining. AGEs are naturally occurring within tissue.[19] 8 weeks may have been too short of a time for AGEs to become overexpressed in the diabetic heart tissue and longer timepoints may be needed to see

over accumulation of AGEs in the tissue. Also, the AGE marker utilized for this study is a pan AGE marker. Other specific AGE markers, such as carboxymethyl lysine, could show significant differences between the hearts.[21] Diabetic hearts had noticeably increased lipid accumulation when compared to normal hearts. This has also been noted in literature.[22,23]

Programmed cellular death or apoptosis is another hallmark of DCMP. Metabolic changes, such as FFA usage and oxidative stress, lead to apoptosis. Caspase-3, an apoptosis marker, was significantly increased in diabetic rat hearts. Apoptosis has been shown to be increased in the STZ diabetic rat hearts.[24,25]

As oxidative stress is increased in the diabetic environment, we examined antioxidant defense mechanisms to determine if there were differences between the hearts.[26] SOD-2 and glutathione, endogenous cellular antioxidants, were investigated.[27] SOD-2 expression was sequestered in the myocardium of diabetic rat hearts, while SOD-2 was homogenously throughout normal hearts. SOD-2 and glutathione were both significantly reduced in diabetic rat hearts, illustrating that antioxidant defense mechanisms within these hearts are either hindered within the diabetic environment or have been depleted through excessive utilization.

ER stress has also been shown to be increased in the diabetic environment due to misfolded or unfolded proteins within the ER.[28] In this state, PERK is activated and triggers the unfolded protein response (UPR) pathway to control protein quality.[29] In diabetic rat hearts it was found that there was an upward trend of PERK, showing that ER

stress was slightly higher in diabetic rat hearts. This is however, one of three major pathways that can be activated and one facet of the story.

### 3.5 Conclusions

STZ type 1 diabetic rat models are useful for investigating ECM and cellular changes associated with DCMP in vivo, however there are discrepancies within the severity of diabetes in this model and systemic STZ administration does not allow for a full recapitulation diabetes seen in human patients. The tools and methods we employed in this diabetic rat heart study are suitable for analysis and highlighted DCMP alterations. These techniques will be useful for future studies into this disease.

### 3.6 Chapter 3 References


1 Forbes JM, Cooper ME, 1997 ADA clinical practice recommendations, up O the, Tight blood pressure control and risk of macrovascular and microvascular complications in type 2 diabetes: UK 38 UPDSG, Abbott C, *et al.* Mechanisms of diabetic complications. *Physiol Rev* 2013;**93**:137–88. https://doi.org/10.1152/physrev.00045.2011.

2 McGuire DK, Marx N. *Diabetes in Cardiovascular Disease: A Companion to Braunwald's Heart Disease*. 1st ed. Philadelphia, PA: Saunders; 2015.

3 Maisch B, Alter P, Pankuweit S. Diabetic cardiomyopathy--fact or fiction? *Herz* 2011;**36**:102–15. https://doi.org/10.1007/s00059-011-3429-4.

4 Yokoe S, Asahi M, Takeda T, Otsu K, Taniguchi N, Miyoshi E, *et al.* Inhibition of phospholamban phosphorylation by O-GlcNAcylation: Implications for diabetic cardiomyopathy. *Glycobiology* 2010;**20**:1217–26. https://doi.org/10.1093/glycob/cwq071.

5 Jia G, Hill MA, Sowers JR. Diabetic cardiomyopathy: An update of mechanisms contributing to this clinical entity. *Circ Res* 2018;**122**:624–38. https://doi.org/10.1161/CIRCRESAHA.117.311586.

6 Fuentes-Antras J, Picatoste B, Gomez-Hernandez A, Egido J, Tunon J, Lorenzo O. Updating experimental models of diabetic cardiomyopathy. *J Diabetes Res* 2015;**2015**:. https://doi.org/10.1155/2015/656795.

7 Bugger H, Abel ED. Rodent models of diabetic cardiomyopathy. *Dis Model Mech* 2009;**2**:454–66. https://doi.org/10.1242/dmm.001941.

8 Bugger H, Abel ED. Molecular mechanisms of diabetic cardiomyopathy. *Diabetologia* 2014;**57**:660–71. https://doi.org/10.1007/s00125-014-3171-6.

9 Lin Y, Kuro-o M, Sun Z. Genetic deficiency of anti-aging gene klotho exacerbates

early nephropathy in STZ-induced diabetes in male mice. *Endocrinology* 2013;**154**:3855–63. https://doi.org/10.1210/en.2013-1053.
10 Szasz T, Wenceslau CF, Burgess B, Nunes KP, Webb RC. Toll-like receptor 4 activation contributes to diabetic bladder dysfunction in a murine model of type 1 diabetes. *Diabetes* 2016;**65**:3754–64. https://doi.org/10.2337/db16-0480.
11 Bolzán AD, Bianchi MS. Genotoxicity of Streptozotocin. *Mutat Res - Rev Mutat Res* 2002;**512**:121–34. https://doi.org/10.1016/S1383-5742(02)00044-3.
12 Kume E, Aruga C, Ishizuka Y, Takahashi K, Miwa S, Itoh M, *et al.* Gene expression profiling in streptozotocin treated mouse liver using DNA microarray. *Exp Toxicol Pathol* 2005;**56**:235–44. https://doi.org/10.1016/j.etp.2004.09.002.
13 Wold LE, Ren J. Streptozotocin directly impairs cardiac contractile function in isolated ventricular myocytes via a p38 map kinase-dependent oxidative stress mechanism. *Biochem Biophys Res Commun* 2004;**318**:1066–71. https://doi.org/10.1016/j.bbrc.2004.04.138.
14 Lashin O, Romani A. Hyperglycemia does not alter state 3 respiration in cardiac mitochondria from type-I diabetic rats. *Mol Cell Biochem* 2004;**267**:31–7. https://doi.org/10.1023/B:MCBI.0000049360.75392.89.
15 Singh VP, Le B, Khode R, Baker KM, Kumar R. Intracellular Angiotensin II Production in Diabetic Rats Is Correlated With Cardiomyocyte Apoptosis, Oxidative Stress , and Cardiac Fibrosis. *Diabetes* 2008;**57**:3297–306. https://doi.org/10.2337/db08-0805.
16 Chen YF, Shibu MA, Fan MJ, Chen MC, Viswanadha VP, Lin YL, *et al.* Purple rice anthocyanin extract protects cardiac function in STZ-induced diabetes rat hearts by inhibiting cardiac hypertrophy and fibrosis. *J Nutr Biochem* 2016;**31**:98–105. https://doi.org/10.1016/j.jnutbio.2015.12.020.
17 Yang L, Zhao D, Ren J, Yang J. Endoplasmic reticulum stress and protein quality control in diabetic cardiomyopathy. *Biochim Biophys Acta* 2015;**1852**:209–18. https://doi.org/10.1016/j.bbadis.2014.05.006.
18 Turner NA. Inflammatory and fibrotic responses of cardiac fibroblasts to myocardial damage associated molecular patterns (DAMPs). *J Mol Cell Cardiol* 2016;**94**:189–200. https://doi.org/10.1016/j.yjmcc.2015.11.002.
19 Bodiga VL, Eda SR, Bodiga S. Advanced glycation end products: Role in pathology of diabetic cardiomyopathy. *Heart Fail Rev* 2014. https://doi.org/10.1007/s10741-013-9374-y.
20 Chong CR, Clarke K, Levelt E. Metabolic remodelling in diabetic cardiomyopathy. *Cardiovasc Res* 2017;**113**:422–30. https://doi.org/10.1093/cvr/cvx018.
21 Weiss MF, Erhard P, Kader-Attia FA, Wu YC, Deoreo PB, Araki A, *et al.* Mechanisms for the formation of glycoxidation products in end-stage renal disease. *Kidney Int* 2000;**57**:2571–85. https://doi.org/10.1046/j.1523-1755.2000.00117.x.
22 Inoue T, Inoguchi T, Sonoda N, Hendarto H, Makimura H, Sasaki S, *et al.* GLP-1 analog liraglutide protects against cardiac steatosis, oxidative stress and apoptosis in streptozotocin-induced diabetic rats. *Atherosclerosis* 2015;**240**:250–9.

https://doi.org/10.1016/j.atherosclerosis.2015.03.026.
23 Naidu PB, Ponmurugan P, Begum MS, Mohan K, Meriga B, Ravindarnaik R, *et al.* Diosgenin reorganises hyperglycaemia and distorted tissue lipid profile in high-fat diet-streptozotocin-induced diabetic rats. *J Sci Food Agric* 2015;**95**:3177–82. https://doi.org/10.1002/jsfa.7057.
24 Amin AH, El-Missiry MA, Othman AI. Melatonin ameliorates metabolic risk factors, modulates apoptotic proteins, and protects the rat heart against diabetes-induced apoptosis. *Eur J Pharmacol* 2015;**747**:166–73. https://doi.org/10.1016/j.ejphar.2014.12.002.
25 Huang PC, Wang GJ, Fan MJ, Asokan Shibu M, Liu YT, Padma Viswanadha V, *et al.* Cellular apoptosis and cardiac dysfunction in STZ-induced diabetic rats attenuated by anthocyanins via activation of IGFI-R/PI3K/Akt survival signaling. *Environ Toxicol* 2017;**32**:2471–80. https://doi.org/10.1002/tox.22460.
26 Faria A, Persaud SJ. Cardiac oxidative stress in diabetes: Mechanisms and therapeutic potential. *Pharmacol Ther* 2017;**172**:50–62. https://doi.org/10.1016/j.pharmthera.2016.11.013.
27 Huynh K, Bernardo BC, McMullen JR, Ritchie RH. Diabetic cardiomyopathy: Mechanisms and new treatment strategies targeting antioxidant signaling pathways. *Pharmacol Ther* 2014;**142**:375–415. https://doi.org/10.1016/j.pharmthera.2014.01.003.
28 Tse G, Lai ETH, Tse V, Yeo JM. Molecular and Electrophysiological Mechanisms Underlying Cardiac Arrhythmogenesis in Diabetes Mellitus. *J Diabetes Res* 2016;**2016**:. https://doi.org/10.1155/2016/2848759.
29 Stratmann B, Tschoepe D. The diabetic heart: sweet, fatty and stressed. *Expert Rev Cardiovasc Ther* 2011;**9**:1093–6. https://doi.org/10.1586/erc.11.109.

# CHAPTER 4: ASSESMENT OF A 2D IN VITRO HUMAN CARDIOMYOCYTE DIABETIC CARDIAC MODEL

## 4.1 Introduction

Cardiomyocyte (CM) adaptations in response to the diabetic environment are of interest in the beginning stages of diabetic cardiomyopathy (DCMP). CMs are responsible for contraction of the myocardium and when they are compromised, so is overall functionality of the heart.[1] Hyperglycemia and dyslipidemia in the diabetic milieu, lead to a loss of metabolic flexibility within the cell.[2] Free fatty acids are preferentially used as an energy source, followed by lipid accumulation and peroxidation, with the over formation of reactive oxygen species (ROS).[3] ROS is produced faster than the cell can eliminate it through endogenous antioxidant defenses, causing oxidative stress.[4,5] Cellular autophagy and apoptosis follow prolonged oxidative stress.[6,7] Within this diabetic climate, advanced glycation endproducts (AGEs) aggregate, forming irreversibe crosslinks, with a decrease in matrix metalloproteinase (MMP) activity.[8] This imbalance gives rise to tissue fibrosis. CMs become hypertrophic as they must work that much harder to maintain efficiency to compensate for CM loss and tissue stiffening.[9] Overtime, this can lead to heart failure.

To understand CM modifications in the diabetic environment, two-dimensional (2D) cell culture of this cell type has been employed with the addition of glucose to the cell culture media. Cells such as neonatal rat CMs, induced pluripotent stem cells (iPSCs), progenitor CMs, immortalized CMs, and embryonic stem cells (ESCs) have been utilized for these studies and have shown to be altered under these conditions.[10–15] We chose to investigate human progenitor CMs (hCMs) as they are commercially

available, able to expand in culture, adult human cells, and there were no ethical concerns attached, as there are with ESCs.[16] We hypothesized that we would see alterations and responses in these hCMs known in the diabetic state by culturing them with additional glucose. The goal of this initial study was to determine if these cells would be suitable for the creation of a three-dimensional (3D), dynamic in vitro model of DCMP.

## 4.2 Materials and Methods

### *4.2.1 Materials*

Progenitor human cardiac myocytes (hCM) were from Promocell GmbH (Heidelberg, Germany). Dulbecco's Modified Eagle Medium (DMEM) and antibiotic / antimycotic were from Corning Incorporated (Oneonta, NY). Fetal Bovine Serum (FBS) was from Atlanta Biologicals (Atlanta, GA). Bicinchoninic acid protein assay was from Pierce Biotech (Rockford, IL). Electrophoresis apparatus, gel imager and imaging software, chemicals, and molecular weight standards were from Bio-rad (Hercules, CA). BM Chemiluminescence Western Blotting kit (Mouse/ Rabbit) was obtained from Roche (Indianapolis, IN). Paraformaldehyde was from Electron Microscopy Sciences (Hartfield, PA). Triton X-100 was from Alfa Aesar (Ward Hill, MA). Bovine Serum Albumin was from Rockland Immunochemicals Inc. (Limerick, PA). The following antibodies were used: rabbit anti-superoxide dismutase-2 (Abcam, ab13534), rabbit anti-caspase-3 (Millipore, 06-735 or Abcam, ab32042), rabbit anti-receptor for advanced glycation endproducts (Abcam, ab37647), mouse anti-N-epsilon-(carboxylmethyl)lysine (R&D Systems, MAB3247), rabbit anti-light chain 3B (Abcam, ab48394), and rabbit anti-protein kinase RNA-like endoplasmic reticulum kinase (Abcam, ab192591). Alexa

Fluor® fluorescent secondary antibodies (mouse and rabbit) were purchased from Molecular Probes (Eugene, OR). All other chemicals were of the highest purity and purchased from Sigma-Aldrich Corporation (Lakewood, NJ).

*4.2.2 Culture of Human Cardiomyocytes*

Progenitor human cardiac myocytes (hCMs) were cultured for 14 days in normal glucose and high glucose media. Normal and diabetic media constituted of Dulbecco's Modified Eagle Medium (DMEM), 10% Fetal Bovine Serum (FBS), and 1% antibiotic/antimycotic (penicillin-streptomycin), with 5mM (1g/L) and 25mM (4.5g/L) glucose, respectively.

*4.2.3 Immunofluorescence for Caspase-3, SOD-2 and CML/RAGE*

Immunofluorescence was used for the visualization of caspase-3, superoxide dismutase 2 (SOD-2,) and carboxymethyl lysine/receptor for advanced glycation endproduct (CML/RAGE) in normal and high glucose conditioned hCMs. Cells were fixed with 4% warm paraformaldehyde for 20 minutes and then permeabilized with 0.2% Triton X-100 (10 minutes) at room temperature. A blocking solution of 5% bovine serum albumin and 0.05% Triton X-100 was then applied for 45 minutes. Cells were incubated in primary antibodies (rabbit anti-caspase-3 Abcam 1ug/mL, rabbit anti-SOD-2 at 4ug/mL, or mouse anti-CML at 1ug/mL and rabbit anti-RAGE at 1ug/mL) in a 1 to 1 mixture of blocking solution to phosphate buffered saline for 2 hours. For negative controls, a 1 to 1 solution of blocking solution to phosphate buffered saline was used, without primary antibodies. Alexa Fluor® fluorescent secondary antibodies (anti-rabbit or anti-mouse) were applied for 1 hour at room temperature. Cell nuclei were stained

with 4',6-diamidino-2-phenylindole (DAPI) and a Zeiss Axiovert 40CFL microscope with AxioVision Release 4.6.3 digital imaging software, UV light box, and filter from Carl Zeiss MicroImaging, Inc. (Thornwood, NY), was utilized to obtain immunofluorescence images.

*4.2.4 Detection of Caspase-3, SOD-2, CML, and LC3B*

Western blotting was employed to compare amounts of caspase-3, SOD-2, CML, light chain 3B (LC3B), and protein kinase RNA-like endoplasmic reticulum kinase (PERK) between normal glucose (n=3,4,4,4,4 respectively) and high glucose (n=3,4,4,5,3 respectively) conditions. Proteins were extracted by radioimmunoprecipitation assay (RIPA) extraction buffer (50mM Tris-HCl pH 7.4, 150mM sodium chloride (NaCl), 1mM ethylenediaminetetraacetic acid (EDTA), 1% Triton X-100, 1% Sodium Deoxycholate, 0.1% sodium dodecyl sulfate (SDS), with protease inhibitor cocktail). Protein concentrations in the samples were found using a bicinchoninic acid protein (BCA) assay. For each sample, 20ug of protein per lane was loaded and a pre-stained molecular weight standard was loaded in one of the lanes. Protein from the gels were transferred to polyvinylidine fluoride membranes. Primary antibodies (rabbit anti-caspase-3 Millipore 1ug/mL, rabbit anti-SOD-2 1ug/mL, mouse anti-CML 1ug/mL, rabbit anti-LC3B 1ug/mL, or rabbit anti-PERK 1ug/mL) were applied overnight at 4°C. The secondary antibody from the anti-mouse/rabbit kit was then applied for 45 minutes at room temperature. The polyvinylidine fluoride membranes were fluorescently tagged with detection solution from the anti-mouse/rabbit kit (1 minute) and then imaged using

the Chemi-Doc™ XRS+ system from Bio-rad (Hercules, CA). Relative band intensities were determined using Bio-rad Image Lab Software Version 5.1, beta build 1.

Relative amounts of caspase-3 within cell cultures were examined with the ApoTarget Caspase-3 / CPP32 Colorimetric Protease Assay from Invitrogen (Carlsbad, CA). Manufacturer's protocol was followed. Total protein was measured via a BCA assay and 100ug was used per sample (n=2 per group). Intensities were measured using the Synergy H1 Hybrid Reader System from BioTek (Winooski, VT).

*4.2.5 Matrix Metalloproteinase Activity Analysis*

Protein extracts from hCMs were taken from normal (n=4) and high (n=4) glucose groups using the RIPA buffer extraction method (above). Protein concentrations in the samples were found using a BCA assay. For each sample, 20ug of protein per lane were loaded into a gelatin zymography gel, as was a pre-stained molecular weight standard into a separate lane. After electrophoresis separation, the zymography gel was washed in a triton-X solution and matrix metalloproteinases (MMPs) were activated with a brij-35 development buffer for 24 hours at 37 degrees C. After staining with Coomassie, MMP clear bands were imaged using the Chemi-Doc™ XRS+ system and evaluated by densitometry using the using Bio-rad Image Lab Software.

*4.2.6 Lipid Accumulation and Peroxidation Staining*

Intracellular lipid accumulation was visualized via Oil Red O staining. Briefly, cells were fixed in 4% paraformaldehyde, rinsed in distilled deionized water ($ddH_2O$), rinsed in 60% isopropanol, and stained in 0.3% Oil Red O in isopropanol solution. Cells were then rinsed twice in 60% isopropanol, stained in a 1 to 1 hematoxylin to $ddH_2O$

solution, and rinsed in $ddH_2O$. Light images were taken on a Zeiss Axiovert 40CFL microscope with AxioVision Release 4.6.3 digital imaging software from Carl Zeiss MicroImaging, Inc. (Thornwood, NY).

Lipid peroxidation was investigated in normal and high glucose hCM cultures by employing the Click-iT® Lipid Peroxidation Detection with Linoleamide Alkyne Kit from Molecular Probes (Eugene, OR). Manufacturer protocol was utilized. Cells nuclei were stained with DAPI and imaged via the immunofluorescence protocol previously discussed (above).

*4.2.7 Reactive Oxygen Species Generation Analysis*

Reactive oxygen species (ROS) generation in normal and high glucose hCM cultures were determined by utilizing the CellROX® Oxidative Stress Reagents Kit from Molecular Probes (Eugene, OR). Manufacturer protocol was utilized. Cell nuclei were stained with DAPI and imaged using immunofluorescence protocol mentioned previously (above).

*4.2.8 Autophagy Inspection*

Autophagy in normal and high glucose conditioned hCMs was studied by utilizing the LC3B Antibody Kit for Autophagy from Invitrogen (Carlsbad, CA). Manufacturer protocol was utilized. Cell nuclei were stained with DAPI and immunofluorescence images were captured as discussed before (above).

*4.2.9 Statistical Inquiry*

Results are expressed at mean ± standard deviation (SD). Statistical analysis was performed between groups utilizing Welch's two-tailed t-test in excel. Significance was determined with an alpha (α) value of 0.05.

## 4.3 Results

*4.3.1 Advanced Glycation Endproducts and Matrix Metalloproteinase Activity*

Analysis of in vitro 2D hCM cultures after two weeks in normal or high glucose was performed to determine if there were noticeable changes in expression of advanced glycation endproducts (AGEs) with their receptor (RAGE) and matrix metalloproteinase (MMP) activity. Immunofluorescence images of carboxymethyl lysine (CML), an AGE, and RAGE, showed greater expression of both in high glucose hCM cultures when compared to hCM cultured in normal glucose (**Figure 4.2**). Based on western blotting, CML illustrated an upward trend in high glucose hCM treated cells. There was a downward trend in MMP activity in high glucose cultured hCM as revealed by gelatin zymography of protein lysates (**Figure 4.1**).

*4.3.2 Lipotoxicity and Reactive Oxygen Species Formation*

Determination of lipotoxicity and reactive oxygen species (ROS) in normal and high glucose hCM cultures was executed with oil red O lipid staining and specialized kits for lipid peroxidation and ROS detection. By using the Click-iT® Lipid Peroxidation Detection with Linoleamide Alkyne Kit, we were able to observe increased lipid peroxidation within hCM cultured in high glucose (**Figure 4.3**). hCM cultured in high glucose also showed higher lipid accumulation as visualized by oil red O lipid staining.

ROS aggregation was examined with the CellROX® Oxidative Stress Reagents Kit. It was noticed that high glucose hCM had more formation of ROS, than normal glucose hCM.

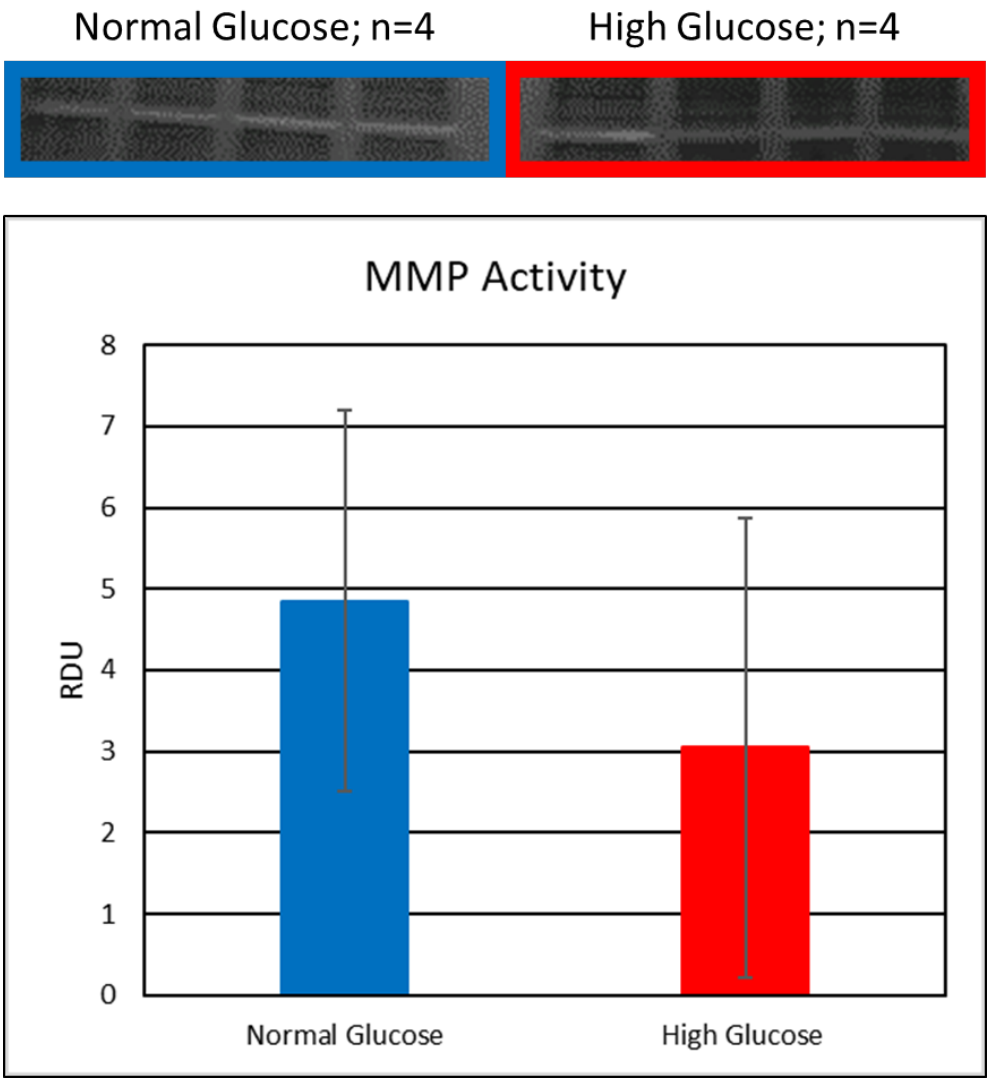


**Figure 4.1:** Matrix metalloproteinase (MMP) activity analysis. Gelatin zymography was used to compare MMP activity in high and normal glucose hCM conditions. RDU=relative densitometry units.

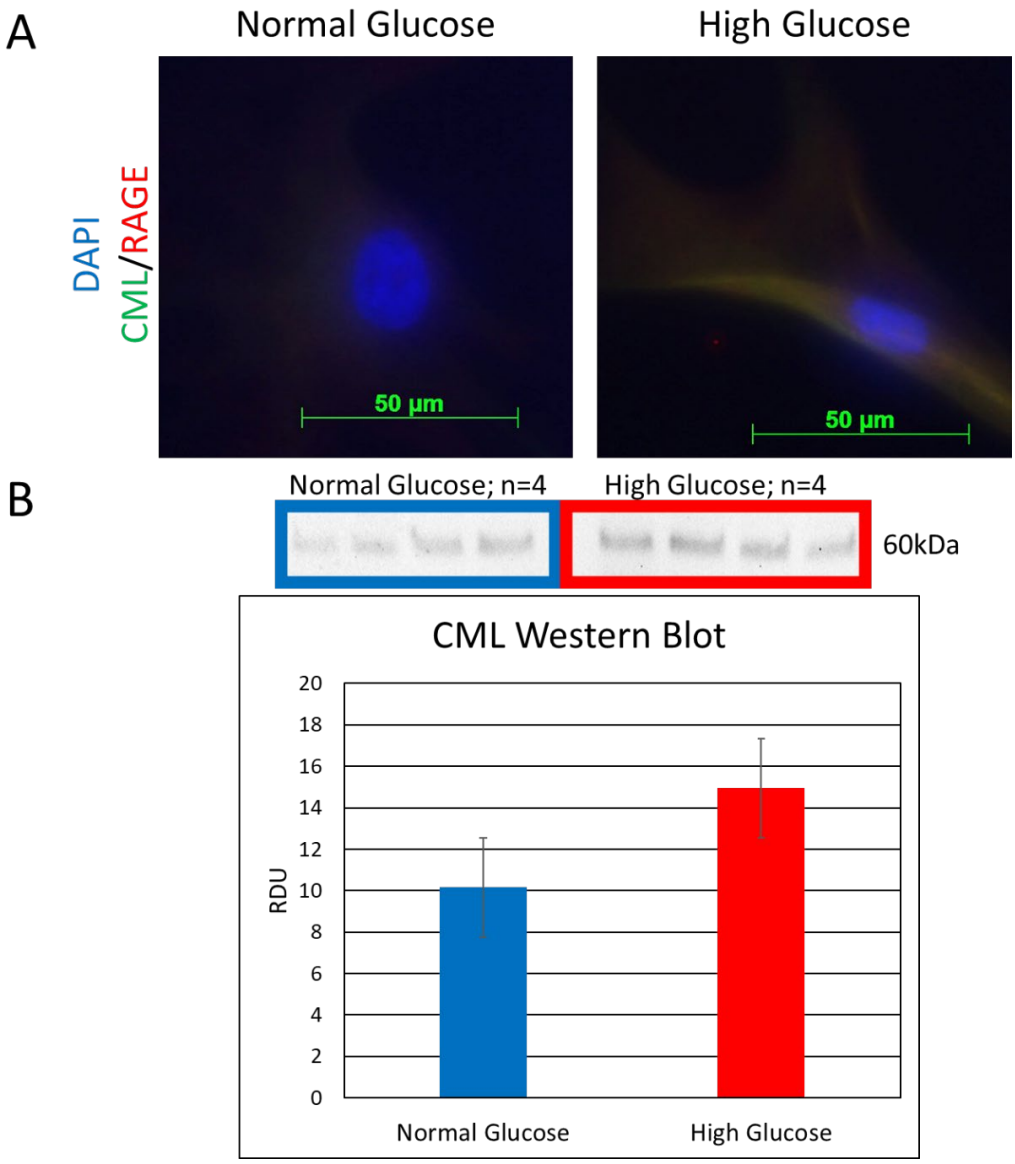


**Figure 4.2:** Advanced glycation endproducts and their receptor in hCM high and normal glucose cell culture. (A) Immunofluorescence staining for an advanced glycation endproduct, carboxymethyl lysine (CML, green), receptor for advanced glycation endproducts (RAGE, red), and staining with 4',6-diamidino-2-phenylindole (DAPI) for nuclei (blue) in hCM cell cultures. Negative controls not shown. (B) Western blotting for CML in hCM cultures. RDU=relative densitometry units.

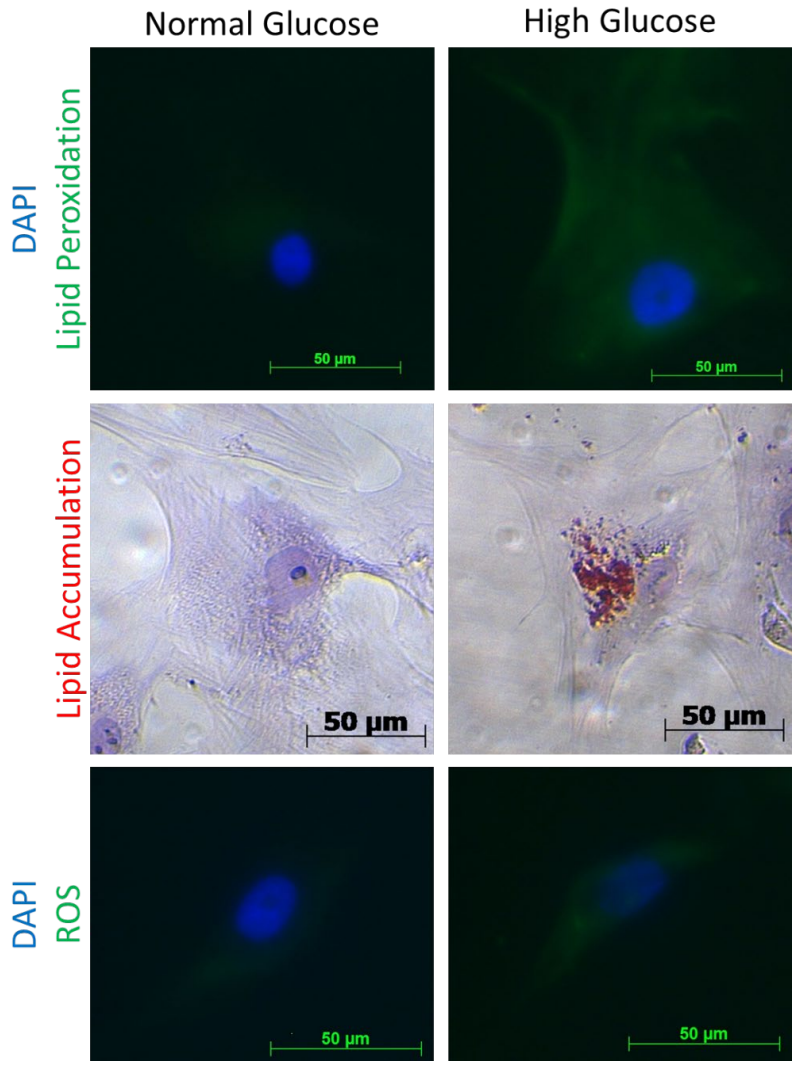


**Figure 4.3:** Lipotoxicity and reactive oxygen species formation in hCM culture. Lipid peroxidation staining (green) of hCM in normal and high glucose conditions with Click-iT® Lipid Peroxidation Detection with Linoleamide Alkyne Kit and nuclei staining (blue) with DAPI (top). Oil red O lipid staining (red) in hCM culture (middle) with cell hematoxylin staining (purple). Reactive oxygen species (ROS) visualization (green) in hCM culture with CellROX® Oxidative Stress Reagents Kit and DAPI nuclei staining (blue).

*4.3.3 Endoplasmic Reticulum Stress and Superoxide Dismutase-2 Antioxidant Defense*

Endoplasmic reticulum stress was analyzed with a marker, protein kinase RNA-like endoplasmic reticulum kinase (PERK). Western blotting detection showed no statistical difference between groups (**Figure 4.4**). Endogenous antioxidant defenses against ROS were assessed in normal and high glucose conditioned hCM by investigating expression of superoxide dismutase-2 (SOD-2), a cellular mitochondrial scavenger. Immunofluorescence staining of SOD-2 in hCM showed that this protein was expressed in both normal and high glucose cultures (**Figure 4.5**). Western blotting protein analysis of SOD-2, also confirmed this, as there was no difference in expression between groups.

*4.3.4 Apoptosis and Autophagy*

Programmed cellular apoptotic death and autophagic organelle recycling were assessed in hCM normal and high glucose cultures to see if high glucose conditions induced these outcomes, as seen in diabetic conditions. Immunofluorescence staining for caspase-3, an apoptosis marker, illustrated higher caspase-3 expression in high glucose hCM when compared to normal glucose hCM (**Figure 4.6**). Examination of caspase-3 in protein lysates by an assay revealed an upward trend of apoptosis in hCM in high glucose, however western blotting of caspase-3 western blotting showed no difference between the two groups. Visualization of light chain 3B (LC3B), an autophagy marker, was performed with the LC3B Antibody Kit for Autophagy and showed increased expression in high glucose hCM (**Figure 4.7**). Western blotting investigation of LC3B demonstrated an upward trend with high glucose conditioning of hCM compared to normal hCM.

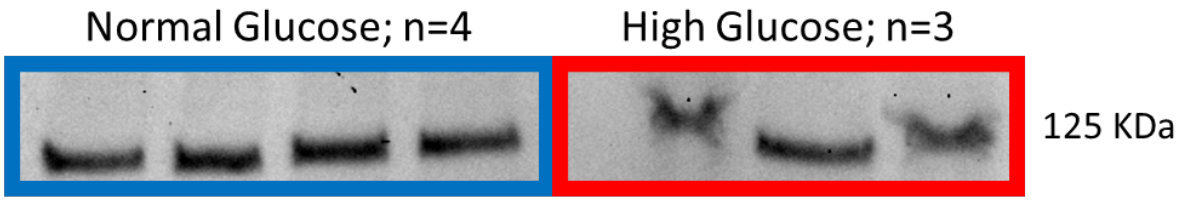


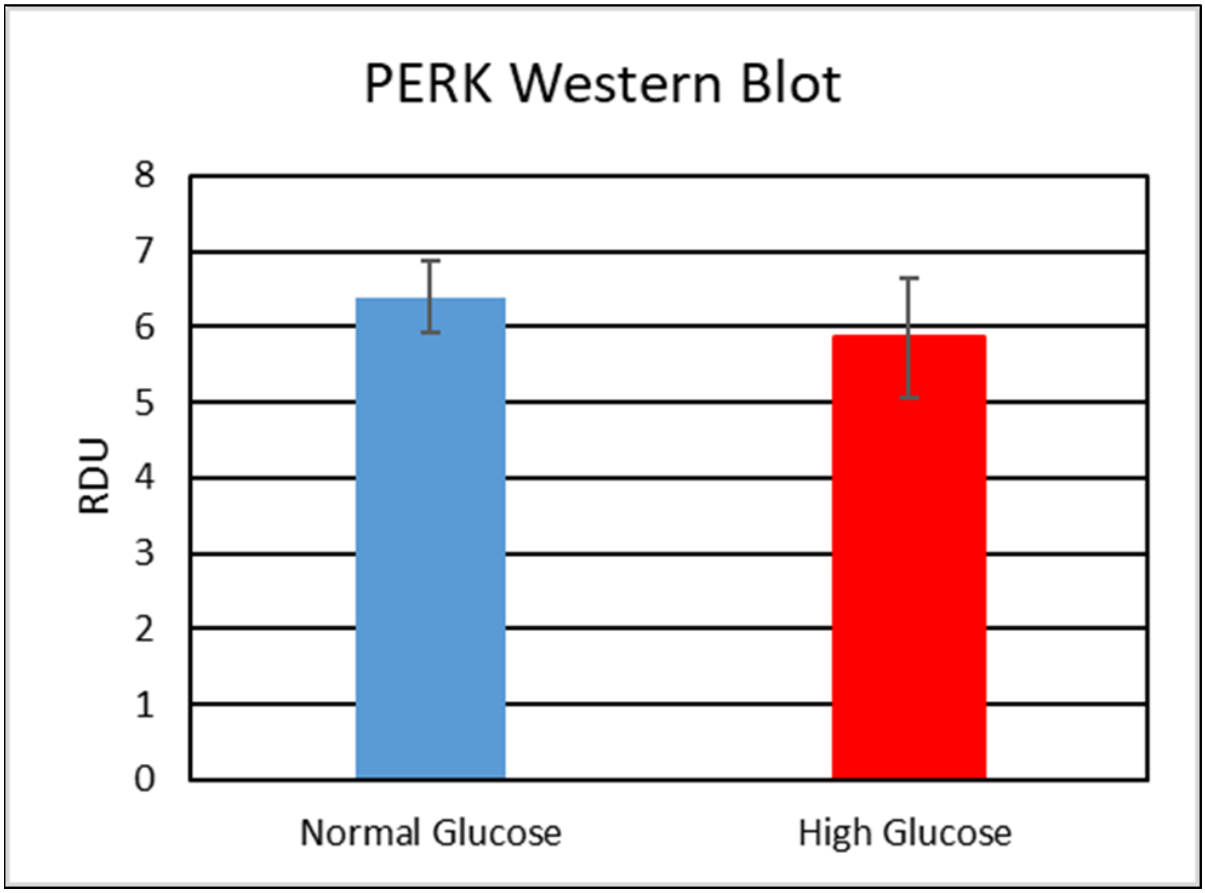


**Figure 4.4:** Endoplasmic reticulum stress examination in normal and high glucose hCM culture. Western blotting of protein kinase RNA-like endoplasmic reticulum kinase (PERK), an ER stress marker. RDU= relative densitometry units.

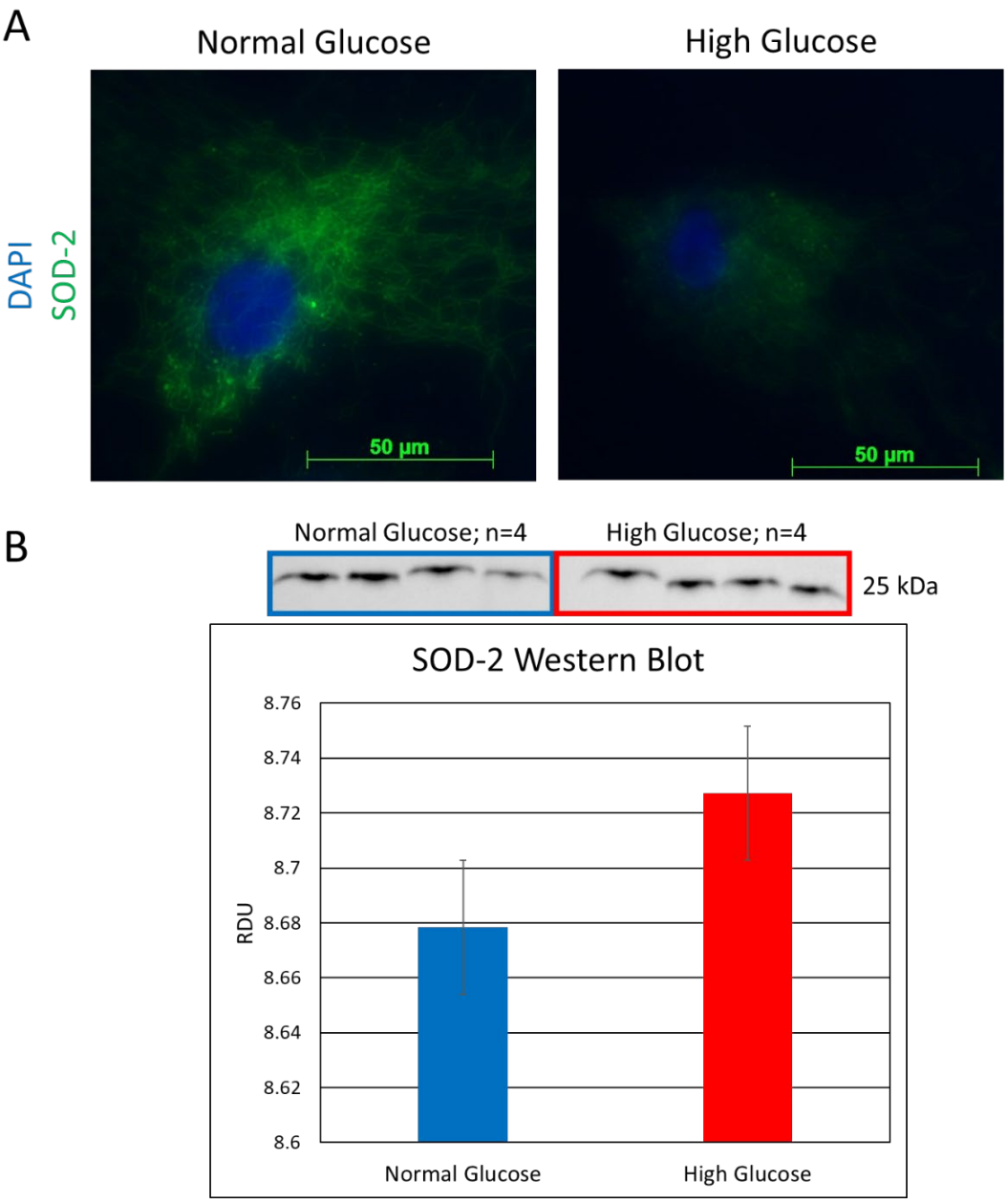


**Figure 4.5:** Analysis of superoxide dismutase-2 (SOD-2) antioxidant defense in high and normal glucose hCM cultures. (A) Immunofluorescence staining of SOD-2 (green) with DAPI (blue) nuclei staining of hCM. Negative controls not shown. (B) Western blotting for SOD-2 expression in hCM culture. RDU=relative densitometry units.

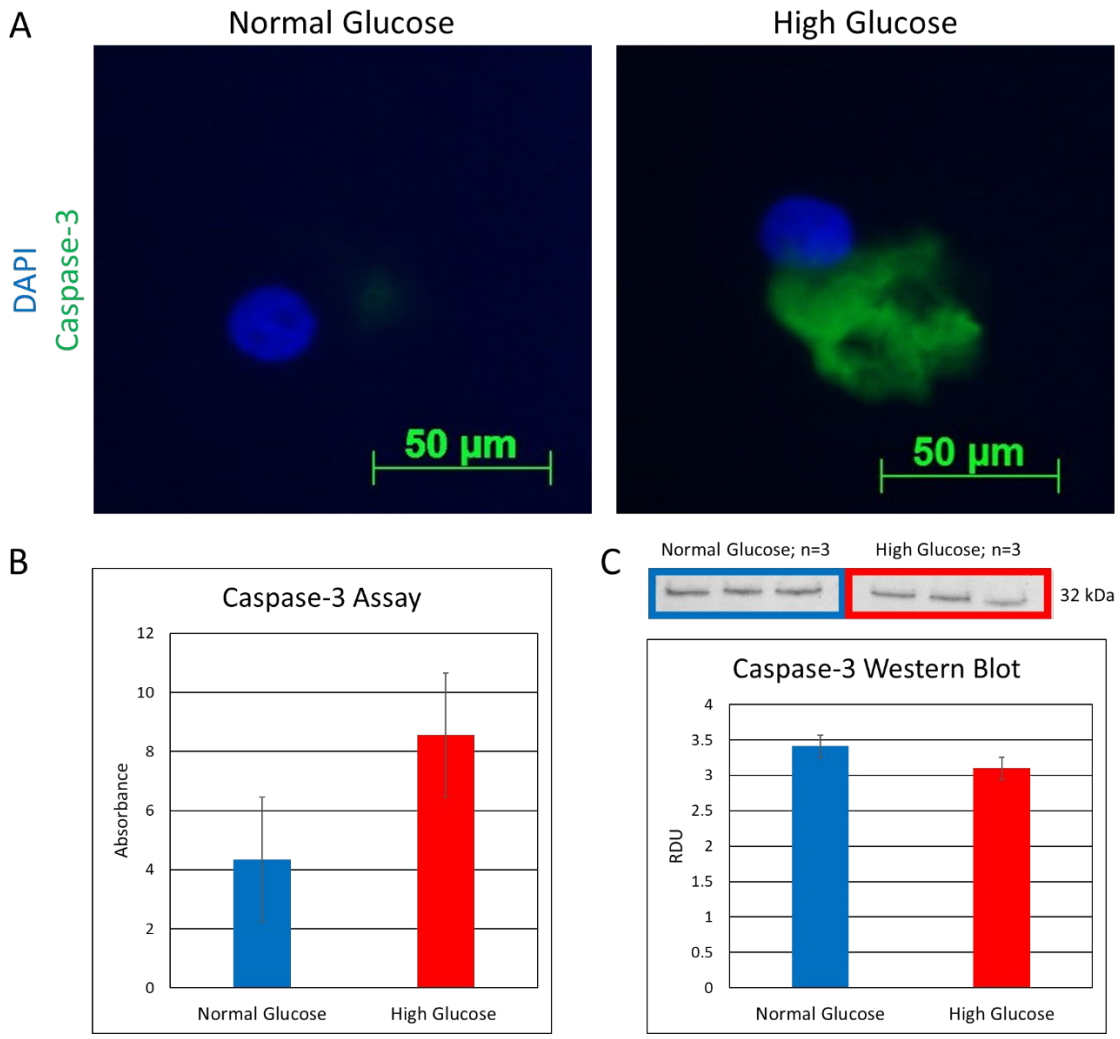


**Figure 4.6:** Apoptosis in hCM normal and high glucose culture. (A) Immunofluorescence for caspase-3 (green), an apoptosis marker, with DAPI (blue) nuclei staining in hCM culture. Negative controls not shown. (B) Caspase-3 assay and (C) western blotting was used for caspase-3 for apoptosis detection in normal and high glucose conditioning of hCM. RDU=relative densitometry units.

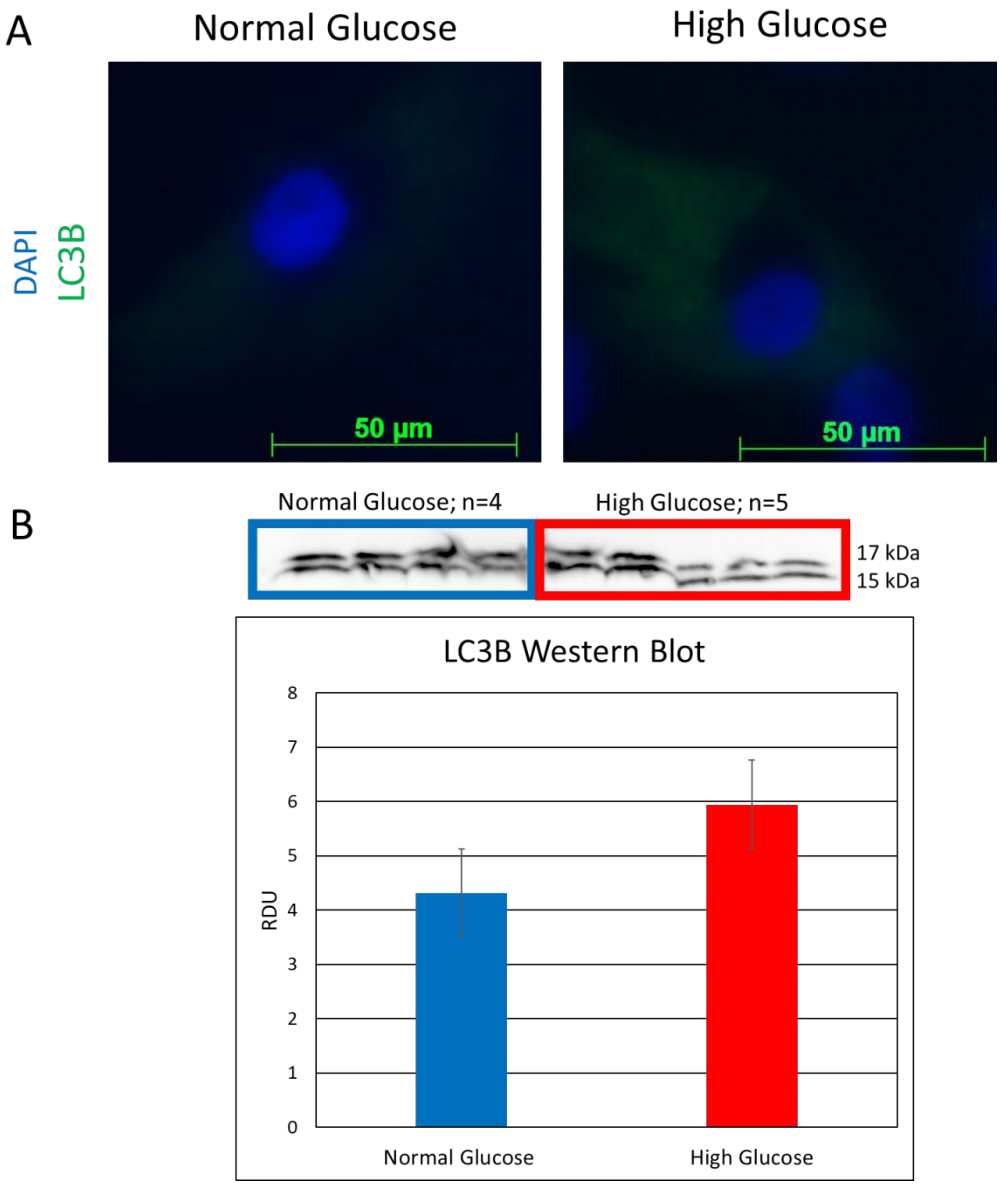


**Figure 4.7:** Autophagy investigation in high and normal glucose environments for hCM. (A) Autophagy visualization in hCM employing light chain 3B (LC3B, green) Antibody Kit for Autophagy staining with nuclei staining via DAPI (blue). Negative controls not shown. (B) Western blotting of hCM protein lysates for LC3B, an autophagy marker. RDU=relative densitometry units.

## 4.4 Discussion

Cell culture has provided a simple and controllable in vitro model over the years to study normal cellular function and disease related alterations that occur within specific cardiac cell types, such as CMs, fibroblasts, endothelial, and smooth muscle cells.[17–19] These studies have provided starting points for research into regulatory pathways important for healthy cell function, as well as underlying mechanisms of pathological disease progression. Modifications at the micro cellular level ultimately lead to macro functional problems at the tissue, organ, and system levels. Understanding how specialized cells within a tissue operate and adapt within a disease are the keys to diagnosis of the patient and provide targets for treatment.

While cell culture is great for initial studies, its simplistic and static nature does have some pitfalls. The human body is a highly complicated and dynamic machine with many mechanisms still to be understood. Cell culture models are reproducible and cell media is easily tailored with the addition of chemicals, however diseases exist on a spectrum and across multiple systems in the body.[20] Media does not include important aspects, such as paracrine factors from other cells. Crosstalk via paracrine factors between cells and cell types within an altered state can influence how they themselves change in response, such as CM hypertrophy and fibroblast proliferation in cardiac disease.[21] In standard culture, cells are grown on a 2D negatively charged polystyrene surface. Extracellular matrix components, such as collagen and fibronectin, can be used as surface coatings to better mimic the physiologic environment, however, this still does not capture the sophistication of the human body.[22]

We sought to investigate and characterize cells in an in vitro 2D DCMP model before pursuing usage within a more complicated 3D in vitro disease model. Early alterations of CMs are still not understood within this disease, making it difficult to determine targeted therapies and diagnostic markers for DCMP.[23] Throughout the years, CMs, such as neonatal rat CMs, iPSCs differentiated into CMs, progenitor CMs, immortalized CMs, and ESCs, have been utilized by many research groups for understanding cellular adaptations in myocardial diseases as well as diabetic studies.[10,13–15,24,25] For our study we decided to use human progenitor CMs (hCMs), as they were commercially available, able to expand in culture, adult human cells, and there were no ethical concerns attached, like ESCs.[16] It is important to note that while these cells are isolated from adult hearts, they have characteristics unlike adult CMs, such as the ability to proliferate and potential to differentiate. These specific cells from the manufacturer have been used for many applications such as inflammatory, hypoxic, metabolic, toxicity, and pharmacological studies.[13,26–31]

For this preliminary study of a simple 2D DCMP model, the "diabetic" environment was produced by the addition of glucose to culture media. After two weeks, cells were analyzed for alterations known to exist within DCMP, such as lipid accumulation and peroxidation, ROS formation, increased cell death and autophagy, accumulation of AGEs with increased expression of their receptor, RAGE, endoplasmic reticulum (ER) stress, changes in endogenous antioxidant defense mechanisms, and lessened MMP activity.[32,33] This was performed to determine if these cells would be suitable for future studies.

Hallmarks of diabetes and DCMP include the accumulation of AGEs and increased expression of its receptor, RAGE.[34,35] The hyperglycemic environment leads to the buildup of these irreversible crosslinks, which can detrimentally alter the extracellular matrix.[36] As the diabetic state is highly inflammatory, RAGE becomes overexpressed via a positive feedback cycle.[37] This was also shown to be the case within our in vitro model as CML, an AGE, and RAGE expression were increased when cultured in high glucose. We also investigated MMP activity, as in DCMP it is inhibited.[38] Within our model, there was a downward trend in the high glucose groups.

Hyperglycemia and dyslipidemia in diabetes cause loss of metabolic plasticity, leading to a surge in usage of free fatty acids.[32] From this imbalance oxidative stress, ER stress, lipid peroxidation, and lipid aggregation originate.[5] There were noted increases of all these features, except for ER stress, in the high glucose cultures of hCM. Increases in all of these traits have been previously reported in high glucose studies involving neonatal and adult rat CMs, hiPSCs, and progenitor hCM sourced from the same company.[10,12,13,39,40] ER stress was not shown to be increased in high glucose cell culture conditions, however this study was only for two weeks and only a marker for one of three pathways activated by ER stress was investigated. It may be worthwhile to look at other pathway markers, as they may activated at earlier timepoints.

These metabolic disturbances and unbalanced state can lead to overwhelmed antioxidant defense mechanisms followed by enhanced cellular organelle recycling via autophagy and increased programmed cell death through apoptosis.[6,41] There were no differences seen in the expression of SOD-2, an endogenous mitochondrial defense

mechanism, between the two groups within two weeks. Autophagy and apoptosis were increased in high glucose hCM. Escalation of apoptosis in inflated glucose conditions has been seen in hiPSCs differentiated into CMs and neonatal rat CMs.[10,11]

### 4.5 Conclusions

Cell culture is a good stepping stone for initial investigations of homeostatic cellular functions and pathological alterations of specific cell types, however it is unable to recapitulate the complexity or diversity of the human body. Progenitor hCM utilized for this preliminary study responded to the "diabetic" environment induced with the addition of glucose for two weeks. They will be useful in building a tissue engineered DCMP model to study early cellular changes in a 3D and dynamic in vitro model.

### 4.6 Chapter 4 References


1 Iaizzo PA. Handbook of cardiac anatomy, physiology, and devices, third edition. *Handb Card Anatomy, Physiol Devices, Third Ed* 2015:1–817. https://doi.org/10.1007/978-3-319-19464-6.

2 Maisch B, Alter P, Pankuweit S. Diabetic cardiomyopathy - Fact or fiction? *Herz* 2011;**36**:102–15. https://doi.org/10.1007/s00059-011-3429-4.

3 Ni R, Cao T, Xiong S, Ma J, Fan G, Lace JC, *et al.* Free Radical Biology and Medicine Therapeutic inhibition of mitochondrial reactive oxygen species with mito-TEMPO reduces diabetic cardiomyopathy 2016;**90**:12–23. https://doi.org/10.1016/j.freeradbiomed.2015.11.013.

4 Octavia Y, Brunner-La Rocca HP, Moens AL. NADPH oxidase-dependent oxidative stress in the failing heart: From pathogenic roles to therapeutic approach. *Free Radic Biol Med* 2012;**52**:291–7. https://doi.org/10.1016/j.freeradbiomed.2011.10.482.

5 Faria A, Persaud SJ. Cardiac oxidative stress in diabetes: Mechanisms and therapeutic potential. *Pharmacol Ther* 2017;**172**:50–62. https://doi.org/10.1016/j.pharmthera.2016.11.013.

6 Kobayashi S, Liang Q. Autophagy and mitophagy in diabetic cardiomyopathy. *Biochim Biophys Acta - Mol Basis Dis* 2015;**1852**:252–61. https://doi.org/10.1016/j.bbadis.2014.05.020.

7 Ouyang C, You J, Xie Z. The interplay between autophagy and apoptosis in the diabetic heart. *J Mol Cell Cardiol* 2014. https://doi.org/10.1016/j.yjmcc.2013.10.014.

8 Bodiga VL, Eda SR, Bodiga S. Advanced glycation end products: Role in pathology of diabetic cardiomyopathy. *Heart Fail Rev* 2014. https://doi.org/10.1007/s10741-013-9374-y.
9 Falcão-Pires I, Leite-Moreira AF. Diabetic cardiomyopathy: Understanding the molecular and cellular basis to progress in diagnosis and treatment. *Heart Fail Rev* 2012;**17**:325–44. https://doi.org/10.1007/s10741-011-9257-z.
10 Guo S, Yao Q, Ke Z, Chen H, Wu J, Liu C. Resveratrol attenuates high glucose-induced oxidative stress and cardiomyocyte apoptosis through AMPK. *Mol Cell Endocrinol* 2015;**412**:85–94. https://doi.org/10.1016/j.mce.2015.05.034.
11 Ng K-M, Lau Y-M, Dhandhania V, Cai Z-J, Lee Y-K, Lai W-H, *et al.* Empagliflozin Ammeliorates High Glucose Induced-Cardiac Dysfuntion in Human iPSC-Derived Cardiomyocytes. *Sci Rep* 2018;**8**:14872. https://doi.org/10.1038/s41598-018-33293-2.
12 Drawnel FM, Boccardo S, Prummer M, Delobel F, Graff A, Weber M, *et al.* Disease modeling and phenotypic drug screening for diabetic cardiomyopathy using human induced pluripotent stem cells. *Cell Rep* 2014;**9**:810–21. https://doi.org/10.1016/j.celrep.2014.09.055.
13 Maalouf RM, Eid AA, Gorin YC, Block K, Escobar GP, Bailey S, *et al.* Nox4-derived reactive oxygen species mediate cardiomyocyte injury in early type 1 diabetes. *Am J Physiol Cell Physiol* 2012;**302**:C597-604. https://doi.org/10.1152/ajpcell.00331.2011.
14 Jeyabal P, Thandavarayan RA, Joladarashi D, Suresh Babu S, Krishnamurthy S, Bhimaraj A, *et al.* MicroRNA-9 inhibits hyperglycemia-induced pyroptosis in human ventricular cardiomyocytes by targeting ELAVL1. *Biochem Biophys Res Commun* 2016;**471**:423–9. https://doi.org/10.1016/j.bbrc.2016.02.065.
15 Yang P, Chen X, Kaushal S, Reece EA, Yang P. High glucose suppresses embryonic stem cell differentiation into cardiomyocytes: High glucose inhibits ES cell cardiogenesis. *Stem Cell Res Ther* 2016;**7**:1–13. https://doi.org/10.1186/s13287-016-0446-5.
16 Chaudhuri R, Ramachandran M, Moharil P, Harumalani M, Jaiswal AK. Biomaterials and cells for cardiac tissue engineering: Current choices. *Mater Sci Eng C* 2017;**79**:950–7. https://doi.org/10.1016/j.msec.2017.05.121.
17 Nuamnaichati N, Sato VH, Moongkarndi P, Parichatikanond W, Mangmool S. Sustained β-AR stimulation induces synthesis and secretion of growth factors in cardiac myocytes that affect on cardiac fibroblast activation. *Life Sci* 2018;**193**:257–69. https://doi.org/10.1016/j.lfs.2017.10.034.
18 Malavolta M, Costarelli L, Giacconi R, Basso A, Piacenza F, Pierpaoli E, *et al.* Changes in Zn homeostasis during long term culture of primary endothelial cells and effects of Zn on endothelial cell senescence. *Exp Gerontol* 2017;**99**:35–45. https://doi.org/10.1016/j.exger.2017.09.006.
19 Li L, Mao D, Li C, Li M. miR-145-5p Inhibits Vascular Smooth Muscle Cells (VSMCs) Proliferation and Migration by Dysregulating the Transforming Growth Factor-b Signaling Cascade. *Med Sci Monit* 2018;**24**:4894–904. https://doi.org/10.12659/MSM.910986.

20 Hoes MF, Bomer N, van der Meer P. Concise Review: The Current State of Human in vitro Cardiac Disease Modeling: A Focus on Gene Editing and Tissue Engineering. *Stem Cells Transl Med* 2018:1–9. https://doi.org/10.1002/sctm.18-0052.
21 Camelliti P, Borg TK, Kohl P. Structural and functional characterisation of cardiac fibroblasts. *Cardiovasc Res* 2005;**65**:40–51. https://doi.org/10.1016/j.cardiores.2004.08.020.
22 Abdal Dayem A, Lee S, Y. Choi H, Cho SG. The Impact of Adhesion Molecules on the In Vitro Culture and Differentiation of Stem Cells. *Biotechnol J* 2018;**13**:1–10. https://doi.org/10.1002/biot.201700575.
23 McGuire DK, Marx N. *Diabetes in Cardiovascular Disease: A Companion to Braunwald's Heart Disease*. 1st ed. Philadelphia, PA: Saunders; 2015.
24 Hartman ME, Dai DF, Laflamme MA. Human pluripotent stem cells: Prospects and challenges as a source of cardiomyocytes for in vitro modeling and cell-based cardiac repair. *Adv Drug Deliv Rev* 2016;**96**:3–17. https://doi.org/10.1016/j.addr.2015.05.004.
25 Geraets IME, Chanda D, van Tienen FHJ, van den Wijngaard A, Kamps R, Neumann D, *et al.* Human embryonic stem cell-derived cardiomyocytes as an in vitro model to study cardiac insulin resistance. *Biochim Biophys Acta - Mol Basis Dis* 2018;**1864**:1960–7. https://doi.org/10.1016/j.bbadis.2017.12.025.
26 Büchner N, Ale-Agha N, Jakob S, Sydlik U, Kunze K, Unfried K, *et al.* Unhealthy diet and ultrafine carbon black particles induce senescence and disease associated phenotypic changes. *Exp Gerontol* 2013;**48**:8–16. https://doi.org/10.1016/j.exger.2012.03.017.
27 El-battrawy I, Tülümen E, Lang S, Akin I, Behnes M, Zhou X, *et al.* Expression of Inflammation-related Intercellular Adhesion Molecules in Cardiomyocytes In Vitro and Modulation by Pro-inflammatory Agents. *In Vivo (Brooklyn)* 2016;**30**:213–8.
28 Feijóo-Bandín S, Rodríguez-Penas D, García-Rúa V, Mosquera-Leal A, Otero MF, Pereira E, *et al.* Nesfatin-1 in human and murine cardiomyocytes: Synthesis, secretion, and mobilization of GLUT-4. *Endocrinology* 2013;**154**:4757–67. https://doi.org/10.1210/en.2013-1497.
29 Moe KT, Khairunnisa K, Yin NO, Chin-Dusting J, Wong P, Wong MC. Tumor necrosis factor-α-induced nuclear factor-kappaB activation in human cardiomyocytes is mediated by NADPH oxidase. *J Physiol Biochem* 2014;**70**:769–79. https://doi.org/10.1007/s13105-014-0345-0.
30 Nehra S, Bhardwaj V, Ganju L, Saraswat D. Nanocurcumin prevents hypoxia induced stress in primary human ventricular cardiomyocytes by maintaining mitochondrial homeostasis. *PLoS One* 2015;**10**:1–26. https://doi.org/10.1371/journal.pone.0139121.
31 Seemann I, Te Poele JAM, Song JY, Hoving S, Russell NS, Stewart FA. Radiation- and anthracycline-induced cardiac toxicity and the influence of ErbB2 blocking agents. *Breast Cancer Res Treat* 2013;**141**:385–95. https://doi.org/10.1007/s10549-013-2707-7.

32 Chong CR, Clarke K, Levelt E. Metabolic remodelling in diabetic cardiomyopathy. *Cardiovasc Res* 2017;**113**:422–30. https://doi.org/10.1093/cvr/cvx018.
33 Lee WS, Kim J. Diabetic cardiomyopathy: Where we are and where we are going. *Korean J Intern Med* 2017;**32**:404–21. https://doi.org/10.3904/kjim.2016.208.
34 Basta G. Receptor for advanced glycation endproducts and atherosclerosis: From basic mechanisms to clinical implications. *Atherosclerosis* 2008;**196**:9–21. https://doi.org/10.1016/j.atherosclerosis.2007.07.025.
35 Goldin A, Beckman JA, Schmidt AM, Creager MA. Advanced glycation end products: Sparking the development of diabetic vascular injury. *Circulation* 2006;**114**:597–605. https://doi.org/10.1161/CIRCULATIONAHA.106.621854.
36 Koulis C, Watson AMD, Gray SP, Jandeleit-Dahm KA. Linking RAGE and Nox in diabetic micro- and macrovascular complications. *Diabetes Metab* 2015;**41**:272–81. https://doi.org/10.1016/j.diabet.2015.01.006.
37 Soro-paavonen A, Watson AMD, Li J, Paavonen K, Koitka A, Calkin AC, *et al.* Receptor for Advanced Glycation End Products ( RAGE ) Atherosclerosis in Diabetes. *Vascular* 2008;**57**:13–5. https://doi.org/10.2337/db07-1808.
38 Lewandowski KC, Banach E, Bieńkiewicz M, Lewiński A. Matrix metalloproteinases in type 2 diabetes and non-diabetic controls: Effects of short-term and chronic hyperglycaemia. *Arch Med Sci* 2011;**7**:294–303. https://doi.org/10.5114/aoms.2011.22081.
39 Sedlic F, Muravyeva MY, Sepac A, Sedlic M, Williams AM, Yang M, *et al.* Targeted Modification of Mitochondrial ROS Production Converts High Glucose-Induced Cytotoxicity to Cytoprotection: Effects on Anesthetic Preconditioning. *J Cell Physiol* 2017;**232**:216–24. https://doi.org/10.1002/jcp.25413.
40 Younce CW, Wang K, Kolattukudy PE. Hyperglycaemia-induced cardiomyocyte death is mediated via MCP-1 production and induction of a novel zinc-finger protein MCPIP. *Cardiovasc Res* 2010;**87**:665–74. https://doi.org/10.1093/cvr/cvq102.
41 Huynh K, Bernardo BC, Mcmullen JR, Ritchie RH. Pharmacology & Therapeutics Diabetic cardiomyopathy : Mechanisms and new treatment strategies targeting antioxidant signaling pathways. *Pharmacol Ther* 2014;**142**:375–415. https://doi.org/10.1016/j.pharmthera.2014.01.003.

# CHAPTER 5: ELECTROMECHANICAL BIOREACTOR FOR CARDIAC TISSUE ENGINEERING

## 5.1 Introduction

Tissue engineering holds a great promise to regenerate myocardial tissue in order to replace and restore function to the diseased tissue. To do this a robust system is needed to condition the construct (i.e. the scaffold and cells) prior to implantation for tissue maturation. Physiological electromechanical stimuli are crucial in this process as they improve maturation, structure, and function of cardiomyocytes (CMs) in vitro.[1] Electrical stimulation of CMs has been shown to affect cell alignment, differentiation, metabolic activity, protein synthesis, connexin 43 expression, conduction velocity, calcium handling, and force generation.[2] These changes have been induced with physiological electrical properties such as rectangular shape and 2ms duration at 5V/cm and 1Hz.[3] Mechanical strain is important for CM alignment and development and expression of t-tubules, myofilaments, sarcomeric organization, gap junctions, desmosomes, adherens junctions.[4]

As of now, combinational electromechanical bioreactors have only tested animal cells in gels at low cyclic stretch or decellularized myocardium for a short duration.[5,6] However, many discrepancies exist between animal and human CMs, gels may not withstand the highly dynamic environment seen in vivo, and scaffolds tested would be too small to be translatable for use in a human patient.[7,8] To meet this need, we developed a physiologically relevant electromechanical bioreactor system. We hypothesized that by combining this with a methodology for reproducible myocardial-like tissues utilizing decellularized porcine myocardium, previously developed in our lab, seeded with human

CMs we would be able to create a robust platform for tissue engineered myocardium preconditioning.

## 5.2 Materials and Methods

### *5.2.1 Materials*

Primary human cardiac myocytes (hCM) were from Promocell GmbH (Heidelberg, Germany). Dulbecco's Modified Eagle Medium (DMEM) and antibiotic/antimycotic were from Corning Incorporated (Oneonta, NY). Fetal Bovine Serum (FBS) was from Atlanta Biologicals (Atlanta, GA). A FX-5000™ Compression System and Bioflex® 6-well plates were from Flexcell International Corp. (Burlington, NC, USA). Bicinchoninic acid protein assay was from Pierce Biotech (Rockford, IL). Carbon electrodes were from Alfa Aesar (Haverhill, MA). Platinum wire was purchased from Ladd Research Industries (Williston, VT). The Vectastain Elite kit, ABC diaminobenzidine tetrahydrochlorine peroxidase substrate kit, and Vectashield mounting medium were from Vector Laboratories (Burlingame, CA). The following antibodies were used: rabbit anti-sarcomeric α-actinin (Abcam, ab90776), rabbit anti-connexin-43 (Abcam, ab11370), rabbit anti-GATA-4 (Abcam, ab84593), rabbit anti-desmin (Abcam, ab15200), rabbit anti-laminin (Abcam, ab11575), and rabbit anti-collagen IV (Abcam, ab6586). Biotinylated anti-rabbit IgG was purchased from Vector Laboratories (Burlingame, CA). Movat's Pentachrome Kit and Masson's Trichrome Kit were from Poly Scientific (Bay Shore, NY). All other chemicals were of the highest purity and purchased from Sigma-Aldrich Corporation (Lakewood, NJ).

*5.2.2 Decellularization of Porcine Myocardium Scaffold*

Whole, healthy, porcine hearts were obtained from a local abattoir and decellularized utilizing a previously published method.[9] Briefly, after harvesting whole hearts were immediately injected with warm 50mM ethylenediamenetetraacetic acid (EDTA) in phosphate buffered saline (PBS) into the coronary arteries to prevent clotting. Hearts were transported on ice for processing. Pulmonary veins were cannulated with a threaded plug and zip-ties, to ensure proper circulation of solution and decellularization through the left side of the heart. Excess adipose and connective tissue were cleaned from the aorta, aortic leaflets were removed, and aorta was connected to a perfusion decellularization system. The hydrostatic driven perfusion decellularization system contained a multichannel peristaltic pump (Masterflex; Cole-Parmer) and a series of reservoirs that circulated 3.5L of solution through and around each heart (**Figure 5.1**). Decellularization was performed utilizing 1% sodium dodecyl sulfate (SDS) solution changes and a DNAse/RNase treatment. Distilled deionized water ($ddH_2O$) and PBS were employed for washes. Scaffolds were stored in PBS with 0.02% sodium azide and 0.001% protease inhibitor cocktail (Sigma) at 4 degrees C until tissue preparation.

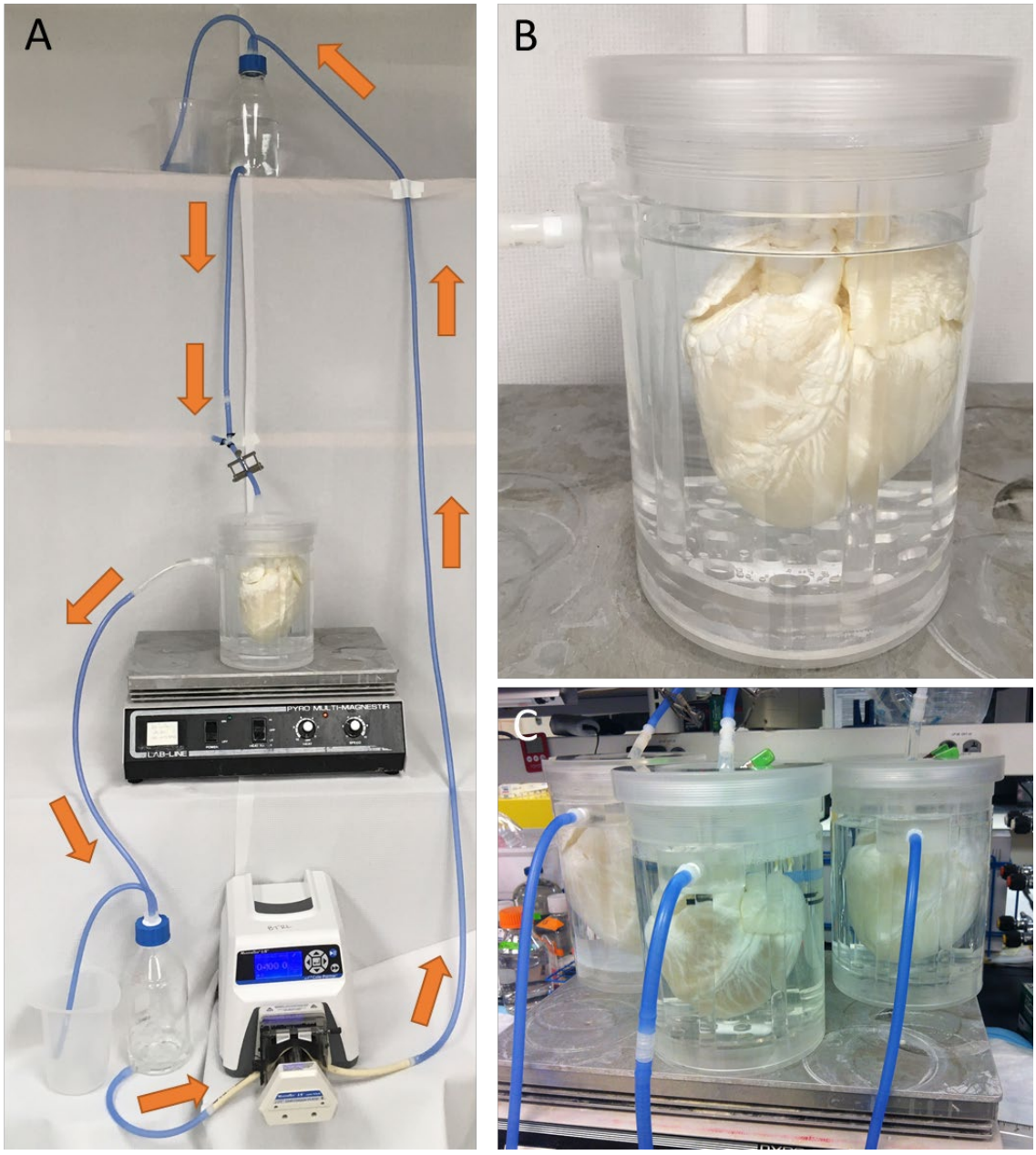


**Figure 5.1:** Decellularized porcine myocardium scaffold preparation. (A) Whole heart perfusion decellularization setup utilizing hydrostatic pressure and peristaltic pump. (B) Container housing one heart. (C) System can decellularize three hearts simultaneously.

*5.2.3 Tissue Preparation and Sterilization*

Decellularized porcine myocardium from the left ventricle was sliced to 2mm by 4cm by 2 cm via a specialized tissue slicer. Briefly, the scaffold was cut into 4 cm by 2 cm pieces using a 3D printed template. These constructs were placed flat on aluminum foil at -20 degrees Celsius until frozen, then cut into 2 mm slices utilizing microtome blades integrated into a custom tissue slicer designed in SolidWorks and 3D printed in digital acrylonitrile butadiene styrene (ABS). After sizing, the tissue was washed in three rinses of PBS (30 min, 2 hr, 30 min) and then sterilized in sterile 0.01% peracetic acid in PBS for 2 hours. Excess peracetic acid was removed through three washes of sterile PBS (30 min, 2hr, 30 min). Scaffolds were stored in sterile PBS at 4 degrees Celsius until cell seeding preparation.

*5.2.4 Adaptation of Flexcell Bioflex® 6-Well Plates for Tissue and Electrode Integration*

To accommodate cell-seeded scaffolds and an electrical stimulus similar to physiological conditions, Flexcell Bioflex® 6-well plates were modified. Digital ABS plastic inserts with lock-in-groove rings were designed using SolidWorks, 3D printed, to hold constructs in place via a clamping mechanism. The inserts were designed to hold two cylindrical (cut to 3 mm diameter) carbon electrodes parallel to each other to transfer an electrical stimulus across the cell-seeded scaffold in each well. Flexcell Bioflex® 6-well plates were cut for addition of a positive/negative connector for connection of external wires for electrical stimuli. Carbon electrodes were internally connected to the connector by platinum wire secured around the center of the electrode and covered with shrink tube and tubing with the lead soldered to a positive or negative wire. The positive

and negative wires from the platinum wires were soldered to the connector. Before ethylene oxide sterilization of the modified Flexcell Bioflex® 6-well plate, continuity was tested with a voltmeter.

*5.2.5 Flexcell FX-5000™ Compression System Modifications*

A FX-5000™ Compression System sold by Flexcell International Corporation was modified to allow for mechanical and electrical stimulation of the hCM cell seeded decellularized porcine myocardium scaffolds. The system purchased included a baseplate allowing for four Flexcell Bioflex® 6-well plates with membranes to be sealed airtight against it. Compressed air travelling through the baseplate served to mechanically stimulate cells in the wells by pushing the membrane and integrated tissue upward. Pressure was regulated by the main controller containing pressure regulators, transducers, and valves.

To more properly model diastole and systole of the left ventricular wall, the cyclic pressure waveform was modelled using provided Flexcell software, at 1.17 Hz (~70 beats per minute) with an amplitude of 0-120-0 mmHg (350 msec duration) with a static at 0 mmHg (450 msec duration). A pressure transducer was added to monitor real-time pressure applied to the silicone membrane and was acquired by a data acquisition module in a custom-written LabView program. Another LabView program triggered a square-wave electrical pulse of 5V (2.78V/cm$^2$, 20 msec-width) at the rising edge of every pressure wave for a coordinated pulse.

*5.2.6 Cell Culture, Seeding and Viability*

Progenitor human cardiac myocytes (hCMs) were expanded in Dulbecco's Modified Eagle Medium (DMEM), 10% Fetal Bovine Serum (FBS), and 1% antibiotic/antimycotic (penicillin-streptomycin). Sized, sterile, decellularized porcine myocardium was incubated overnight at 37 degrees Celsius in cell culture medium comprised of Dulbecco's Modified Eagle's medium (DMEM), 10% fetal bovine serum (FBS), and 1% antibiotic/antimycotic (penicillin-streptomycin). Before seeding, scaffolds were incubated 2 hours at 37°C in 6 well plates to allow removal of excess medium. Scaffolds were secured into two modified Flexcell Bioflex® 6-well plates (Flexcell International Corp., Burlington, NC, USA) and progenitor human cardiomyocytes (hCM) at passage 6 were aseptically injected (2 million per scaffold) and dropwise seeded (1 million per scaffold) with a sterile 26 ½ gauge needle. Control scaffolds were not seeded with hCM. Both plates were placed in an incubator for 1 hour to allow for hCM attachment and 4 mL of cell culture media (DMEM, 10% FBS, 1% Ab/Am) was placed in each well. Tissue was statically cultured for 3 days before exposure to dynamic stimuli. Before subjecting tissue (with cells or without cells) to the electrical stimulus and physiological cyclic pressures (0-120-0 mmHg), preconditioning was performed at two days with a cyclic waveform of 0-40-0 mmHg, followed by two days of a cyclic waveform of 0-80-0 mmHg. Media was changed every day and 7 mL was added to each well to cover the dynamic tissue and account for evaporation. Static scaffolds were controls and media was changed every day at 4 mL per well. Cell viability was confirmed

with a LIVE/DEAD® Viability/Cytotoxicity kit for Mammalian Cells from Molecular Probes (Eugene, OR).

*5.2.7 Histological and Immunohistochemical Analysis*

Samples were fixed in 10% formalin for 48 hours, processed, paraffin-embedded, and sectioned to 5um. Sections were rehydrated and examined via histological staining with hematoxylin and eosin (H&E), Masson's trichrome and Movat's pentachrome. Manufacturer's protocol was utilized for each stain.

Immunohistochemistry (IHC) was performed for detection of sarcomeric α-actinin, connexin-43, GATA-4, desmin, laminin, and collagen IV. Briefly, antigen retrieval was performed on rehydrated paraffin sections (5um) with heated (90-100 degrees Celsius, 10 min) 10mM citric acid (pH=7.4). Slides were permeabilized with 0.025% Triton X-100 for 5 minutes and then incubated in normal blocking serum for 45 minutes. Primary antibodies (rabbit anti-sarcomeric α-actinin 2ug/mL dilution, rabbit anti-connexin-43 2ug/mL dilution, rabbit anti-desmin 2ug/mL dilution, rabbit anti-GATA-4 4ug/mL dilution, rabbit anti-collagen IV 2ug/mL dilution, or rabbit anti-laminin 4ug/mL dilution) were incubated overnight at 4 degrees Celsius. Negative controls were obtained by omitting the primary antibody. Endogenous peroxidases were blocked with 0.3% hydrogen peroxide in 0.3% normal horse serum for 30 minutes. The secondary biotinylated anti-rabbit or anti-mouse antibody was applied for 30 minutes. Antibody staining was visualized using the Vector ABC peroxidase substrate kit and then lightly counterstained with diluted hematoxylin, before mounting. A Zeiss Axiovert 40CFL

microscope with AxioVision Release 4.6.3 digital imaging software (Carl Zeiss MicroImaging, Inc. Thornwood, NY) was utilized to obtain images.

## 5.3 Results

### *5.3.1 Decellularization of Porcine Myocardium Efficacy*

To decellularized whole porcine hearts for scaffolds, a perfusion system previously developed within our group was employed to use the vasculature of the hearts to perform cellular removal (**Figure 5.1**).[9] With this technique, three whole porcine hearts can be decellularized simultaneously. This decellularization platform combined with solutions specific to our method were seen in appearance and histological analysis of hematoxylin and eosin (H&E), Masson's trichrome, and Movat's pentachrome staining, to eradicate cells and residual materials (**Figure 5.2**). Our methods were harsh enough to eliminate cells, while gentle enough to retain the collagenous extracellular matrix, as shown in Masson's trichrome and Movat's pentachrome staining of fresh and decellularized hearts.

### *5.3.2 Efficiency of Scaffold Preparation*

By utilizing a custom 3D printed tissue slicer with integrated microtome blades, we were able to separate reproducible 4cm by 2cm by 2mm pieces of decellularized left ventricular porcine myocardium from endocardium and epicardium (**Figure 5.3**). Through our scaffold methodology of decellularization and preparation, hCM seeded on these scaffolds were viable at 1 hour and 3 days after seeding (**Figure 5.4**). Cells cultured statically for 21 days on these scaffolds were alive (**Figure 5.8**). hCM cultured for 3 days static, followed by 4 days dynamic conditioning, and then subjected to physiological

electrical and mechanical conditions for 14 days were also viable on these scaffolds (**Figure 5.8**). Few dead cells were found (images not shown).

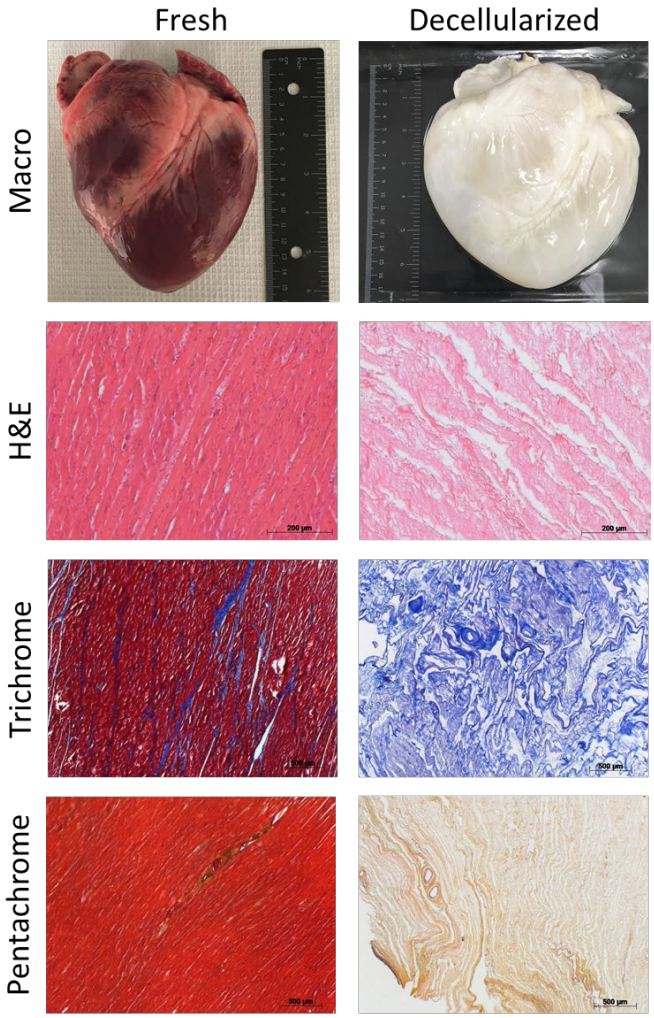


**Figure 5.2:** Comparison of fresh and decellularized porcine hearts. Images of hearts (top). Histological staining of fresh and decellularized tissue (middle to bottom) via hematoxylin and eosin (H&E; purple=nuclei, pink=tissue), Masson's trichrome (red=muscle fibers, blue=collagen, black=nuclei) and Movat's pentachrome (black=nuclei or elastic fibers, yellow=collagen or reticular fibers, blue=ground substance or mucin, bright red=fibrin, red=muscle).

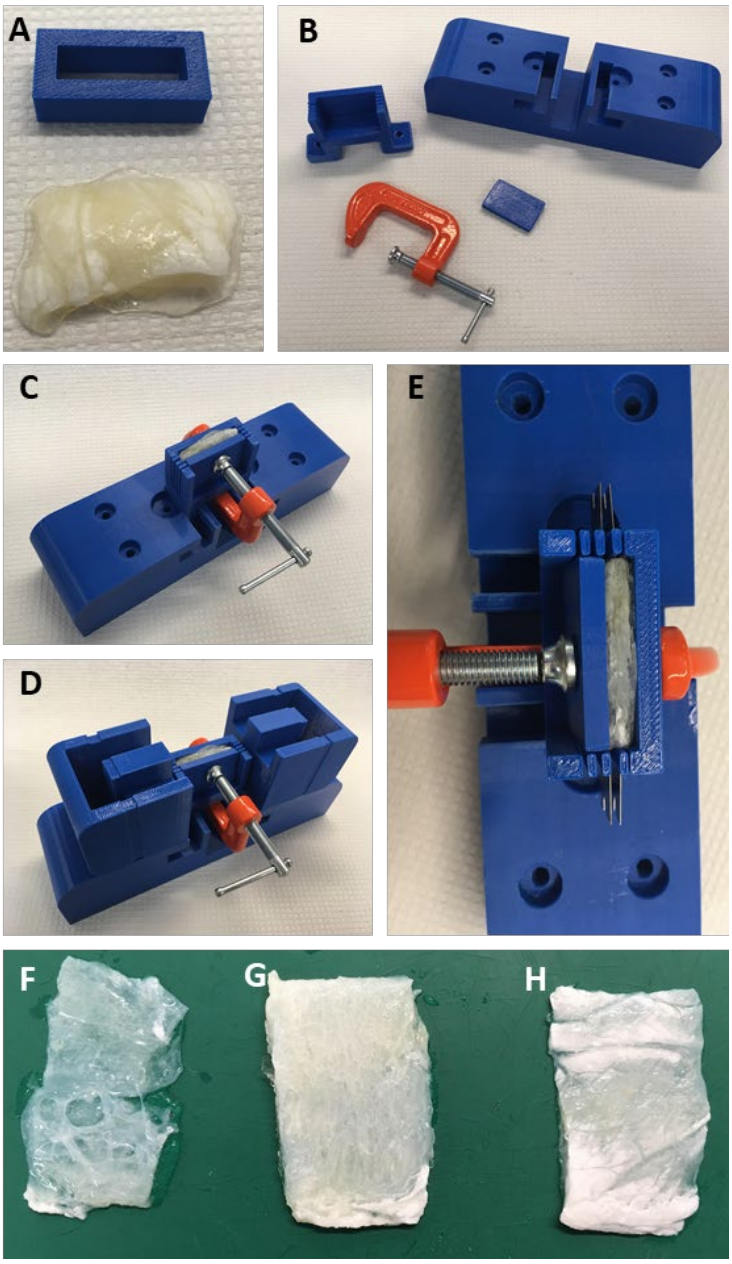


**Figure 5.3:** Custom 3D printed tissue slicer for extraction of left ventricular myocardium from decellularized porcine heart. Images show isolation of decellularized myocardium from a piece utilizing a template (A) and tissue slicer (B) after clamping frozen tissue in the system (C) and cutting via secured microtome blades (D, E). The tissue slicer separated the heart wall into endocardium (F), myocardium (G), and epicardium (H).

*5.3.3 Investigation of Modified Flexcell FX-5000™ Compression System and Plates*

By modifying a Flexcell FX-5000™ compression system and Flexcell Bioflex® 6-well plates with membranes, we were able design a platform for electrical and mechanical stimulation of tissue seeded with hCM. 3D printed ABS well plate inserts were sturdy for the experimental duration under dynamic and static conditions. These inserts were able to securely hold the tissue in place for 18 days, as well as provide housing for carbon electrodes and wiring after cutting excess plastic from the plates (**Figure 5.5**). The baseplate of this system holding the altered well plates was able to be contained within a standard cell culture incubator with room to spare (**Figure 5.6**). Additional programs written in LabVIEW to provide electrical stimulus and examine pressure exerted on the tissue were able to be run on the computer purchased with the system. Modelling of the electrical pulse between electrodes in COMSOL confirmed current handling in this system (**Figure 5.6**). By utilizing a ramping up regimen for dynamic tissue before physiological conditions, as illustrated in **Figure 5.7**, this system supported hCM for 14 days in this state (**Figure 5.8**).

*5.3.4 Cellular Analysis*

There was high cell viability after the duration of the experiment in both the dynamic and static groups seeded with hCM (**Figure 5.8**). Cells were aligned and found throughout the tissue in the dynamic group, while cells in the static group were spherical and not aligned. Few dead cells were found (images not shown). Hematoxylin and eosin (H&E) staining of both groups showed hCM on the surface and within the scaffold. As

seen in **Figure 5.9**, cells in dynamic and static scaffolds stained positive for cardiomyocyte markers such as connexin-43, sarcomeric α-actinin, desmin, and GATA-4.

*5.3.5 Extracellular Matrix Investigation*

When investigating scaffolds that were dynamically and statically conditioned, with or without cells, it was found that samples from all groups all had collagen IV present, with muscle fibers and elastin fibers missing (**Figure 5.10, Figure 5.11**). Scaffolds seeded with hCM stained for nuclei. As visualized by immunohistochemistry (IHC) staining in **Figure 5.10**, laminin presence was more noticeable in scaffolds seeded with cells, when compared to those without cells.

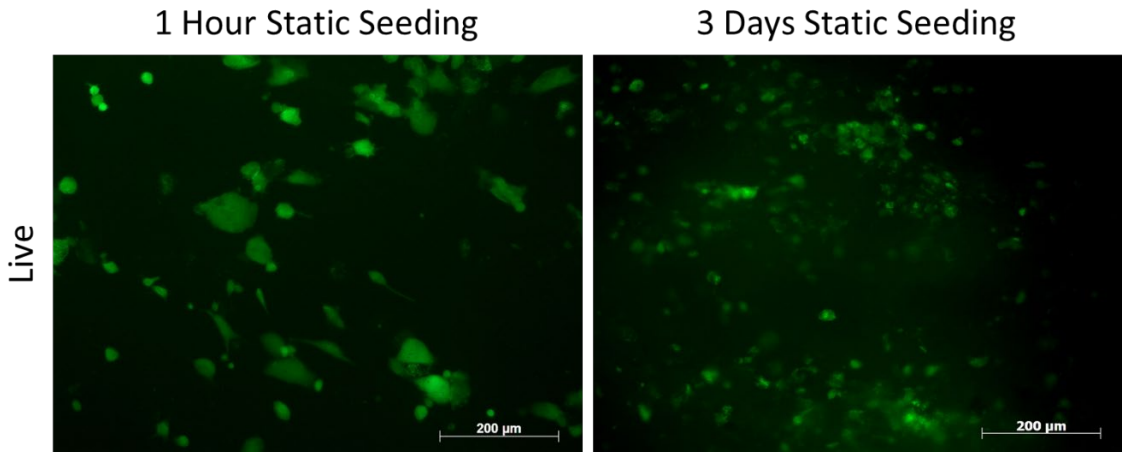


**Figure 5.4:** Viability of human cardiomyocytes (hCM) after seeding. Live images show viable (green) hCM after 1 hour (left) and 3 days (right) of static seeding.

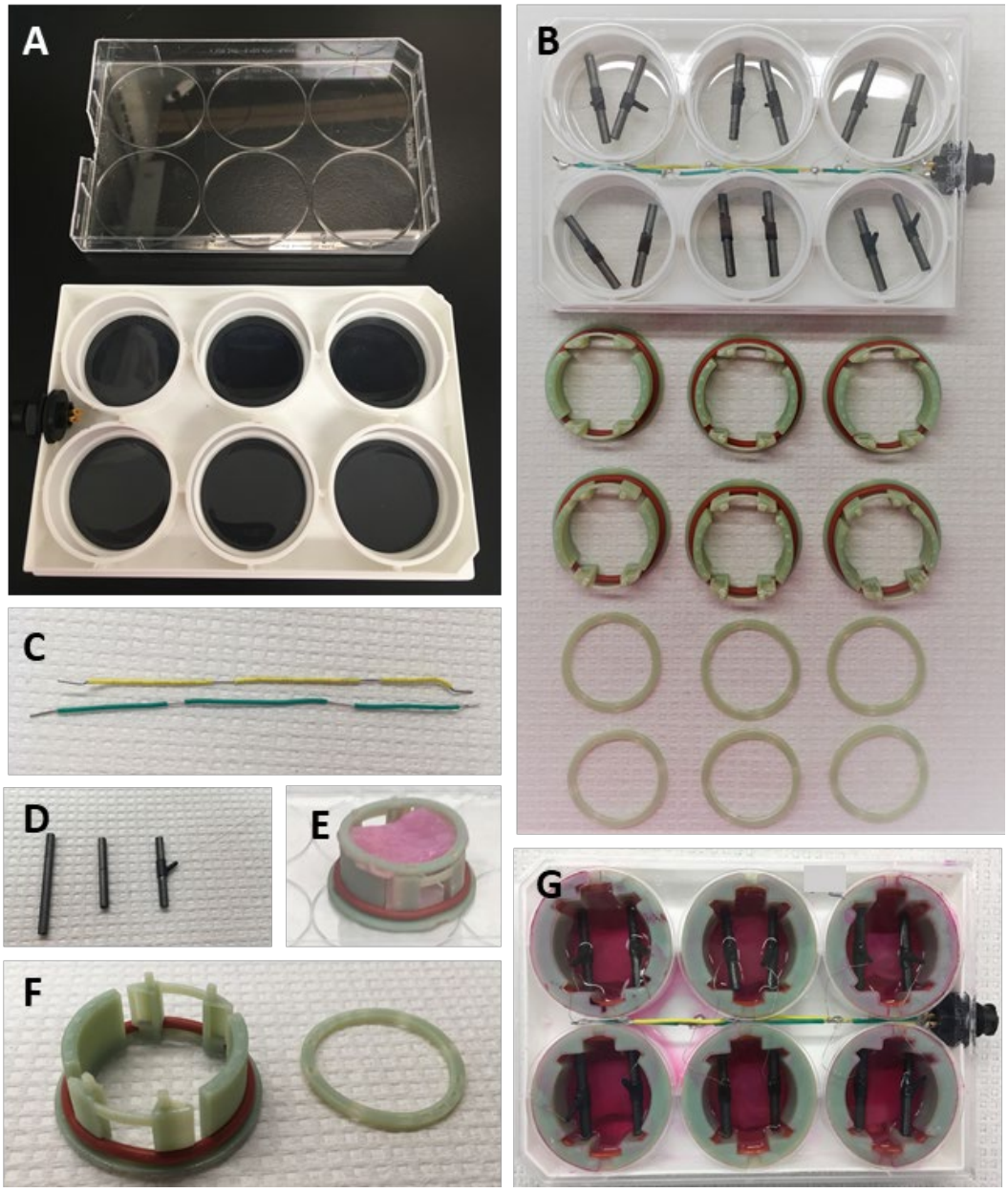


**Figure 5.5:** Modifications of Flexcell plates and mounting prepared tissue. Uncoated Flexcell plates cut for insertion of connector (A) for positive and negative wires (C) to deliver stimulus to electrodes (D). 3D printed tissue holding inserts (F) hold tissue via a clamping ring (E). All components (B) assembled with tissue (G) and cells are ready for the modified Flexcell system.

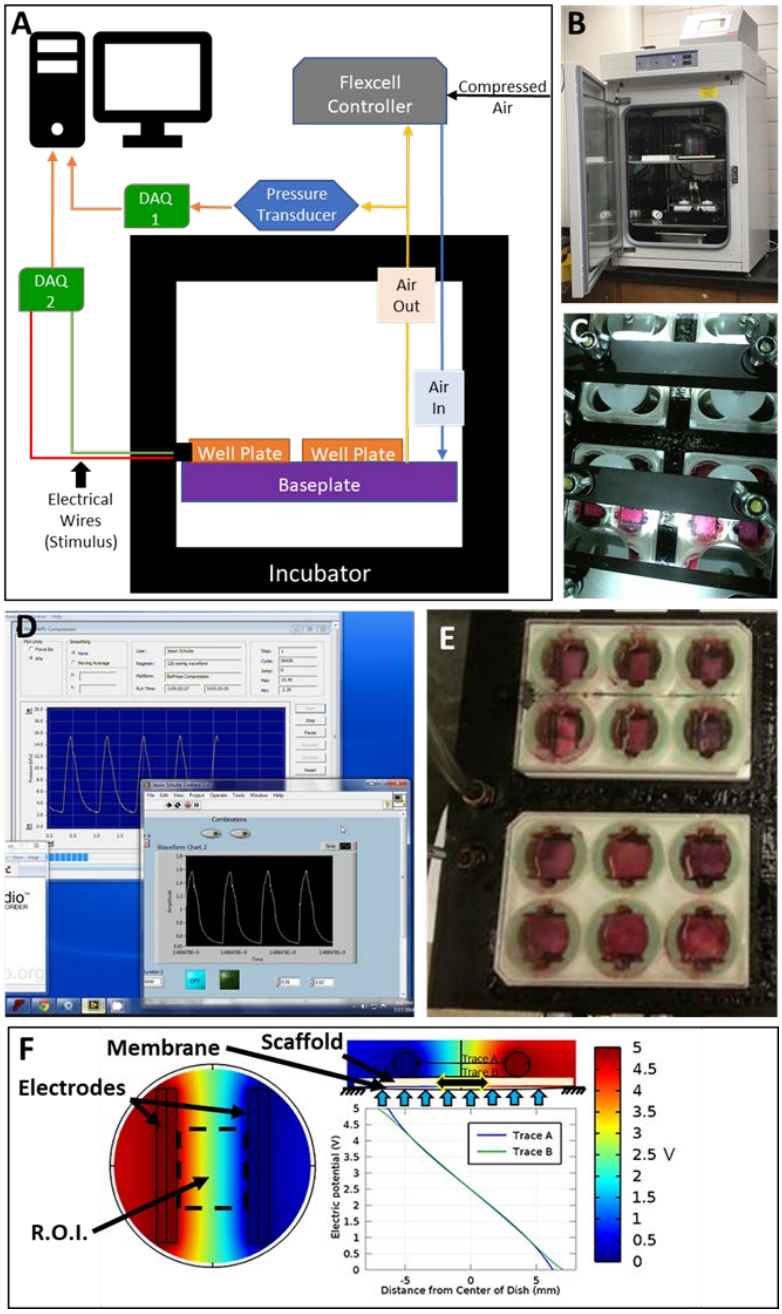


**Figure 5.6:** Flexcell setup and monitor. A diagram illustrating the modified Flexcell setup (A) shows addition of data acquisition (DAQ) devices for monitoring pressure and delivering electrical stimulus included with the Flexcell controller, monitor, and baseplate holding modified well plates. An incubator (B) houses the modified well plates clamped

to the baseplate (C). The system is controlled via a computer and monitor (D) utilizing Flexcell software to deliver air to the baseplate and an original LabVIEW program to deliver an electrical stimulus to the tissue. The baseplate can hold up to four well plates (E). 5 volts travel between the electrodes as shown by COMSOL modelling (F).

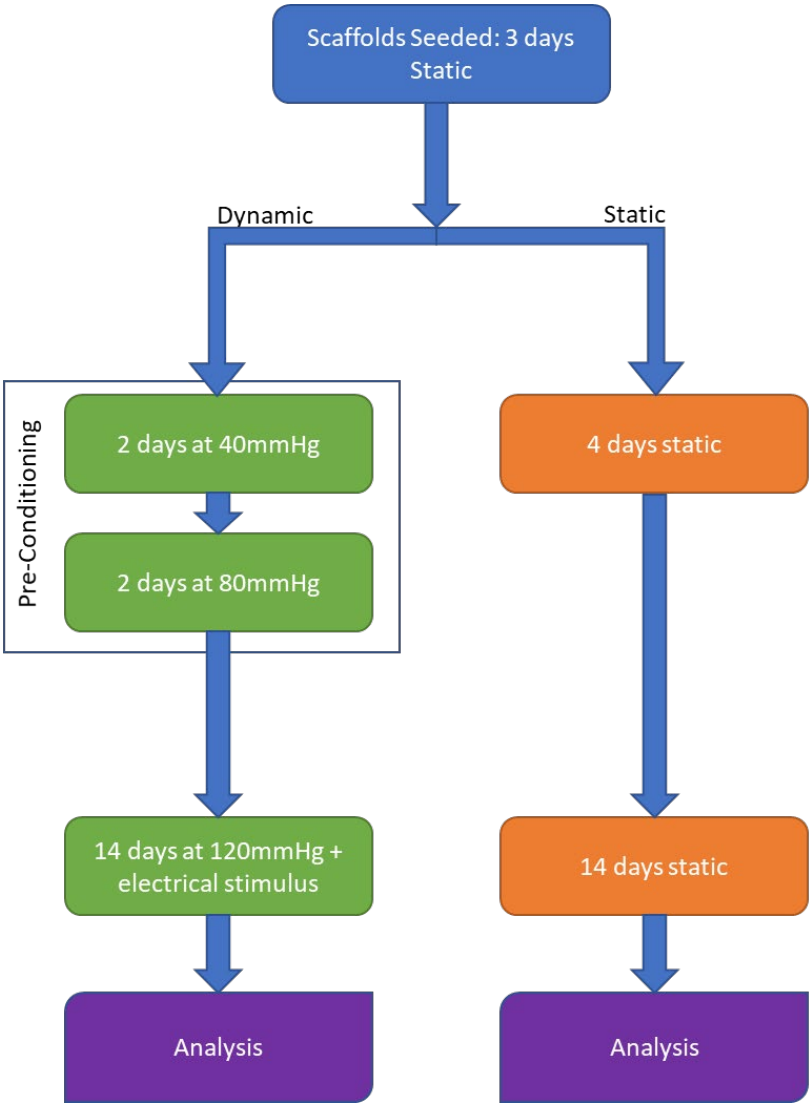


**Figure 5.7:** Workflow of experimental set-up for dynamic and static tissues. Tissue was preconditioned in the dynamic system for 4 days before electrical stimulus and exposure to normal native cyclic pressure of a 120mmHg.

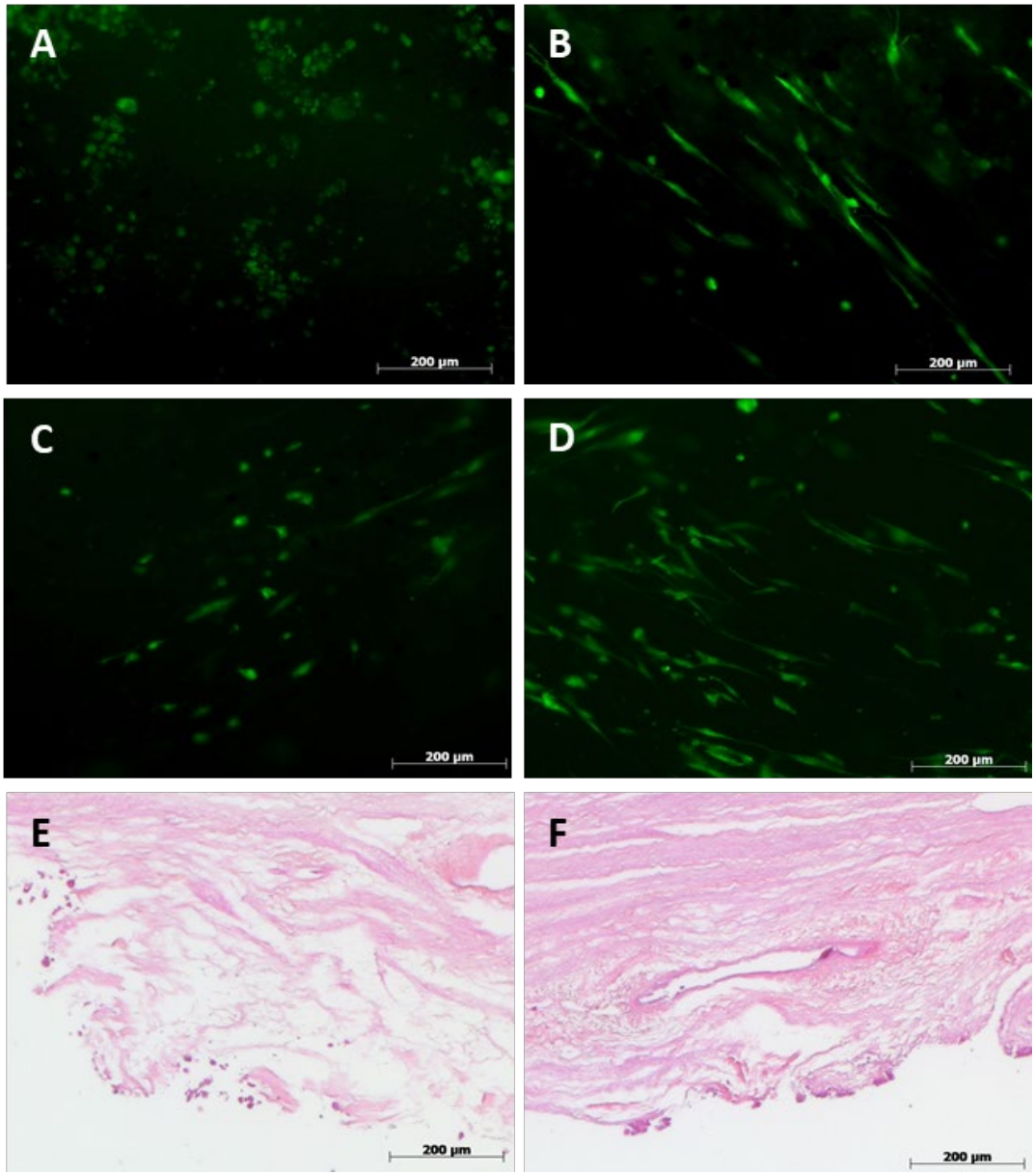


**Figure 5.8:** Cellular viability and presence in dynamic and static conditions. Live assay of decellularized porcine myocardium cultured with hCM after 18 days static culture (A) and 18 days of dynamic culture on side (B), inside (C), and other side (D) of the tissue. Green= live cells. Hematoxylin and eosin staining of cells (purple) show presence in tissue (pink) after 18 days of static (E) or dynamic (F) culture.

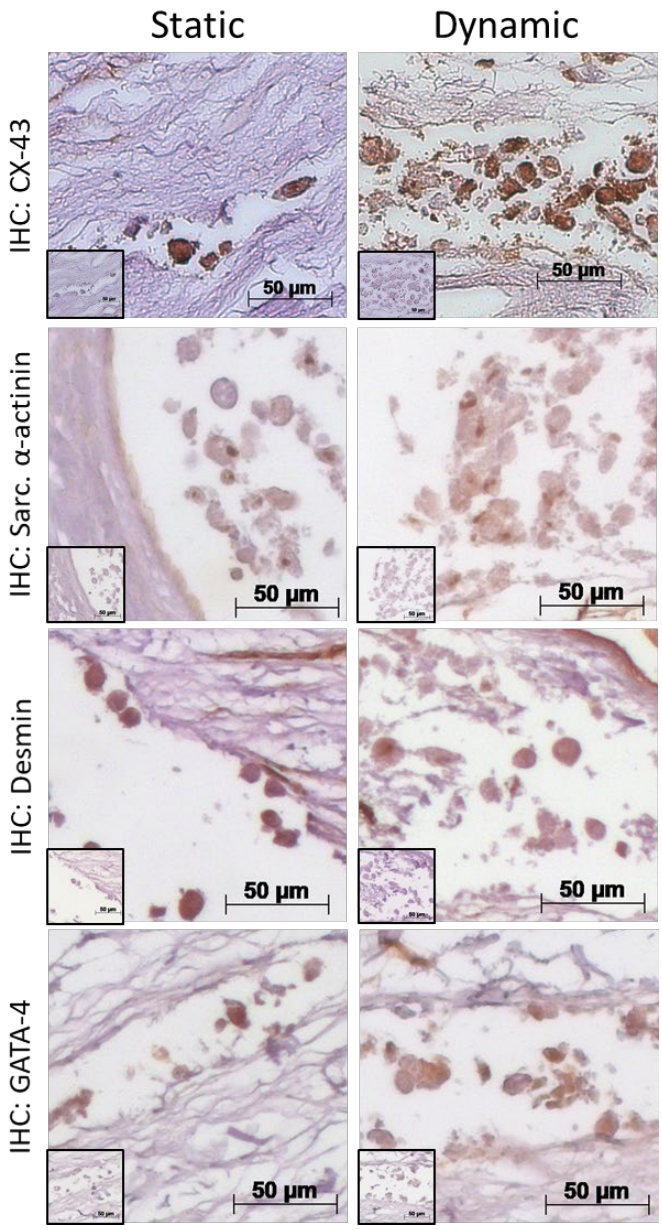


**Figure 5.9:** Cellular analysis of human cardiomyocytes (hCM) in static and dynamic conditions. Immunohistochemical (IHC) staining of cardiomyocyte markers after 18 days of static and dynamic culture highlight connexin-43 (CX-43), sarcomeric alpha-actinin (Sarc. α-actinin), desmin, and GATA-4. (brown=positive; purple=tissue; inserts=negative controls)

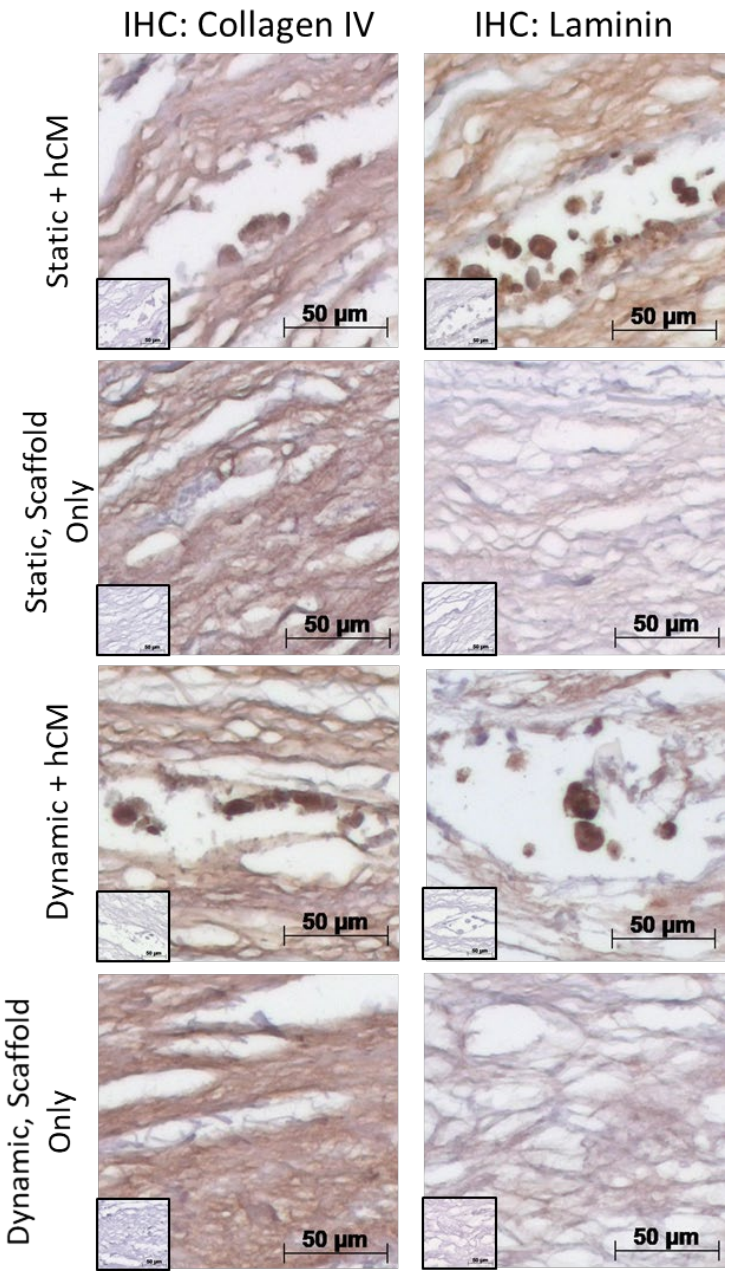


**Figure 5.10:** Collagen IV and laminin extracellular matrix analysis on scaffolds subjected to static and dynamic conditions with and without human cardiomyocytes (hCM). Immunohistochemical (IHC) staining of collagen IV and laminin in groups. (brown=positive; purple=tissue; inserts= negative controls)

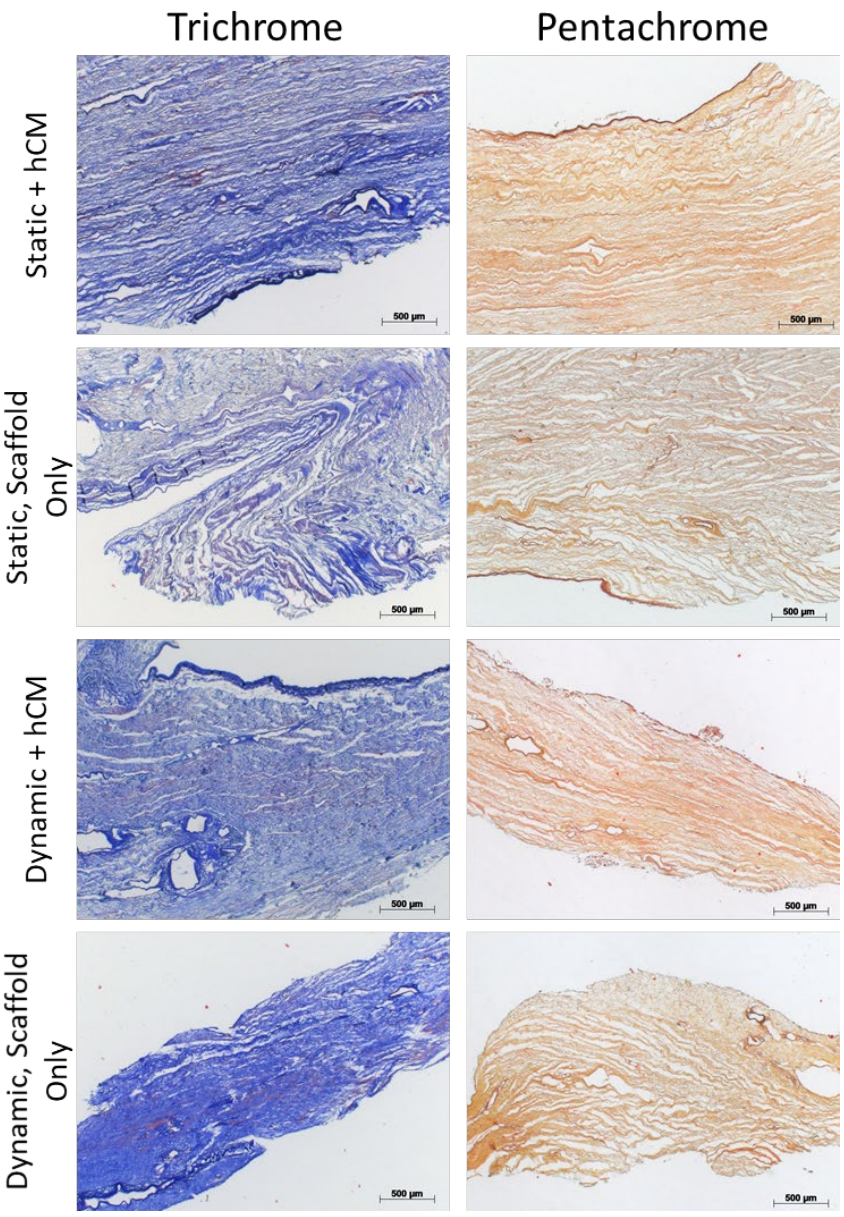


**Figure 5.11:** Extracellular matrix investigation of static and dynamic scaffolds with and without human cardiomyocytes (hCM). Masson's trichrome (red=muscle fibers, blue=collagen, black=nuclei) and Movat's pentachrome (black=nuclei or elastic fibers, yellow=collagen or reticular fibers, blue=ground substance or mucin, bright red=fibrin, red=muscle) staining.

## 5.4 Discussion

Cardiac tissue engineering has emerged as a promising solution for a functional tissue replacement for patients who have experienced a myocardial infarction, which causes myocardial ischemia. Preconditioning is important in developing an engineered tissue that is mature and behaves properly when implanted.[10] Electrical and mechanical stimuli have been proven to be pivotal in this. Currently, combinational electromechanical bioreactors have only tested animal cells encapsulated in gels at low cyclic stretch or seeded in decellularized tissue for a short amount of time.[56] Though, many discrepancies exist between animal and human CMs, physiological conditions could destroy weak gels, and these platforms support small tissues, limiting their translation to human patients.[7,8]

To fill this disparity, we developed a physiologically relevant bioreactor that was able to subject larger (4cm by 2cm by 2mm) and mechanically sound scaffolds with human cells. Within our lab we have produced a complex 3D acellular scaffold from decellularized porcine myocardium, which has been proven to retain mechanical and vascular integrity, and important ECM basal lamina components crucial to recapitulating native myocardium, such as fibronectin, laminin, and collagen IV.[9] Myocardial ECM is very diverse and this specific environment is essential for inherent cellular interactions and tethering.[11,12] By designing a tissue slicer we were able to simply and reproducibly extract myocardium from our scaffold at around a 2mm thickness.

For our cells we decided to employ primary hCM progenitor cells. They have recently been used for research in areas such as cardiotoxicity, therapeutic testing,

scaffold biocompatibility, and the study of pathways involved in oxidative stress.[13–16] These cells are more cost effective than induced pluripotent stem cells (iPSCs), can proliferate, and express cardiac markers, such as sarcomeric α-actin, making them ideal for our research.[17]

We were able to create tissue engineered myocardium my combining hCM and our scaffold. This myocardium was supported in our electromechanical bioreactor for 14 days at physiologically relevant conditions with mechanical and electrical stimuli after an initial ramping up period in order to acclimate the hCM to this highly dynamic environment. Not only was this system able to maintain viable cells for 14 days, but dynamic scaffolds had live hCM throughout the tissue and on both surfaces that were aligned, while statically cultured tissue engineered myocardium had spherical cells localized to one surface. Morphologically, our dynamic myocardium is more similar to cellular alignment of native myocardium and with this system we can support these cells within our 2mm thick tissues.

CM markers were evaluated as a checkpoint to determine if our electromechanical bioreactor allowed for the preservation of the CM phenotype in our scaffolds. To do so we investigated connexin 43, sarcomeric α-actinin, desmin, and GATA-4 in dynamic and static conditions. Connexin 43 or gap junction protein, plays a key role in synchronous cellular contraction and the exchange of molecules, such as calcium, between cells.[18,19] Sarcomeric α-actinin and desmin are integral parts of the sarcomere in CMs and contribute to its contraction and overall functionality.[19–21] GATA-4 is crucial for CM development, differentiation, as it is only expressed by CMs and is a transcriptional

regulator for cardiac genes.[16,19] These proteins were all found to be expressed by hCM in scaffolds cultured in dynamic or static conditions.

Our scaffold was also inspected with and without cells to determine if our dynamic conditioning would adversely alter the ECM, as it could compromise overall function of our tissue engineered myocardium. Scaffolds were not adversely altered in the course of 14 days within the electromechanical bioreactor. All scaffolds dynamically and statically conditioned, with and without cells, were shown to retain collagen IV and laminin, important ECM proteins. Collagen IV provides the supportive framework for the ECM and cells to interact.[22] Laminins are glycoproteins located mainly in the basal lamina and are vital for cell-ECM attachment, cell differentiation, survival, and migration.[23] Dynamic and static scaffolds with cells had increased expression of laminin compared to scaffolds without cells, which is promising. This shows the hCM are integrating and interacting with the ECM, by connecting to and secreting their own matrix proteins.

**5.5 Conclusions**

Tremendous strides have been made in cardiac tissue engineering, with even more to come. We are the first to our knowledge to subject acellular porcine scaffolds seeded with hCM to physiological electromechanical conditions for 14 days. We found that dynamic tissues had cellular alignment and cells throughout the tissue, while static tissue did not. This bioreactor system for myocardium was able to support human cells expressing cardiomyocyte markers for 14 days at physiological conditions, without

altering the ECM. This platform has great potential for myocardial tissue preconditioning and could be useful for disease modeling.

## 5.6 Chapter 5 References


1 Hirt MN, Hansen A, Eschenhagen T. Cardiac tissue engineering : State of the art. *Circ Res* 2014;**114**:354–67. https://doi.org/10.1161/CIRCRESAHA.114.300522.

2 Kofron CM, Mende U. In vitro models of the cardiac microenvironment to study myocyte and non-myocyte crosstalk: bioinspired approaches beyond the polystyrene dish. *J Physiol* 2017;**595**:3891–905. https://doi.org/10.1113/JP273100.

3 Nunes SS, Miklas JW, Liu J, Aschar-Sobbi R, Xiao Y, Zhang B, *et al.* Biowire: A platform for maturation of human pluripotent stem cell-derived cardiomyocytes. *Nat Methods* 2013;**10**:781–7. https://doi.org/10.1038/nmeth.2524.

4 Zimmermann WH, Schneiderbanger K, Schubert P, Didié M, Münzel F, Heubach JF, *et al.* Tissue engineering of a differentiated cardiac muscle construct. *Circ Res* 2002;**90**:223–30. https://doi.org/10.1161/hh0202.103644.

5 Morgan KY, Black LD. Mimicking Isovolumic Contraction with Combined Electromechanical Stimulation Improves the Development of Engineered Cardiac Constructs. *Tissue Eng Part A* 2014;**20**:1654–67. https://doi.org/10.1089/ten.tea.2013.0355.

6 Wang B, Wang G, To F, Butler JR, Claude A, McLaughlin RM, *et al.* Myocardial scaffold-based cardiac tissue engineering: Application of coordinated mechanical and electrical stimulations. *Langmuir* 2013;**29**:11109–17. https://doi.org/10.1021/la401702w.

7 Fuentes-Antras J, Picatoste B, Gomez-Hernandez A, Egido J, Tunon J, Lorenzo O. Updating experimental models of diabetic cardiomyopathy. *J Diabetes Res* 2015;**2015**:. https://doi.org/10.1155/2015/656795.

8 Chaudhuri R, Ramachandran M, Moharil P, Harumalani M, Jaiswal AK. Biomaterials and cells for cardiac tissue engineering: Current choices. *Mater Sci Eng C* 2017;**79**:950–7. https://doi.org/10.1016/j.msec.2017.05.121.

9 Schulte JB, Simionescu A, Simionescu DT. The acellular myocardial flap: a novel extracellular matrix scaffold enriched with patent microvascular networks and biocompatible cell niches. *Tissue Eng Part C Methods* 2013;**19**:518–30. https://doi.org/10.1089/ten.TEC.2012.0536.

10 Gaetani R, Doevendans PAF, Messina E, Sluijter JPG. Tissue Engineering for Cardiac Regeneration 2011;**6**:1–27. https://doi.org/10.1007/8415_2011_82.

11 Kelly DJ, Rosen AB, Schuldt AJT, Kochupura P V, Doronin S V, Potapova I a, *et al.* Increased myocyte content and mechanical function within a tissue-engineered myocardial patch following implantation. *Tissue Eng Part A* 2009;**15**:2189–201. https://doi.org/10.1089/ten.tea.2008.0430.

12 Badylak SF. The extracellular matrix as a biologic scaffold material. *Biomaterials*

2007;**28**:3587–93. https://doi.org/10.1016/j.biomaterials.2007.04.043.
13 Hernández-Córdova R, Mathew DA, Balint R, Carrillo-Escalante HJ, Cervantes-Uc JM, Hidalgo-Bastida LA, *et al.* Indirect three-dimensional printing: A method for fabricating polyurethane-urea based cardiac scaffolds. *J Biomed Mater Res Part A* 2016;**104**:1912–21. https://doi.org/10.1002/jbm.a.35721.
14 El-battrawy I, Tülümen E, Lang S, Akin I, Behnes M, Zhou X, *et al.* Expression of Inflammation-related Intercellular Adhesion Molecules in Cardiomyocytes In Vitro and Modulation by Pro-inflammatory Agents. *In Vivo (Brooklyn)* 2016;**30**:213–8.
15 Ruiz-esparza GU, Segura-ibarra V, Cordero-reyes AM, Keith A, Serda RE, Cruz-solbes AS, *et al.* A specifically designed nanoconstruct associates, internalizes, traffics in cardiovascular cells, and accumulates in failing myocardium: a new strategy for heart failure diagnostics and therapeutics. *Eur J Hear Fail* 2017;**18**:169–78. https://doi.org/10.1002/ejhf.463.A.
16 Kuo CY, Chiu YC, Lee AYL, Hwang TL. Mitochondrial Lon protease controls ROS-dependent apoptosis in cardiomyocyte under hypoxia. *Mitochondrion* 2015;**23**:7–16. https://doi.org/10.1016/j.mito.2015.04.004.
17 Kai D, Prabhakaran MP, Jin G, Ramakrishna S. Biocompatibility evaluation of electrically conductive nanofibrous scaffolds for cardiac tissue engineering. *J Mater Chem B* 2013;**1**:2305–14. https://doi.org/10.1039/c3tb00151b.
18 Sarig U, Sarig H, de-Berardinis E, Chaw SY, Nguyen EBV, Ramanujam VS, *et al.* Natural myocardial ECM patch drives cardiac progenitor based restoration even after scarring. *Acta Biomater* 2016;**44**:209–20. https://doi.org/10.1016/j.actbio.2016.08.031.
19 Lux M, Andrée B, Horvath T, Nosko A, Manikowski D, Hilfiker-Kleiner D, *et al.* In vitro maturation of large-scale cardiac patches based on a perfusable starter matrix by cyclic mechanical stimulation. *Acta Biomater* 2016;**30**:177–87. https://doi.org/10.1016/j.actbio.2015.11.006.
20 Chan Y-C, Ting S, Lee Y-K, Ng K-M, Zhang J, Chen Z, *et al.* Electrical Stimulation Promotes Maturation of Cardiomyocytes Derived from Human Embryonic Stem Cells. *J Cardiovasc Transl Res* 2013;**6**:989–99. https://doi.org/10.1007/s12265-013-9510-z.
21 Davidson MM, Nesti C, Palenzuela L, Walker WF, Hernandez E, Protas L, *et al.* Novel cell lines derived from adult human ventricular cardiomyocytes. *J Mol Cell Cardiol* 2005;**39**:133–47. https://doi.org/10.1016/j.yjmcc.2005.03.003.
22 Zamilpa R, Lindsey ML. Extracellular matrix turnover and signaling during cardiac remodeling following MI: Causes and consequences. *J Mol Cell Cardiol* 2010;**48**:558–63. https://doi.org/10.1016/j.yjmcc.2009.06.012.
23 Mouw JK, Ou G, Weaver VM. Extracellular matrix assembly: A multiscale deconstruction. *Nat Rev Mol Cell Biol* 2014;**15**:771–85. https://doi.org/10.1038/nrm3902.

# CHAPTER 6: TISSUE ENGINEERING MODELS OF DIABETIC CARDIAC PATHOLOGY

## 6.1 Introduction

There is no cure for DCMP, except for heart transplantation which has a very long wait list.[1] Treatment for this disease is lumped in with other cardiomyopathies and heart failure, however these therapies only treat the symptoms and downstream complications that accompany heart failure without addressing origins of the problem.[2] As DCMP progresses, significant changes are seen in heart mass, size and wall thickness, in conjunction with abnormal diastolic and/or systolic function.[3] Patients at the end stage of DCMP experience symptoms associated with heart failure, such as shortness of breath, fluid retention, dizziness, and coughing.[4] Patients with heart failure have a 5-year mortality of approximately 50%.[1]

Understanding the underlying mechanisms in the early stages of DCMP are crucial for diagnosis and targeted therapies early on. As of now, knowledge of this disease has relied on rodent models, cell culture models, and cadaveric human patient hearts.[5,6] Human cadaveric hearts with DCMP have been excellent for elucidating end stage cellular and extracellular changes and rodent and cell culture models have been utilized to fill in the gaps. Problems arise within rodent models as they have varying progressions of diabetes, circulating lipid concentrations, cardiomyocyte electrophysiological properties, higher beats per minute, and inflammatory responses when compared to human diabetic patients.[7–9] Human cells have been studied to investigate specific cell type alterations

associated with the diabetic environment, however this is an oversimplified 2D static environment, lacking an extracellular matrix (ECM).[10]

Tissue engineering holds much promise in bridging this gap. 3D organotypic tissue engineered models allow for studies of individual cell types in a dynamic, controllable and repetitive environment.[11] Other research groups have tried to fill this need but have failed to either produce a complex and dynamic 3D ECM environment or have examined animal cells, instead of human cells.[12,13] We hypothesized that if we combined human cardiomyocytes (hCMs) and an acellular porcine myocardium scaffold within (1) a perfusion 3D Kube minibioreactor or (2) an electromechanical bioreactor supplemented with high glucose, that we would be able to detect early alterations associated with DCMP. These platforms could be useful for determining and testing targeted therapeutics, as well as markers for prompt diagnosis of DCMP in diabetic patients.

## 6.2 Materials and Methods

### *6.2.1 Materials*

Primary human cardiac myocytes (hCM) were from Promocell GmbH (Heidelberg, Germany). Dulbecco's Modified Eagle Medium (DMEM) and antibiotic/antimycotic were from Corning Incorporated (Oneonta, NY). Fetal Bovine Serum (FBS) was from Atlanta Biologicals (Atlanta, GA). 3D Kubes were purchased from Kiyatec (Greenville, SC). A multichannel peristaltic pump was from Cole-Parmer (Vernon Hills, IL). A FX-5000™ Compression System and Bioflex® 6-well plates were from Flexcell International Corp. (Burlington, NC, USA). Carbon electrodes were from Alfa Aesar

(Haverhill, MA). Platinum wire was purchased from Ladd Research Industries (Williston, VT). Bicinchoninic acid protein assay was from Pierce Biotech (Rockford, IL). Electrophoresis apparatus, gel imager and imaging software, chemicals, and molecular weight standards were from Bio-rad (Hercules, CA). Clean-Blot$^{TM}$ IP Western Blot Detection kit was obtained from Thermo Fisher Scientific Inc. (Waltham, MA). The Vectastain Elite kit, ABC diaminobenzidine tetrahydrochlorine peroxidase substrate kit, and Vectashield mounting medium were from Vector Laboratories (Burlingame, CA). The following antibodies were used: rabbit anti-superoxide dismutase-2 (Abcam, ab13534), rabbit anti-advanced glycation endproducts (Abcam, ab23722), rabbit anti-light chain 3B (Abcam, ab48394), rabbit anti-caspase-3 (Millipore, 06-735 and Thermo Fisher, MA1-16843), mouse anti-N-epsilon-(carboxylmethyl)lysine (R&D Systems, MAB3247), rabbit anti-inositol-requiring enzyme 1 (Abcam, ab48187), and rabbit anti-protein kinase RNA-like endoplasmic reticulum kinase (Abcam, ab192591). Biotinylated anti-rabbit IgG and anti-mouse IgG were purchased from Vector Laboratories (Burlingame, CA). Movat's Pentachrome Kit and Masson's Trichrome Kit were from Poly Scientific (Bay Shore, NY). All other chemicals were of the highest purity and purchased from Sigma-Aldrich Corporation (Lakewood, NJ).

*6.2.2 Decellularization of Porcine Myocardium Scaffold*

Whole, healthy, porcine hearts were obtained from a local slaughterhouse and decellularized utilizing a previously published method (see Chapter 5).[14] Briefly, pulmonary veins were cannulated, excess adipose and connective tissue were cleaned from the aorta, aortic leaflets were removed, and aorta was connected to a perfusion

decellularization system. Decellularization was performed with 1% sodium dodecyl sulfate (SDS) solution changes and a DNAse/RNase treatment. Washes of distilled deionized water ($ddH_2O$) and PBS were used for cleaning. Scaffolds were stored in PBS with 0.02% sodium azide and 0.001% protease inhibitor cocktail (Sigma) at 4 degrees Celsius until tissue bioreactor use in either the 3D Kube minibioreactor or modified electromechanical Flexcell bioreactor.

### *6.2.3 Tissue Preparation and Sterilization*

For the 3D Kube minibioreactor, decellularized porcine myocardium scaffolds were removed using a 5mm round biopsy punch. For the electromechanical bioreactor, decellularized porcine myocardium was extracted from the left ventricle was sliced to 2mm by 4cm by 2 cm via a specialized tissue slicer (see Chapter 5). Briefly, the scaffold was cut into 4 cm by 2 cm pieces using a 3D printed template, frozen at 20 degrees Celsius, then cut into 2 mm slices with a custom designed 3D printed tissue slicer.

After isolation, the scaffolds were washed in three rinses of PBS (30 min, 2 hr, 30 min) and then sterilized in sterile 0.01% peracetic acid in PBS for 2 hours. Excess peracetic acid was removed through three washes of sterile PBS (30 min, 2hr, 30 min). Scaffolds were stored in sterile PBS at 4 degrees Celsius until cell seeding preparation.

### *6.2.4 Adaptation of Well Plates and FX-5000™ Compression System Modifications*

To accommodate cell-seeded scaffolds and an electrical stimulus like physiological conditions, Flexcell Bioflex® 6-well plates were modified as previously described (see Chapter 5). Briefly, inserts were designed to hold constructs in place and to hold two

wired carbon electrodes parallel to each other to transfer an electrical stimulus across the cell-seeded scaffold in each well. Flexcell Bioflex® 6-well plates were cut for addition of a positive/negative connector for connection of external wires and electrodes were bridged with platinum wires for electrical stimuli. Continuity was tested with a voltmeter and plates were sterilized with ethylene oxide.

A FX-5000™ Compression System sold by Flexcell International Corporation was modified to allow for mechanical and electrical stimulation of the hCM cell seeded decellularized porcine myocardium scaffolds (see Chapter 5). The cyclic pressure waveform to mimic diastole and systole of the left ventricular wall was modelled using provided Flexcell software, at 1.17 Hz (~70 beats per minute) with an amplitude of 0-120-0 mmHg (350 msec duration) with a static at 0 mmHg (450 msec duration). This was confirmed with the addition of a pressure transducer and a data acquisition module in a custom-written LabView program. Another LabView program triggered a square-wave electrical pulse of 5V (2.78V/cm$^2$, 20 msec-width) at the rising edge of every pressure wave for a coordinated pulse.

*6.2.5 Cell Culture and Expansion*

Progenitor human cardiac myocytes (hCMs) were expanded in normal glucose. They were then cultured for 14 days in normal glucose or high glucose media before seeding on prepared and sterilized decellularized porcine myocardial scaffolds. Normal and high glucose media constituted of Dulbecco's Modified Eagle Medium (DMEM), 10% Fetal

Bovine Serum (FBS), and 1% antibiotic/antimycotic (penicillin-streptomycin), with 5mM (1g/L) and 25mM (4.5g/L) glucose, respectively.

*6.2.6 3D Kube Minibioreactor Setup*

For the 3D Kube minibioreactor systems, sterile scaffolds were then placed in normal glucose media constituted of DMEM, 10% FBS, and 1% antibiotic/antimycotic (penicillin-streptomycin) overnight at 37 degrees Celsius. The next day, these scaffolds were injected with a 26½ gauge needle aseptically with hCM with 200,000 cells per scaffold. After 48 hours of static resting in either normal (n=11) or high (n=10) glucose media, two bioreactors (one normal and one with high glucose media) were aseptically assembled utilizing 3D Kubes to house the respective reseeded scaffolds. The bioreactors were housed in an incubator (37°C, 5% $CO_2$). A multi-channel peristaltic pump provided a flow rate of 1mL/min from a fluid reservoir. 1% antibiotic/antimycotic was injected every 3.5 days into the closed system to replenish degraded antibiotics and media was changed every week for each bioreactor. The scaffolds were subjected to these conditions for 14 days then analyzed (**Table 6.1**). Cell viability was confirmed with a LIVE/DEAD® Viability/Cytotoxicity kit for Mammalian Cells from Molecular Probes (Eugene, OR).

| 3D Kube Minibioreactor | | | | |
|---|---|---|---|---|
| Conditions | # Samples: Protein | # Samples: Histology | # Samples: Live/Dead | # Samples: Cryosections |
| Normal Glucose | 6 | 2 | 1 | 1 |
| High Glucose | 6 | 2 | 1 | 1 |

**Table 6.1:** Sample size and analysis for 3D Kube minibioreactor.

*6.2.7 Electromechanical Bioreactor Setup*

Sized, sterile, decellularized porcine myocardium was incubated overnight at 37 degrees Celsius in cell culture medium comprised of Dulbecco's Modified Eagle's medium (DMEM), 10% fetal bovine serum (FBS), and 1% antibiotic/antimycotic (penicillin-streptomycin). Before seeding, scaffolds were incubated 2 hours at 37°C in 6 well plates to allow removal of excess medium. Scaffolds were secured into two modified Flexcell Bioflex® 6-well plates (Flexcell International Corp., Burlington, NC, USA) and progenitor human cardiomyocytes (hCM) at passage 6 were aseptically injected and dropwise seeded (2 million per scaffold) with a sterile 26 ½ gauge needle. Plates were placed in an incubator for 1 hour to allow for hCM attachment and then 4 mL of cell culture media (normal or high glucose, depending on expansion conditions) was added to each well. Tissue was statically cultured for 3 days before subjecting tissue cultured in either normal or high glucose to preconditioning in the bioreactor. Preconditioning was performed with a cyclic waveform of 0-40-0 mmHg for two days, followed by two days with a cyclic waveform of 0-80-0 mmHg, and then tissue engineered myocardium was subjected to 0-120-0 mmHg cyclic waveform with electrical stimuli for 14 days. Normal and high glucose media was changed every day and 7 mL was added to each well to cover the dynamic tissue and account for evaporation. Cell viability was confirmed with a LIVE/DEAD® Viability/Cytotoxicity kit for Mammalian Cells from Molecular Probes (Eugene, OR). Samples were divided and processed for analysis (**Table 6.2, Figure 6.1**).

| Electromechanical Bioreactor | | |
|---|---|---|
| Conditions | # Samples: Protein, RNA, and Histology | # Samples: Live/Dead, Cryosections |
| Normal Glucose | 11 | 1 |
| High Glucose | 11 | 1 |

**Table 6.2:** Sample size and analysis for electromechanical bioreactor.

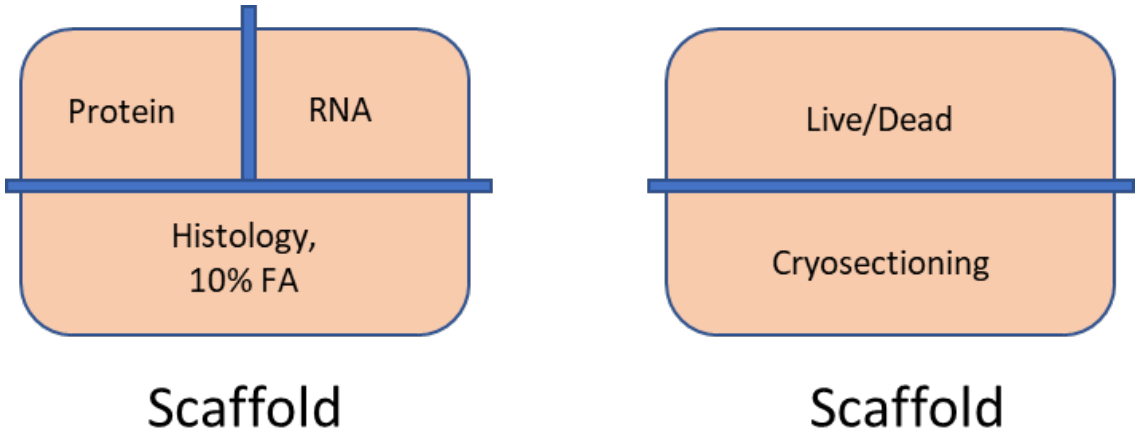


**Figure 6.1:** Division of electromechanical scaffolds for analysis.

*6.2.8 Histological Analysis*

After 14 days in either the 3D Kube minibioreactor or electromechanical bioreactor, normal and high glucose samples were fixed in 10% formalin for 48 hours and histologically processed, paraffin embedded, and sectioned on slides. Rehydrated paraffin sections (5um) were stained with hematoxylin and eosin (H&E), Movat's pentachrome, and Masson's trichrome kits for normal and high glucose samples. Manufacturer's guidelines were followed for these.

Immunohistochemistry (IHC) was performed for detection of superoxide dismutase-2 (SOD-2), light chain 3B (LC3B), carboxymethyl lysine (CML), inositol-

requiring enzyme 1 (IRE-1) and caspase-3 to compare high and normal glucose samples. Briefly, antigen retrieval was performed on rehydrated paraffin sections (5um) with heated (90-100 degrees C, 10 min) 10mM citric acid (pH=7.4). Slides were permeabilized with 0.025% Triton X-100 for 5 minutes and then incubated in normal blocking serum for 45 minutes. Primary antibodies (rabbit anti-SOD-2 1ug/mL dilution, rabbit anti-LC3B 5ug/mL dilution, rabbit anti-IRE-1 4ug/mL, mouse anti-CML 2ug/mL, or rabbit anti-caspase-3 4ug/mL dilution) were incubated overnight at 4 degrees Celsius. Negative controls were obtained by omitting the primary antibody. Endogenous peroxidases were blocked with 0.3% hydrogen peroxide in 0.3% normal horse serum for 30 minutes. The secondary biotinylated anti-rabbit antibody was applied for 30 minutes. Antibody staining was visualized using the Vector ABC peroxidase substrate kit and then lightly counterstained with diluted hematoxylin, before mounting. A Zeiss Axiovert 40CFL microscope with AxioVision Release 4.6.3 digital imaging software (Carl Zeiss MicroImaging, Inc. Thornwood, NY) was utilized to obtain images.

*6.2.9 Lipid Staining*

Lipid accumulation was visualized in both bioreactor system samples via oil red O on cryosectioned normal and high glucose samples. Slides were fixed in 4% paraformaldehyde, rinsed in distilled, deionized water ($ddH_2O$), rinsed in 60% isopropanol, and stained in 0.3% Oil Red O in isopropanol solution. Slides were then rinsed twice in 60% isopropanol, stained in a 1 to 1 hematoxylin in $ddH_2O$ solution, rinsed in $ddH_2O$, and mounted with aqueous Vectashield mounting medium. Light images were taken on a Zeiss Axiovert 40CFL microscope, as described before.

*6.2.10 Detection of Caspase-3, SOD-2, CML, AGE, LC3B, and PERK*

Western blotting was employed to compare amounts of caspase-3, SOD-2, CML, advanced glycation endproducts (AGEs), LC3B, and protein kinase RNA-like endoplasmic reticulum kinase (PERK) between normal glucose and high glucose conditioned samples run in the electromechanical bioreactor for 14 days. Proteins were extracted by radioimmunoprecipitation assay (RIPA) extraction buffer (50mM Tris-HCl pH 7.4, 150mM sodium chloride (NaCl), 1mM ethylenediaminetetraacetic acid (EDTA), 1% Triton X-100, 1% Sodium Deoxycholate, 0.1% sodium dodecyl sulfate (SDS), with protease inhibitor cocktail). Protein concentrations in the samples were found using a bicinchoninic acid protein (BCA) assay. For each sample, 20ug of protein per lane was loaded and a pre-stained molecular weight standard was loaded in one of the lanes. Protein from the gels were transferred to polyvinylidine fluoride membranes. Primary antibodies (mouse anti-caspase-3 1ug/mL, rabbit anti-SOD-2 1ug/mL, mouse anti-CML 1ug/mL, rabbit anti-AGE 1ug/mL, rabbit anti-LC3B 1ug/mL, or rabbit anti-PERK 1ug/mL) were applied overnight at 4°C. The secondary antibody from the anti-mouse/rabbit kit was then applied for 45 minutes at room temperature. The polyvinylidine fluoride membranes were fluorescently tagged with detection solution from the anti-mouse/rabbit kit (1 minute) and then imaged using the Chemi-Doc™ XRS+ system from Bio-rad (Hercules, CA). Relative band intensities were determined using Bio-rad Image Lab Software Version 5.1, beta build 1 and values were analyzed.

Relative amounts of caspase-3 between groups in the electromechanical bioreactor were examined with the ApoTarget Caspase-3 / CPP32 Colorimetric Protease

Assay from Invitrogen (Carlsbad, CA). Manufacturer's protocol was followed. Total protein was measured via a BCA assay and 100ug was used per sample (n=5 per group). Intensities were measured using the Synergy H1 Hybrid Reader System from BioTek (Winooski, VT).

### *6.2.11 Matrix Metalloproteinase Activity Analysis*

Matrix Metalloproteinase (MMP) activity in high and normal glucose media and tissue protein lysates were analyzed by gelatin zymography. For media analysis, 10uL of normal or high glucose media per sample was loaded into a gelatin zymography gel with 1x sample buffer. For protein lysate analysis, 20ug of protein was loaded. A pre-stained molecular weight standard was loaded into a separate lane for each gel. After electrophoresis separation, the zymography gel was washed in a triton-X solution and MMPs were activated with a brij-35 development buffer for 24 hours at 37 degrees Celsius. After staining with Coomassie and destaining, MMP clear bands were imaged using the Chemi-Doc™ XRS+ system and evaluated by densitometry using the using Bio-rad Image Lab Software.

### *6.2.12 Statistical Analysis*

Results are expressed at mean ± standard deviation (SD). Statistical analysis was performed between groups utilizing Welch's two-tailed t-test in excel. Significance was determined with an alpha ($\alpha$) value of 0.05.

## 6.3 Results

### *6.3.1 3D Kube Minibioreactor Results*

#### *6.3.1.1 Analysis of Cell Seeding and Viability in 3D Kube Minibioreactor*

Constructs were placed in either a high or normal glucose 3D Kube minibioreactor under perfusion conditions in an incubator (**Figure 6.2**). Before placing hCM seeded scaffolds into the 3D Kube minibioreactor, analysis of cell viability was performed after sitting statically for 48 hours to allow for hCM attachment. As seen in **Figure 6.3**, hCMs seeded in the scaffold were viable at 48 hours after injection. Scaffolds from both high and normal glucose dynamically conditioned in the 3D Kube minibioreactor for 14 days had live cells (**Figure 6.3**). As revealed in **Figure 6.4**, hematoxylin and eosin (H&E) staining of these samples after conditioning showed hCM within the decellularized porcine myocardium scaffolds.

#### *6.3.1.2 Investigation of Matrix Metalloproteinase Activity and AGEs*

Matrix metalloproteinase (MMP) activity and advanced glycation endproduct (AGE) formation within high and normal glucose 3D Kube minibioreactor samples were determined with a gelatin zymography and protein western blotting analysis, respectively. As shown in **Figure 6.5**, there were no significant differences between groups in overall MMP, MMP9, and MMP2 activity. Protein analysis of AGEs revealed no significant differences between the two groups (**Figure 6.6**).

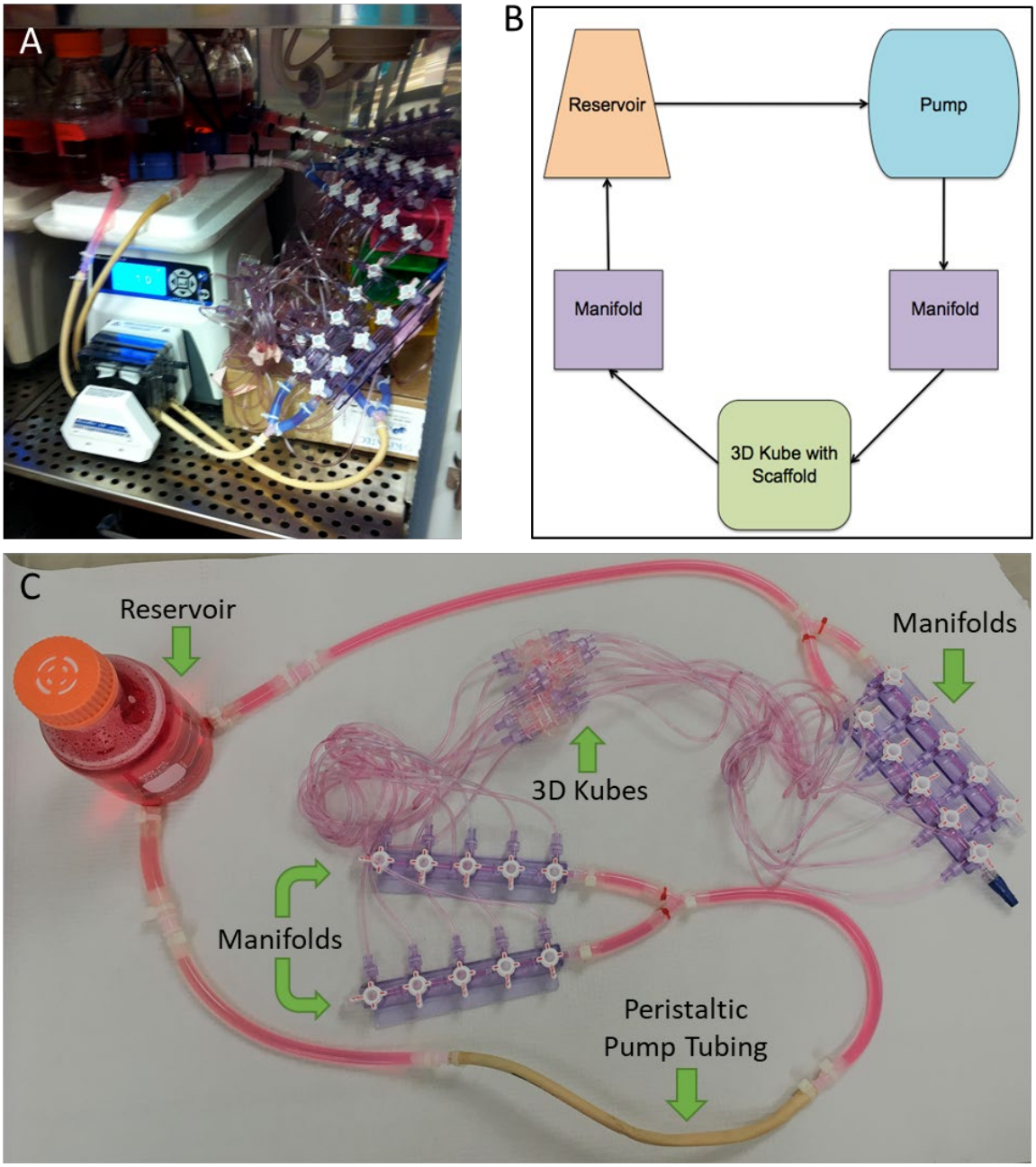


**Figure 6.2:** Set-Up of 3D Kube minibioreactor. (A) Minibioreactor was housed in incubator. (B) Diagram illustrating media flow in the system. (C) 3D Kube minibioreactor platform fully assembled with tubing, manifolds, reservoir, and 3D Kubes housing seeded constructs.

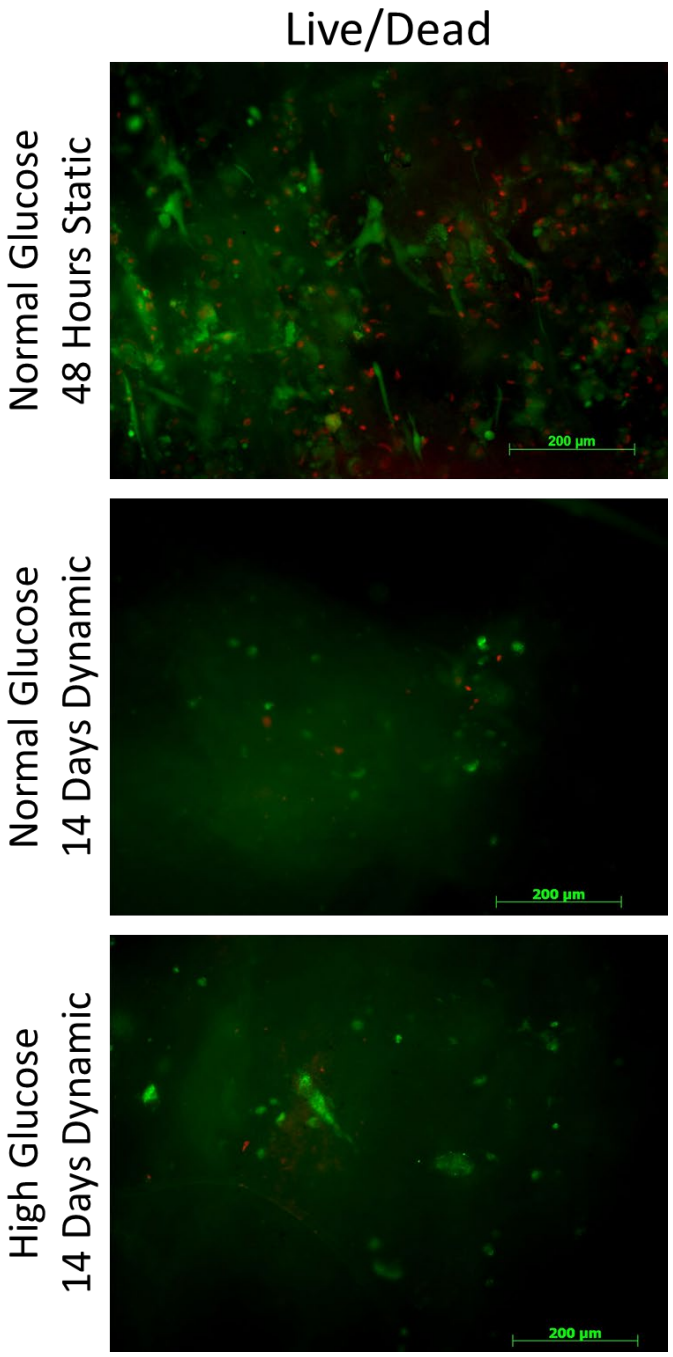


**Figure 6.3:** Viability analysis of hCM seeded on decellularized porcine myocardium scaffolds. Static seeding after 48 hours (top), and dynamic minibioreactor conditioned normal (middle) and high (bottom) glucose after 14 days. (green=live cells, red=dead cells).

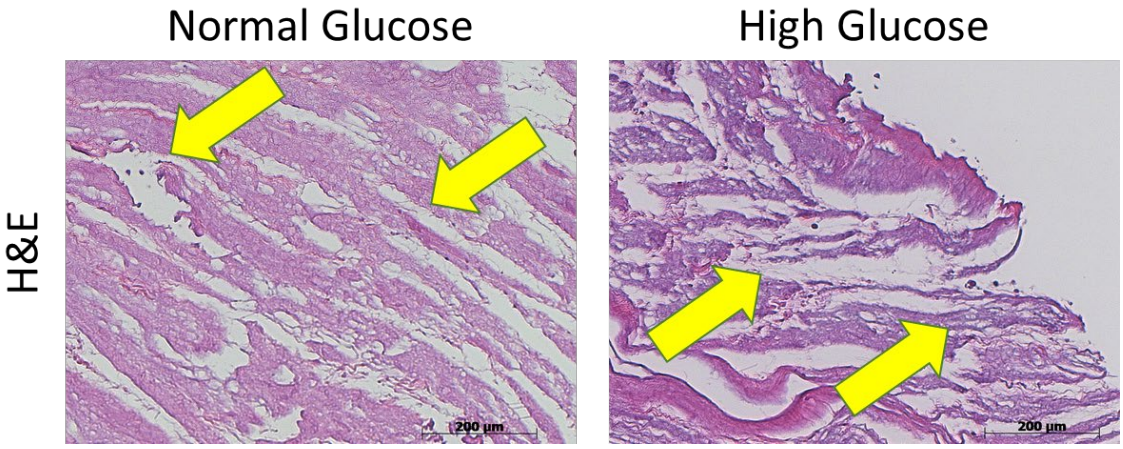


**Figure 6.4:** Hematoxylin and eosin (H&E) staining of samples after 14 days in 3D Kube minibioreactor. Normal (left) and high (right) glucose showed cells (purple) and tissue (pink).

*6.3.1.3 Antioxidant Defenses and Lipid Accumulation*

Antioxidant defense mechanisms were investigated with immunohistochemical (IHC) staining and western blotting for protein analysis. Superoxide dismutase 2 (SOD-2), an endogenous antioxidant defense mechanism, was shown to be present in both high and normal glucose samples stained via IHC (**Figure 6.7**). SOD-2 had an upward trend in the high glucose group as seen in western blotting. Lipid accumulation was visualized with staining and was only found in high glucose samples (**Figure 6.8**).

*6.3.1.4 Examination of Apoptosis and Autophagy*

Caspase-3 was employed to determine programed death or apoptosis within samples. This protein was present in both normal and high glucose conditioned groups, as seen with IHC staining (**Figure 6.9**). IHC staining of samples for light chain 3B (LC3B), an

autophagic marker, revealed its presence in both groups (**Figure 6.10**). Western blotting analysis showed significantly higher expression of LC3B in the high glucose group.

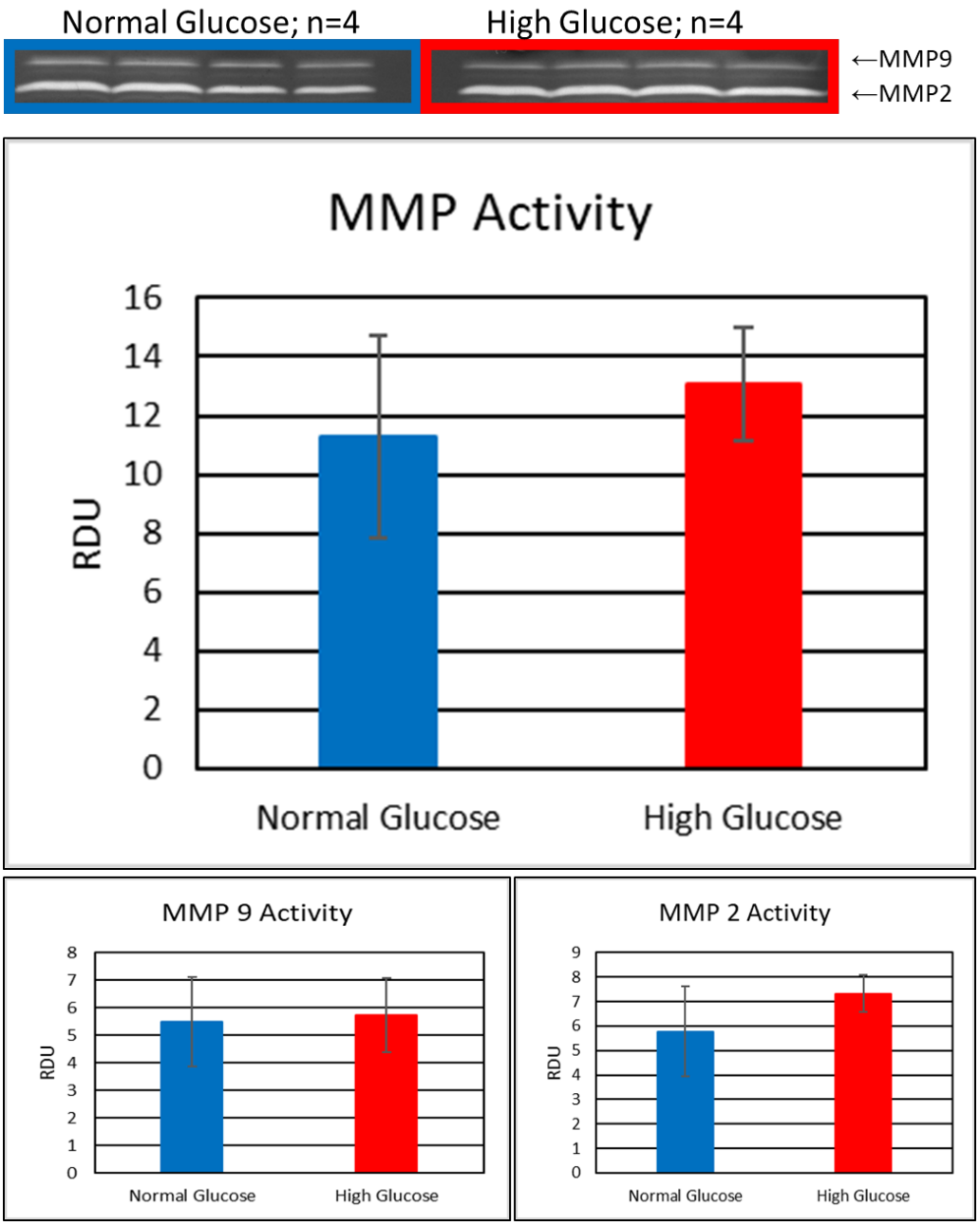


**Figure 6.5:** Overall matrix metalloproteinase (MMP), MMP9, and MMP2 activity in 3D Kube normal and high glucose media via gelatin zymography. RDU= relative densitometry units.

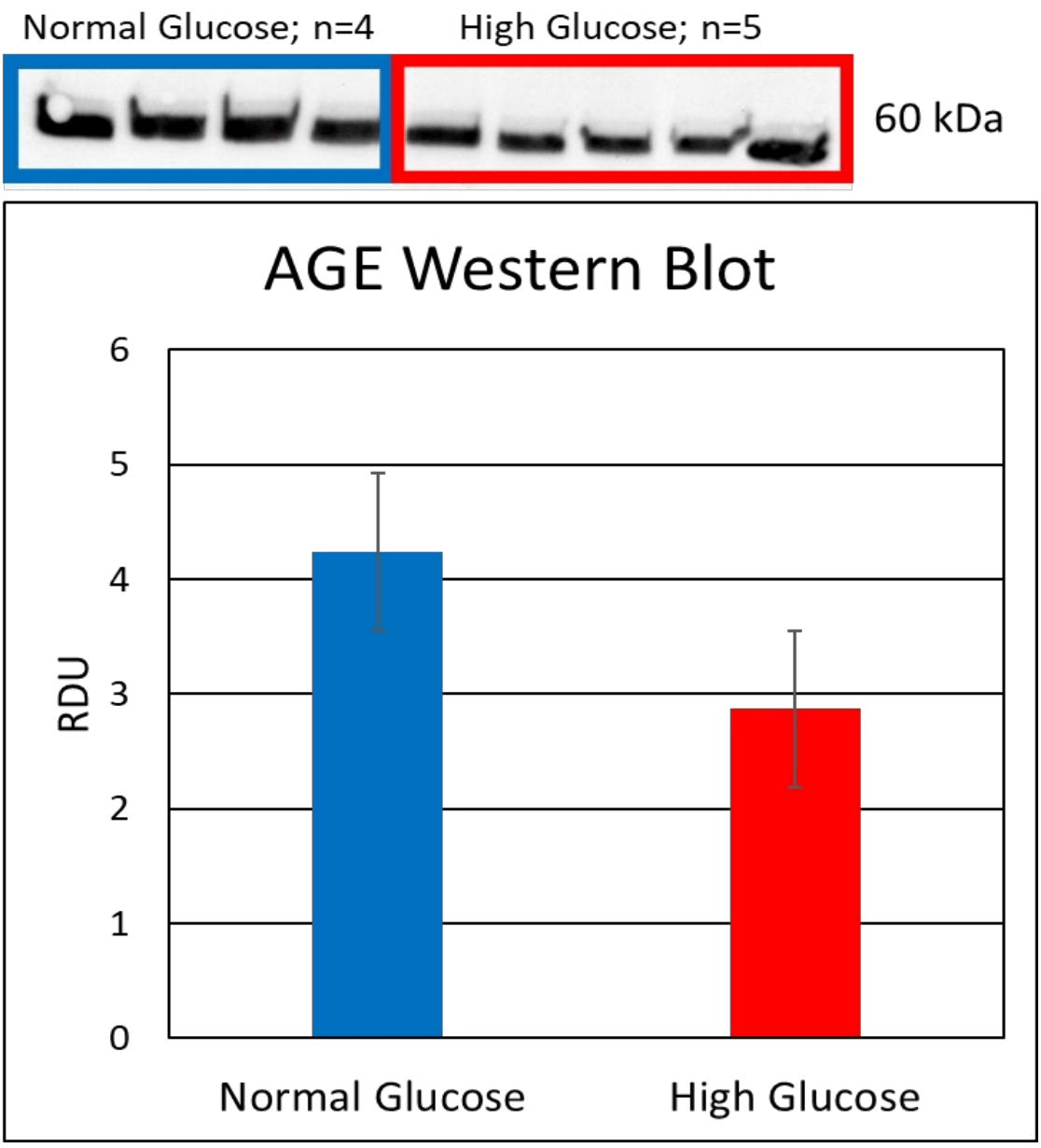


**Figure 6.6:** Detection of advanced glycation endproducts (AGEs) in 3D Kube minibioreactor samples by employing western blotting. RDU= relative densitometry units.

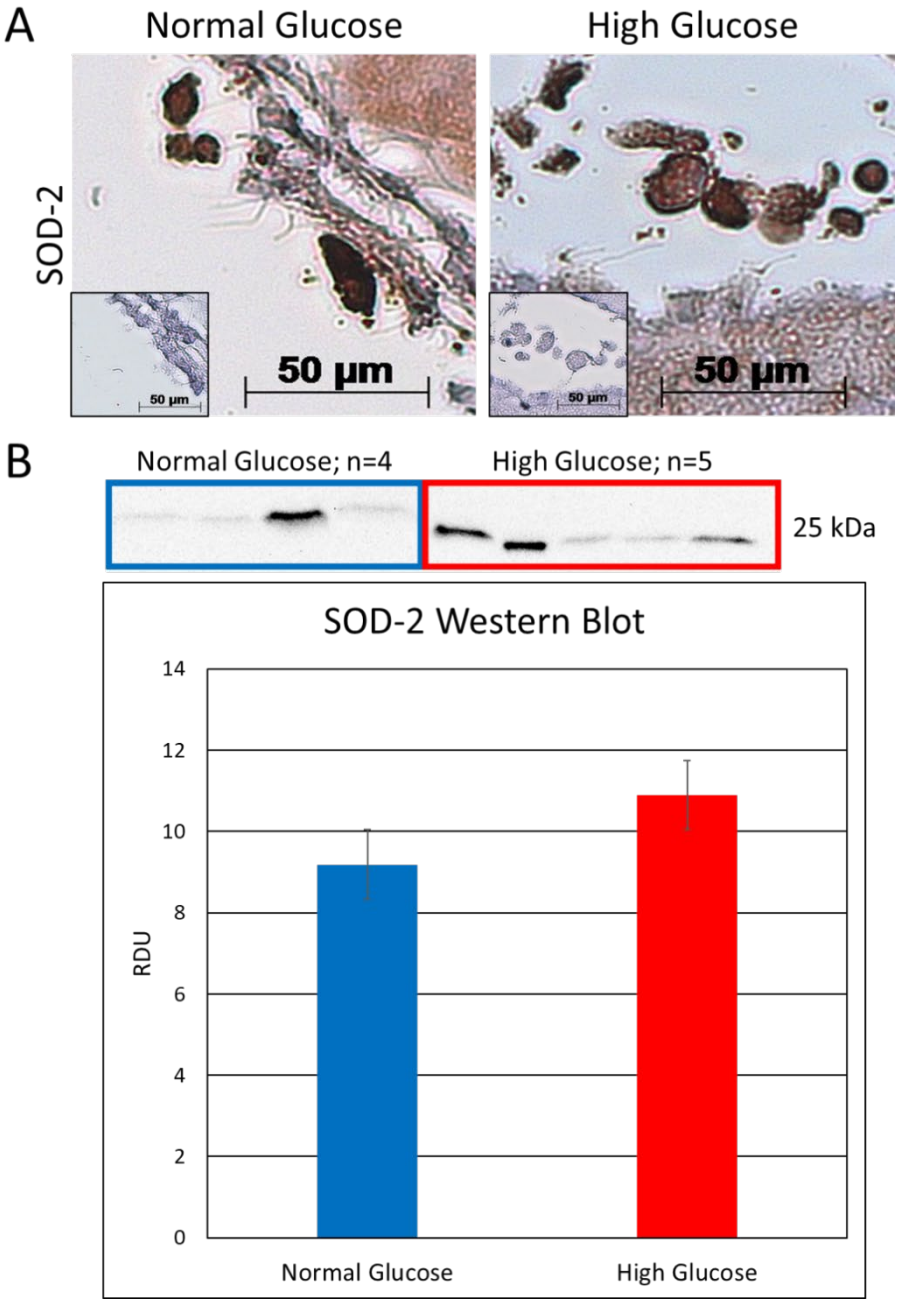


**Figure 6.7:** Investigation of antioxidant superoxide dismutase 2 (SOD-2) in 3D Kube normal and high glucose groups. (A) Immunohistochemical (IHC) staining of samples for SOD-2 visualization. (brown=positive, dark purple=nuclei; inserts=negative controls) (B) SOD-2 protein western blotting analysis of the two groups. RDU= relative densitometry units.

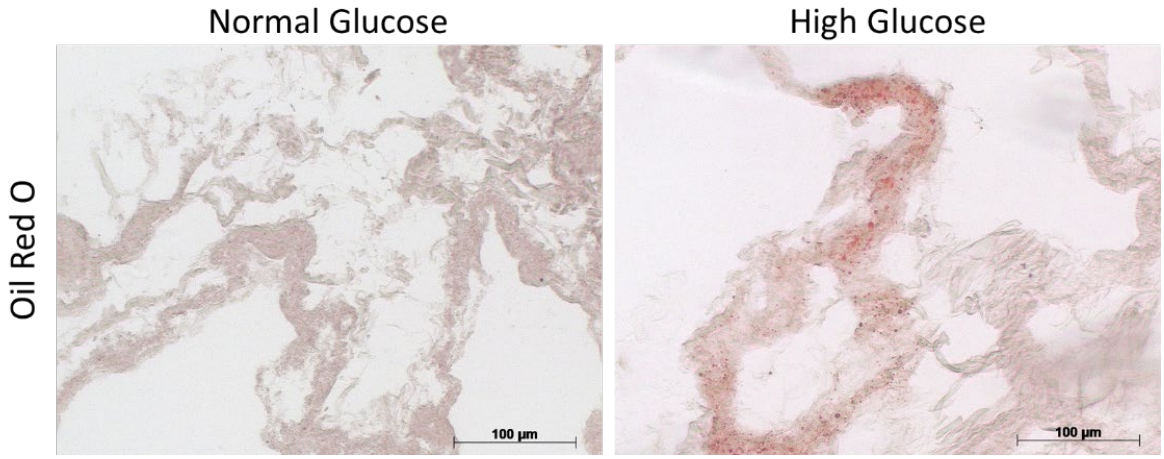


**Figure 6.8:** Staining for lipid accumulation in normal and high glucose samples. Red= lipids.

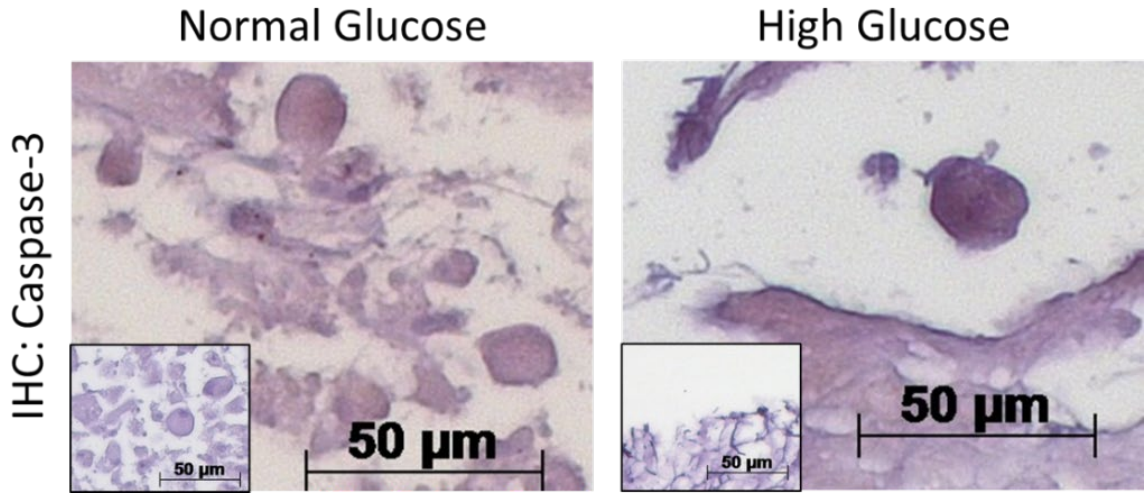


**Figure 6.9:** Visualization of apoptosis marker caspase-3 in normal and high glucose 3D Kube minibioreactor samples via immunohistochemistry (IHC). (brown=positive, dark purple=nuclei; inserts=negative controls).

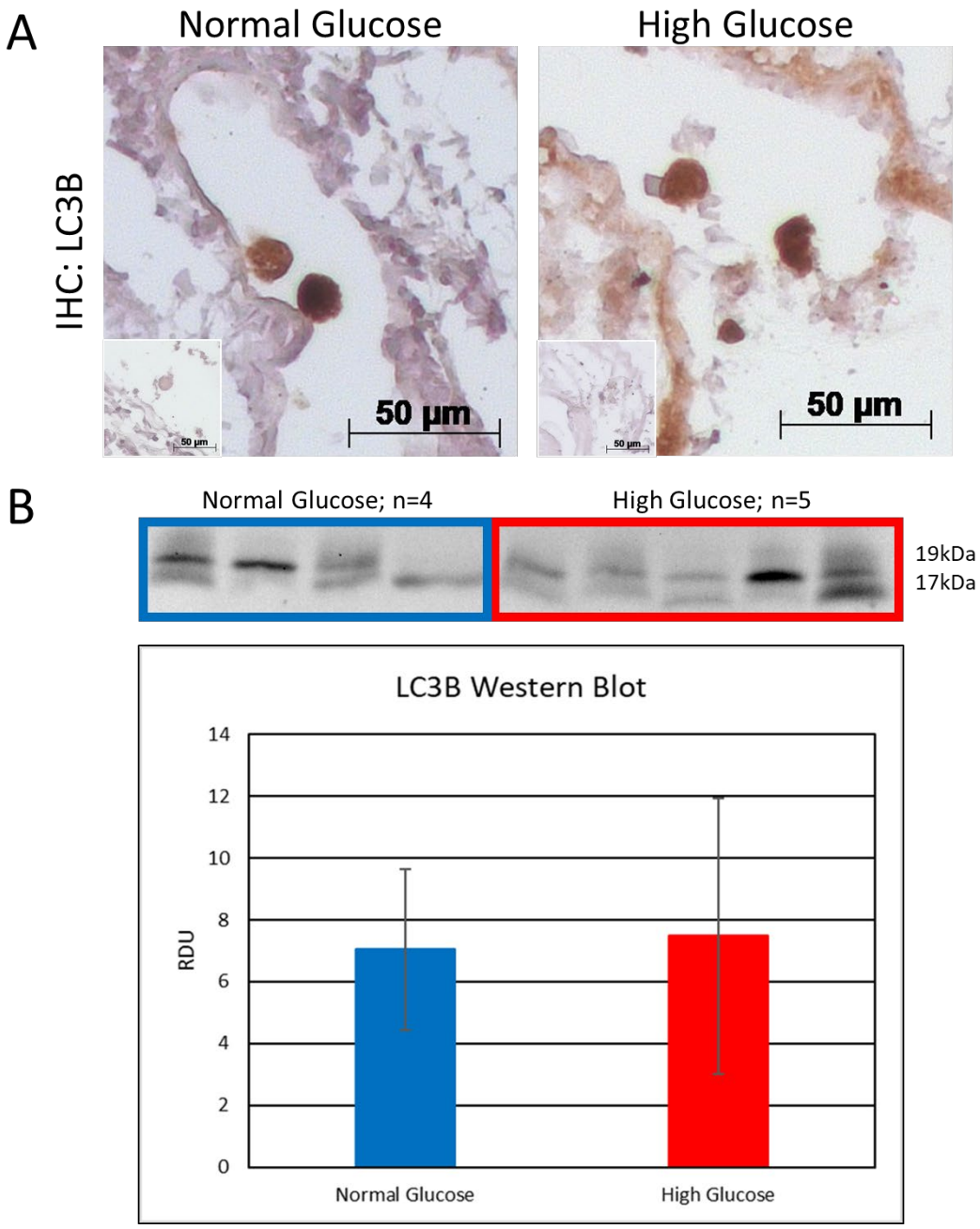


**Figure 6.10:** Inquiry of light chain 3B (LC3B), a marker of autophagy, between 3D Kube groups. (A) Immunohistochemical (IHC) staining of samples for LC3B. (brown=positive, dark purple=nuclei; inserts=negative controls) (B) Western blotting analysis of LC3B in groups. RDU= relative densitometry units. * indicates statistical difference.

### *6.3.2 Electromechanical Bioreactor Results*

#### *6.3.2.1 Analysis of Cell Seeding and Viability in Electromechanical Bioreactor*

Before mounting into the electromechanical bioreactor, we determined that hCM seeded on decellularized porcine myocardium were viable after one hour and three days after static seeding (**Figure 6.11**). After 14 days under dynamic conditions, engineered tissues contained live cells in both normal and high glucose conditions (**Figure 6.12**). Trichrome and pentachrome staining both showed hCM integrated within the collagen ECM scaffold (**Figure 6.13**).

#### *6.3.1.2 Investigation of Matrix Metalloproteinase Activity and AGEs*

MMP activity and accumulation of AGEs were examined in electromechanically stimulated normal and high glucose conditioned engineered tissues and media. When investigating MMP activity in media samples, there were no differences found between the two groups for overall MMP, MMP9 and MMP2 activity (**Figure 6.14**). MMP activity in tissue lysates showed no significant difference in overall MMP, MMP9, and active MMP2, with significantly higher pro MMP2 and overall MMP2 in high glucose conditions, as seen in **Figure 6.15**. Carboxymethyl lysine (CML), an AGE, was shown to be present in both groups with IHC staining and slightly greater in the high glucose group with western blot analysis (**Figure 6.16**). Western blotting for AGE detection indicated comparable amounts in both groups.

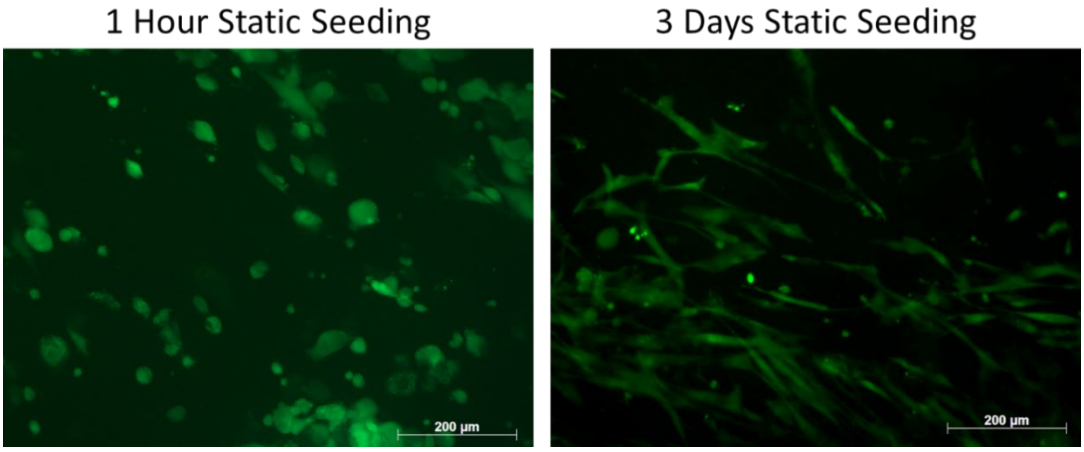


**Figure 6.11:** Viability of human cardiomyocytes (hCM) after seeding. Live images show viable (green) hCM after 1 hour (left) and 3 days (right) of static seeding.

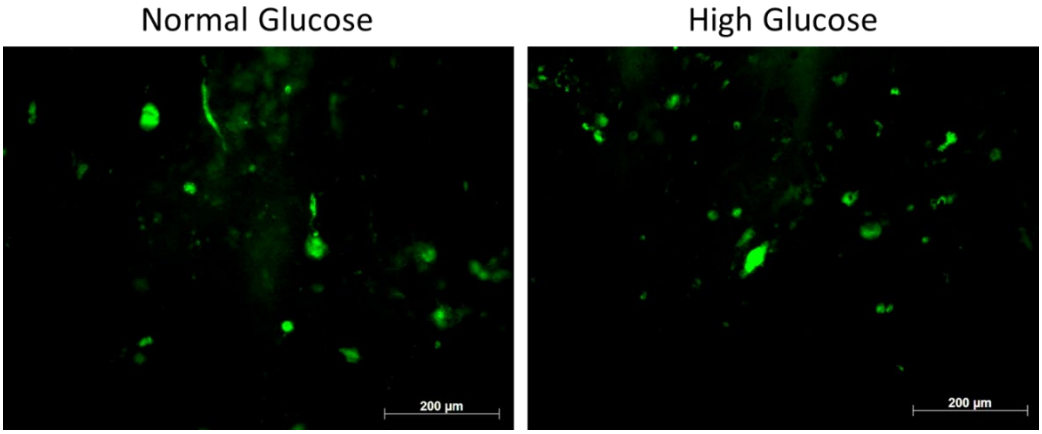


**Figure 6.12:** Cellular viability after 14 days of electromechanical stimuli in normal and high glucose conditions. Green= live cells.

*6.3.1.3 Examination of Cellular Antioxidant Defenses, Autophagy, and Apoptosis*

Cellular changes known as DCMP hallmarks were studied such as antioxidant defense mechanisms, autophagy, and apoptosis. Superoxide dismutase 2 (SOD-2), an endogenous antioxidant, was visible in both normal and high glucose bioreactor samples

with IHC staining (**Figure 6.17**). SOD-2 protein detection with western blotting revealed a greater inclination in high glucose samples. IHC staining and western blotting of light chain 3B (LC3B), an autophagy protein, indicated similar amounts in each group (**Figure 6.18**). Caspase-3, an apoptosis marker, stained in both groups (**Figure 6.19**). Protein analysis of caspase-3 revealed an upward trend in high glucose samples with western blotting and similar expression in both with a caspase-3 assay.

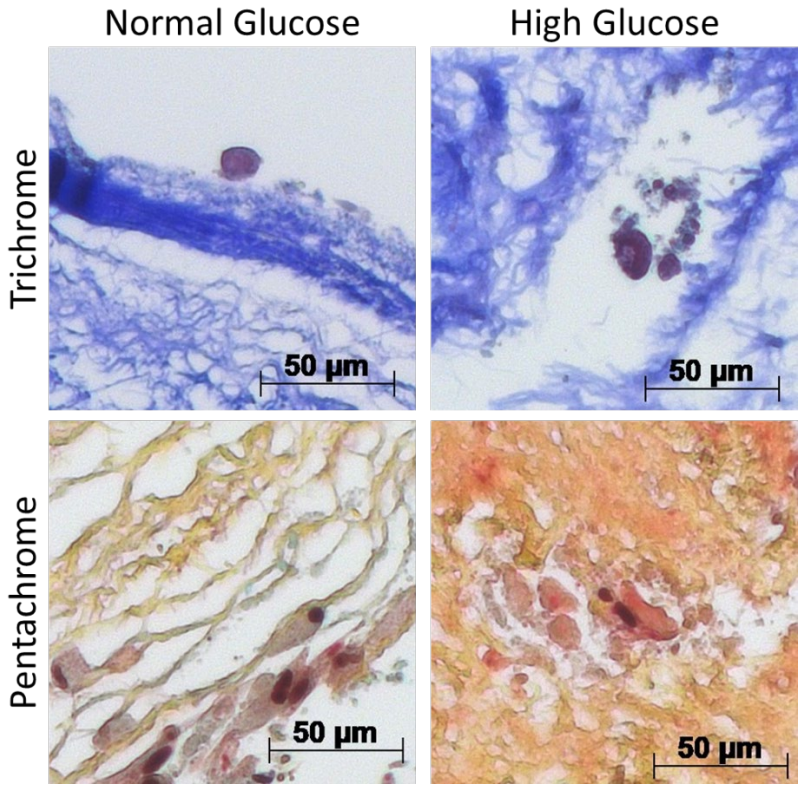


**Figure 6.13:** Cell and ECM visualization in electromechanical normal and high glucose samples. Masson's trichrome (red=muscle fibers, blue=collagen, black=nuclei) and Movat's pentachrome (black=nuclei or elastic fibers, yellow=collagen or reticular fibers, blue=ground substance or mucin, bright red=fibrin, red=muscle) staining of groups from normal and high glucose conditions.

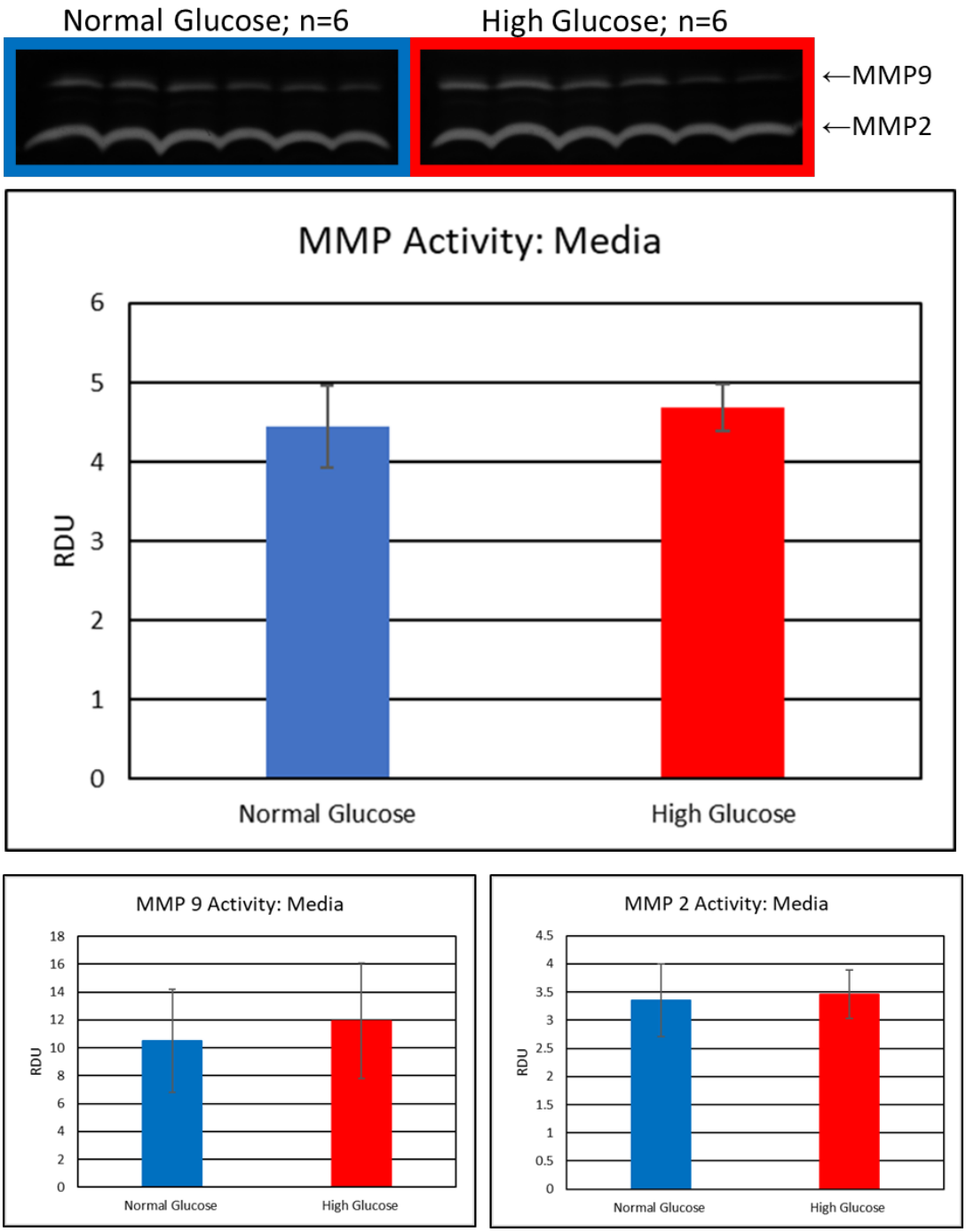


**Figure 6.14:** Matrix metalloproteinase (MMP) activity in media from electromechanically conditioned normal and high glucose samples via gelatin zymography. MMP activity results for all MMPs, MMP9, and MMP2 in media. RDU= relative densitometry units.

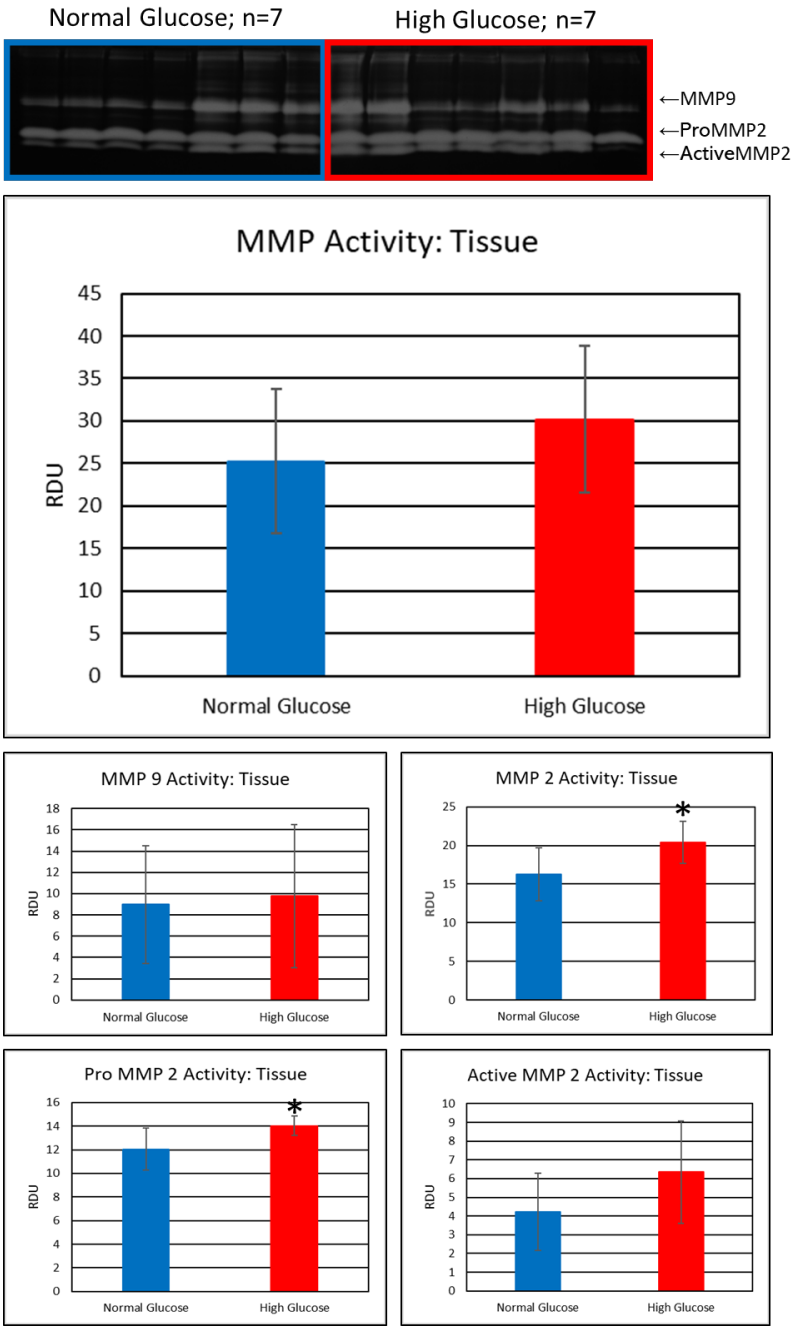


**Figure 6.15:** Matrix metalloproteinase (MMP) activity in tissue lysates from electromechanically conditioned normal and high glucose samples via gelatin zymography. MMP activity results for all MMPs, MMP9, MMP2, proMMP2, and activeMMP2 in tissue. RDU= relative densitometry units. * indicates statistically significant difference.

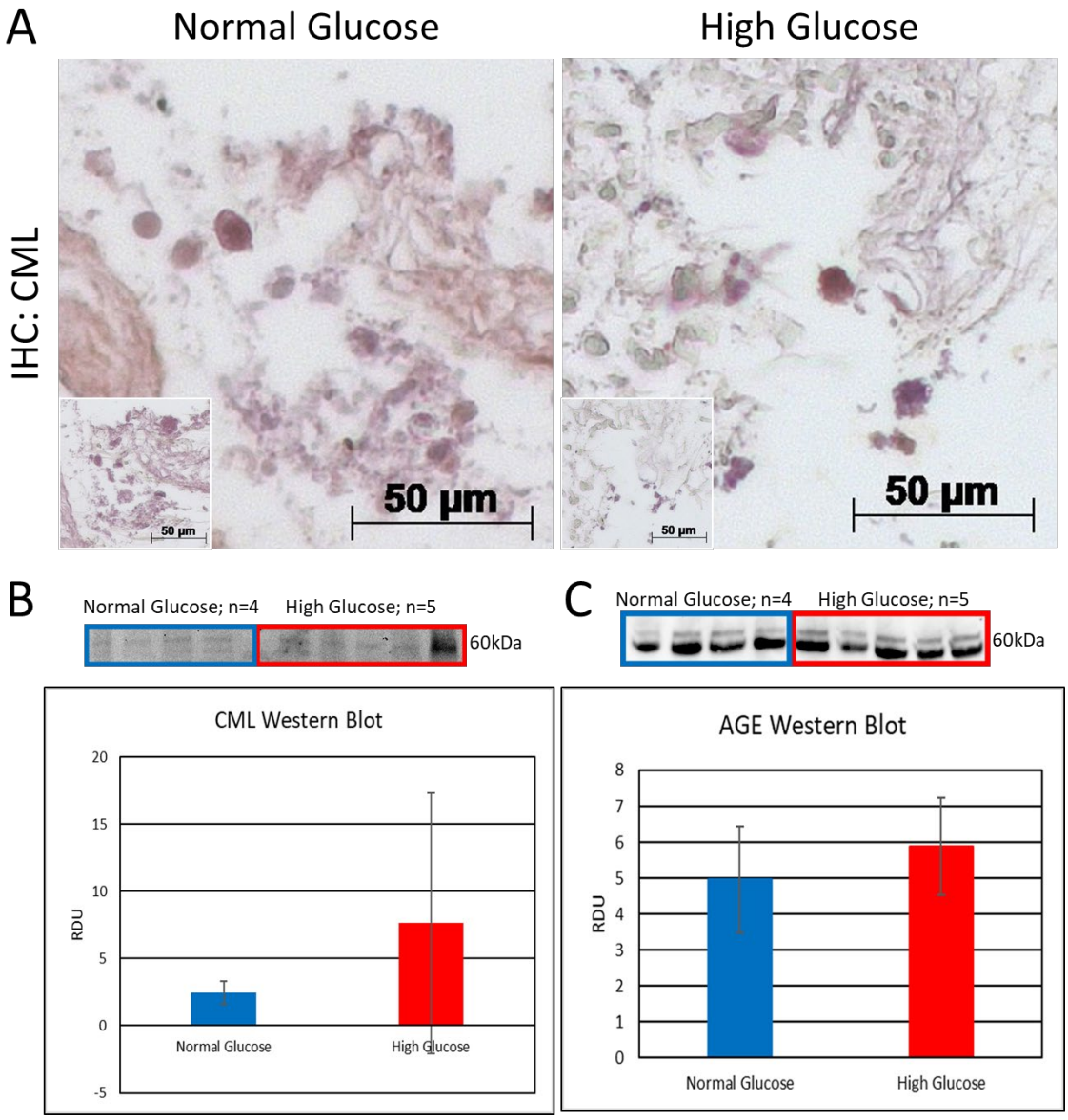


**Figure 6.16:** Investigation of advanced glycation endproducts (AGEs) in normal and high glucose groups electromechanically stimulated. (A) Immunohistochemical (IHC) staining of samples for carboxymethyl lysine (CML), an AGE. (brown=positive, dark purple=nuclei; inserts=negative controls) (B) Western blotting analysis of CML in groups. (C) Western blotting analysis for AGE in samples. RDU= relative densitometry units.

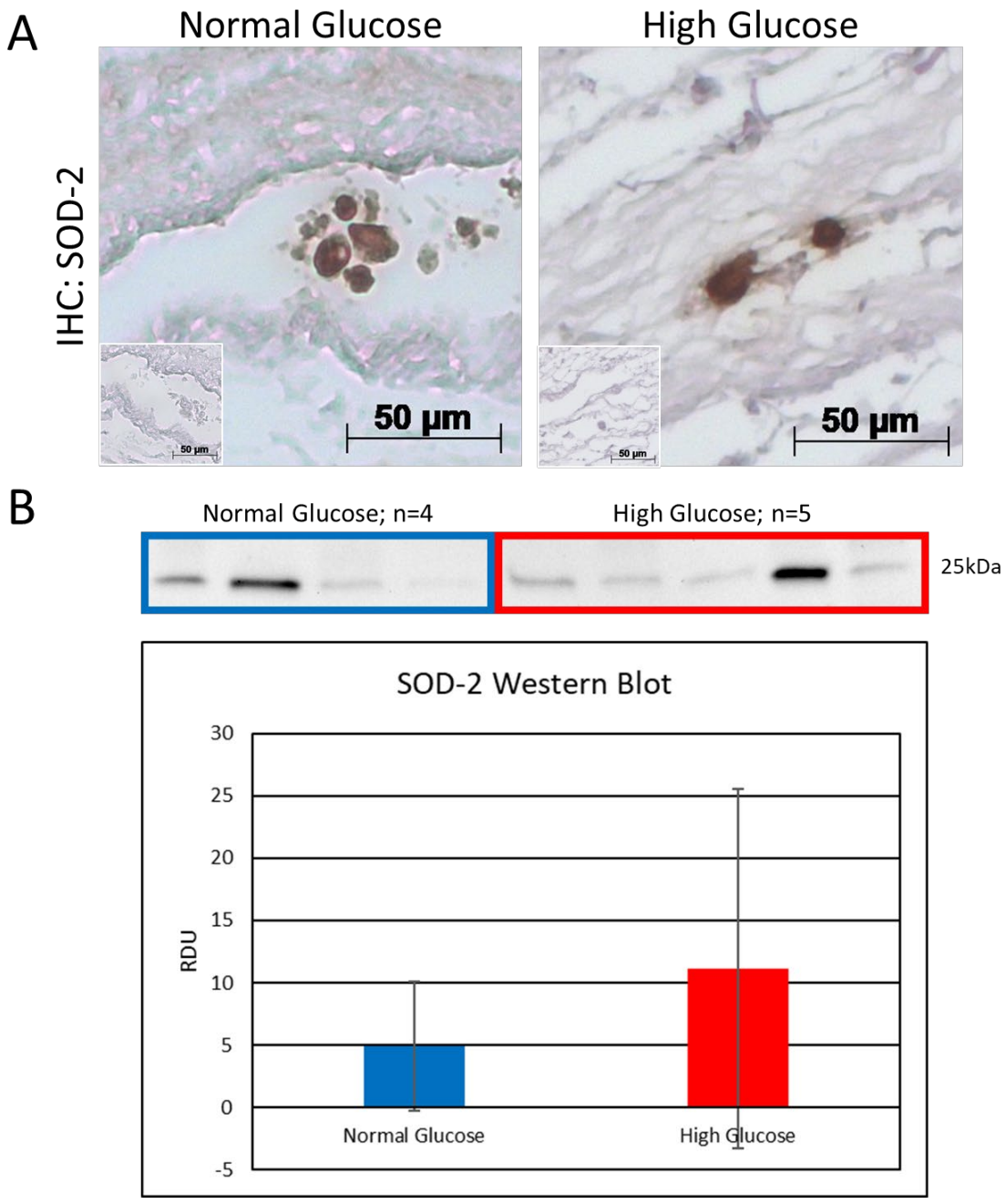


**Figure 6.17:** Examination of antioxidant superoxide dismutase 2 (SOD-2) in electromechanical bioreactor normal and high glucose groups. (A) Immunohistochemical (IHC) staining of samples for SOD-2 visualization. (brown=positive, dark purple=nuclei; inserts=negative controls) (B) SOD-2 protein western blotting analysis of the two groups. RDU= relative densitometry units.

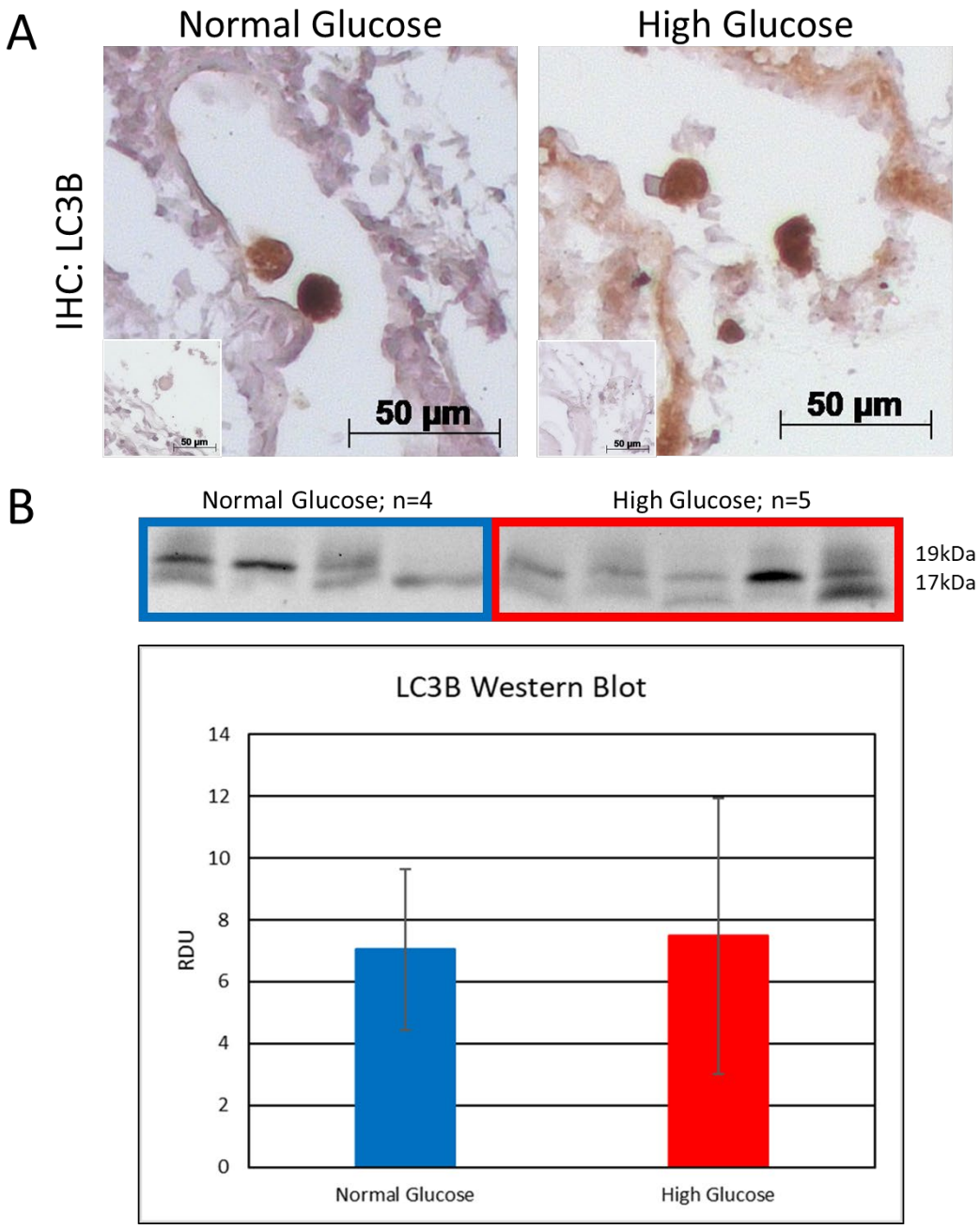


**Figure 6.18:** Inquiry of light chain 3B (LC3B), a marker of autophagy, between electromechanical bioreactor groups. (A) Immunohistochemical (IHC) staining of samples for LC3B. (brown=positive, dark purple=nuclei; inserts=negative controls) (B) Western blotting analysis of LC3B in groups. RDU= relative densitometry units.

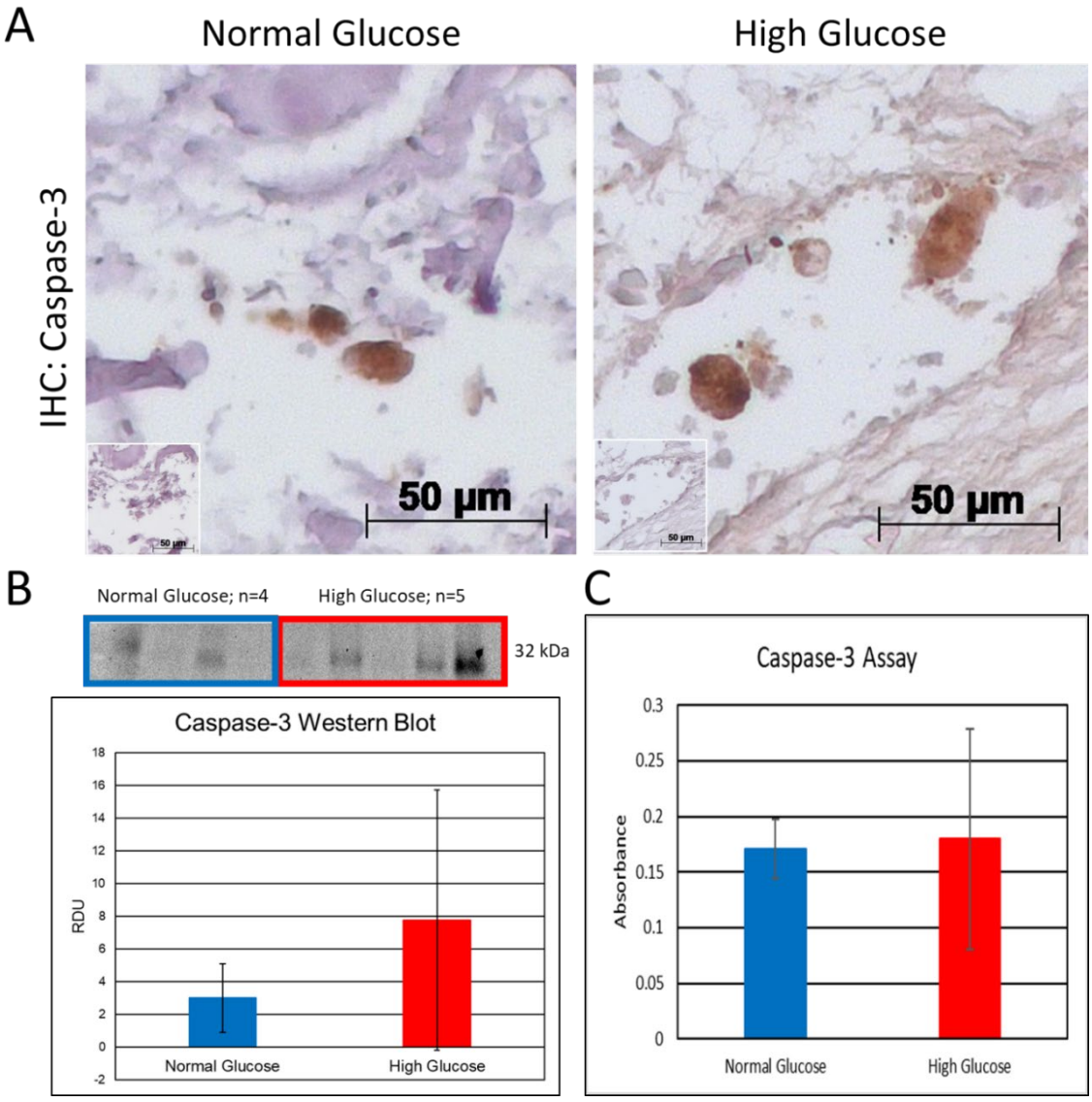


**Figure 6.19:** Analysis of apoptosis marker, caspase-3, in electromechanically conditioned normal and high glucose groups. (A) Immunohistochemical (IHC) staining of samples for caspase-3 visualization. (brown=positive, dark purple=nuclei; inserts=negative controls) (B) Caspase-3 protein western blotting analysis of the two groups. RDU= relative densitometry units. (C) Results from ApoTarget caspase-3 assay.

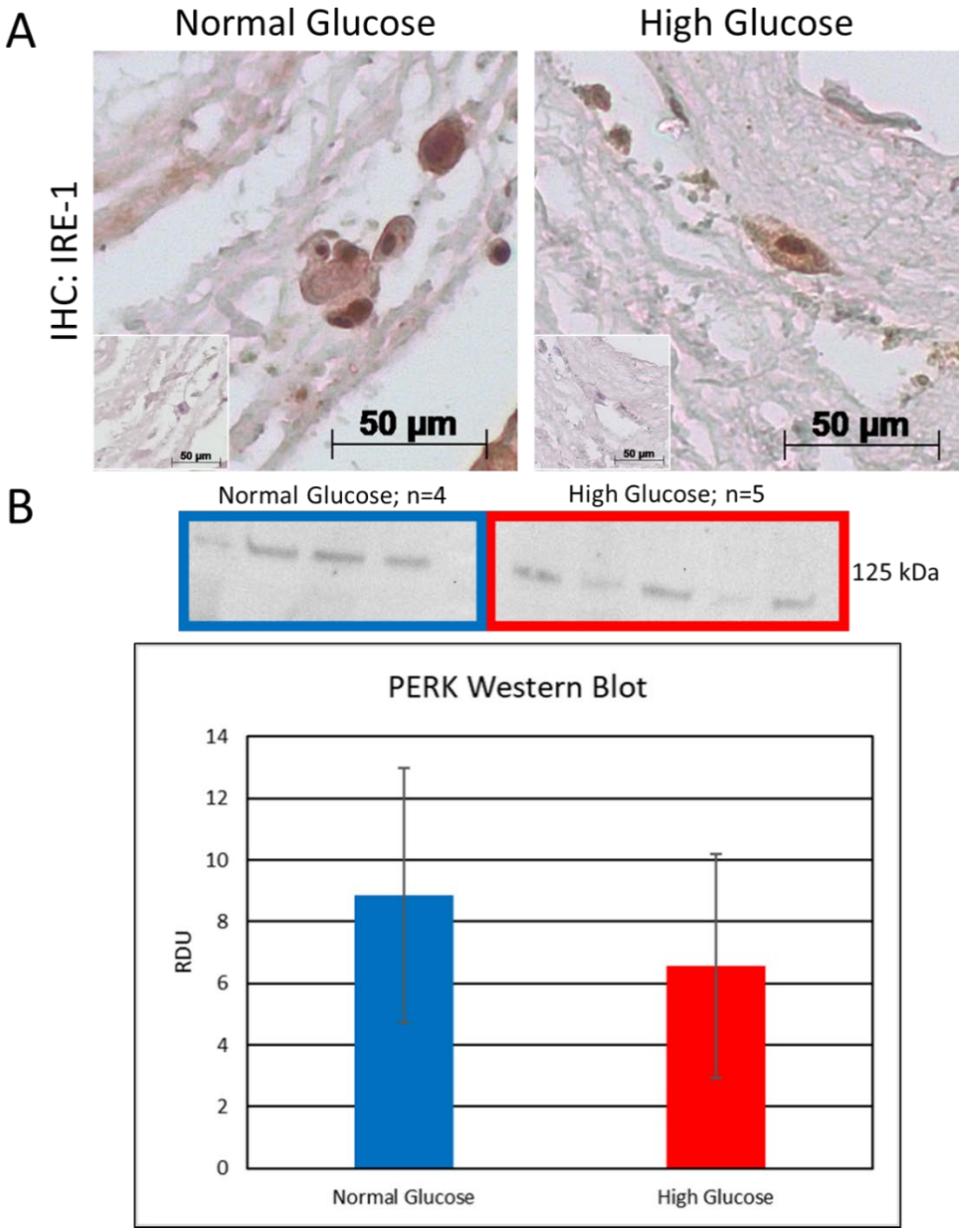


**Figure 6.20:** Endoplasmic reticulum (ER) stress inspection in normal and high glucose electromechanical samples. (A) Immunohistochemical (IHC) staining of inositol requiring enzyme-1 (IRE-1) in samples. (brown=positive, dark purple=nuclei; inserts=negative controls) (B) Western blotting of protein kinase RNA-like ER kinase (PERK) in the two groups. RDU= relative densitometry units.

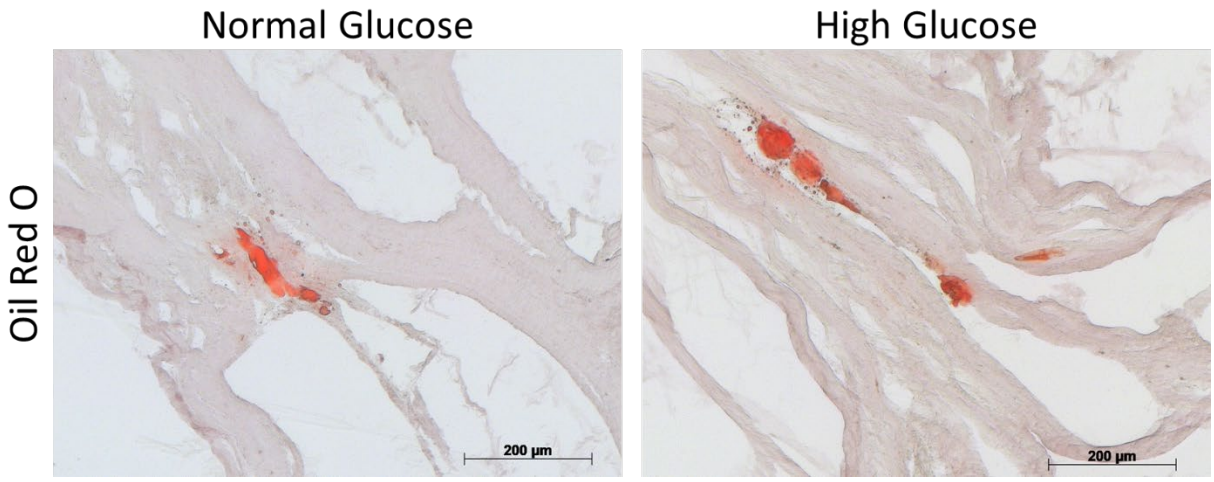


**Figure 6.21:** Staining for lipid accumulation in electromechanical bioreactor normal and high glucose samples. Red= lipids.

*6.3.2.4 Endoplasmic Reticulum Stress and Lipid Accumulation*

Evaluation of endoplasmic reticulum (ER) stress and lipid accumulation was performed, as they are traits of DCMP. IHC staining of inositol requiring enzyme-1 (IRE-1), an ER stress marker, showed existence in both normal and high glucose conditions (**Figure 6.20**). Western blotting of another ER stress protein, protein kinase RNA-like ER kinase (PERK) showed no difference between groups. Oil red O staining revealed lipids within normal and high glucose samples, with more accrual in high glucose conditions (**Figure 6.21**).

## 6.4 Discussion

DCMP is diagnosed once symptoms, including but not limited to, shortness of breath, angina, and fluid retention, are present in the patient.[15] Currently, no cure exists for DCMP and its treatment is grouped with other heart failures.[16] To diagnose and treat

or even reverse early stages of this disease, understanding the underlying mechanisms of its progression is key. As of now, animal models and cell cultures have been utilized to elucidate these initial changes.[5] However, there are discrepancies that exist between rodent models and human patients, such as differing heart beats per minute, circulating lipid concentrations, CM electrophysiological properties, diabetes disease progression, and inflammatory response.[7] Within rodent models, it is also difficult to study how individual cell types respond in a diseased state. In cell culture, specific cell types can be investigated, but it lacks a dynamic 3D ECM environment.

Recently, the field of tissue engineering has moved towards mimicking diseases by employing organotypic models that are physiologically relevant and reproducible, with the intent to study specific cell changes within a disease and determine definitive interactions to halt and reverse disease progression.[17–19] Tissue engineering holds substantial promise for addressing these needs, as it encompasses a wide variety of disciplines and organotypic 3D models are attractive as they are controllable, repetitive, and more cost efficient than animal testing.[11]

Other groups have attempted to bridge this gap for the study of DCMP but have failed to either produce a complex and dynamic 3D ECM environment or have utilized animal cells, instead of human cells.[10,12,13] Within our lab we have produced a complex 3D acellular scaffold from decellularized porcine myocardium, which has been proven to retain mechanical and vascular integrity, and important ECM basal lamina components crucial to recapitulating native myocardium, such as fibronectin, laminin, and collagen IV.[14] Myocardial ECM is very diverse and this specific environment is essential for

inherent cellular interactions and tethering.[20,21] Cell – ECM interactions in DCMP are especially pivotal in this disease, as myocardial fibrosis causes CMs to overcompensate to contract the left ventricle, leading to CM death and hypertrophy.[22]

Primary hCM progenitor cells have recently been used for research in areas such as cardiotoxicity, therapeutic testing, scaffold biocompatibility, and the study of pathways involved in oxidative stress.[23–26] They are more cost effective than induced pluripotent stem cells (iPSCs), can proliferate, and express cardiac markers, such as sarcomeric α-actin, making them ideal for CM investigation.[27] We have shown these cells respond to biochemical cues, such as normal (1 g/L) and high (4.5 g/L) glucose, in their milieu (see Chapter 4).

We examined two DCMP tissue engineering platforms generated within our lab. We chose to combine hCM and decellularized acellular porcine myocardium in either (1) a 3D Kube perfusion minibioreactor or (2) an electromechanical bioreactor we developed. 3D Kubes have been employed by researchers for disease modelling, tissue angiogenesis investigations, and cell differentiation and seeding studies.[28–31] Our electromechanical bioreactor has been shown to not alter the CM phenotype or ECM in normal conditions (see Chapter 5). Each were able to be housed within separate incubators and supported viable hCM in these scaffolds for 14 days in either normal or high glucose conditions.

To investigate these models, we explored some known hallmarks of DCMP. Within the hyperglycemic and dyslipidemic diabetic environment there is a loss of metabolic plasticity and cells rely mainly in free fatty acids for energy.[32] This leads to lipid peroxidation and accumulation, as well as prolonged accrual of reactive oxygen species

with oxidative stress as antioxidant defense mechanisms are overwhelmed.[33] In this prolonged state, there is an increase in, endoplasmic reticulum (ER) stress, autophagy, and apoptosis.[34,35] Hyperglycemia also increases accumulation of irreversible crosslinks formed by AGEs and hindered MMP activity, leading to fibrosis.[36]

In examining early MMP activity and AGE buildup, we saw no differences in overall MMP activity in media and AGE expression between the normal and high glucose groups in either bioreactor system. This could be due to the experimental duration of 14 days being too short to see noticeable changes in AGE accumulation from protein lysates and overall MMP activity in media. Media analysis could be useful for determining specific diagnostic markers for patient blood testing. There were no differences in overall MMP, MMP9, and active MMP2 activity in tissue lysates. We did however, see a significant increase in overall MMP2 and pro MMP2 activity in high glucose electromechanical tissue lysates. At this early point we may be seeing initial stages of unbalanced MMP activity, as MMP2 is heightened in inflammation, and we know later on, in established diabetic patients' serum, MMPs are significantly lowered.[37,38] We were able to see higher lipid accumulation within the high glucose tissue in both platforms. This is promising as this is a trait of diabetes.[39]

Cellular alterations in hCM such as endogenous antioxidant defense mechanisms, autophagy, apoptosis, and ER stress were inspected. SOD-2, an endogenous antioxidant defense mechanism, was slightly elevated in high glucose samples in both systems. Autophagy was significantly increased within the 3D Kube minibioreactor high glucose group and no difference was seen between groups in the electromechanical bioreactor.

Apoptosis was seen in both states in the minibioreactor system and there was a slight increase in apoptosis in the high glucose electromechanically conditioned samples. ER stress was only examined in the electromechanical platform and no differences were found between groups. In examining early changes, it is important to note that there are some alterations that may occur before others and some that may not occur until later stages DCMP. These changes occur over the course of years. Currently, our understanding of initial stages of this disease is limited and these results are promising as we know that within the cell, autophagy has been shown to be increased in hyperglycemia and after a prolonged state, it can lead to apoptosis.[40] In evaluating longer timepoints with these models, we could determine specifically when these modifications in hCM are occurring in the progression of DCMP.

While this 3D Kube minibioreactor is a promising model for DCMP, there are some drawbacks with this platform. Due to the small size of the 3D Kube chambers, protein extraction and analysis is limited, as is sample throughput. Even though this perfusion system is dynamic in nature, it lacks physiological myocardial conditions such as, electrical and mechanical stimuli. The electromechanical bioreactor provides these conditions; however, it is not a perfusion system and media must be changed every day to support cell viability. Because of this, changes in DCMP and diabetes may not have shown, as they are caused by accrual of proteins and toxic intermediates within the body.

## 6.5 Conclusions

Currently, limitations in animal and cell culture models of DCMP constrain our understanding of early alterations of specific cell types in this disease. Elucidating initial modifications are important for targeted therapies and patient diagnosis. Tissue engineering can bridge this gap with controllable, reproducible, and cost-effective organotypic models. We were able to combine acellular porcine myocardium and hCM within (1) 3D Kube minibioreactors and (2) an electromechanical bioreactor with added glucose for a DCMP tissue engineered models. Within these disease models, some early alterations in hCM and ECM were seen. While these systems are promising on their own, a more appropriate platform could be developed by combining these two.

## 6.6 Chapter 6 References


1 Bonow RO, Mann DL, Zipes DP, Libby P. *Braunwald's Heart Disease*. 9th ed. Saunders; 2011.

2 Murarka S, Movahed MR. Diabetic cardiomyopathy. *J Card Fail* 2010;**16**:971–9. https://doi.org/10.1016/j.cardfail.2010.07.249.

3 Seferović PM, Paulus WJ. Clinical diabetic cardiomyopathy: A two-faced disease with restrictive and dilated phenotypes. *Eur Heart J* 2015;**36**:1718–27. https://doi.org/10.1093/eurheartj/ehv134.

4 Fang ZY, Prins JB, Marwick TH. Diabetic cardiomyopathy: evidence, mechanisms, and therapeutic implications. *Endocr Rev* 2004;**25**:543–67. https://doi.org/10.1210/er.2003-0012.

5 Bugger H, Abel ED. Rodent models of diabetic cardiomyopathy. *Dis Model Mech* 2009;**2**:454–66. https://doi.org/10.1242/dmm.001941.

6 Michaelson J, Hariharan V, Huang H. Hyperglycemic and hyperlipidemic conditions alter cardiac cell biomechanical properties. *Biophys J* 2014;**106**:. https://doi.org/10.1016/j.bpj.2014.04.040.

7 Fuentes-Antras J, Picatoste B, Gomez-Hernandez A, Egido J, Tunon J, Lorenzo O. Updating experimental models of diabetic cardiomyopathy. *J Diabetes Res* 2015;**2015**:. https://doi.org/10.1155/2015/656795.

8 Bayeva M, Sawicki KT, Ardehali H. Taking diabetes to heart--deregulation of myocardial lipid metabolism in diabetic cardiomyopathy. *J Am Hear Assoc*

2013;**2**:e000433. https://doi.org/10.1161/JAHA.113.000433.
9 Aamodt JM, Grainger DW. Extracellular matrix-based biomaterial scaffolds and the host response. *Biomaterials* 2016;**86**:68–82. https://doi.org/10.1016/j.biomaterials.2016.02.003.
10 Maalouf RM, Eid AA, Gorin YC, Block K, Escobar GP, Bailey S, *et al.* Nox4-derived reactive oxygen species mediate cardiomyocyte injury in early type 1 diabetes. *AJP Cell Physiol* 2012;**302**:C597–604. https://doi.org/10.1152/ajpcell.00331.2011.
11 Vunjak Novakovic G, Eschenhagen T, Mummery C. Myocardial tissue engineering: In vitro models. *Cold Spring Harb Perspect Med* 2014;**4**:. https://doi.org/10.1101/cshperspect.a014076.
12 Drawnel FM, Boccardo S, Prummer M, Delobel F, Graff A, Weber M, *et al.* Disease modeling and phenotypic drug screening for diabetic cardiomyopathy using human induced pluripotent stem cells. *Cell Rep* 2014;**9**:810–20. https://doi.org/10.1016/j.celrep.2014.09.055.
13 Song H, Zandstra PW, Radisic M. Engineered heart tissue model of diabetic myocardium. *Tissue Eng Part A* 2011;**17**:1869–78. https://doi.org/10.1089/ten.TEA.2010.0617.
14 Schulte JB, Simionescu A, Simionescu DT. The acellular myocardial flap: a novel extracellular matrix scaffold enriched with patent microvascular networks and biocompatible cell niches. *Tissue Eng Part C Methods* 2013;**19**:518–30. https://doi.org/10.1089/ten.TEC.2012.0536.
15 McGuire DK, Marx N. *Diabetes in Cardiovascular Disease: A Companion to Braunwald's Heart Disease*. 1st ed. Philadelphia, PA: Saunders; 2015.
16 Battiprolu PK, Wang Z V., Hill JA. Diabetic Cardiomyopathy: Mediators and Mechanisms. *Diabetes Cardiovasc. Dis. A Companion to Braunwald's Hear. Dis.* 2015. p. 290–301.
17 Kofron CM, Mende U. In vitro models of the cardiac microenvironment to study myocyte and non-myocyte crosstalk: bioinspired approaches beyond the polystyrene dish. *J Physiol* 2017;**595**:3891–905. https://doi.org/10.1113/JP273100.
18 Smith AST, Macadangdang J, Leung W, Laflamme MA, Kim DH. Human iPSC-derived cardiomyocytes and tissue engineering strategies for disease modeling and drug screening. *Biotechnol Adv* 2017;**35**:77–94. https://doi.org/10.1016/j.biotechadv.2016.12.002.
19 Hirt MN, Sorensen NA, Bartholdt LM, Boeddinghaus J, Schaaf S, Eder A, *et al.* Increased afterload induces pathological cardiac hypertrophy: a new in vitro model. *Basic Res Cardiol* 2012;**107**:307. https://doi.org/10.1007/s00395-012-0307-z.
20 Kelly DJ, Rosen AB, Schuldt AJT, Kochupura P V, Doronin S V, Potapova I a, *et al.* Increased myocyte content and mechanical function within a tissue-engineered myocardial patch following implantation. *Tissue Eng Part A* 2009;**15**:2189–201. https://doi.org/10.1089/ten.tea.2008.0430.
21 Badylak SF. The extracellular matrix as a biologic scaffold material. *Biomaterials* 2007;**28**:3587–93. https://doi.org/10.1016/j.biomaterials.2007.04.043.

22 Falcão-Pires I, Leite-Moreira AF. Diabetic cardiomyopathy: Understanding the molecular and cellular basis to progress in diagnosis and treatment. *Heart Fail Rev* 2012;**17**:325–44. https://doi.org/10.1007/s10741-011-9257-z.
23 Hernández-Córdova R, Mathew DA, Balint R, Carrillo-Escalante HJ, Cervantes-Uc JM, Hidalgo-Bastida LA, *et al.* Indirect three-dimensional printing: A method for fabricating polyurethane-urea based cardiac scaffolds. *J Biomed Mater Res Part A* 2016;**104**:1912–21. https://doi.org/10.1002/jbm.a.35721.
24 El-battrawy I, Tülümen E, Lang S, Akin I, Behnes M, Zhou X, *et al.* Expression of Inflammation-related Intercellular Adhesion Molecules in Cardiomyocytes In Vitro and Modulation by Pro-inflammatory Agents. *In Vivo (Brooklyn)* 2016;**30**:213–8.
25 Ruiz-esparza GU, Segura-ibarra V, Cordero-reyes AM, Keith A, Serda RE, Cruz-solbes AS, *et al.* A specifically designed nanoconstruct associates, internalizes, traffics in cardiovascular cells, and accumulates in failing myocardium: a new strategy for heart failure diagnostics and therapeutics. *Eur J Hear Fail* 2017;**18**:169–78. https://doi.org/10.1002/ejhf.463.A.
26 Kuo CY, Chiu YC, Lee AYL, Hwang TL. Mitochondrial Lon protease controls ROS-dependent apoptosis in cardiomyocyte under hypoxia. *Mitochondrion* 2015;**23**:7–16. https://doi.org/10.1016/j.mito.2015.04.004.
27 Kai D, Prabhakaran MP, Jin G, Ramakrishna S. Biocompatibility evaluation of electrically conductive nanofibrous scaffolds for cardiac tissue engineering. *J Mater Chem B* 2013;**1**:2305–14. https://doi.org/10.1039/c3tb00151b.
28 Srivastava S, Pasipanodya JG, Ramachandran G, Deshpande D, Shuford S, Crosswell HE, *et al.* A Long-term Co-perfused Disseminated Tuberculosis-3D Liver Hollow Fiber Model for Both Drug Efficacy and Hepatotoxicity in Babies. *EBioMedicine* 2016;**6**:126–38. https://doi.org/10.1016/j.ebiom.2016.02.040.
29 Portalska KJ, Chamberlain MD, Lo C, Blitterswijk C van, Sefton M V, Boer J de. Collagen modules for in situ delivery of mesenchymal stromal cell-derived endothelial cells for improved angiogenesis. *J Tissue Eng Regen Med* 2016;**10**:363–73. https://doi.org/10.1002/term.
30 Abbott RD, Raja WK, Wang RY, Stinson JA, Glettig DL, Burke KA, *et al.* Long term perfusion system supporting adipogenesis. *Methods* 2015;**84**:84–9. https://doi.org/10.1016/j.ymeth.2015.03.022.
31 Ruiz-Cantu L, Gleadall A, Faris C, Segal J, Shakesheff K, Yang J. Characterisation of the surface structure of 3D printed scaffolds for cell infiltration and surgical suturing. *Biofabrication* 2016;**8**:. https://doi.org/10.1088/1758-5090/8/1/015016.
32 Bugger H, Abel ED. Molecular mechanisms of diabetic cardiomyopathy. *Diabetologia* 2014;**57**:660–71. https://doi.org/10.1007/s00125-014-3171-6.
33 Huynh K, Bernardo BC, Mcmullen JR, Ritchie RH. Pharmacology & Therapeutics Diabetic cardiomyopathy : Mechanisms and new treatment strategies targeting antioxidant signaling pathways. *Pharmacol Ther* 2014;**142**:375–415. https://doi.org/10.1016/j.pharmthera.2014.01.003.
34 Huang PC, Wang GJ, Fan MJ, Asokan Shibu M, Liu YT, Padma Viswanadha V, *et*

*al.* Cellular apoptosis and cardiac dysfunction in STZ-induced diabetic rats attenuated by anthocyanins via activation of IGFI-R/PI3K/Akt survival signaling. *Environ Toxicol* 2017;**32**:2471–80. https://doi.org/10.1002/tox.22460.

35 Kobayashi S, Liang Q. Autophagy and mitophagy in diabetic cardiomyopathy. *Biochim Biophys Acta - Mol Basis Dis* 2015;**1852**:252–61. https://doi.org/10.1016/j.bbadis.2014.05.020.

36 Bodiga VL, Eda SR, Bodiga S. Advanced glycation end products: Role in pathology of diabetic cardiomyopathy. *Heart Fail Rev* 2014. https://doi.org/10.1007/s10741-013-9374-y.

37 Lewandowski KC, Banach E, Bieńkiewicz M, Lewiński A. Matrix metalloproteinases in type 2 diabetes and non-diabetic controls: Effects of short-term and chronic hyperglycaemia. *Arch Med Sci* 2011;**7**:294–303. https://doi.org/10.5114/aoms.2011.22081.

38 Cui N, Hu M, Khalil RA. *Biochemical and Biological Attributes of Matrix Metalloproteinases*. vol. 147. 1st ed. Elsevier Inc.; 2017.

39 Asghar O, Al-Sunni A, Khavandi K, Khavandi A, Withers S, Greenstein A, *et al.* Diabetic cardiomyopathy. *Clin Sci* 2009;**116**:741–60. https://doi.org/10.1042/CS20080500.

40 Ouyang C, You J, Xie Z. The interplay between autophagy and apoptosis in the diabetic heart. *J Mol Cell Cardiol* 2014. https://doi.org/10.1016/j.yjmcc.2013.10.014.

# CHAPTER 7: CONCLUSIONS AND RECOMMENDATIONS FOR FUTURE WORK

## 7.1 CONCLUSIONS

As the epidemic of diabetes continues to rise, it follows that instances of cardiovascular disease, such as diabetic cardiomyopathy, hypertension, and atherosclerosis in diabetic patients also rise.[1,2] Diabetic cardiomyopathy (DCMP) occurs in diabetic patients as a ventricular dysfunction independent of coronary artery disease, hypertension or valvular abnormalities.[3] Through cascading events over time, hyperglycemia and dyslipidemia can lead to this myocardial disease. Dyslipidemia leads to heightened utilization of circulating free fatty acids (FFA) that creates a highly oxidative environment that supersedes the endogenous antioxidant defense mechanism of cells, preceding oxidative stress, lipotoxicity, autophagy, and apoptosis of cardiomyocytes.[4] Hyperglycemia causes the formation and accumulation of advanced glycation endproducts (AGEs) in the extracellular matrix, leading to fibrosis. These alterations in the myocardium can lead to cardiac inefficiency and heart failure.[5]

Currently, mainly rodent models and two dimensional (2D) cell cultures have been employed to analyze early changes associated with DCMP. However, there are notable differences between rodents and humans that provide challenges when studying DCMP and 2D cultures lack a dynamic, three dimensional (3D) environment crucial to the progression of this disease.[6] As of now, DCMP diagnosis and treatment is lumped in with other cardiomyopathies and heart failure, with an emphasis on blood glucose

control.[2] Treatments for this disease do not target the source of the problem, only treat the symptoms. A more accurate model is needed to investigate specific cell type early cellular and extracellular modifications of DCMP for diagnosis and determine and test potential therapies. We believe tissue engineering can be used to bridge this gap. The tissue engineering paradigm can be utilized to developing a reproducible, native-like tissue engineered model of the myocardium by combining a scaffold, cells, and biochemical and physical stimuli to model DCMP.

We have shown that tools and methods used in our lab were able to detect known extracellular matrix (ECM) and cellular changes associated with DCMP in a streptozotocin (STZ) type 1 diabetic rat model. Furthermore, through examination of human cardiomyocytes (hCM), we were able to prove that these cells respond to hyperglycemia within their milieu. These techniques are useful for analyzing and detecting DCMP alterations in cells and the ECM such as, lipid accumulation, endogenous antioxidant mechanisms, advanced glycation endproduct (AGE) buildup, matrix metalloproteinase (MMP) activity, apoptosis, autophagy, endoplasmic reticulum (ER) stress, and perivascular and interstitial fibrosis.

We produced a physiologically relevant electromechanical bioreactor within our lab and method for reproducible scaffolds from decellularized porcine myocardium. Through our in house decellularization procedure of whole porcine hearts, we were able to remove porcine cells efficiently while keeping important myocardial ECM proteins such as collagen IV and laminin intact. By designing and 3D printing a tissue slicer, myocardium was easily extracted for use. This myocardial scaffold supported viable

hCM for 18 days. Our electromechanical bioreactor sustained hCM seeded on and in these scaffolds for 14 days at mechanical and electrical physiological conditions. Cells were aligned, found throughout the scaffolds, and maintained the cardiomyocyte phenotype. The ECM was found to be unaltered in these dynamic conditions.

We examined cardiac tissue engineered constructs in: (1) a perfusion 3D Kube minibioreactor and (2) the electromechanical bioreactor customized in our lab. Each platform contained decellularized myocardium seeded with human cardiomyocytes for two weeks; "diabetic" conditions were simulated by increased glucose concentration. Within these models some early alterations of DCMP were seen. We found were able to better mimic physiological conditions with our electromechanical bioreactor, compared to static and non-diabetic conditions, as well as to 2D cell culture.

Our electromechanical tissue engineering platform shows promise for unveiling early cellular and matrix modifications in DCMP. The potential for this system is enormous; it could be useful for studying other cardiac diseases in many human cell types, testing potential therapies and drugs, and preconditioning tissue engineered myocardium prior to implantation.

### 7.2 Project Challenges and Considerations

Challenges in this project arose in seeding cells into decellularized porcine myocardium. Injection seeding of myocardium resulted in pockets of cells within the scaffold, which does not resemble the highly populated native myocardium. Dynamic stimulation, either perfusion or electromechanical, for the duration of 14 days did not

promote homogenous hCM migration into the scaffold. Cell seeding strategies are being investigated under other projects within our lab.

Another challenge during this project was related to protein analysis of tissues cultured in the 3D Kube minibioreactor system. The tissue housed within 3D Kubes are very small and only so many cells can be seeded on them, this led to very low protein amounts. Protein lysates needed to be concentrated with spin columns before protein analysis with western blotting to be able to load 20ug per well. This limited proteins that were analyzed and led to a lower n-value.

Our electromechanical bioreactor was able to house larger scaffolds seeded with hCM, which mitigated the protein analysis problem seen with the 3D Kube minibioreactor. This system, however, is not perfusion based, so media was changed every day. As DCMP and diabetes progress by the accumulation of proteins and toxic intermediates, this platform may not allow for early alterations in cells and the ECM to occur. This is currently being developed within our lab.

A consideration for future DCMP models would include; the addition a known amount of lipids in media with the hyperglycemic environment to simulate dyslipidemia; increase in pressure to mimic hypertension; and addition of high cholesterol. Other Another consideration would be employing insulin to simulate a diabetic state with treatment to determine if cells are still altered. Fibroblasts should also be investigated in future research, as they are vital players in ECM turnover, are adversely affected in diabetes, and secrete important paracrine factors. More timepoints should be studied to

see when cellular and matrix changes are occurring. Microarrays for gene analysis would be useful for this. For a diagnostic potential, media should also be investigated for markers that could be targets for patient blood testing.

## 7.3 Recommendations for Future Work

### *7.3.1 Analysis of Perfusion Electromechanical Platform*

The electromechanical bioreactor is now being modified to be perfusion based within our lab as of now. Testing of this platform will be performed to ensure hCM and human cardiac fibroblasts (FBs) maintain phenotype and the ECM is not adversely affected. hCM and FBs will be cultured and expanded until enough cells needed for seeding are reached. Decellularized porcine myocardium will be extracted with the tissue slicer, sterilized with peracetic acid, and left overnight in media (Dulbecco's modified eagle medium, 10% fetal bovine serum, 1% antibiotic/antimycotic) at 37 degrees Celsius. Scaffolds will either be seeded with 3 million hCM or hFB per scaffold via dropwise and injection seeding. Some scaffolds will be seeded with both hCM (1.2 million; 40%) and hFB (1.8 million; 60%). Controls will have no cells. They will sit statically in the incubator for 1 hour, then 4mL of media will be added. Seeded scaffolds will remain in the incubator, static, for 3 days, with media changes each day. A PrestoBlue and live/dead assay will be performed as a checkpoint at this time.

After this duration, scaffolds will be placed within modified 6-well plates of the perfusion electromechanical bioreactor system housed in an incubator and for two days will be subjected to a 0-40-0 mmHg waveform, followed by two days at 0-80-0 mmHg.

Once this conditioning period is complete, myocardial-like tissue will be exposed to the 0-120-0 mmHg waveform with electrical stimulus. Static scaffolds in 6 well plates will be run in tandem as a control with 4mL of media changed every two days. Media in the electromechanical perfusion system will be changed once a week with supplemental antibiotic injections 3.5 days after media changes. Media will be collected from static and dynamic groups every week and frozen for examination.

| Perfusion Electromechanical Bioreactor | | | |
|---|---|---|---|
| Groups | | Samples Per Timepoint (2,4,6,8 weeks) | |
| Static or Dynamic | Cells on Scaffold | Histology; Protein; RNA | PrestoBlue & Live/Dead |
| Static | hCM | 5 | 1 |
| Static | hFB | 5 | 1 |
| Static | hCM + hFB | 5 | 1 |
| Static | No cells | 5 | 1 |
| Dynamic | hCM | 5 | 1 |
| Dynamic | hFB | 5 | 1 |
| Dynamic | hCM + hFB | 5 | 1 |
| Dynamic | No cells | 5 | 1 |

**Table 7.1**: Sample analysis of perfusion electromechanical bioreactor.

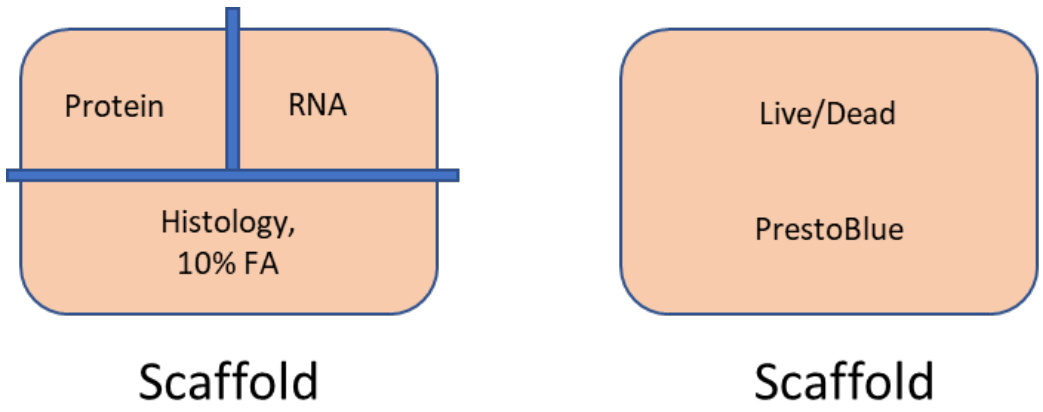


**Figure 7.1:** Diagram of dissection of scaffolds for analysis.

Timepoints analyzed will be two, four, six, and eight weeks. In order to have a high and desired n-value outlined in **Table 7.1**, this experiment will need to be performed four times. One myocardial-like tissue from each group will be assessed by PrestoBlue and a live/dead assay to determine cell viability at each timepoint. Scaffolds will be dissected as shown in **Figure 7.1**. Half of each scaffold will be placed in 10% formalin for 48 hours, processed, embedded, and sectioned to 5um on slides. Slides will be stained with hematoxylin and eosin, Movat's pentachrome, Masson's trichrome, and immunohistochemically stained for: cardiomyocyte markers such as, sarcomeric α-actinin, connexin 43, desmin, and GATA-4; fibroblast markers such as vimentin, prolyl 4-hydroxylase, and heat shock protein 47; and ECM proteins such as, collagen IV and laminin. One-fourth of each myocardial-like tissue will be used for protein isolation and flash frozen before stored in the -80-degree Celsius freezer until extraction via homogenizer and radioimmunoprecipitation assay (RIPA) buffer. Total protein from these samples will be determined by bicinchoninic acid (BCA) assay. Western blotting protein for cardiomyocyte markers such as, sarcomeric α-actinin, connexin 43, desmin, and GATA-4, and ECM proteins such as, collagen IV and laminin will be investigated. Matrix metalloproteinase (MMP) activity will be examined in media and lysates by gelatin zymography. One-fourth of each scaffold will be flash frozen and stored in -80-degree Celsius freezer for ribonucleic acid (RNA) isolation. RNA samples will be sent away for microarray analysis for cardiomyocyte genes such as, GATA4 and myosin heavy chain-β; fibroblast genes such as, vimentin, collagen I and III, and fibroblast specific protein 1; and any other genes of interest.

*7.3.2 Preliminary Dyslipidemic and High Cholesterol Testing*

Preliminary testing of addition of FFAs and cholesterol will be performed to determine if they harm cell viability in culture. hCM and hFBs will need to be cultured in serum free conditions, so known amounts of cholesterol and FFAs can be added. hCM and hFBs (2:3 seeding ratio), hCM alone, and hFB alone will be cultured in 48 well plates and subjected to various conditions for 12, 24, 48, and 72 hour, and 1 and 2 week timepoints for viability and cytotoxicity with PrestoBlue, live/dead, and MTS assays. Cholesterol (Sigma-Aldrich, catalogue #: C3045) will be dissolved in ethanol and added to serum free media in a range of normal at 1g/L (100mg/dL) to high at 2.5g/L (250mg/dL) cholesterol. Palmitic acid (Sigma-Aldrich, catalogue #: P0500) and oleic acid (Sigma-Aldrich, catalogue #: O1008), main fatty acids in human nutrition, will be conjugated to bovine serum albumin and added to serum free media in a range from 0.25mmol/L to 0.5mmol/L, as previously studied.[7] Final concentrations in media will be assessed after sterile filtration with colorimetric enzymatic assays LabAssay™ Cholesterol and LabAssay™ Phospholipid (FUJIFILM, Wanko Chemicals) before addition to cells. Conditions and analysis will be performed as shown in **Figure 7.2** and **Figure 7.3**.

Once testing determines optimal high and normal concentrations of cholesterol and FFAs in cell culture, secondary preliminary testing will assess these in the two cell types (hCM + hFB, hCM, and hFB) with combinations of these in normal (1g/L) and high (4.5g/L) glucose at the same timepoints (12, 24, 48, and 72 hours, and 1 and 2

weeks). Cell viability and cytotoxicity with be analyzed with PrestoBlue, live/dead, and MTS assays at these timepoints as shown in **Figure 7.4**.

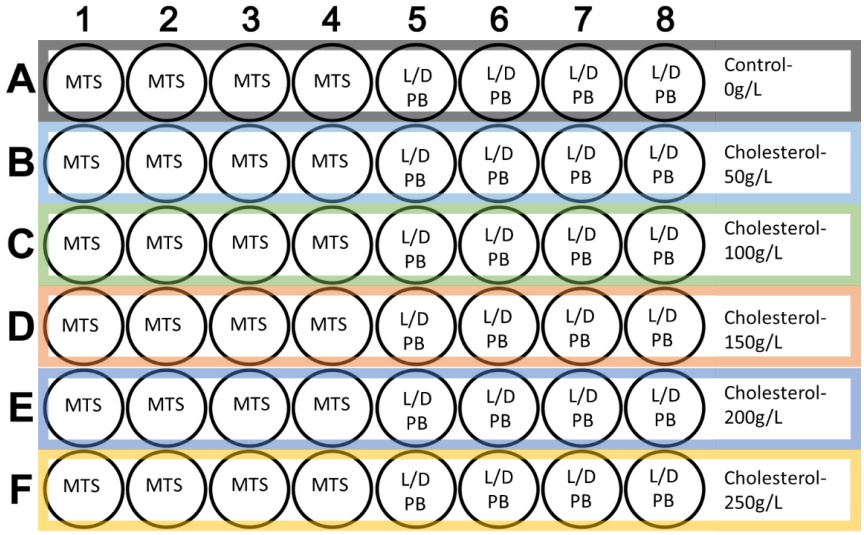


**Figure 7.2:** 48 well plate layout of cholesterol testing. One plate for each timepoint and one cell type or combination. MTS=MTS assay. L/D=live/dead. PB=PrestoBlue.

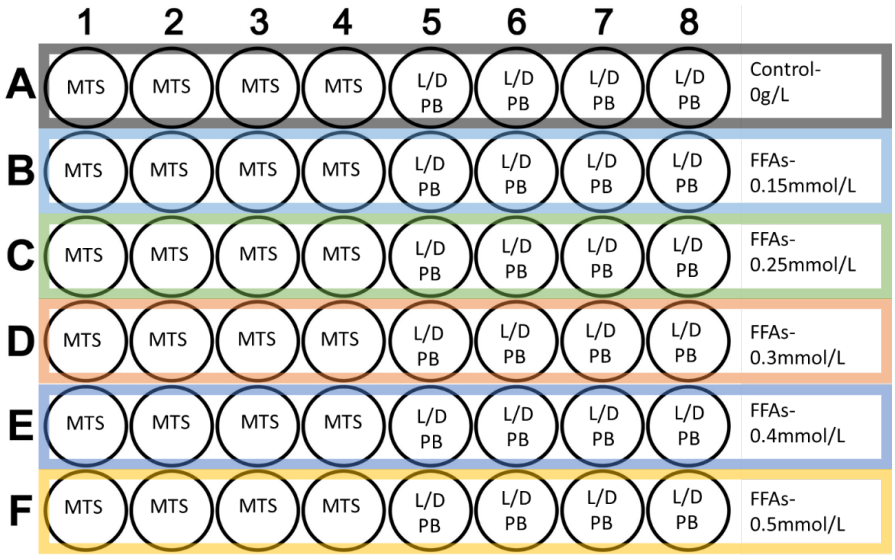


**Figure 7.2:** 48 well plate layout of FFA testing. One plate for each timepoint and one cell type or combination. MTS=MTS assay. L/D=live/dead. PB=PrestoBlue.

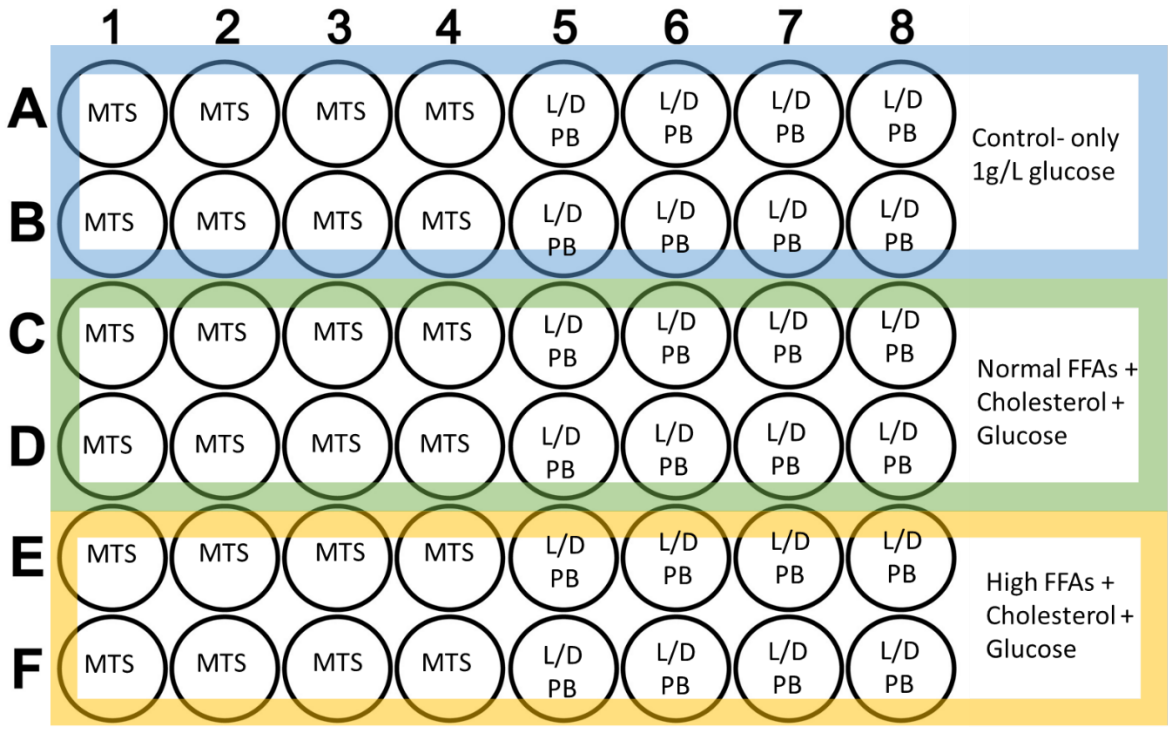


**Figure 7.4:** 48 well plate layout of combinational testing. One plate for each timepoint and one cell type or combination. MTS=MTS assay. L/D=live/dead. PB=PrestoBlue.

*7.3.3 Perfusion Electromechanical Platform: DCMP Model*

The same dynamic experimental setup described in *7.3.1* will be used, however in order to model a "diabetic" environment, glucose will be added (4.5 g/L), along with high FFAs and cholesterol (determined in *7.3.2*) to serum free media in the perfused electromechanical bioreactor. Normal serum free media (1 g/L glucose, normal FFAs and cholesterol) will be run in tandem as a control. All scaffolds seeded with hCM, hFB, and hCM and hFB will be conditioned as described before, then subjected to physiological conditions in the perfused electromechanical system. Timepoints analyzed will be two, four, six, and eight weeks at normal and "diabetic" conditions for all three cell groups

(**Table 7.2**). Media will also be collected and samples at two, four, six, and eight weeks will be analyzed. Multiple bioreactor runs will be done for a high n-value and separate runs will be done for normal and "diabetic" conditions. A total of 8 runs will be performed (normal vs. "diabetic" at four timepoints). A PrestoBlue and live/dead assay will be used to determine cell viability at these timepoints in normal and "diabetic" groups. Myocardial-like tissue will be saved for paraffin and frozen cryosection histological staining, protein, and RNA analysis as shown in **Figure 7.1** and **Table 7.2**. Examination of DCMP hallmarks such as lipid accumulation, endogenous antioxidant mechanisms, AGE buildup, MMP activity, apoptosis, autophagy, ER stress, and fibrosis will be completed as detailed in Chapter 6. Tissue and media will be sent away for microRNA analysis.

| Perfusion Electromechanical Bioreactor | | | | |
|---|---|---|---|---|
| Run | Groups | | Samples Per Timepoint (2,4,6,8 weeks) | |
| | Condition | Cells on Scaffold | Histology; Protein; RNA | PrestoBlue & Live/Dead |
| 1 | Normal | hCM | 7 | 1 |
| 1 | Normal | hFB | 7 | 1 |
| 1 | Normal | hCM + hFB | 7 | 1 |
| 2 | "Diabetic" | hCM | 7 | 1 |
| 2 | "Diabetic" | hFB | 7 | 1 |
| 2 | "Diabetic" | hCM + hFB | 7 | 1 |

**Table 7.2**: Sample analysis of perfusion electromechanical bioreactor DCMP model.

## 7.4 Chapter 7 References


1 International Diabetes Federation. *Eighth edition 2017*. 2017.

2 McGuire DK, Marx N. *Diabetes in Cardiovascular Disease: A Companion to Braunwald's Heart Disease*. 1st ed. Philadelphia, PA: Saunders; 2015.

3 Lee WS, Kim J. Diabetic cardiomyopathy: Where we are and where we are going. *Korean J Intern Med* 2017;**32**:404–21. https://doi.org/10.3904/kjim.2016.208.

4 Bugger H, Abel ED. Molecular mechanisms of diabetic cardiomyopathy. *Diabetologia* 2014;**57**:660–71. https://doi.org/10.1007/s00125-014-3171-6.
5 Wang J, Song Y, Wang Q, Kralik PM, Epstein PN. Causes and characteristics of diabetic cardiomyopathy. *Rev Diabet Stud* 2006;**3**:108–17. https://doi.org/10.1900/RDS.2006.3.108.
6 Bugger H, Abel ED. Rodent models of diabetic cardiomyopathy. *Dis Model Mech* 2009;**2**:454–66. https://doi.org/10.1242/dmm.001941.
7 Dyntar D, Eppenberger-Eberhardt M, Maedler K, Pruschy M, Eppenberger HM, Spinas GA, *et al.* Glucose and Palmitic Acid Induce Degeneration of Myofibrils and Modulate Apoptosis in Rat Adult Cardiomyocytes. *Diabetes* 2001;**50**:2105–13. https://doi.org/10.2337/diabetes.50.9.2105.

# APPENDICES

# Appendix A

## Abbreviations

| | |
|---|---|
| 2D | two dimensional |
| 3D | three dimensional |
| ABS | acrylonitrile butadiene styrene |
| ACE | angiotensin converting enzyme |
| ADSC | adipose derived stem cell |
| AGE | advanced glycation endproduct |
| Akt | protein kinase B |
| ATF4 | activating transcription factor 4 |
| ATF6 | activating transcription factor 6 |
| ATP | adenosine 5'-triphosphate |
| BCA | bicinchoninic acid protein assay |
| BiP | binding protein |
| BMDSC | bone marrow derived stem cell |
| CD36 | cluster of differentiation 36 |
| CHOP | CCAAT/-enhancer-binding protein homologous protein |
| CM | cardiomyocyte |
| cm | centimeters |
| CML | carboxymethyl lysine |
| CPC | cardiac progenitor cell |
| CSC | cardiac stem cell |

| | |
|---|---|
| DAPI | 4’,6-diamidino-2-phenylindole |
| DAQ | data acquisition |
| DCMP | diabetic cardiomyopathy |
| $ddH_2O$ | distilled deionized water |
| Decell | decellularization |
| DMEM | Dulbecco’s modified eagle medium |
| DNA | deoxyribonucleic acid |
| DPP-4 | dipeptidyl peptidase inhibitor |
| DSC2 | desmocollin-2 |
| EC | endothelial cell |
| ECM | extracellular matrix |
| EDTA | Ethylenediaminetetraacetic acid |
| eIF2α | eukaryotic translation initiation factor 2 alpha |
| eNOs | endothelial nitric oxide synthases |
| EPC | endothelial progenitor cell |
| ER | endoplasmic reticulum |
| ERAD | endoplasmic reticulum associated degradation |
| ESC | embryonic stem cell |
| FB | fibroblast |
| FBS | fetal bovine serum |
| FFA | free fatty acid |
| g | gram |

| | |
|---|---|
| GFP | green fluorescent protein |
| GLP-1 | glucagon-like peptide 1 |
| GLUT4 | glucose transporter 4 |
| H&E | hematoxylin and eosin |
| HCl | hydrochloric acid |
| hCM | human cardiomyocyte |
| Hz | hertz |
| $I_{Ca\text{-}L}$ | L-type calcium ion channel |
| IHC | immunohistochemistry |
| iPSC | induced pluripotent stem cell |
| IRE-1 | inositol-requiring enzyme 1 |
| IRS-1 | insulin receptor substrate 1 |
| $I_{to}$ | outward potassium current |
| JNK | Jun N terminal kinase |
| JUP | armadillo proteins plakiglobin |
| L | liter |
| LC3B | light chain 3B |
| min | minute |
| mL | milliliter |
| mM | millimolar |
| mmHg | millimeter of mercury |
| MMP | matrix metalloproteinase |

| | |
|---|---|
| MRI | magnetic resonance imaging |
| MSC | mesenchymal stem cell |
| msec | millisecond |
| NaCl | sodium chloride |
| NADPH | nicotinamide adenine dinucleotide phosphate |
| NCX | $Na^{+2}/Ca^{+2}$ exchanger |
| NIH | National Institute of Health |
| NOS | nitric oxide synthase |
| Nrf2 | (erythroid-derived 2)-related factor2 |
| OCT | optimal cutting temperature |
| PDK4 | pyruvate dehydrogenase kinase 4 |
| PERK | protein kinase RNA-like ER kinase |
| PET | positron emission tomography |
| PI3K | phosphoinositide 3-kinase |
| PKC | protein kinase C |
| PLB | phosphorylated phospholamban |
| PPAR- α | peroxisome proliferator-activated receptor alpha |
| RAGE | receptor for advanced glycation endproducts |
| RDU | relative densitometry units |
| RGD | arginylglycylaspartic acid |
| RIPA | Radioimmunoprecipitation assay |
| RNA | ribonucleic acid |

| | |
|---|---|
| ROS | reactive oxygen species |
| RyRs | ryanodine receptor |
| sarc. α-actinin | sarcomeric α-actinin |
| SD | standard deviation |
| SDS | sodium dodecyl sulfate |
| SEM | scanning electron microscopy |
| SERCA | sarcoplasmic/endoplasmic reticulum $Ca^{+2}$-ATPase |
| SMC | smooth muscle cell |
| SOD | superoxide dismutase |
| STZ | streptozotocin |
| TGF-β | transforming growth factor-beta |
| TIMP | tissue inhibitor of matrix metalloproteinase |
| TNFα | tumor necrosis factor alpha |
| Tris | tris(hydroxymethyl)aminomethane |
| TZD | thiazolindinediones |
| ug | microgram |
| um | micrometer |
| UPR | unfolded protein response |
| UV | ultraviolet |
| V | volts |
| XPB-1 | X-box binding protein 1 |
| ZDF | Zucker diabetic fatty rat |

| | |
|---|---|
| α | alpha |
| α-SMactin | alpha smooth muscle actin |